frontiers | Research Topics

Nuclear power cooling-water system disaster-causing organisms: Outbreak and aggregation mechanisms, early-warning monitoring, prevention and control

Edited by
Huang Honghui, Wei Wu and Kaizhi Li

Published in
Frontiers in Marine Science

ISSN 1664-8714
ISBN 978-2-8325-2857-0
DOI 10.3389/978-2-8325-2857-0

About Frontiers

Frontiers is more than just an open access publisher of scholarly articles: it is a pioneering approach to the world of academia, radically improving the way scholarly research is managed. The grand vision of Frontiers is a world where all people have an equal opportunity to seek, share and generate knowledge. Frontiers provides immediate and permanent online open access to all its publications, but this alone is not enough to realize our grand goals.

Frontiers journal series

The Frontiers journal series is a multi-tier and interdisciplinary set of open-access, online journals, promising a paradigm shift from the current review, selection and dissemination processes in academic publishing. All Frontiers journals are driven by researchers for researchers; therefore, they constitute a service to the scholarly community. At the same time, the *Frontiers journal series* operates on a revolutionary invention, the tiered publishing system, initially addressing specific communities of scholars, and gradually climbing up to broader public understanding, thus serving the interests of the lay society, too.

Dedication to quality

Each Frontiers article is a landmark of the highest quality, thanks to genuinely collaborative interactions between authors and review editors, who include some of the world's best academicians. Research must be certified by peers before entering a stream of knowledge that may eventually reach the public - and shape society; therefore, Frontiers only applies the most rigorous and unbiased reviews. Frontiers revolutionizes research publishing by freely delivering the most outstanding research, evaluated with no bias from both the academic and social point of view. By applying the most advanced information technologies, Frontiers is catapulting scholarly publishing into a new generation.

What are Frontiers Research Topics?

Frontiers Research Topics are very popular trademarks of the *Frontiers journals series*: they are collections of at least ten articles, all centered on a particular subject. With their unique mix of varied contributions from Original Research to Review Articles, Frontiers Research Topics unify the most influential researchers, the latest key findings and historical advances in a hot research area.

Find out more on how to host your own Frontiers Research Topic or contribute to one as an author by contacting the Frontiers editorial office: frontiersin.org/about/contact

Nuclear power cooling-water system disaster-causing organisms: Outbreak and aggregation mechanisms, early-warning monitoring, prevention and control

Topic editors

Huang Honghui — South China Sea Fisheries Research Institute, Chinese Academy of Fishery Sciences (CAFS), China

Wei Wu — University of Southern Mississippi, United States

Kaizhi Li — South China Sea Institute of Oceanology, Chinese Academy of Sciences (CAS), China

Citation

Honghui, H., Wu, W., Li, K., eds. (2023). *Nuclear power cooling-water system disaster-causing organisms: Outbreak and aggregation mechanisms, early-warning monitoring, prevention and control*. Lausanne: Frontiers Media SA. doi: 10.3389/978-2-8325-2857-0

Table of contents

frontiers | Frontiers in Marine Science

TYPE Editorial
PUBLISHED 14 June 2023
DOI 10.3389/fmars.2023.1218776

OPEN ACCESS

EDITED AND REVIEWED BY
Ilaria Corsi,
University of Siena, Italy

*CORRESPONDENCE
Honghui Huang
huanghh@scsfri.ac.cn

RECEIVED 08 May 2023
ACCEPTED 22 May 2023
PUBLISHED 14 June 2023

CITATION
Huang H, Wu W and Li K (2023) Editorial: Nuclear power cooling-water system disaster-causing organisms: outbreak and aggregation mechanisms, early-warning monitoring, prevention and control. *Front. Mar. Sci.* 10:1218776. doi: 10.3389/fmars.2023.1218776

Editorial: Nuclear power cooling-water system disaster-causing organisms: outbreak and aggregation mechanisms, early-warning monitoring, prevention and control

Honghui Huang[1]*, Wei Wu[2] and Kaizhi Li[3]

[1]Guangdong Provincial Key Laboratory of Fishery Ecology and Environment, South China Sea Fisheries Research Institute, Chinese Academy of Fishery Sciences (CAFS), Guangzhou, China, [2]School of Ocean Science and Engineering, University of Southern Mississippi Ocean Springs, Ocean Springs, MS, United States, [3]South China Sea Institute of Oceanology, Chinese Academy of Sciences (CAS), Guangzhou, China

KEYWORDS

nuclear power plant (NPP), marine organisms, outbreak and aggregation mechanisms, early-warning monitoring, prevention and control strategy

Editorial on the Research Topic

Nuclear power cooling-water system disaster-causing organisms: outbreak and aggregation mechanisms, early-warning monitoring, prevention and control

The outbreaks of aquatic organisms have become more frequent due to the changing global climate and human activities, resulting in negative impacts on the sustainability of marine ecosystems and causing economic losses in local communities (Gobler, 2020; Prakash, 2021). Generally, these outbreaks are indicative of serious environmental disturbances and potential regime shifts in marine ecosystems (Wollrab et al., 2021; Chust et al., 2022). Meanwhile, they are particularly prevalent in waters adjacent to nuclear power plants (NPP), where they may be related to thermal discharge from the plants' cooling water (Lucas et al., 2014; Wu et al., 2023). Besides their ecological and economic impacts, these outbreaks can lead to costly shutdowns, equipment damage, and safety hazards of NPP.

Nevertheless, the processes, mechanisms, potential impact, and prevention and control strategies of disaster-causing organisms (DCO) remain unclear. Furthermore, with the increasing demand for renewable energy to combat climate change, the construction of new NPP is expected to rise (Khttab, 2021). To achieve the dual goals of healthier aquatic ecosystems and operation safety of NPP, urgent research is needed to investigate this issue comprehensively. This specific Research Topic includes twelve original research articles, a brief research article, and an article on methods, which cover organisms such as bacteria, phytoplankton, zooplankton, benthos, and fish.

The thermal discharge from NPP can increase the temperature of the surrounding water, causing changes in the local ecosystem and potentially harming marine organisms. Plankton are highly sensitive to changes in temperature, and even small increases in water temperature caused by thermal discharge can result in significant shifts in their abundance and community structure (Beninca et al., 2011). Liu et al. found that the metabolism of plankton community was enhanced in moderately warm regions, with higher gross primary production and community respiration than in regions with high and extremely high temperatures; meanwhile, the metabolism was evidently inhibited in warmer regions, showing exhibiting heterotrophic metabolism state. Hu et al. detected a rapid photosynthetic and physiological response of phytoplankton to the elevated temperature and a shift in the size-fractioned structure in the thermal discharge area, consequently, the high-temperature inhibition might stimulate the stress response of the common phytoplankton and promote high frequency of harmful algal blooms. However, a sudden drop in temperature caused by the shutdown of power plants may also affect the health and behavior of organisms. The impact of the upper and lower incipient lethal temperatures decreased during fish development, from yolk-sac larvae to juveniles, especially in response to cold shocks, indicating that later developmental stages are more tolerant of temperature fluctuations (Tian et al.). Because of their limited migration ability, relatively long lifespan, and sensitivity to environmental changes, benthos are usually considered to be an effective indicators for assessing ecosystem health (Borja et al., 2016). A test of the adaptability and vulnerability of gastropods under controlled temperature suggested that constant increases in water temperature can be fatal to the slow-moving gastropods, with cellular atrophy and necrosis (Shaikh et al.).

Marine organisms can affect the operations and safety of NPP, therefore, understanding the spatial and temporal patterns of marine organisms can help identify areas of high risk for cooling water blockage, enable the implementation of preventative and control strategies, and inform the design of mitigation measures to minimize the impacts on marine ecosystems. According to a survey conducted in Daya Bay, there was a noticeable seasonal shift in abundance and taxonomic composition of zooplankton communities. Because of their large body size and massive abundance in spring, certain kollaplankton could potentially cause severe damage to the NPP cooling system. In addition, the blooms of *Centropages tenuiremis* during spring and *Penilia avirostris* during summer could potentially lure in groups of larval or adult pelagic fish, thereby posing a threat to the security of the cooling system (Wu et al.). In extreme weather conditions like the typhoon, the threat posed by benthic organisms to the cooling-water system of NPP cannot be ignored. Cai et al. depicted the spatial and seasonal distributions of ten benthic macrofauna species which have the potential to blockage the cooling-water system of Daya NPP, and examined the environmental conditions for these species. Biofouling is a key factor affecting the safety of the water intake of the cooling-water system of coastal NPP. Lin et al. conducted a 1-year simulated concrete panel test in Xinghua Bay (China) from 2020 to 2021 and observed that fouling organisms had the highest attachment period between June and October. The study recommends implementing targeted prevention and control measures during this period, considering the larval attachment period of different dominant groups of fouling organisms.

Uncovering the mechanisms of the outbreak and aggregation of DCO is crucial to developing effective prevention and control strategies. Bacteria communities are essential in the marine ecosystem since they contribute to biochemical reactions and are involved in the chemical transformations of virtually all elements. Shi et al. investigated the community profiles of bacterioplankton, particle-attached bacteria, and colony-attached bacteria during a *Phaeocystis globosa* bloom. The results showed that the diversity of bacterioplankton and particle-attached bacteria communities significantly decreased as the bloom progressed from the exponential to the decline phase. In the decline phase of the bloom, Bacteroidota and Verrucomicrobiota were found to be the dominant and highly abundant bacteria in the bacterioplankton community, while Verrucomicrobiota dominated the particle-attached bacteria community. Large jellyfish constitute the main groups of DCO. The researchers analyzed the aggregation processes and interactions of two scyphozoan jellyfish species, *Nemopilema nomurai* and *Aurelia coerulea*, in the intake area of NPP in Eastern Liaodong Bay (China). They observed a rapid increase in the individual growth and relative biomass (RB) of the jellyfish from late June to July, followed by a rapid decrease thereafter. The RB of *N. nomurai* was found to be positively correlated with sea surface temperature (SST) and negatively correlated with levels of dissolved oxygen (DO) in the region. As SST increased, RB also increased, but it decreased with increasing DO levels. On the other hand, the RB of *A. coerulea* was negatively correlated with that of *N. nomurai*, and the two species showed alternating peaks of biomass over time. This pattern may be due to the fact that the two jellyfish species occupy similar ecological niches.

Early-warning monitoring systems are also essential in preventing and controlling outbreaks of DCO. Several studies have explored different approaches to monitor and predict the abundance and movements of DCO. For instance, Li et al. applied a three-dimensional numerical current–wave-coupled model to simulate the causes of blocking events near the Changjiang NPP, highlighting the windage effect and surface Stokes drift induced by waves as the primary causes. Lou et al. utilized the Lagrangian flow network (LFN) to map the transport pathways and aggregation areas of *Acetes*. Huo et al. developed a deep learning algorithm to predict the biomass of DCO, while Li et al. employed a seafloor *in situ* integrated monitoring system (IMSDCO) equipped with optical microscopic imagers and hydrometric sensors to automate the monitoring process. Fu et al. created a 3-dimensional numerical model (TELEMAC-3D) to determine the impingement probability of DCO under various environmental conditions.

In summary, the proliferation of organisms in nuclear power plant cooling-water systems is a serious issue that poses risks to both the safety of the plants and the health of marine ecosystems. However, by enhancing our understanding of these organisms, developing monitoring systems, and implementing prevention and control measures, we can ensure the safety and reliability of nuclear power while also protecting marine ecosystems. This is crucial not only for environmental conservation, but also for

sustaining human life and ensuring long-term sustainability. Looking forward, continued research and innovation in this area will be essential for addressing the challenges posed by DCO in cooling-water systems. Additionally, increasing public awareness of these issues can help encourage greater investment in research and development, as well as the implementation of effective prevention and control measures. Ultimately, by working together to address these challenges, we can ensure the safe and reliable operation of nuclear power plants while also protecting the health and diversity of marine ecosystems for future generations.

Author contributions

HH wrote the manuscript of the Editorial, the other guest editors of the Research Topic reviewed and revised the manuscript. All authors contributed to the article and approved the submitted version.

Funding

We gratefully acknowledge the National Key Research and Development Program of China (2018YFC1407501), the Central Public-interest Scientific Institution Basal Research Fund, CAFS (NO.2020TD15), the Central Public-interest Scientific Institution Basal Research Fund South China Sea Fisheries Research Institute, CAFS (2021SD03).

Acknowledgments

We would like to thank the editors of Frontiers in Marine Science for their support on the Research Topic. We appreciate all the reviewers, who have paid their time and expertise on the articles. We thank the authors, who are willing to submit and publish their manuscript in the Research Topic.

Conflict of interest

The authors declare that the research was conducted in the absence of any commercial or financial relationships that could be construed as a potential conflict of interest.

Publisher's note

References

Beninca, E., Dakos, V., Van Nes, E. H., Huisman, J., Scheffer, M., et al. (2011). Resonance of plankton communities with temperature fluctuations. *Am. Nat.* 178 (4), E85–E95. doi: 10.1086/661902

Borja, A., Elliott, M., Andersen, J. H., Berg, M., Carstensen, J., Halpern, B. S., et al. (2016). Overview of integrative assessment of marine systems: the ecosystem approach in practice. *Front. Mar. Sci.* 20. doi: 10.3389/fmars.2016.00020

Chust, G., González, M., Fontán, A., Revilla, M., Alvarez, P., Santos, M., et al. (2022). Climate regime shifts and biodiversity redistribution in the bay of Biscay. *Sci. Total Environ.* 803, 149622. doi: 10.1016/j.scitotenv.2021.149622

Gobler, C. J. (2020). Climate change and harmful algal blooms: insights and perspective. *Harmful algae* 91, 101731. doi: 10.1016/j.hal.2019.101731

Khttab, K. (2021). Nuclear power reactors in the world. *Atom Dev.* 33 (2), 43–55. https://www.iaea.org/publications/14989/nuclear-power-reactors-in-the-world

Lucas, C. H., Gelcich, S., and Uye, S. I. (2014). Living with Jellyfish: Management and Adaptation Strategies. In: Pitt, K., Lucas, C. (eds) Jellyfish Blooms. (Dordrecht: Springer). doi: 10.1007/978-94-007-7015-7_6

Prakash, S. (2021). Impact of climate change on aquatic ecosystem and its biodiversity: an overview. *Int. J. Biol. Innov.* 3 (2), 312–317. doi: 10.46505/IJBI.2021.3210

Wollrab, S., Izmest'yeva, L., Hampton, S. E., Silow, E. A., Litchman, E., Klausmeier, C. A., et al. (2021). Climate change–driven regime shifts in a planktonic food web. *Am. Nat.* 197 (3), 281–295. doi: 10.1086/712813

Wu, J., Kong, J., Laws, E. A., Liu, X., Wang, C., Chen, J., et al. (2023). The link between marine thermal discharges and nemopilema nomurai blooms around nuclear power plants. *Ecosystem Health Sustainability* 9, 0009. doi: 10.34133/ehs.0009

frontiers | Frontiers in Marine Science

TYPE Brief Research Report
PUBLISHED 07 October 2022
DOI 10.3389/fmars.2022.1006551

OPEN ACCESS

EDITED BY
Kaizhi Li,
South China Sea Institute of Oceanology (CAS), China

REVIEWED BY
Zeng Jiangning,
Ministry of Natural Resources, China
Yang-Guang Gu,
South China Sea Fisheries Research Institute (CAFS), China

*CORRESPONDENCE
Sher Khan Panhwar
sk.panhwar@uok.edu.pk

SPECIALTY SECTION
This article was submitted to Marine Pollution, a section of the journal Frontiers in Marine Science

RECEIVED 29 July 2022
ACCEPTED 16 September 2022
PUBLISHED 07 October 2022

CITATION
Shaikh W, Panhwar SK and Yaqoob N (2022) Thermal tolerance and critical maxima examined in marine gastropods inhabiting around Karachi Nuclear Power Plant.
Front. Mar. Sci. 9:1006551.
doi: 10.3389/fmars.2022.1006551

Thermal tolerance and critical maxima examined in marine gastropods inhabiting around Karachi Nuclear Power Plant

Wajiha Shaikh[1], Sher Khan Panhwar[1]* and Nadeem Yaqoob[2]

[1]Centre of Excellence in Marine Biology, University of Karachi, Karachi, Pakistan, [2]Pakistan Isotope Application Division, PINSTECH, Islamabad, Pakistan

Bensthic communities along the coastal basins are an indication of ecosystem health but highly susceptible owing to manmade activities. This study envisages thermal tolerance in sea snails *Monodonta canalifera*, *Nerita albicilla* and *Tylothais savignyi* inhabiting around the outfall and intake structures of Karachi Nuclear Power Plant (KANUPP). To test the adaptability and vulnerability, a lethality test protocol under controlled temperature was applied in the laboratory where they were exposed at 25, 30, 35, and 40°C, which was raised to 45°C after an acclimation period of 1 week. The critical thermal maximum (CT_{max}) for the three species was found to be between 39 and 42°C, whereas the lethal temperature (LT_{50}) tests revealed that at the utmost 45°C was lethal for *M. canalifera*. The correlation between LT_{50} and CT_{maxima} (R = 0.47, p = 0.00) and LT_{50} and body sizes reveals that the thermal adaptability in *N. albicilla* and *T. savignyi* (R = 0.65, p = 0.00) was relatively higher than that at 45°C given in the laboratory. In addition, microscopic changes due to temperature, which appeared in the foot (adhesive part) of each species, were deduced from the histological examination. The outcomes of this study would help to underline the ecosystem health around KANUPP and highlight precautionary measures required for the newly established K2/K3 power units to safeguard habitat.

KEYWORDS

sea snails, thermal tolerance, foot histology, outfall structure, nuclear power units Karachi

Introduction

The Karachi Nuclear Power Plant (KANUPP) was established a semicentury back, with a capacity of 137 MWe energy generated using 140 tonnes of seawater per hour for the cooling system. A constant increase of energy demand in the Karachi metropolis was overwhelming and thus led to the establishment of K2/K3 power units with a capability of

2,200 KWe to satisfy the power needs. Therefore, seawater intake for cooling purposes and use in power generation has significantly soared. This mass-level water consumption is expected to bring some changes in water temperature and can harm the aquatic ecosystem. However, it would be better to provide energy to the public with the sustainable use of coastal resources. Here we provide data on how an increase in temperature can harm sessile organisms in natural environment and on using indoor experimental practices. It is commonly concurred that the world's ocean and air temperatures have warmed by 0.6°C in the early 21st century and now reached 2.0–4.5°C (IPCC, 2007). The Arabian Sea deep water temperature rose by 0.65°C and that of coastal waters by 0.86°C; therefore, a low warming tendency persists (Rana et al., 2014). Tropical countries can contribute 6–10°C by means of cooling systems (Poornima et al., 2006), and this is 8–12°C in temperate areas (Hoffmeyer et al., 2005). It is estimated that high-capacity power plants of about 1,000 MWe would need more water, and this water, when released back into the sea, would surely create pollution and harm fish stocks. Thus, temperature is a significant abiotic factor in marine environments (Webb et al., 2008), driving other important changes at the community level by affecting organisms and their distributions, species composition as well as the entire ecosystem (Dallas, 2012). Fluctuations in temperature may alter its physiological functions such as growth rate (Vannote and Sweeney, 1980; Farooq et al., 2017), feeding rate (Kishi et al., 2005), metabolic rate (Eriksen, 1964; Brockington and Clarke, 2001; Ganser et al., 2015), fecundity (Byrne and Przeslawski, 2013), larval dispersal (O'Connor et al., 2007), reproduction (Tropea et al., 2015), immunity (Green et al., 2014), emergence (McKie et al., 2004), behavior (Mora and Ospina, 2001), and, ultimately, survival (Mairaj et al., 2021).

Intertidal ecological systems have been portrayed as "harbingers of fate" (Helmuth, 2002) or "early indicators" (Wethey and Woodin, 2008) for environmental impacts interceded by environmental changes. These types of systems are contrastingly not the same as most tropical conditions since they show massive thermal changes with time and area, with a large portion of the variety happening day by day and between tidal cycles (Helmuth et al., 2002). Thermal range fluctuates broadly among species. Many life forms can endure harsh temperatures in a short time by changing their physical systems under thermal pressure (Jiang et al., 2008). The thermal resistances of organisms are because of long-term natural selection and evolution under ecological systems, and organisms that adjust to elevated temperatures, which is referred to as thermal resilience, are better compared to the ones that desire decreased temperatures (Pörtner, 2001). The rocky intertidal zones are considered as physically complex and variable coastal environments on earth; therefore, thermal effluents are problematic primarily for benthic organisms (Warwick, 1993). Huge numbers of benthic species are sessile or stationary, and even numerous errant species move less throughout their lifetime—so they are defenseless against thermal discharge—since they have a restricted capacity to get away (Bamber and Spencer, 1984). Mollusks are the most important members of the benthic community in rocky intertidal zones. The capability of intertidal mollusk to endure high temperatures is identified with their location in the intertidal zone and their geological dispersal (Markel, 1971).

Upon exposure to heat, marine snails normally undergo a reversible condition of unconsciousness. This abstraction includes foot detachment from the substratum and becoming unsteady, with the foot expansion studied (Sandison, 1967; Fraenkel, 1968). Moreover, the response to thermal stress among various aquatic macroinvertebrates differs among taxa. Some common behavioral responses are loss of grip, which results in detachment from a substrate or rapid movement, ultimately proceeding to immobility and becoming irresponsive when stimulated with a jet of water (Dallas and Ketley, 2011). A microscopic study of snail foot can show the robust cellular deformation due to excessive temperatures (Pavlasek, 1950). In addition, the main part of the snail's body is the muscular foot, which is well known for slime that secretes visco-elastic mucus gels and that functions to include feeding, protection, reproduction, locomotion, lubrication, defense, and adhesion (Pavlasek, 1950). Increasing the exposure temperature (48, 50, and 52°C) can increase the mucus secretion with enlargement and necrosis of mucocytes (Dittbrenner et al., 2009).

The basic ideas are as follows: (1) to determine the adaptability and vulnerability of sea snails *Nerita albicella*, *Monodonta canalifera*, and *Tylothais savignyi* dwelling around the intake and outfall structures of Karachi Nuclear Power Plant to demonstrate thermal acclimation and their tolerance to maximum temperatures, (2) to examine LT_{50} depending on size and age, and (3) to provide microscopic changes in the foot due to temperature under controlled conditions.

Materials and methods

Collection of test organisms

The test organisms *M. canalifera* (Lamarck, 1816), *N. albicella* (Linnaeus, 1758), and *T. savignyi* (Deshayes, 1844) were collected from the intake and outfall structures of Karachi Nuclear Power Plant near Paradise Point, Karachi, in October 2017. The specimens were hand-picked or dislodged from rock boulders by adopting random sampling method.

In situ temperature

Seawater temperature of each location was recorded by using hydro-lab (HL-4) USA. The *in situ* water temperature at the outfall was recorded as 24–31°C, with 28°C representing an intermediate

value, whereas an average temperature (24 to 25°C) was recorded from the intake structures during the sampling period.

Field observations, handling, and experiment procedures

Prior to placing the specimens in buckets, a few moments were spent to look into the behavior of sea snails in the natural ecosystem. In the laboratory prior temperature tests, the organisms were acclimatized at 25°C and maintained for 1 week before the experiments commenced. Later on, the snails were transferred into an already adjusted glass aquarium of dimension 44 × 30 × 31 cm (length × width × depth), each trial of both tests (CT_{max} and LT_{50}) lost water through evaporation and was thus added with seawater to maintain the water level. A steady adjustment of temperature was made using a thermostat, keeping in mind the photoperiod time 16:08 LD. The circulating pump ensured that the percentage saturation of dissolved oxygen remained above 70% during the experiments so that the tanks were well aerated using compressed air passed through multiple airstones.

Critical thermal maxima (CT_{max}) test

Thirty individuals of each species were used to test CT_{max} following their random selection and transfer into aquariums for exposure. Two replicates of each exercise were adopted. During the test phase, the water temperature was allowed to stabilize at 25°C for 30 min after it was raised at 1 to 2 min manually with an aquarium heater/thermostat until the individuals were in a state of heat coma. Simultaneously, snail reaction to heating was observed continuously, where critical thermal endpoint was recorded for each species.

Lethal temperature (LT_{50}) test

The lethality test was deduced from 10 individuals of each species which were allowed to adjust in separate experimental aquariums at constant temperatures, *i.e.*, 25, 30, 35, 40, and 45°C, whereas 25°C was set for the control. Four treatments at 30, 35, 40, and 45°C with each of the replicates—thus a total of n = 300 individuals—were used. The test groups were heated for 4 days subsequently until the target temperature was reached. Constant behavioral adaptations for survival were recorded every 24 h.

Behavioral changes

Data on those organisms were included in the results, which were recovered from the critical thermal maxima test, whereas dead organisms at lethal temperature were separated immediately. The shell identification, photograph, lengths, and weights data were recorded for each individual. For the histological examination of the foot, each dead snail was fixed in Davidson fixative for 48 h. After that, the materials were dehydrated at increasing ethanol concentrations and then embedded in paraffin. The wax blocks were sectioned at 4 µm, using a microtome with tungsten knives, and stained with hematoxylin–eosin. The permanent slides were prepared and archived.

Statistical analysis

All statistical analyses were made using R software. Kruskal–Wallis one-way ANOVA and LSD (0.05) multiple comparisons were tested for CT_{max}. The calculations were made following the expression used (Diaz et al., 2011). The trimmed Spearman–Karber test (95% CI) was applied on the data of LT_{50} using 24-, 48-, 72-, and 96-h data. A linear model was applied on the snail body sizes against treatment temperature.

Results

Critical thermal maxima (CT_{max})

Evaluation of thermal tolerance in *M. canalifera* (CT_{max} 40.50 ± 0.28 SE), *N. albicilla* (CT_{max} 39.33 ± 0.17 SE), and *T. savignyi* (CT_{max} 42.17 ± 0.17 SE) was undertaken in this study. It was revealed that each species displays a critical behavior against different temperatures (Figure 1). This was validated by Kruskal–Wallis one-way analysis of variance and the mean ranks of CT_{max}. These values were significantly different among the three test species and significant at p = 0.05. All species showed a common behavioral response to elevated temperature. These values were observed when the test species became unresponsive to touch and showed detachment from the wall and base of the tanks.

Lethal temperature (LT_{50} test)

In the laboratory, aquariums were set up (control = 24.9 ± 0.48, T^1 = 30.6 ± 1.28, T^2 = 35.3 ± 0.93,T^3 = 40.3 ± 0.72, T^4 = 44.5 ± 0.57), and all species were kept for 96 h, whereas LT_{50} and 95% confidence limits were estimated through trimmed Spearman–Karber analysis which showed that the thermal tolerance of *N. albicella* and *T. savignyi* increases significantly with increasing exposure duration. In the case of *M. canalifera*, the thermal tolerance inversely decreases with increasing exposure within 72 h (Figure 2). Linear regression was applied to test the relationship between body size and lethal temperature applied on

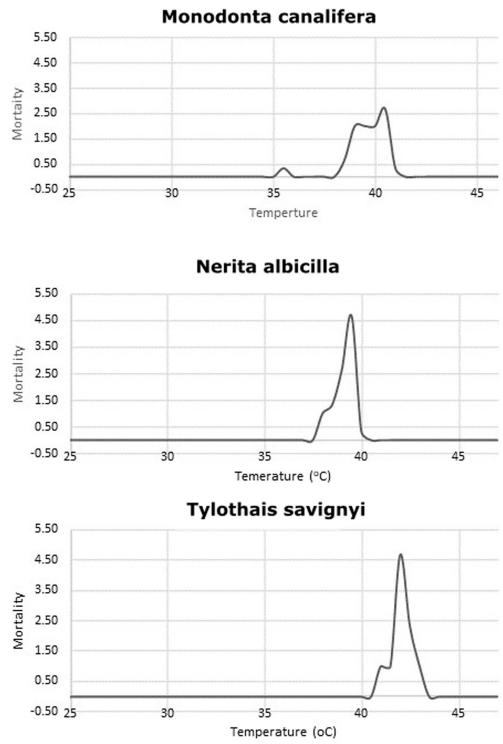

FIGURE 1
CT_{max} rise of temperature to determine the maximum critical temperature where the activities of organisms stop.

three species of gastropods; it shows an inverse relationship between LT_{50} and body size (Figure 3). Linearity between lethal temperatures and median critical thermal maxima was calculated as $R^2 = 0.47$, which defines a variation in CT_{max} to validate the efficacy of short-term estimates so as to predict long-term variation (Figure 4). The survival number of three gastropod species within 96 h of LT_{50} test indicates that the majority of individuals of *N. albicella* and *T. savignyi* endured various temperatures for up to 96 h, thus indicating their higher tolerance to elevated temperatures. However, individuals of *M.*

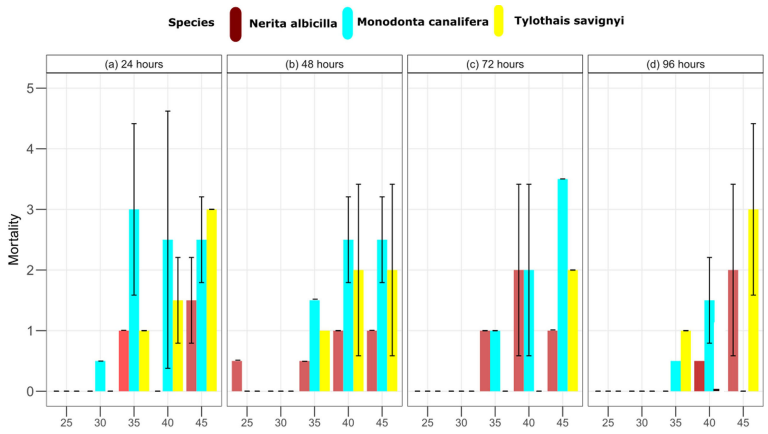

FIGURE 2
LT_{50} at constant temperatures of 25, 30, 35, 40, and 45°C at 24-, 48-, 72-, and 96-h duration.

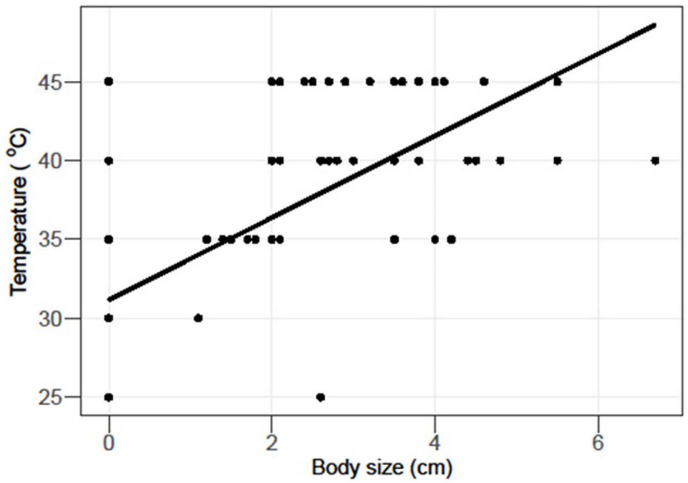

FIGURE 3
Linear regression applied to test LT_{50} and body sizes of *Nerita albicilla, Tylothias savignyi* and *Monodonta canalifera*. The coefficient of correlation (*R*) shows inverse relation between LT_{50} and body sizes.

canalifera survived with the lowest number at 96 h, indicating their sensitivity to warm water (Figure 5).

Histopathological alterations in the foot

The foot tissue of control snails mainly contained columnar muscle cells, mucocytes, and normal epithelium. No histological alteration in the foot of three gastropod species was observed at 25°C (control) and 30°C (treatment I) (Figures 6A, B). These changes occurred at an exposure temperature of 35°C (treatment II) and became more adverse at exposure temperatures of 40°C (treatment III) and 45°C (treatment IV). The most conspicuous effects were observed in treatments II, III, and IV as deduced from a microscopic examination of the foot. When the temperature reached 40°C, the epithelium (outer covering) started rupturing, and the microvilli started to be denatured with deranged cilia. A further increase in temperature at 45°C

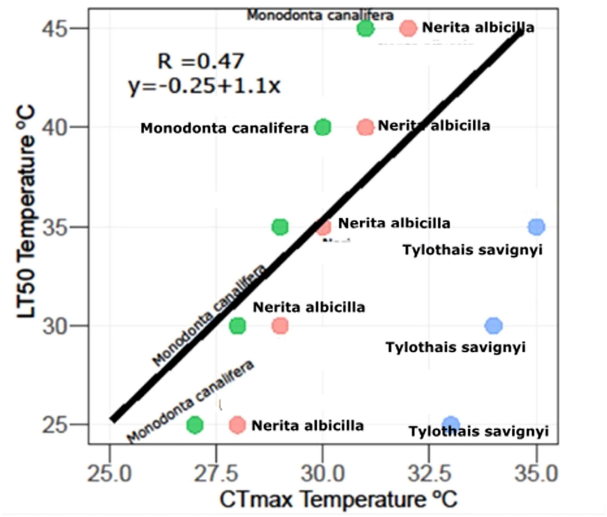

FIGURE 4
Relationship between L_{50} and CTmaxima statistically tested in three snails presented in this study.

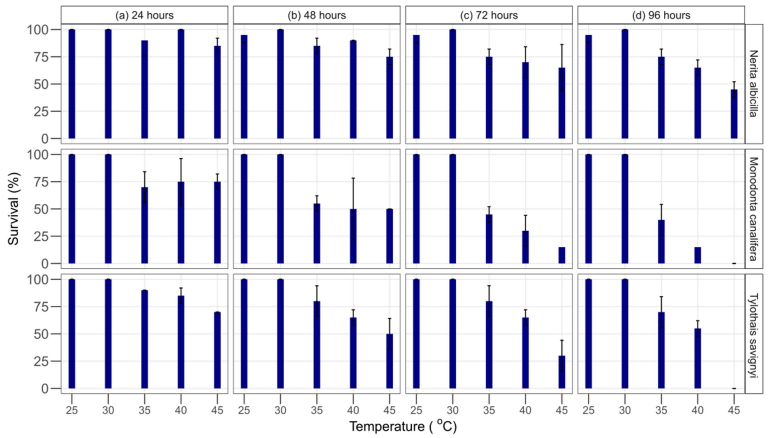

FIGURE 5
Survival % of *Monodonta canalifera, Nerita albicilla*, and *Tylothias savignyi* at constant temperatures of 25, 30, 35, 40, and 45°C at duration **(A)** 24 hours, **(B)** 48 hours, **(C)** 72 hours, **(D)** 96 hours.

resulted in eroded epithelium and scattered and deranged cilia with deformed microvilli. The eroded epithelium, disruption of columnar muscle fibers with gap between the cells, and empty and shrunken mucocytes can be seen (Figures 6C, D). The eroded epithelium and cilia (ci) formed spaces and gaps between the muscle fibers and deformed microvilli (Figure 6E). Comparison and validation of the cellular structure of the normal foot of organisms sampled from the

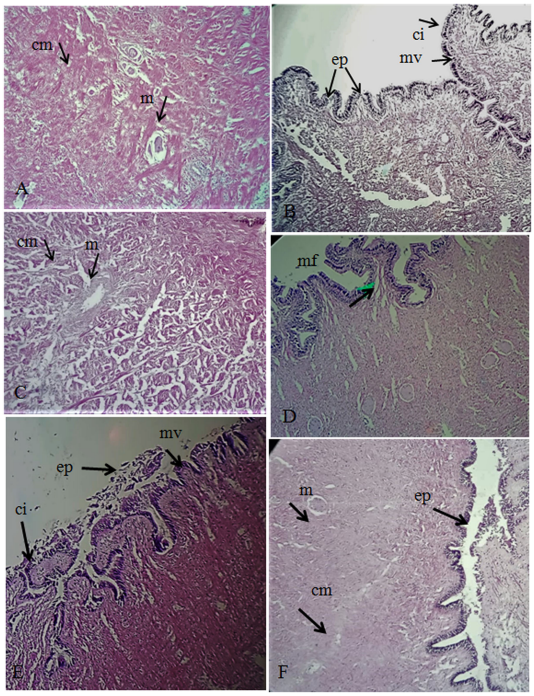

FIGURE 6
(A) Foot tissue (TS) of control snail showing normal columnar muscle cells (cm) and mucocytes (m). **(B)** Foot TS of control snail showing normal epithelium. **(C)** Foot TS of exposed snails showing emptied and shrinkage mucocytes (m) and deranged columnar muscle fibers (cm) with increased spaces in between them (arrow). **(D)** The epithelium (ep) was partially damaged, and the microvilli (mv) started to denature with deranged cilia. **(E)** The ep was eroded and the cilia (ci) scattered and deranged with deforming microvilli (mv). **(F)** Normal foot TS of snail from the intake structure of KANUPP, showing normal epithelium (ep), microvilli (mv), and columnar muscle fibers (cm).

intake and those taken from the treatments were conducted in the laboratory (Figure 6F).

Discussion

This study unveils temperature tolerance in sea snails inhabiting around Karachi Nuclear Power Units and the utmost level where they can survive, are vulnerable, or die in natural and captive environments. Three commonly occurring species showed a variable level of tolerance—for example, *N. albicella* and *T. savignyi* had a higher range of temperature, whereas *M. canalifera* was relatively much sensitive to the temperature. Moreover, it is obvious that coastal degradation can worsen with the increase in temperature by power units or other industrial units on the sea basin, which can cause damage to coastal ecosystems and make sessile organisms vulnerable around the outfall of the power plant. It is assumed that temperature is one of the major ecological factors since it influences the living region (Pörtner, 2001). Increased seawater temperature and its effects on marine biota have already gained a lot of attention and have become a notable issue when developing or planning a coastal power plant unit. Therefore, experiments on the capability of aquatic organisms, especially benthic species, are necessary to check their tolerance to elevated temperature in relation to their long-term management. CTM has proven to be a simple approach for assessing aquatic macro-invertebrates to the upper thermal limits because it requires minimum collection and experimental effort. The LT_{50} trials, on the other hand, took longer and required a larger number of test organisms to get consistent and reliable results. Its calculation also gives a longer-term understanding of the impact of increased water temperatures on the survival of aquatic macro-invertebrates (Dallas and Ketley, 2011). Therefore, in this study, we examined three different benthic species inhabiting near the intake and outfall of KNPC with both test CT_{max} and LT_{50} in order to check whether the occasionally released warm water from the outfall have some impacts on benthic organisms upon shorter and longer thermal exposure. Hence, the experiment revealed clear intraspecific differences among all three species: *M. canalifera* was the most thermally sensitive because its LT_{50} values progressively increased with time. Its mean thermal tolerance declined with time, in contrast to *N. albicilla* and *Tylothias savignyi*. Their LT_{50} values progressively decreased with time. These species are not sensitive to slowly change relative to the water temperature and are able to adopt to temperature changes with time. Our behavioral observation revealed that *M. canalifera* showed an adverse reaction upon continuous heating by losing its operculum. However, *N. albicella* and *T. savignyi* also showed an instantaneous reaction to heating by detachment from the base and walls of the aquarium and also displayed foot expansion. The CT_{max} results show the lowest thermal tolerance of *Nerita albicella* in comparison to *M. canalifera* and *T. savignyi*. In contrast to the 96-h temperature exposure, we can say that *N. albicella* has a lower ability to recover from temporary thermal induction, as its behavior in rapid temperature change showed unconsciousness, although soon after the end of the experiment, it was back to its normal state and started to attach to the wall of the aquarium. Hence, it is assumed that the difference of the results in both tests is due to exposure period. Further studies are still needed on the time limitation of thermal limits for different gastropods if we wish to assess the impact of extreme events (*e.g.*, heat exposure) on different populations. The correlation of the LT_{50} data with the CT_{max} in Figure 4 indicates that temperature stress may be important in determining the distributions of several of the species investigated (Figure 2). In particular, the maximum recorded temperatures exceeded the 96-h LT_{50} values of *M. canalifera*. High temperature is more likely to be an important factor limiting lotic invertebrates in the water body near KANUPP. The behavioral observation during the overall experiment depicted snails as susceptible to drying up during action rather than pulling back into their shell and staying idle at high and possibly distressing surrounding temperatures. Subsequently, they can endure a critical range of temperatures when inactive (Marshall and McQuaid, 2011; Marshall et al., 2011), but it may lead to predation and limiting their distribution in the wild, ultimately threatening their life. The analysis of histopathological alteration offers information about the general health status of this species because it reflects cellular and subcellular morphological changes. There is evidence that thermal induction causes histological alteration in the foot of the tested snails. The atrophic tubules were rarely observed in lower temperature exposures, *i.e.*, 25–30°C; however, atrophy gradually increased, even showing necrosis after higher thermal exposures at 35, 40, and 45°C. These alterations affect the mucus-secreting cells, leading to loss of mobility. On further exposure, a final consequence of this impairment is leading the snail to death. Generally, both the release of mucus and the hypertrophy of mucus cells seem to be involved in the adaptation of snails to extreme temperatures.

Various examinations on temperature influence due to coastal power plants have been recorded, such as Branett in 1972 who carried out studies on the outfall area of Hunterston Power Plant and suggested that the gastropods' growth is disturbed and that spawning time was advanced by 3 months as the water temperature is raised. Other investigations found that the majority of benthic organisms, including gastropods, were affected due to the high temperature near the outfall region of Brazil Nuclear Power Plant (Teixeira et al., 2012). Among gastropods, we found that most studies about thermal tolerance have been carried out with *Nerita* spp. The lethal temperature of *N. albicilla* is described to be at 50°C, with severe effects on

enzymatic activity that ultimately results in loss of activity (Dong et al., 2018). Another research about the episodic exposure to extreme temperature for *N. albicilla* is described at 39.6°C (Waltham and Sheaves, 2020). The thermoregulation of *Nerita atramentosa* was also tested, and it describes the endpoint as 45°C (Caddy-Retalic et al., 2011). Hence, the mortality or disappearance of gastropods may occur if the temperature increments were beyond their adaptive ranges.

Conclusion

This study increases our understanding on how sessile organisms can recover from sudden heat shocks and that they already have the ability to cope with shorter thermal exposures but cannot survive longer thermal induction even for a few days. Besides this, thermal exposure is independent of the size of the organism that is vulnerable either to shorter or larger or to constant thermal exposure which may lead to death. Hence, it is clear that constant increases in water temperature caused by the outfall structure of the power plant can be lethal to slow-moving organisms. The LT_{50} and CT_{max} test demonstrate that the temperature tolerance in two species remained at around 45°C for *N. albicilla* and *T. savignyi*, whereas *M. canalifera* can endure >45°C on constant exposure that may lead to an assumption of whether populations can possibly increase or become extinct. Moreover, the histological study of the foot demonstrates cellular atrophy and necrosis in the three species of sea snail.

Data availability statement

The raw data supporting the conclusions of this article will be made available by the authors without undue reservation.

Author contributions

WS conducted the field and laboratory exercises. SKP designed and supervised research, and finalized the manuscript. NY helped in improving the quality of the manuscript. All authors contributed to the article and approved the submitted version.

Acknowledgments

This research work was financially supported by PAEC/PMDC-West projects and a part of the PhD dissertation of WS. This part of research is dedicated to late Dr. Azhar Mashiatullah, Ex-Head, Isotope Division, PINSTECH-Islamabad, for his encouragements, affection, and care that will always be kept in our hearts: “love you, Sir”.

Conflict of interest

The authors declare that the research was conducted in the absence of any commercial or financial relationships that could be construed as a potential conflict of interest.

Publisher’s note

References

Bamber, R. N., and Spencer, J. F. (1984). The benthos of a coastal power station thermal discharge canal. *J. Mar. Biol. Assoc. United Kingdom.* 64 (3), 603–623. doi: 10.1017/S0025315400030290

Brockington, S., and Clarke, A. (2001). The relative influuence of temperature and food on the metabolism of a marine invertebrates. *J. Exp. Mar. Biol. Ecol.* 258, 87–99. doi: 10.1016/S0022-0981(00)00347-6

Byrne, M., and Przeslawski, R. (2013). Multistressor impacts of warming and acidification of the ocean on marine invertebrates. *Life histories Integr. Comp. Biol.* 53 (3), 582–596. doi: 10.1093/icb/ict049

Caddy-Retalic, S., Benkendorff1, K., and Fairweather, P. G. (2011). Visualizing hotspots: applying thermal imaging to monitor internal temperatures in intertidal gastropods. *Molluscan Res.* 31 (2), 106–113. ISSN 1323-5818.

Dallas, H. F., and Ketley, Z. A. (2011). Upper thermal limits of aquatic macroinvertebrates: Comparing critical thermal maxima with 96-LT50 values. *J. Thermal Biol.* 36 (6), 322–327. doi: 10.1007/s10750-011-0856-4

Dallas, H. F., and Rivers Moore, N. A. (2012). Critical thermal maxima of aquatic macroinvertebrates: towards identifying bioindicators of thermal alteration. *Hydrobiologia.* 679 (1), 61–76. doi: 10.1007/s10750-011-0856-4

Deshayes, G. P., and Milne-Edwards, H. (1844). Histoire naturelle des animaux sans vertèbres présentant les caractères généraux et particuliers de ces animaux leur distribution leurs classes leurs familles leurs genres et la citation des principales espèces qui s'y rapportent, par J. B. P. A. de Lamarck. *Deuxième* édition, *Tome dixième. Histoire des Mollusques*. J. B. Baillière: Paris. 638 pp. Available at: http://www.biodiversitylibrary.org/item/64020

Diaz, F., Salas, A., Re, A. D., Gonzalez, M., and Reyes, I. (2011). Thermal preference and tolerance of Megastrea (Lithopoma) undosa (Wood 1828; Gastropoda: turbinidae). *J. Thermal Biol.* 36 (1), 34–37. doi: 10.1016/j.jtherbio.2010.10.004

Dittbrenner, N., Lazzara, R., Köhler, H. R., Mazzia, C., Capowiez, Y., and Triebskorn, R. (2009). Heat tolerance in Mediterranean land snails: histopathology after exposure to different temperature regimes. *J. Molluscan Stud.* 75 (1), 9–18. doi: 10.1093/mollus/eyn033

Dong, Y. W., Liao, M. L., Meng, X. L., and Somero, G. N. (2018). Structural flexibility and protein adaptation to temperature: Molecular dynamics analysis of malate dehydrogenases of marine molluscs. *Proc. Natl. Acad. Sci.* 115 (6), 1274–1279. doi: 10.1073/pnas.1718910115

Eriksen, C. (1964). Evidence of a spring rise in metabolic rate in the burrowing mayfluy ephemera simulans walker. *Hydrobiologia.* 23, 506–510. doi: 10.1073/pnas.1718910115

Farooq, N., Qamar, N., and Panhwar, S. K. (2017). Characterization of feeding habits, prey diversity and diet overlap of two sympatric species: Bronze catfish, Netuma bilineata (Valenciennes 1840) and blacktip sea catfish, Plicofollis dussumieri (Valenciennes 1840) in the northern Arabian Sea. *J. Appl. Ichthyology.* 33, 709–719. doi: 10.1111/jai.13377

Fraenkel, G. S. (1968). The heat resistance of intertidal snails at bimini, bahamas; ocean springs, mississippi; and woods hole, Massachusetts. *Physiol. Zoology.* 41, 1–13. doi: 10.1086/physzool.41.1.30158481

Ganser, A. M., Newton, T. J., and Haro, R. J. (2015). Efects of elevated water temperature on physiological responses in adult freshwater mussels. *Freshw. Biol.* 60, 1705–1716. doi: 10.1111/fwb.12603

Green, T. J., Montagnani, C., Benkendor, K., and Robinson, N. (2014). Ontogeny and water temperature influuences the antiviral response of the pacific oyster, crassostrea gigas. *Fish Shellfish Immunol.* 36 (1), 151–157. doi: 10.1016/j.fsi.2013.10.026

Helmuth, B. (2002). How do we measure the environment? linking intertidal thermal physiology and ecology through biophysics. *Integr. Comp. Biol.* 42 (4), 837–845. doi: 10.1093/icb/42.4.837

Helmuth, B., Harley, C. D., Halpin, P. M., O'Donnell, M., Hofmann, G. E., and Blanchette, C. A. (2002). Climate change and latitudinal patterns of intertidal thermal stress. *Science.* 298 (5595), 1015–1017. doi: 10.1126/science.1076814

Hoffmeyer, M. S., Biancalana, F., and Berasategui, A. (2005). Impact of a power plant cooling system on copepod and meroplankton survival (Bahía blanca estuary, Argentina). *Iheringia Série Zoologia.* 95 (3), 311–318. doi: 10.1590/S0073-47212005000300011

IPCC (2007). "Climate change: the physical science basis. contribution of working group I to the fourth assessment," in *Report of the intergovernmental panel on climate change*. Eds. S. Solomon, D. Qin, M. Manning, Z. Chen, M. Marquis, K. B. Averyt, M. Tignor and H. I. Miller (Cambridge, United Kingdom and New York, NY, USA: Cambridge University Press), 996.

Jiang, Z., Zeng, J., Chen, Q., Huang, Y., Xu, X., Liao, Y., et al. (2008). Tolerance of copepods to short-term thermal stress caused by coastal power stations. *J. Thermal Biol.* 33 (7), 419–423. doi: 10.1016/j.jtherbio.2008.06.008

Kishi, D., Murakami, M., Nakano, S., and Maekawa, K. (2005). Water temperature determines strength of top down control in a stream food web. *Freshw. Biol.* 50 (8), 1315–1322. doi: 10.1111/j.1365-2427.2005.01404

Lamarck, J. B. (1816). Liste des objets représentés dans les planches de cette livraison. In: Tableau encyclopédique et méthodique des trois règnes de la Nature. Mollusques et Polypes divers. Agasse, Paris. 16 pp.

Linnaeus, C. (1758). Systema Naturae per regna tria naturae, secundum classes, ordines, genera, species, cum characteribus, differentiis, synonymis, locis. Editio decima, reformata [*10th* revised edition], vol. 1:824 pp. Laurentius Salvius: Holmiae. Available at: https://biodiversitylibrary.org/page/726886

Mairaj, M., Panhwar, S. K., Qamar, N., and Rashid, S. (2021). Indus river estuary: an assessment of potential risk of contaminants and ecosystem susceptibility. *SN Appl. Science.* 3, 730. doi: 10.1007/s42452-021-04721-2

Markel, R. P. (1971). Temperature relations in two species of tropical western American littorines. *Ecology.* 52 (6), 1126–1130. doi: 10.2307/1933823

Marshall, D. J., Dong, Y. W., McQuaid, C. D., and Williams, G. A. (2011). Thermal adaptation in intertidal snail echinolittorina malaccana contradicts current theory by revealing the crucial roles of resting metabolism. *J. Exp. Biol.* 214 (27), 3649–3657. doi: 10.1242/jeb.059899

Mckie, B.,. G., Cranston, P. S., and Pearson, R. G. (2004). Gondwanan mesotherms and cosmopolitan eurytherms: Effects of temperature on the development and survival of Australian chironomidae (Diptera) from tropical and temperate populations. *Mar. Freshw. Res.* 55 (8), 759–767. doi: 10.1071/MF04023

Mora, C., and Ospina, A. (2001). Tolerance to high temperatures and potential impact of sea warming on reef fishes of gorgona island (tropical eastern pacific). *Mar. Biol.* 139 (4), 765–769. doi: 10.1007/s002270100626

O'Connor, M. I., Bruno, J. F., Gaines, S. D., Halpern, B. S., Lester, S. E., and Kinlan, B. P. (2007). Temperature control of larval dispersal and the implications for marine ecology, evolution, and conservation. *Proc. Natl. Acad. Sci. U.S.A.* 104 (4), 1266–1271. doi: 10.1073/pnas.0603422104

Pavlasek, J. (1950). Morfologie a biologie hlemyzde zahradniho (Helix pomatia L.) vzhledem k potravinarstvi. *Disertacni prace, VSV Brno*, 120s.

Poornima, E. H., Rajaduraia, M., Rao, V. N. R., Narasimhan, S. V., and Venugopalan, V. P. (2006). Use of coastal waters as condenser coolant in electric power plants: Impaction on phytoplankton and primary productivity. *J. Thermal Biol.* 31 (7), 556–564. doi: 10.1016/j.jtherbio.2006.05.009

Pörtner, H. (2001). Climate change and temperature-dependent biogeography: oxygen limitation of thermal tolerance in animals. *Naturwissenschaften.* 88 (4), 137–146. doi: 10.1007/s001140100216

Rana, A. S., Zaman, Q., Afzal, M., and Haroon, M. A. (2014). Characteristics of sea surface temperature of the Arabian Sea coast of Pakistan and impact of tropical cyclones on SST. *Pakistan J. Meteorology.* 11 (21), 61–70.

Sandison, E. E. (1967). Respiratory response to temperature and temperature tolerance of some intertidal gastropods. *J. Exp. Mar. Biol. Ecology.* 1 (2), 271–281. doi: 10.1016/0022-0981(67)90019-6

Teixeira, T. P., Neves, L. M., and Araújo, F. G. (2012). Thermal impact of a nuclear power plant in a coastal area in Southeastern Brazil: Effects of heating and physical structure on benthic cover and fish communities. *Hydrobiologia*. 684 (1), 161–175. doi: 10.1007/s10750-011-0980-1

Tropea, C., Stumpf, L., and Lopez Greco, L. S. (2015). Effect of temperature on biochemical composition, growth and reproduction of the ornamental red cherry shrimp neocaridina heteropoda (Decapoda, caridea). *Public Library Sci. One* 10 (3), e0119468. doi: 10.1371/journal.pone.0119468

Vannote, R., and Sweeney, B. (1980). Geographic analysis of thermal equilibria: A conceptual model for evaluating the effect of natural and modified thermal regimes on aquatic insect communities. *Am. Naturalist.* 115, 667–695. doi: 10.1086/283591

Waltham, N. J., and Sheaves, M. (2020). Thermal exposure risks to mobile tropical marine snails: Are eco-engineered rock pools on seawalls scale-specific enough for comprehensive biodiversity outcome? *Mar. pollut. Bulletin.* 156, 111237. doi: 10.1016/j.marpolbul.2020.111237

Warwick, R. M. (1993). Environmental impact studies on marine communities: pragmatical considerations. *Aust. J. Ecology.* 18, 63–80. doi: 10.1111/j.1442-9993.1993.tb00435

Webb, B. W., Hannah, D. M., Moore, R. D., Brown, L. E., and Nobilis, F. (2008). Recent advances in stream and river temperature research. *Hydrological Processes: Int. J.* 22 (7), 902–918. doi: 10.1007/s10750-008-93

Wethey, D. S., and Woodin, S. A. (2008). Ecological hindcasting of biogeographic responses to climate change in the European intertidal zone. *Hydrobiologia.* 606 (1), 139–151. doi: 10.1007/s10750-008-9338-8

frontiers | Frontiers in Marine Science

TYPE Original Research
PUBLISHED 09 November 2022
DOI 10.3389/fmars.2022.1037137

OPEN ACCESS

EDITED BY
Huang Honghui,
South China Sea Fisheries Research Institute (CAFS), China

REVIEWED BY
Anglu Shen,
Shanghai Ocean University, China
Si Zhu,
Ocean University of China, China
Yonghua Jiang,
Jimei University, China
Zhiyong Wang,
Jimei University, China

*CORRESPONDENCE
Yibo Liao
liaoyb@sio.org.cn

†These authors have contributed equally to this work and share first authorship

SPECIALTY SECTION
This article was submitted to Marine Pollution, a section of the journal Frontiers in Marine Science

RECEIVED 05 September 2022
ACCEPTED 19 October 2022
PUBLISHED 09 November 2022

CITATION
Tian S, Zhou K, Liao Y, Tang Y, Liu Q, Zhang R, Shou L and Zeng J (2022) Effects of temperature shock on the survival of different life stages of large yellow croaker (*Larimichthys crocea*) by simulated power plant cooling water.
Front. Mar. Sci. 9:1037137.
doi: 10.3389/fmars.2022.1037137

Effects of temperature shock on the survival of different life stages of large yellow croaker (*Larimichthys crocea*) by simulated power plant cooling water

Sujie Tian[1†], Konglin Zhou[2†], Yibo Liao[1*], Yanbin Tang[1], Qinghe Liu[1], Rongliang Zhang[1], Lu Shou[1] and Jiangning Zeng[1]

[1]Key Laboratory of Marine Ecosystem Dynamics, Second Institute of Oceanography, Ministry of Natural Resources, Hangzhou, China, [2]Fujian Key Laboratory on Conservation and Sustainable Utilization of Marine Biodiversity, Fuzhou Institute of Oceanography, Minjiang University, Fuzhou, China

Seawater temperatures have increased with global climate change. Coolant water discharged from coastal nuclear power-generating and coal-powered plants, coupled with already increasing seawater temperatures, can adversely affect local fish communities. A sudden drop in temperature caused by the winter shutdown of power plants can also affect fish health and behavior. To assess the effects of temperature change on fish populations, we subjected early life stages of the once commercially important large yellow croaker (*Larimichthys crocea*) to various water temperature experiments. Fertilized eggs showed the highest hatching rate at 23.4°C and the lowest rate of deformity in hatched larvae at 23.0°C. We determined the incipient lethal temperature for each life stages using derivation models. Ranges between the upper and lower incipient lethal temperatures increased during development from yolk-sac larvae to juveniles, especially in response to cold shock, indicating that later developmental stages in this species are more tolerant of temperature fluctuations. However, thermal tolerance is not solely determined by life stage. Our results suggest that rapid changes in seawater temperature caused by power plant coolant water discharges may significantly affect early developmental stages of fish. Critical thermal maximum tests indicate that the seawater heating rate is significantly negatively correlated with survival time and affects the critical thermal maximum value of *L. crocea*. On the basis of our determination of incipient lethal temperatures, emergency measures could be taken to avoid adverse economic and ecological impacts due to changes in seawater temperature caused by coolant water discharges.

KEYWORDS

temperature tolerance, *Larimichthys crocea*, coolant water, heat shock, cold shock

Introduction

Sea surface temperature (SST) is affected by various factors, and changes in SST can affect recruitment in fish populations (Almodóvar et al., 2012; Cheung et al., 2013). Marine fishes are sensitive to temperature change, which affects their energy distribution (Trancart et al., 2016). Low amplitude in temperature rising greatly increases fish activity and affects their feeding behavior (Biro et al., 2010). If a physiologically optimum temperature is exceeded, then the increased metabolic rate and decreased energy intake can reduce growth rates (Killen et al., 2010). At high water temperatures, fish populations without adequate food sources can experience increased mortality (Biro et al., 2007; Munday et al., 2008).

Between 1950 and 1980, the large yellow croaker (*Larimichthys crocea*, Richardson) was a commercially important marine fish species in China; however, the fishery collapsed in the 1980s. Even after implementation of a fishing moratorium, stocks never fully recovered to satisfy market demands, and the population of *L. crocea* remained depressed (Chen and Zhang, 1984; Xu and Liu, 2007; Xu and Chen, 2011; Zhang et al., 2018). Conversely, according to the Chinese Fishery Statistical Yearbook, *L. crocea* has become the dominant species in mariculture, with a 9.46% growth rate in farming scale and a 14.11% increase in seeding from 2003 to 2020. Most farming of *L. crocea* occurs is in Fujian Province. The inadequacy of offshore farming models and a lack of data on the temperature tolerance of *L. crocea* at different life stages can be problematic for farmers when faced with sudden changes in SST due to external factors such as coolant water discharges from power plants (Cai et al., 2020).

Waste heat generated by power plants is generally removed using water, for which reason many power plants are built along coasts where coolant water is readily available (Rosen, 2001; Aminov et al., 2017). Affected by warm water discharged from these power plants, the offshore seawater temperatures increase. Discharge of heated coolant water from coastal power plants can exacerbate the rise in coastal water temperatures already caused by climate change, resulting in an increase of approximately 5°C in waters thousands of meters away from the discharge port, which can affect nearshore benthic, planktonic, and nektonic organisms (Ma et al., 2016; Lee et al., 2018). In addition, the temperature drop caused by stopping the discharge of coolant water can also have adverse effects. Power plants can shut down for several reasons such as electricity overproduction, material replacement, or maintenance, resulting in abrupt water temperature decreases in adjacent receiving waters (Zhao et al., 2006; Madden et al., 2013; Buhariwalla et al., 2016). For fish, such sudden cold shocks can increase the number of mitochondria in cells, increase respiratory and energy consumption rates, damage the respiratory system, or cause mortality (Guderley, 2004; Begriche et al., 2006; Kavanagh et al., 2010).

To understand the effects of temperature changes on fish populations, there are well-established methods of separately determining the incipient lethal temperature (ILT) and critical thermal maximum (CTMax) for a species (Beitinger et al., 2000; Golovanov, 2012). The ILT represents the tolerance limit of the species, which is the temperature at which half of the test animals die when exposed to a series of higher or lower temperatures after acclimation to the relevant temperature for a particular environment (Brett, 1952; Jobling, 1981). In this study, the upper and lower ILTs (ULIT and LLIT, respectively) were determined for different life stages of *L. crocea* to simulate the effects of temperature shock caused by coolant water discharges. CTMax represents the thermal resistance of a species, which is determined by increasing the water temperature at a constant rate until the fish lose equilibrium and opercular movement ceases (Otto, 1973; Becker and Genoway, 1979). CTMax was calculated to simulate the effects of coolant water discharged at different rates on fish populations. The hatching rate of eggs exposed to different temperatures was also determined to simulate the effects of coolant water discharge (Okamura et al., 2007). We report UILT, LILT, and CTMax values for different developmental stages of *L. crocea* and discuss the differences in temperature tolerance among different life history stages of this species. In addition, we suggest management measures that could be taken to avoid adverse economic and ecological impacts due to coolant water discharges.

Materials and methods

Preparation of test animals and seawater

Experiments were performed with four developmental stages of *L. crocea* (fertilized eggs, yolk-sac larvae, larvae, and juveniles). Test animals were provided by the Ningbo Marine and Fishery Research Institute, and their body sizes are shown in Table 1. The fish were kept in natural sand-filtered seawater with a normal saturation oxygen level, constant temperature (22°C), constant salinity (25.6‰), and a natural light regime.

Heat-shock seawater was heated using a titanium heating rod (Armaturenbau, 100–2,000 W) and calibrated using a precision thermometer (Korea A-MI 211H; range, 0°C–90°C; sensitivity, 0.1°C). Cold-shock seawater was prepared using a

TABLE 1 Length and weight of *Larimichthys crocea* at different developmental stages: yolk-sac larvae (LY), larvae (LL), and juveniles (LJ).

Stages	LY	LL	LJ
Length (cm)	< 1	3.21 ± 0.56	17.02 ± 2.05
Weight (g)		0.23 ± 0.14	56.29 ± 19.55

cooling incubator (Yi Heng LRH-150; range, 0°C–60°C; sensitivity, 0.1°C). Aeration and natural light were maintained, and temperature was measured at regular intervals with a mercury thermometer.

Fertilized egg hatching experiments

At the beginning of the experiment, healthy fertilized eggs were transferred directly from 22°C seawater to prepared seawater (15°C, 18°C, 21°C, 24°C, 27°C, 30°C, and 33°C) in 500-ml beakers. One hundred eggs were placed in each beaker, and each temperature test was replicated three times. We observed the eggs hatch and hatched larvae development until all eggs hatched or sank to the bottom. The hatching rate was calculated by dividing the number of eggs hatched by the total number of eggs in each beaker, and the deformity rate was calculated by determining the proportion of hatched larvae exhibiting spinal deformity, tail curvature, or fin membrane decay (Figure 1).

Temperature jump experiments

Yolk-sac larvae were removed from the acclimation environment to the 500-ml beakers, which contained 22°C, 24°C, 26°C, 28°C, 30°C, 32°C, and 34°C seawater for the heat-shock experiments, and 22°C, 19°C, 16°C, 13°C, and 10°C seawater for the cold-shock experiments. Experimental control groups maintained at 22°C were used in both heat-shock and cold-shock experiments to simulate natural ambient seawater unaffected by coolant water discharges.

Mortality of larvae and juveniles spiked in two sequential experimental groups (30°C and 32°C) in the heat-shock experiments, which required adding one intermediate temperature level at 31°C. Furthermore, in the cold-shock experiments, some larvae and juveniles exhibited no effects at 10°C, which required adding four lower experimental temperature levels (8°C, 6°C, 4°C, and 2°C). Consequently, larvae and juveniles were removed from the acclimation environment and placed in 5- and 50-L tanks, which contained seawater maintained at 22°C, 24°C, 26°C, 28°C, 30°C, 31°C, 32°C, and 34°C for the heat-shock experiments, and seawater maintained at 22°C, 20°C, 18°C, 16°C, 14°C, 12°C, 10°C, 8°C, 6°C, 4°C, and 2°C for the cold-shock experiments.

A total of 20 yolk-sac larvae, 30 larvae, and 20 juveniles were exposed to each temperature treatment for 48 h, and approximately100–300 rotifers (*Brachionus plicatilis*; Müller) and fish feed were provided daily as food. This frequency of feeding prevented starvation stress, as indicated by the food remaining in the water at the end of the experiment. Each temperature treatment was replicated three times for each of the three growth stages.

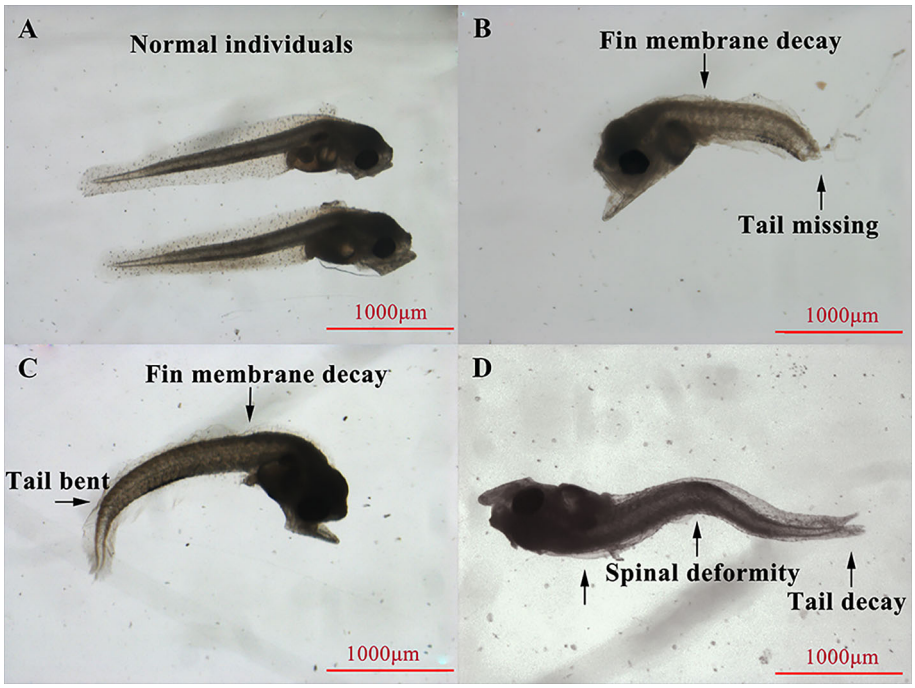

FIGURE 1
Apparent morphology of normal **(A)** and deformed **(B–D)** *Larimichthys crocea* hatched larvae.

The behavioral responses of yolk-sac larvae, larvae, and juveniles were observed continuously over 48 h in each temperature treatment, and the number of dead individuals in each experimental group was recorded. Death was defined as the cessation of opercular movement or the absence of response to touch.

Critical thermal maximum experiments

We measured the reactions of larvae and juveniles exposed to different rates of increase in water temperature. The initial water temperature was 22°C for both larvae and juveniles, and a heating rod was used to control the rate of temperature increase (0.5°C, 3°C, 6°C, and 15°C h^{-1}). For each temperature heating rate exposure, 30 larvae and 20 juveniles were used, and each exposure was replicated three times. Adequate fish feed was provided as food. Throughout the experiment, we noted any larval or juvenile movement disorders, abnormal behaviors, loss of balance, body turnover, or other reactions and recorded the experimental seawater temperature at the time any such observation was made as the CTMax value for that individual. The abnormal subjects were then removed and placed in buffered seawater maintained at 22°C until the CTMax values for all test organisms were observed and recorded.

Statistical analyses

Statistical analyses were performed using SPSS v. 20.0 (IBM Corp., Armonk, NY, USA) and visualized in Origin 2021 (OriginLab, Northampton, MA, USA). Normality and homogeneity of data were assessed using Shapiro–Wilk's and Levene's tests. For data with normal distribution and homogeneity of variance, one-way ANOVA and Duncan tests were used to evaluate differences for overall and pairwise comparisons. For data with non-normal distribution or non-homogeneity of variance, Kruskal–Wallis and Games–Howell tests were used, respectively. Spearman rank correlation analysis was performed to identify relationships between two groups of correlated data.

Results

Fertilized egg temperature tolerance

Hatching and deformity rates for fertilized eggs exposed to different temperatures over 48 h are shown in Figure 2. Significant differences in hatching rates were shown among different treatments (one-way ANOVA, F = 298.598, $P < 0.05$). The highest hatching rate occurred at 21°C and decreased significantly with increased temperature. The lowest larval deformity rates occurred at 21°C and 24°C (Kruskal–Wallis test, $P < 0.05$), and all larvae hatched at either 15°C or 33°C were deformed. Spearman rank correlation test results for hatching and deformity rates are shown in Table 2.

Effects of temperature shock on large yellow croaker

Changes in the mortality of *L. crocea* exposed to cold shock are shown in Figure 3. Mortality rates of yolk-sac larvae increased significantly as temperature decreased (one-way ANOVA, F = 6.684, $P < 0.05$) but did not differ significantly at temperatures >10°C, the point at which 100% mortality occurred.

Larvae were exposed to cold-shock temperatures as low as 6°C, and the mortality rate of larvae in both the 8°C and 6°C experimental groups was 100% (Kruskal–Wallis test, $P < 0.05$).

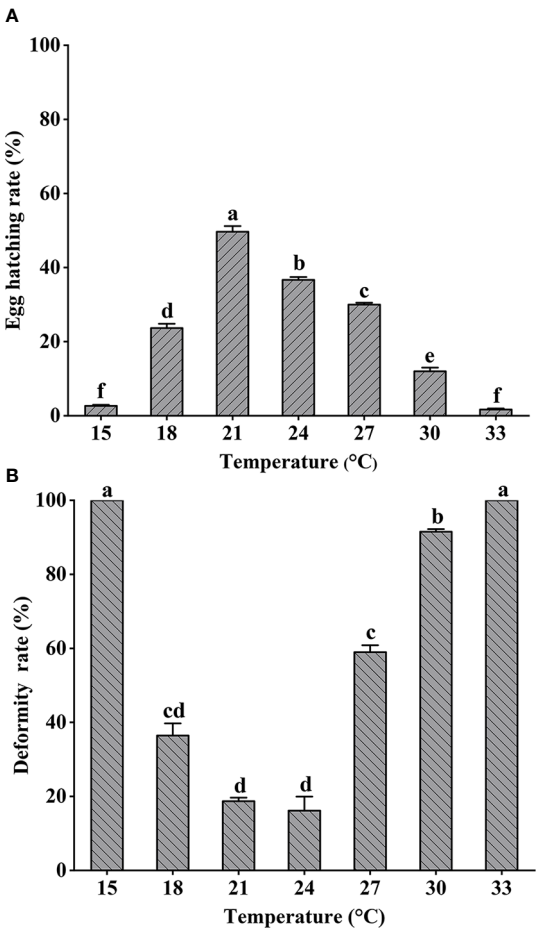

FIGURE 2
Larimichthys crocea fertilized eggs hatching rate **(A)** and hatched larvae deformity rate **(B)** exposed to different temperatures (mean ± SD). Labeled means without a common letter differ ($P < 0.05$).

TABLE 2 Spearman rank correlation analysis results on hatching and deformity rates, individual survival time and heating rate.

	Correlation coefficient	
	Deformity rate	**Heating rate**
Hatching rate	−0.909 **	
Individual survival time		−0.973 **

**Correlation is significant at the 0.01 level (two-tailed).

To avoid unnecessary impacts to test organisms, larvae were not exposed to temperatures lower than 6°C. In contrast to the results of the yolk-sac larvae experiment, larval mortality did not occur until the temperature dropped to 14°C. The mortality rate of larvae exposed to temperatures ≤12°C was significantly higher than the mortality rate of larvae in the 14°C experimental group.

Juveniles were exposed to cold-shock temperatures as low as 2°C, and none exhibited mortality at temperatures ≥10°C.

Changes in the mortality of *L. crocea* exposed to heat shock are shown in Figure 4. After the yolk-sac larvae were acclimated at 22°C, they exhibited a significant increase in mortality in response to a sudden increase in temperature (Kruskal–Wallis test, $P < 0.05$) (Figure 4A). The mortality rate was less than 20% for yolk-sac larvae in the 24°C and 26°C experimental groups. All yolk-sac larvae died in the three replicate experimental groups at 34°C.

Larvae did not exhibit any mortality at temperatures ≤28°C; however, larval mortality increased significantly at 30°C, 31°C, and 32°C (Kruskal–Wallis test, $P < 0.05$). Larval mortality at 34°C reached 100%.

Similar to larvae, juveniles did not exhibit any mortality at temperatures ≤28°C; however, at higher temperatures, there was a significant difference in mortality compared to the control group (Kruskal–Wallis test, $P < 0.05$).

We systematically described the mortality of yolk-sac larvae, larvae, and juveniles in different temperature shock experimental groups and used three calculation models to fit the mortality of fish at different life stages exposed to heat shock or cold shock after acclimation at 22°C (Cherry et al., 1977; Urquhart and Koetsier, 2013; Kir, 2020). UILT, LILT, model type, and input parameters are shown in Table 3.

Thermal resistance of larvae and juveniles at different heating rates

Larval and juvenile survival at different heating rates is shown in Figure 5. Average survival time differed significantly among treatments (Kruskal–Wallis test, $P < 0.05$); however, survival times for larvae and juveniles exposed to the same heating rate were not significantly different (paired sample T-test, $P > 0.05$).

CTMax values for larval and juvenile stages at a heating rate of 0.5°C h^{-1} were much higher than for other treatments (paired sample T-test, $P < 0.05$). There was no significant difference in CTMax among treatment groups exposed to heating rates >0.5°C h^{-1}. The trend in CTMax change was similar for larval and juvenile stages (Figure 6).

Discussion

Responses of fertilized eggs to temperature fluctuations

Water temperature affects early fish development (Decuypere and Michels, 2019). Compared with salinity and dissolved oxygen, temperature is worthy of paying more attention during the incubation process (Alderdice and Forrester, 1968; Geist et al., 2011). Lower temperatures can prolong hatching time, whereas higher temperatures can accelerate development (Pauly and Pullin, 1988; Teletchea et al., 2009). We observed this phenomenon in our

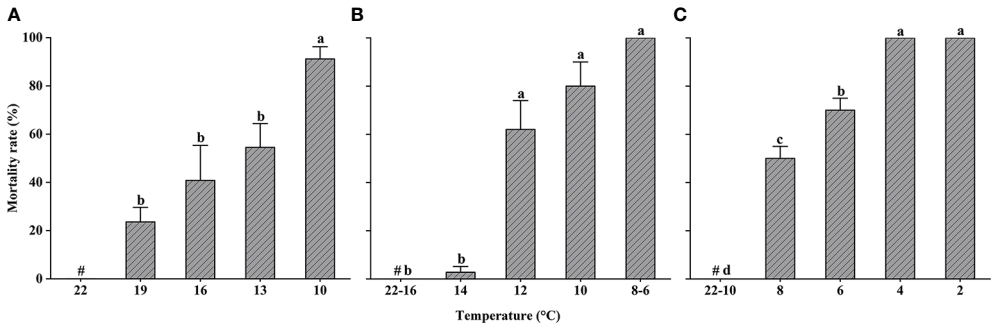

FIGURE 3
Larimichthys crocea yolk-sac larvae **(A)**, larvae **(B)**, and juvenile **(C)** mortality rate in cold-shock treatments (mean ± SD). Labeled means without a common letter differ ($P < 0.05$). **#**Control treatment.

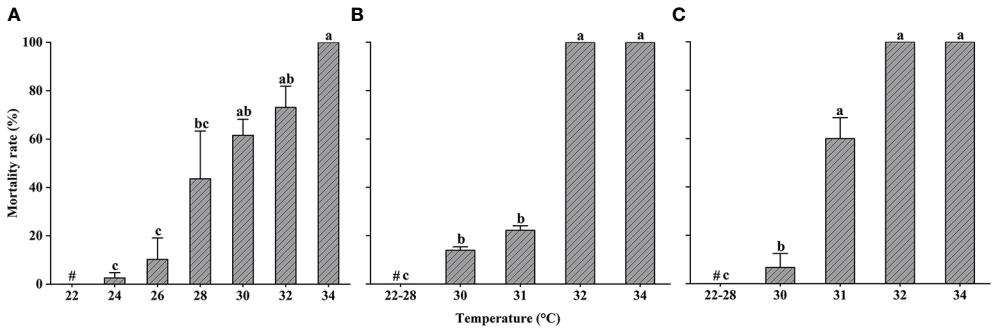

FIGURE 4
Larimichthys crocea yolk-sac larvae **(A)**, larvae **(B)**, and juvenile **(C)** mortality rate in heat-shock treatments (mean ± SD). Labeled means without a common letter differ ($P < 0.05$). #Control treatment.

experiments, as well. During culture of *L. crocea*, Lin et al. (1991) found that the optimum temperature for fertilized eggs was 18°C–24°C. Consistent with this finding, we determined (by curve fitting hatching rate with temperature) that the optimum hatching temperature for *L. crocea* was 23.4°C, which is similar to seawater temperatures where *L. crocea* spawns (Wu et al., 2022). Therefore, discharging of heated coolant water should be avoided during the incubation period if possible. We found that the lowest rate of deformity in hatched larvae occurred at 23°C. In culturing *L. crocea*, a balance must be maintained between the hatching rate and the quality of the hatched larvae. High temperatures can accelerate hatching but can also reduce larval quality due to thermal stress (Ojanguren et al., 1999; Moran et al., 2007). Fluctuations in temperature are known to affect fertilized egg hatching time and rate; however, the impact of such fluctuations on malformation rates in hatched larvae was previously unknown (Koo and Johnston, 1978; Kurokawa et al., 2008). In this study, we found a significant negative correlation between rates of hatching and malformation (Table 2). We also found that temperatures producing the highest hatching rate and the highest quality hatched larvae were similar, indicating that this temperature regime could be successfully employed in *L. crocea* culture.

Tolerance of different life stages to heat and cold shock

Overfishing and lack of protection measures have depleted *L. crocea* stocks (Liu and De Mitcheson, 2008). The discharge of coolant water from power plants near *L. crocea* habitat is known to adversely affect population recruitment; however, few studies have investigated the tolerance of different life stages of *L. crocea* to temperature change (Wu et al., 2022). Understanding the causes of ILT and CTMax for different life stages is essential to restoring wild resources, guiding artificial breeding programs, and warning of likely impacts due to frequent, abnormal, or sudden temperature changes (Wernberg et al., 2012).

Among the multiple factors that affect ILT and CTMax, life stage is considered to be one of the most critical. Some studies have found that younger fish were more thermotolerant (Recsetar et al., 2012; Di Santo and Lobel, 2017), whereas others found that older fish were more tolerant to temperature changes (Charo-Karisa et al., 2005; Moyano et al., 2017). Some researchers have questioned the existence of a life stage effect, noting that the evidence for such an effect was inconclusive and finding little variation in temperature tolerance among fish of different stages (Ospina and Mora, 2004; Recsetar et al., 2012).

TABLE 3 Pearson's r and R^2 for *Larimichthys crocea* yolk-sac larvae (LY), larvae (LL), and juveniles (LJ) about upper and lower incipient lethal temperature (LILT and UILT). Labeled means without a common letter differ ($P < 0.05$).

Type	X = log T			Linear			Logistic		Stages
	T	R^2	P's r	T	R^2	P's r	T	R^2	
LILT	14.32	0.80	−0.90	14.88	0.79	−0.90	14.11	0.76	LY [a]
	11.58	0.83	−0.92	11.92	0.85	−0.93	12.27	0.95	LL [b]
	6.95	0.88	−0.95	7.31	0.94	−0.97	7.53	0.97	LJ [c]
UILT	28.70	0.79	0.89	28.96	0.80	0.90	29.19	0.81	LY [a]
	30.98	0.62	0.81	30.99	0.63	0.82	31.24	0.98	LL [b]
	30.60	0.73	0.87	30.58	0.76	0.88	30.97	0.98	LJ [b]

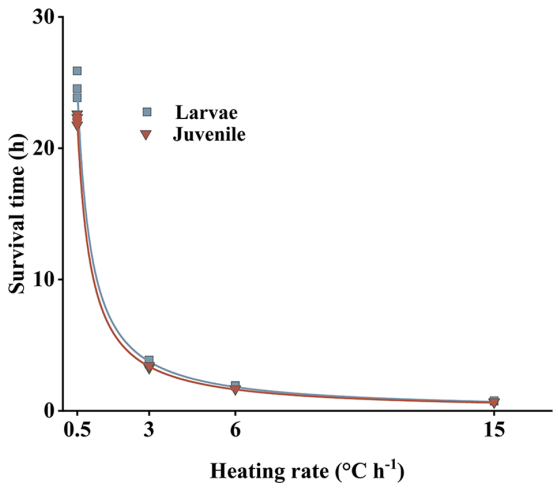

FIGURE 5
Heating rates and survival times of larvae and juveniles *Larimichthys crocea*.

Temperature tolerance has been linked to individual differences in metabolic rate and related to variations in key life history traits that could affect ecological patterns within animal populations (Norin et al., 2015). Therefore, a more likely explanation for changes in temperature tolerance may be related to individual life stage and bottlenecks during life stages. Older fish have more mature organs and physiological systems but require extra energy for activities such as spawning (Baroudy and Elliott, 1994; Dahlke et al., 2020). This could explain the increasing temperature range between LILT and UILT with the growth of *L. crocea*, as well as the lack of change in UILT between the larval and juvenile stages, a finding consistent with that of Baroudy and Elliott (1994).

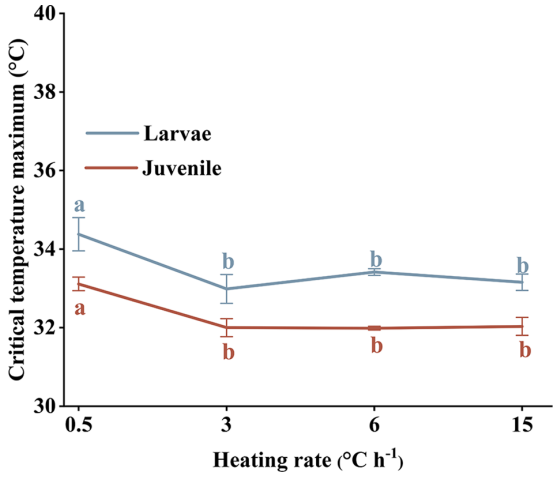

FIGURE 6
Larvae and juveniles *Larimichthys crocea* critical temperature maxima (CTMax) subjected to different heating rates. Labeled means without a common letter differ ($P < 0.05$).

Effect of heating rate on critical temperature maxima

Discharge of power plant coolant water is necessary for power production. Larvae and juvenile fish are strongly motile (Pavlov et al., 2008) and can escape elevated temperatures should they encounter coolant water (Crozier et al., 2008; Rijnsdorp et al., 2009). We describe a power function relationship between individual survival time and heating rate, with a statistically significant negative correlation (Table 2). The absence of any significant differences in larval and juvenile survival times suggests that the escape time for larvae and juveniles was determined more by the heating rate than the growth stage. Therefore, during the discharge of coolant water from power plants, the rate of increase in seawater temperature should be controlled to provide fish in early developmental stages with sufficient escape time to avoid suboptimal temperature conditions, thereby aiding wild population recovery.

When the heating rate exceeds a certain value, CTMax does not change and is generally greater for larvae than juveniles (Elliott and Elliott, 1995; Beitinger and Bennett, 2000; Das et al., 2004). Elliott and Elliott (1995) and Mora and Maya (2006) found that CTMax varied with heating rate, being greatest at 1°C h^{-1}, with any change at increased rates being insignificant. We found that CTMax was highest at a heating rate of 0.5°C h^{-1} and trended downward at higher heating rates and, similarly, fluctuate insignificantly thereafter. Because CTMax does not change significantly at higher heating rates, rapid thermal shock probably causes irreversible impacts (Landsman et al., 2011). If CTMax experiments were performed on a variety of coastal fish species using different rates of temperature increase, then the results could be used to develop and implement appropriate treatment methods and discharge rates to minimize the damage to fish communities caused by heated coolant water.

Conclusion

In this paper, we described the responses of different life history stages of *L. crocea* to temperature change in heat-shock and cold-shock experiments. Fertilized egg hatching and malformation rates were negatively correlated, and the optimum hatching temperature was determined to be 23.4°C. Application of these findings to the culture of *L. crocea* could increase the survival of cultured fish. UILT and LILT values showed that the tolerance of *L. crocea* to temperature fluctuations increased during development from the yolk-sac larval stage to the juvenile stage. We discussed the impact of

individual life stage and bottlenecks in the life cycle of *L. crocea* on ILT variation. As the thermotolerance mechanism in fish matures, the difference between the UILT of larvae and juveniles is less significant than the LILT. The discharge of coolant water and its interruption should be timed to avoid impacts on early life stages with poor tolerance to temperature change. We also found a significant negative correlation between survival time and heating rate. When coolant water is discharged, the rate of temperature increase should be monitored. Controlling the discharge rate of coolant water could provide early life stages of fishes in coastal waters with more time to react to elevated temperatures, thus reducing damage to coastal fisheries.

Data availability statement

The original contributions presented in the study are included in the article/supplementary material. Further inquiries can be directed to the corresponding author.

Ethics statement

The animal study was reviewed and approved by The Institutional Animal Care and Use Committee of Second Institute of Oceanography, Ministry of Natural Resources, China.

Author contributions

ST and KZ contributed equally to this work and share first authorship. ST, KZ: Formal analysis; Methodology; Writing - Original Draft; Writing - review and editing. YL: Resources; Data curation; Project administration. YT, QL, RZ: Writing - Review and Editing. LS, JZ: Supervision; Funding acquisition. All authors contributed to the article and approved the submitted version.

Funding

The present work was supported financially by the National Natural Science Foundation of China (41706125) and the Scientific Research Fund of the Second Institute of Oceanography, MNR, China (JG2209 and JG1914).

Acknowledgments

We thank wordvice (https://www.wordvice.com) for editing a draft of this manuscript.

Conflict of interest

The authors declare that the research was conducted in the absence of any commercial or financial relationships that could be construed as a potential conflict of interest.

Publisher's note

References

Alderdice, D. F., and Forrester, C. R. (1968). Some effects of salinity and temperature on early development and survival of the English sole (*Parophrys vetulus*). *J. Fisheries Res. Board Canada.* 25, 495–521. doi: 10.1139/f68-043

Almodóvar, A., Nicola, G. G., Ayllón, D., and Elvira, B. (2012). Global warming threatens the persistence of Mediterranean brown trout. *Global Change Biol.* 18, 1549–1560. doi: 10.1111/j.1365-2486.2011.02608.x

Aminov, R. Z., Shkret, A. F., and Garievskii, M. V. (2017). Thermal and nuclear power plants: Competitiveness in the new economic conditions. *Thermal Eng* 64, 319–328. doi: 10.1134/S0040601517050019

Baroudy, E., and Elliott, J. M. (1994). The critical thermal limits for juvenile Arctic charr *Salvelinus alpinus*. *J. Fish Biol.* 45, 1041–1053. doi: 10.1111/j.1095-8649.1994.tb01071.x

Becker, C. D., and Genoway, R. G. (1979). Evaluation of the critical thermal maximum for determining thermal tolerance of freshwater fish. *Environ. Biol. Fish* 4, 245–256. doi: 10.1007/bf00005481

Begriche, K., Igoudjil, A., Pessayre, D., and Fromenty, B. (2006). Mitochondrial dysfunction in Nash: Causes, consequences and possible means to prevent it. *Mitochondrion* 6, 1–28. doi: 10.1016/j.mito.2005.10.004

Beitinger, T. L., and Bennett, W. A. (2000). Quantification of the role of acclimation temperature in temperature tolerance of fishes. *Environ. Biol. Fish* 58, 277–288. doi: 10.1023/A:1007618927527

Beitinger, T. L., Bennett, W. A., and Mccauley, R. W. (2000). Temperature tolerances of north American freshwater fishes exposed to dynamic changes in temperature. *Environ. Biol. Fish* 58, 237–275. doi: 10.1023/a:1007676325825

Biro, P. A., Beckmann, C., and Stamps, J. A. (2010). Small within-day increases in temperature affects boldness and alters personality in coral reef fish. *Proc. Biol. Sci.* 277, 71–77. doi: 10.1098/rspb.2009.1346

Biro, P. A., Post, J. R., and Booth, D. J. (2007). Mechanisms for climate-induced mortality of fish populations in whole-lake experiments. *Proc. Natl. Acad. Sci. U S A.* 104, 9715–9719. doi: 10.1073/pnas.0701638104

Brett, J. R. (1952). Temperature tolerance in young pacific salmon, genus *Oncorhynchus*. *J. Fisheries Res. Board Canada.* 9, 265–323. doi: 10.1139/f52-016

Buhariwalla, C. F., Macmillan, J. L., Gregoire, M. J., Dadswell, M. J., and Stokesbury, M. J. W. (2016). Population characteristics of striped bass killed by cold shock during winter shutdown of a power plant in Nova Scotia. *Northeastern Naturalist.* 23, 163–173. doi: 10.1656/045.023.0113

Cai, X., Zhang, J., Lin, L., Li, Y., Liu, X., and Wang, Z. (2020). Study of a noninvasive detection method for the high-temperature stress response of the Large yellow croaker (*Larimichthys crocea*). *Aquac Rep.* 18:100514. doi: 10.1016/j.aqrep.2020.100514

Charo-Karisa, H., Rezk, M. A., Bovenhuis, H., and Komen, H. (2005). Heritability of cold tolerance in Nile tilapia, *Oreochromis niloticus*, juveniles. *Aquaculture* 249, 115–123. doi: 10.1016/j.aquaculture.2005.04.029

Chen, B., and Zhang, C. (1984). Preliminary study on the biological basis of Large yellow croaker fishery in southern fujian. *J. Fujian Fish* 4, 6-16.

Cherry, D. S., Dickson, K. L., Cairns, J.Jr., and Stauffer, J. R. (1977). Preferred, avoided, and lethal temperatures of fish during rising temperature conditions. *J. Fisheries Res. Board Canada.* 34, 239–246. doi: 10.1139/f77-035

Cheung, W. W., Watson, R., and Pauly, D. (2013). Signature of ocean warming in global fisheries catch. *Nature* 497, 365–368. doi: 10.1038/nature12156

Crozier, L. G., Hendry, A. P., Lawson, P. W., Quinn, T. P., Mantua, N. J., Battin, J., et al. (2008). Potential responses to climate change in organisms with complex life histories: Evolution and plasticity in pacific salmon. *Evol. Appl.* 1, 252–270. doi: 10.1111/j.1752-4571.2008.00033.x

Dahlke, F. T., Wohlrab, S., Butzin, M., and Portner, H. O. (2020). Thermal bottlenecks in the life cycle define climate vulnerability of fish. *Science* 369, 65–70. doi: 10.1126/science.aaz3658

Das, T., Pal, A. K., Chakraborty, S. K., Manush, S. M., Chatterjee, N., and Mukherjee, S. C. (2004). Thermal tolerance and oxygen consumption of Indian major carps acclimated to four temperatures. *J. Thermal Biol.* 29, 157–163. doi: 10.1016/j.jtherbio.2004.02.001

Decuypere, E., and Michels, H. (2019). Incubation temperature as a management tool: A review. *World's Poultry Sci. J.* 48, 28–38. doi: 10.1079/wps19920004

Di Santo, V., and Lobel, P. S. (2017). Body size and thermal tolerance in tropical gobies. *J. Exp. Mar. Biol. Ecol* 487, 11–17. doi: 10.1016/j.jembe.2016.11.007

Elliott, J. M., and Elliott, J. A. (1995). The effect of the rate of temperature increase on the critical thermal maximum for parr of Atlantic salmon and brown trout. *J. Fish Biol.* 47, 917–919. doi: 10.1111/j.1095-8649.1995.tb06014.x

Geist, D. R., Abernethy, C. S., Hand, K. D., Cullinan, V. I., Chandler, J. A., and Groves, P. A. (2011). Survival, development, and growth of fall Chinook salmon embryos, alevins, and fry exposed to variable thermal and dissolved oxygen regimes. *Trans. Am. Fisheries Soc* 135, 1462–1477. doi: 10.1577/T05-294.1

Golovanov, V. K. (2012). Influence of various factors on upper lethal temperature (Review). *Inland Water Biol.* 5, 105–112. doi: 10.1134/s1995082911040079

Guderley, H. (2004). Metabolic responses to low temperature in fish muscle. *Biol. Rev. Camb Philos. Soc* 79, 409–427. doi: 10.1017/S1464793103006328

Jobling, M. (1981). Temperature tolerance and the final preferendum-rapid methods for the assessment of optimum growth temperatures. *J. Fish Biol.* 19, 439–455. doi: 10.1111/j.1095-8649.1981.tb05847.x

Kavanagh, K. D., Haugen, T. O., Gregersen, F., Jernvall, J., and Vollestad, L. A. (2010). Contemporary temperature-driven divergence in a Nordic freshwater fish under conditions commonly thought to hinder adaptation. *BMC Evol. Biol.* 10, 350. doi: 10.1186/1471-2148-10-350

Killen, S. S., Atkinson, D., and Glazier, D. S. (2010). The intraspecific scaling of metabolic rate with body mass in fishes depends on lifestyle and temperature. *Ecol. Lett.* 13, 184–193. doi: 10.1111/j.1461-0248.2009.01415.x

Kir, M. (2020). Thermal tolerance and standard metabolic rate of juvenile gilthead seabream (*Sparus aurata*) acclimated to four temperatures. *J. Therm Biol.* 93, 102739. doi: 10.1016/j.jtherbio.2020.102739

Koo, T. S. Y., and Johnston, M. L. (1978). Larva deformity in striped bass, *Morone saxatilis* (Walbaum), and blueback herring, *Alosa aestivalis* (Mitchill), due to heat shock treatment of developing eggs. *Environ. pollut. (1970).* 16, 137–149. doi: 10.1016/0013-9327(78)90128-3

Kurokawa, T., Okamoto, T., Gen, K., Uji, S., Murashita, K., Unuma, T., et al. (2008). Influence of water temperature on morphological deformities in cultured larvae of Japanese eel, *Anguilla japonica*, at completion of yolk resorption. *J. World Aquac Soc* 39, 726–735. doi: 10.1111/j.1749-7345.2008.00208.x

Landsman, S. J., Gingerich, A. J., Philipp, D. P., and Suski, C. D. (2011). The effects of temperature change on the hatching success and larvae survival of largemouth bass *Micropterus salmoides* and smallmouth bass *Micropterus dolomieu*. *J. Fish Biol.* 78, 1200–1212. doi: 10.1111/j.1095-8649.2011.02927.x

Lee, P. W., Tseng, L. C., and Hwang, J. S. (2018). Comparison of mesozooplankton mortality impacted by the cooling systems of two nuclear power plants at the northern Taiwan coast, southern East China Sea. *Mar. pollut. Bull.* 136, 114–124. doi: 10.1016/j.marpolbul.2018.09.003

Lin, D., Zhang, J., Zheng, Z., Weng, Z., and Su, Y. (1991). Studies on the artificial propagation of the Large yellow croake, *Pseudosciaena crocea* (Richardson). *J. Fujian Normal Univ(Natural Sci. Edition).* 7, 71–79.

Liu, M., and De Mitcheson, Y. S. (2008). Profile of a fishery collapse: Why mariculture failed to save the Large yellow croaker. *Fish Fish* 9, 219–242. doi: 10.1111/j.1467-2979.2008.00278.x

Ma, P., Dai, X., Guo, Z., Wei, C., and Ma, W. (2016). Detection of thermal pollution from power plants on china's Eastern coast using remote sensing data. *Stochastic Environ. Res. Risk Assess* 31, 1957–1975. doi: 10.1007/s00477-016-1293-8

Madden, N., Lewis, A., and Davis, M. (2013). Thermal effluent from the power sector: An analysis of once-through cooling system impacts on surface water temperature. *Environ. Res. Letters.* 8:035006. doi: 10.1088/1748-9326/8/3/035006

Mora, C., and Maya, M. F. (2006). Effect of the rate of temperature increase of the dynamic method on the heat tolerance of fishes. *J. Thermal Biol.* 31, 337–341. doi: 10.1016/j.jtherbio.2006.01.005

Moran, D., Smith, C. K., Gara, B., and Poortenaar, C. W. (2007). Reproductive behaviour and early development in yellowtail kingfish (*Seriola lalandi*, valenciennes 1833). *Aquaculture* 262, 95–104. doi: 10.1016/j.aquaculture.2006.10.005

Moyano, M., Candebat, C., Ruhbaum, Y., Alvarez-Fernandez, S., Claireaux, G., Zambonino-Infante, J. L., et al. (2017). Effects of warming rate, acclimation temperature and ontogeny on the critical thermal maximum of temperate marine fish larvae. *PloS One* 12, e0179928. doi: 10.1371/journal.pone.0179928

Munday, P. L., Kingsford, M. J., O'callaghan, M., and Donelson, J. M. (2008). Elevated temperature restricts growth potential of the coral reef fish *Acanthochromis polyacanthus*. *Coral Reefs.* 27, 927–931. doi: 10.1007/s00338-008-0393-4

Norin, T., Malte, H., Clark, T. D., and Konarzewski, M. (2015). Differential plasticity of metabolic rate phenotypes in a tropical fish facing environmental change. *Funct. Ecol* 30, 369–378. doi: 10.1111/1365-2435.12503

Ojanguren, A. F., Reyes-Gavilán, F. G., and Muñoz, R. R. (1999). Effects of temperature on growth and efficiency of yolk utilisation in eggs and pre-feeding larvae stages of Atlantic salmon. *Aquac Int.* 7, 81–87. doi: 10.1023/A:1009214804949

Okamura, A., Yamada, Y., Horie, N., Utoh, T., Mikawa, N., Tanaka, S., et al. (2007). Effects of water temperature on early development of Japanese eel *Anguilla japonica*. *Fisheries Sci* 73, 1241–1248. doi: 10.1111/j.1444-2906.2007.01461.x

Ospina, A. F., and Mora, C. (2004). Effect of body size on reef fish tolerance to extreme low and high temperatures. *Environ. Biol. Fish* 70, 339–343. doi: 10.1023/b:Ebfi.0000035429.39129.34

Otto, R. G. (1973). Temperature tolerance of the mosquitofish, *Gambmia affinis* (Baird and girard). *J. Fish Biol.* 5, 575–585. doi: 10.1111/j.1095-8649.1973.tb04490.x

Pauly, D., and Pullin, R. S. V. (1988). Hatching time in spherical, pelagic, marine fish eggs in response to temperature and egg size. *Environ. Biol. Fish* 22, 261–271. doi: 10.1007/BF00004892

Pavlov, D. S., Mikheev, V. N., Lupandin, A. I., and Skorobogatov, M. A. (2008). Ecological and behavioural influences on juvenile fish migrations in regulated rivers: A review of experimental and field studies. *Hydrobiologia* 609, 125–138. doi: 10.1007/s10750-008-9396-y

Recsetar, M. S., Zeigler, M. P., Ward, D. L., Bonar, S. A., and Caldwell, C. A. (2012). Relationship between fish size and upper thermal tolerance. *Trans. Am. Fisheries Soc* 141, 1433–1438. doi: 10.1080/00028487.2012.694830

Rijnsdorp, A. D., Peck, M. A., Engelhard, G. H., Möllmann, C., and Pinnegar, J. K. (2009). Resolving the effect of climate change on fish populations. *ICES J. Mar. Sci* 66, 1570–1583. doi: 10.1093/icesjms/fsp056

Rosen, M. A. (2001). Energy- and exergy-based comparison of coal-fired and nuclear steam power plants. *Exergy Int. J.* 1, 180–192. doi: 10.1016/S1164-0235(01)00024-3

Teletchea, F., Gardeur, J. N., Kamler, E., and Fontaine, P. (2009). The relationship of oocyte diameter and incubation temperature to incubation time in temperate freshwater fish species. *J. Fish Biol.* 74, 652–668. doi: 10.1111/j.1095-8649.2008.02160.x

Trancart, T., Feunteun, E., Lefrançois, C., Acou, A., Boinet, C., and Carpentier, A. (2016). Difference in responses of two coastal species to fluctuating salinities and temperatures: Potential modification of specific distribution areas in the context of global change. *Estuarine Coast. Shelf Sci* 173, 9–15. doi: 10.1016/j.ecss.2016.02.012

Urquhart, A. N., and Koetsier, P. (2013).). low-temperature tolerance and critical thermal minimum of the invasive oriental weatherfish *Misgurnus anguillicaudatus* Idaho, USA. *Trans. Am. Fisheries Soc* 143, 68–76. doi: 10.1080/00028487.2013.829124

Wernberg, T., Smale, D. A., Tuya, F., Thomsen, M. S., Langlois, T. J., De Bettignies, T., et al. (2012). An extreme climatic event alters marine ecosystem structure in a global biodiversity hotspot. *Nat. Climate Change.* 3, 78–82. doi: 10.1038/nclimate1627

Wu, Y., Yu, X., Suo, N., Bai, H., Ke, Q., Chen, J., et al. (2022). Thermal tolerance, safety margins and acclimation capacity assessments reveal the climate vulnerability of Large yellow croaker aquaculture. *Aquaculture* 561:738665. doi: 10.1016/j.aquaculture.2022.738665

Xu, Z., and Chen, J. (2011). Analysis of migratory route of *Larimichthys crocea* in the East China Sea and yellow Sea. *J. Fisheries China.* 35, 429–437. doi: 10.3724/SP.J.1231.2011.17099

Xu, K., and Liu, Z. (2007). The current stock of Large yellow croaker *Pseudosciaena crocea* in the East China Sea with respects of its stock decline. *J. Dalian Fisheries Univ* 22, 392–396.

Zhang, K., Zhang, J., Xu, Y., Sun, M., Chen, Z., and Yuan, M. (2018). Application of a catch-based method for stock assessment of three important fisheries in the East China Sea. *Acta Oceanol Sinica.* 37, 102–109. doi: 10.1007/s13131-018-1173-9

Zhao, Y., Volovoi, V., Waters, M., and Mavris, D. (2006). A profit-based approach for gas turbine power plant outage planning. *J. Eng. Gas Turbines Power.* 128, 806–814. doi: 10.1115/1.2179466

frontiers | Frontiers in Marine Science

TYPE Original Research
PUBLISHED 06 January 2023
DOI 10.3389/fmars.2022.1107087

OPEN ACCESS

EDITED BY
Huang Honghui,
South China Sea Fisheries Research Institute, Chinese Academy of Fishery Sciences (CAFS), China

REVIEWED BY
Li-Zhe Cai,
Xiamen University, China
Tao Yan,
South China Sea Institute of Oceanology, Chinese Academy of Sciences (CAS), China

*CORRESPONDENCE
Heshan Lin
linheshan@tio.org.cn
Zhongbao Li
200061000013@jmu.edu.cn

†These authors have contributed equally to this work

SPECIALTY SECTION
This article was submitted to Marine Pollution, a section of the journal Frontiers in Marine Science

RECEIVED 24 November 2022
ACCEPTED 13 December 2022
PUBLISHED 06 January 2023

CITATION
Lin H, Huang Y, Lin Y, Zhang S, Yu S, Liu K, Mou J, Lin J, He X, Fu S, Xie W and Li Z (2023) Biofouling characteristics in Xinghua Bay of Fujian, China. *Front. Mar. Sci.* 9:1107087. doi: 10.3389/fmars.2022.1107087

Biofouling characteristics in Xinghua Bay of Fujian, China

Heshan Lin[1,2*†], Yaqin Huang[1,2†], Yingyue Lin[3], Shuyi Zhang[1], Shihao Yu[1], Kun Liu[1], Jianfeng Mou[1], Junhui Lin[1], Xuebao He[1], Sujing Fu[1], Weijie Xie[1] and Zhongbao Li[2*]

[1]Laboratory of Marine Biodiversity, Third Institute of Oceanography, Ministry of Natural Resources, Xiamen, China, [2]Fisheries College, Jimei University, Xiamen, China, [3]Environment and Emergency Department, Fujian Fuqing Nuclear Power Co., Ltd., Fuqing, China

Biofouling is one of the main factors affecting the efficiency and safety of cooling water systems in coastal nuclear power plants. Understanding the population dynamics, succession rules and cumulative effects of major fouling organisms is the basis for targeted prevention and control. A 1-year simulated concrete panel test was conducted from December 2020 to November 2021 in Xinghua Bay, China. A total of 78 species of fouling organisms were recorded by combining the monthly, seasonal, semiannual, annual and monthly cumulative panels, and the community composition was dominated by nearshore warm-water species, making for a typical subtropical inner bay-type community. The fouling organisms had a peak attachment period from June to October. Significantly more attachment was observed during summer (from June to August) than during the other three seasons. The attachment amount in the second half-year (from June to November) was much higher than that in the first half-year (from December to May). The attachment thickness, density, and biomass of the bottom summer panels reached 20 cm, 105,150 ind./m^2, and 19,274.50 g/m^2, respectively, while those of the bottom annual panels were 40 cm, 27,300 ind./m^2, and 17,762.50 g/m^2, respectively. The dominant fouling organisms with calcified shells mainly included *Amphibalanus reticulatus* and *Pernaviridis*. These species had high attachment amounts,could accumulate attachments for a long time, and even might cause secondary blockage, making them the most detrimental to the safety of a cooling system. Moreover,the seasonal upward growth of hydroids and bryozoans can also significantly reduce the efficiency of cooling water intake. We suggest that targeted prevention and control should be carried out according to the larval attachment period of different dominant groups of fouling organisms during June-October, which can greatly improve the prevention and control efficiency. Strengthening the research on the biological cycle phenomenon of the main species and their main environmental impact factors, and establishing a scientific and effective early-warning model are the governance direction of formulating and implementing scientific pollution prevention and control in the future.

KEYWORDS

biofouling, succession, prevention and control, Xinghua Bay, cooling water system, nuclear power plant

1 Introduction

Biofouling is a key factor affecting the safety of the water intake of the cooling water systems of coastal nuclear power plants. In recent decades, biofouling has affected the safety of the cooling water systems of coastal nuclear power plants in various countries around the world. For example, in 1981, the broken shells of *Crassostrea virginica* completely damaged the residual heat removal exchanger of the Brunswick Nuclear Power Plant in the United States. The attachment of fouling organisms hindered the normal cooling water intake of the Madras Atomic Power Station in India (Rajagopal et al., 1991a; Rajagopal et al., 1991b). The attachment of numerous *Dreissena polymorpha* lowered the safety of the cooling water systems of the Kalinin Nuclear Power Plant in Russia and the Pickering Nuclear Generating Station in Canada (Florin et al., 2013; Dixon, 2015). In 2009 and 2016, broken shells impaired the cooling water systems of the Daya Bay Nuclear Power Plant and the Fuqing Nuclear Power Plant in China (Information from internal communication).

Biofouling can reduces the efficiency or causes the failure of water intake facilities (such as barrier nets, tunnels, and gratings). Hard calcified shells in the water flow damage small pipelines, heat exchangers, and valves, thereby affecting the safety of equipment and causing serious economic losses. The reported annual global expenditure on biofouling treatment and prevention in marine projects has been estimated to be 10 billion British pounds (Satpathy, 1990). Biofouling restricts the operational safety of coastal nuclear power plants. Therefore, targeted biofouling prevention is an urgent task for coastal nuclear power plants to reduce the impact of fouling organisms on the water intake of cooling water systems.

Past studies have mostly investigated the impact of biofouling on ships (Callow, 1990), buoys (Yan et al., 2009; Zhang et al., 2015), oil and gas drilling platforms (Sammarco et al., 2004; Yan et al., 2006), farming cages (Greene and Grizzle, 2007), simulated concrete panel test (Wu et al., 2019; Liu et al., 2020; Peng et al., 2020), and other facilities (Qvarfordt et al., 2006; Lin et al., 2017), mainly from the perspectives of the species composition, attachment mechanisms, control technology, ecological effects of biofouling, and alien species (Yan and Yan, 2003; Maruzzo et al., 2011; Pradhan et al., 2011; Zhang et al., 2011; Tasso et al., 2012; Cao et al., 2013). Research on the biofouling of cooling systems of coastal power plants and related prevention and control measures began in the 1970s (Graham et al., 1975). In the early 1990s, Rajagopal et al., (1991a; b) investigated the attachment of fouling organisms to the cooling water pipes of the Madras Atomic Power Station in India through a remotely operated vehicle. Since 2000, the number of relevant studies has gradually increased (Satpathy et al., 2010; Nápoles-Rivera et al., 2012; George et al., 2016; Barath Kumar et al., 2017; Xu et al., 2021). For instance, Florin et al. traced the mussels in the Bothnian Sea that appeared in the vicinity of a nuclear power plant in Sweden (Florin et al., 2013). In recent years, several monitoring and early-warning systems and decision support systems for marine organisms in the cooling water systems of nuclear power plants have been developed and put into practice. (Tang et al., 2017; Zhang et al., 2017; Lu et al., 2018). Wood and Marsh (1999) conducted a comprehensive study on the control of bryozoans. A targeted prevention and control experiment was carried out on the attachment of *Dreissena polymorpha* to the Pickering Nuclear Generating Station. The focus of research on the prevention and control of blockages in the cooling water systems of nuclear power plants has shifted from passive defense measures to active prevention measures and mechanisms.

The impact of biofouling on cooling water systems has gradually attracted the attention of nuclear power plants and safety management departments. However, the relevant research work that has been carried out at present is not targeted enough, and the understanding of the temporal and spatial variation law of the species, quantity, accumulation and succession of marine fouling organisms is insufficient. The investigation and research work is often disconnected from the application management work, so that the corresponding prevention and removal measures are inappropriate. The effective prevention and control of biofouling rely on a full understanding of the attachment patterns and basic biological information of fouling organism communities. Therefore, in this study, we conducted a 1-year simulated concrete panel test in Xinghua Bay to systematically understand the community composition of fouling organisms and the larval attachment period, seasonal succession, cumulative attachment, and spatial distribution of the key fouling organism populations in this sea area, evaluated the current status and impact of biofouling, and developed economical and efficient treatment programs.

2 Materials and methods

2.1 Study area

Xinghua Bay is located northwest of the Taiwan Strait. It is a semiclosed coastal bay. The mouth of the bay faces southeast, and the water flow from the bay passes the Nanri Islands and goes into the Taiwan Strait through the Xinghua waterway and the Nanri waterway. The bay has strong semidiurnal tides. This area is dominated by a subtropical marine monsoon climate, with an average annual water temperature of 19.7°C and a multiyear average seawater salinity of 31.0. The experimental site is located in the northeast of Xinghua Bay, near the Xiaomai Island, about 2.8km away from the water intake of Fuqing Nuclear Power Plant. The sea area is relatively open and the water flow is smooth (Figure 1).

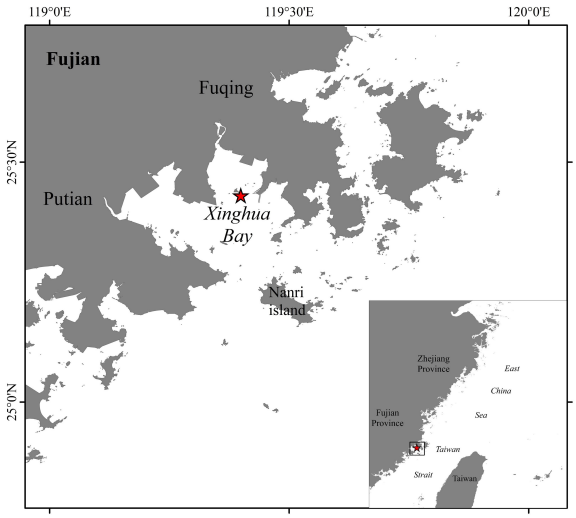

FIGURE 1
Location of biofouling investigation in Xinghua Bay.

2.2 Sampling strategy and laboratory methods

An experimental floating raft (Figure 2) was set up in Xinghua Bay at a water depth of 9 m. Each panel consisted of a 15-cm-long × 15-cm-wide × 2-cm-thick cement concrete test panel (Figure 2) with a surface roughness close to that of the tunnel wall to faithfully simulate the attachment of fouling organisms in actual water intake facilities. A screw hole with a diameter of approximately 0.8-1 cm was drilled at the center of each of the four corners (2.5 cm × 2.5 cm) of each cement slab, and appropriate stainless steel screws were used for fixation. The effective sampling area of each test panel was 200 cm^2. The immersion cycles of the monthly test panels (MTPs), seasonal test panels (STPs), semiannual test panels (SATPs), and annual test panels (ATPs) were monthly, quarterly, semiannually, and annually, respectively. A total of 12 groups of monthly accumulation test panels (MATPs) were immersed in the water at the start, and one group of MATPs was removed every month until all groups of MATPs had been removed after 12 months (Figure 3). Each group of test panels was placed perpendicular to the sea surface in two layers (a top layer and a bottom layer). The top test panels were placed 20-30 cm below the water surface, and the bottom test panels were approximately 5 m below the water surface. The test panels and samples were preserved in a 5% formalin solution. All individuals were identified to the species level or the lowest taxonomic level possible. The biomass was recorded as the wet weight.

A UTBI-001 water temperature data logger was used to simultaneously measure the water temperature of the top and bottom layers once every 2 hours. The measure of transparency was calculated using the secchi disc. The salinity, pH, and dissolved oxygen (DO) of the water body were measured with a YSI ProDSS multiparameter water quality meter.

The dominant species of the fouling organisms were analyzed using the index of relative importance (IRI) as follows:

$$IRI = (W + N) \cdot F \cdot 10^4$$

where W is the percentage of the biomass of a particular species out of the total biomass, N is the percentage of the density of a particular species out of the total density, and F is the frequency of a particular species.

Analyses of the community structure and Bray–Curtis similarity were performed using Primer 7.0. One-way analysis of variance was conducted with SPSS 19.0 to examine the differences in parameters (such as species number, density, and biomass) of the marine fouling community. Diagrams were produced using ArcMap 10.7.

3 Results

3.1 Water temperatures

No significant difference was observed between the water temperatures of the top and bottom layers where the test panels were placed throughout the year. The average water temperature in July–September was higher than 30°C, and the average water temperature in January was the lowest out of the entire year (Figure 4).

FIGURE 2
Test panel, hanging plate fixing device and experimental floating raft.

3.2 Species composition

A total of 78 species of fouling organisms were recognized in this sea area based on the MTPs, STPs, SATPs, ATPs, and MATPs. According to the occurrence frequency and attachment amount, *Amphibalanus reticulatus* was the absolute dominant species in the fouling organism community in this sea area. Other dominant species on the STPs, SATPs, ATPs, and MATPs included *Perna viridis*, *Podocerus brasiliensis* and *Caprella equilibra*. *Anthopleura* sp., *Ectopleura crocea*, *Pennaria disticha*, *Platynereis bicanaliculata* and *Herdmania momus* were also common species in the fouling organism community in this sea area. The adherent algae on the top test panels were the main difference from the bottom test panels. The other species were not significantly different (Figures 5, 6).

3.3 Attachment amount and its spatio-temporal variation

June–October was the peak period of attachment. The attachment density on the bottom panels was the highest in June, reaching 103,650 ind./m^2, and the attachment biomass of the top panels was the highest in July, reaching 7085.5 g/m^2. November to March was the off-season for attachment (Figures 7, 8). Significantly more attachment was observed in summer than in the other three seasons, and the same trend was observed for the second half of the year compared to the first half (Figure 9). The attachment thickness, density, and biomass of the summer (June-August) bottom STP reached 20 cm, 105,150 ind./m^2, and 19,274.50g/m^2, respectively. The attachment thickness, density, and biomass of the annual (December to November of next year) bottom ATP reached 40 cm, 27,300 ind./m^2, and 17,762.50 g/m^2, respectively. The attachment amount on the bottom test panels was slightly higher than that on the top test panels.

3.4 Seasonal succession of communities

The attachment period of the fouling organism community in this sea area can be roughly divided into four stages (Figures 10, 11).

Stage I: From December to February of the following year, the attachment density and biomass were low, and only a small number of hydroids and amphipods were attached. The representative species were *E. crocea* and *C. equilibra*.

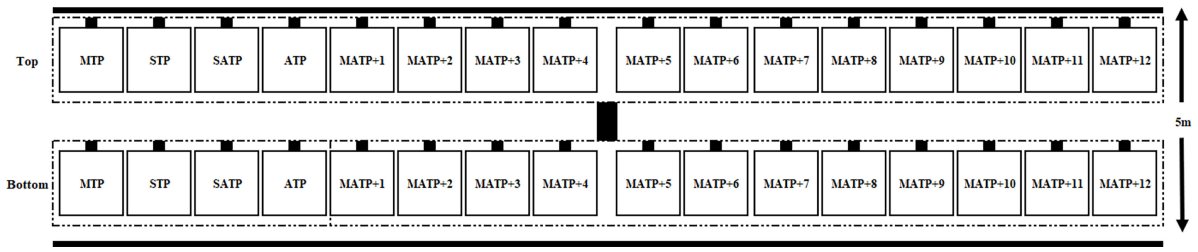

FIGURE 3
Deployment schematic diagram of the test panels installation. MTP, monthly test panel; STP, seasonal test panel; SATP, semi-annual test panel; ATP, annual test panel; MATP, monthly accumulation test panel.

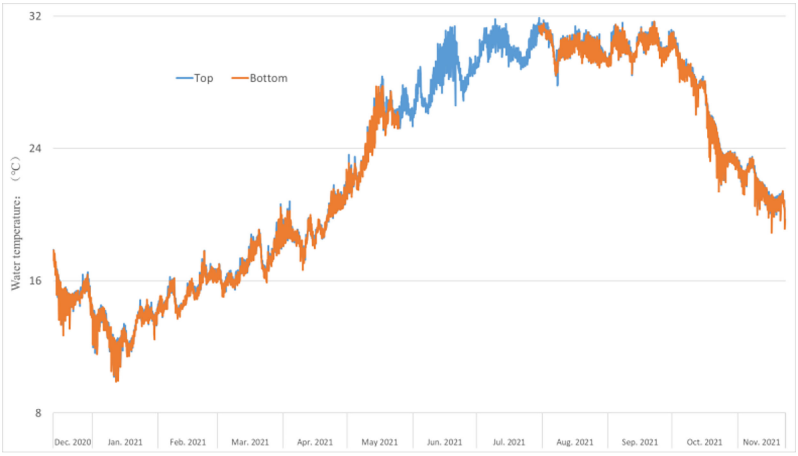

FIGURE 4
Trend chart of monthly average water temperature change from December 2020 to November 2021.

Stage II: From March to May, the community composition was similar to that in Stage I, although the attachment amount was much higher than that in Stage I. The main populations included algae, hydroids and amphipods. The representative species were *Ulva lactuca*, *Stenothoe gallensis*, *C. equilibra*, *Caprella scaura*, and *E. crocea*.

Stage III: From June to October, when attachment plateaued, the attachment density and biomass were high, and the dominant

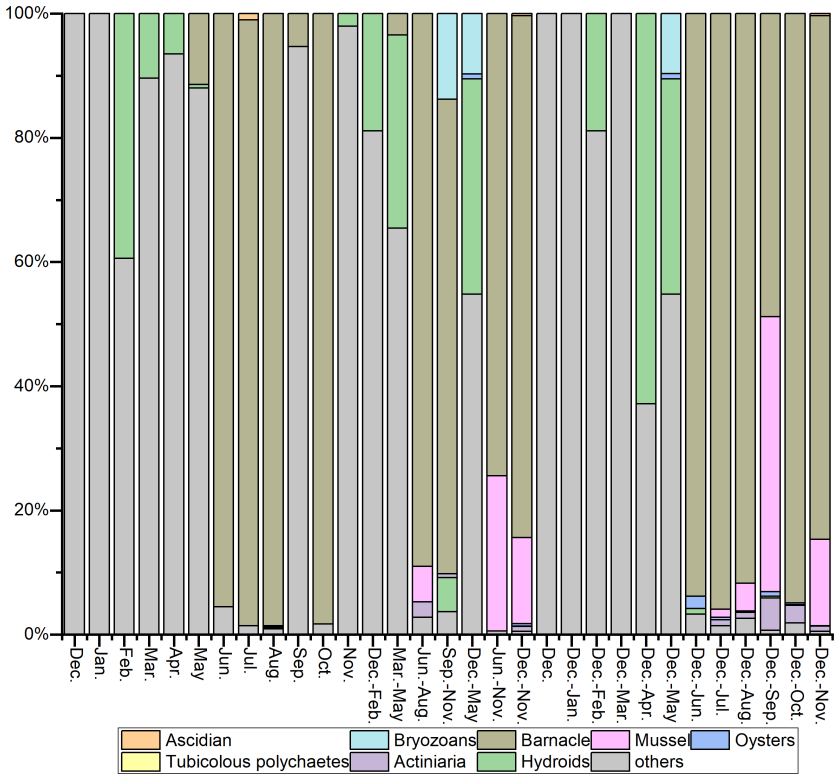

FIGURE 5
Biomass composition of the top test panels of MTPs and MATPs.

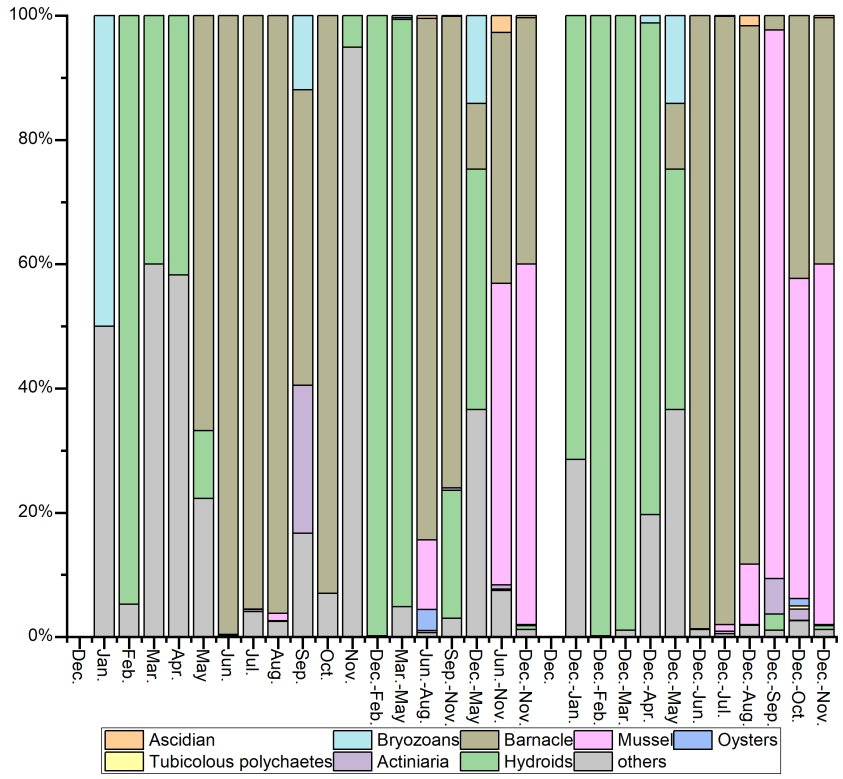

FIGURE 6
Biomass composition of the bottom test panels MTPs and MATPs.

fouling organisms, such as barnacles, mussels, oysters, actiniaria, tubicolous polychaetes, and bryozoans, were all observed. In particular, barnacles were absolutely dominant, and their representative species included *A. reticulatus*, *P. viridis*, *Saccostrea kegaki*, *P. brasiliensis*, and *Elasmopus pectenicrus*.

Stage IV: In November, attachment started gradually declining, and only a small number of hydroids and amphipods were observed. The representative species were *P. brasiliensis* and *P. disticha*.

4 Discussion

4.1 Species composition and its harm

The dominant sessile species with calcified shells are the most detrimental to the safety of cooling water systems, and the most representative sessile species is *A. reticulatus*, which was the dominant species by attachment amount in the fouling organism community in Xinghua Bay. During the peak period, *A. reticulatus* occupied almost the entire surface of the attachment substrate, and the empty shells of *A. reticulatus* and spaces between *A. reticulatus* individuals could also provide habitats, foraging space, and shelter for other migratory species.

The second most dominant species were *P. viridis* and *S. kegaki*, which had relatively large amounts of attachment. These animals can accumulate for a long time and squeeze out other small and medium-sized individuals or even occupy the entire surface of an attachment substrate. Other common fouling species with calcified shells included tubicolous polychaetes (such as Sabellidae and *Hydroides*).

In addition, although algae (such as *Ulva*), hydroids (such as *E. crocea*, *P. disticha*, *Obelia*), Actiniaria (such as *Anthopleura*), Bryozoans (such as *Biflustra grandicella*, *Bugula neritina*), and ascidians (such as *H. momus*) do not firmly attach to the facilities *via* calcified shells, they grow upward in clusters and thus reduce the water intake efficiency (Huang and Cai, 1984; Huang, 2008; Yan et al., 2021).

4.2 Community succession

The biofouling in this sea area underwent approximately four stages. The attachment density and biomass of the fouling

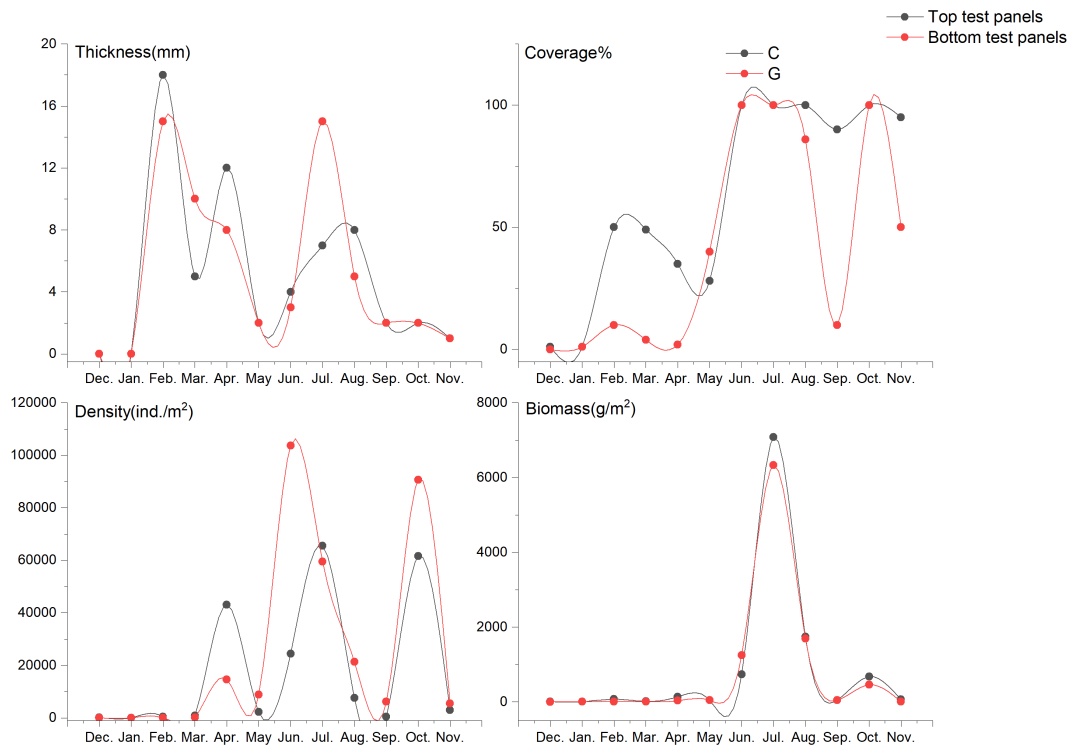

FIGURE 7
The attachment thickness, coverage, density and biomass of MTPs.

organisms were both extremely low from December to February of the following year (*E. crocea* was the dominant species in Stage I), slightly increased from March to May (*Ulva* and *E. crocea* were the dominant species in Stage II), and reached their highest values in June–October when the fouling organisms fully entered the blooming period (especially in July, when the attachment density and biomass of the top MTPs reached 65,500 ind./m^2 and 7085.5 g/m^2, respectively, and the attachment density and biomass of the bottom MTPs reached 59450 ind./m^2 and 6327.5 g/m^2, respectively). Almost all dominant fouling organism populations were observed, and the representative dominant species included *A. reticulatus*, *P. viridis, S. kegaki*, *Anthopleura* sp., *Branchiomma cingulatum*, *B. grandicella*, and *H. momus*. Stage IV (after November) was the off-season for attachment, and only a small number of *P. brasiliensis* and *P. disticha* were observed.

Compared with the results of the previous study conducted in the southeastern waters of the Xinghua Bay (Wu et al., 2019), there is little difference in the community composition, and the main dominant species are still represented by *A. reticulatus, P. viridis, E. crocea, B. grandicella*, etc.. However, the attachment amount of fouling organisms in this survey is significantly higher than the survey results of 2017 to 2018. Taking the bottom summer panels (June-August) as an example, the density and biomass of 2020 to 2021 can reach 105150 ind/m^2 and 19260.0 g/m^2 respectively, which are significantly higher than the 24375 ind/m^2 and 8742.1 g/m^2 investigated during 2017 to 2018. This may be due to the fact that the survey site is located in the central waters, far from the shore, and the environmental conditions are more beneficial for the attachment and growth of fouling organisms.

Barnacles are often the large pioneer adherent species in fouling communities, playing an important role in the succession and development of the communities from scratch and from simple to complex (Yan et al., 2012). In general, barnacle larvae can experience two peaks of attachment. The first-generation larvae reproduced by the previous generation begin to attach in the second half of May, and their number first peaks in June or July and drops greatly in August and September (Huang and Cai, 1984; Lin et al., 2017). In the initial stage, *A. reticulatus* and *Balanus trigonus* were comparable in number, but starting in June, *A. reticulatus* almost completely overwhelmed *B. trigonus*.

With the extension of the immersion cycle of the test panels, *P. viridis* gradually replaced the dominant position of barnacles and even occupied most of the surface of the attachment substrate, squeezing out the living space of other dominant species, such as *A. reticulatus* and *S. kegaki*. At this point, the

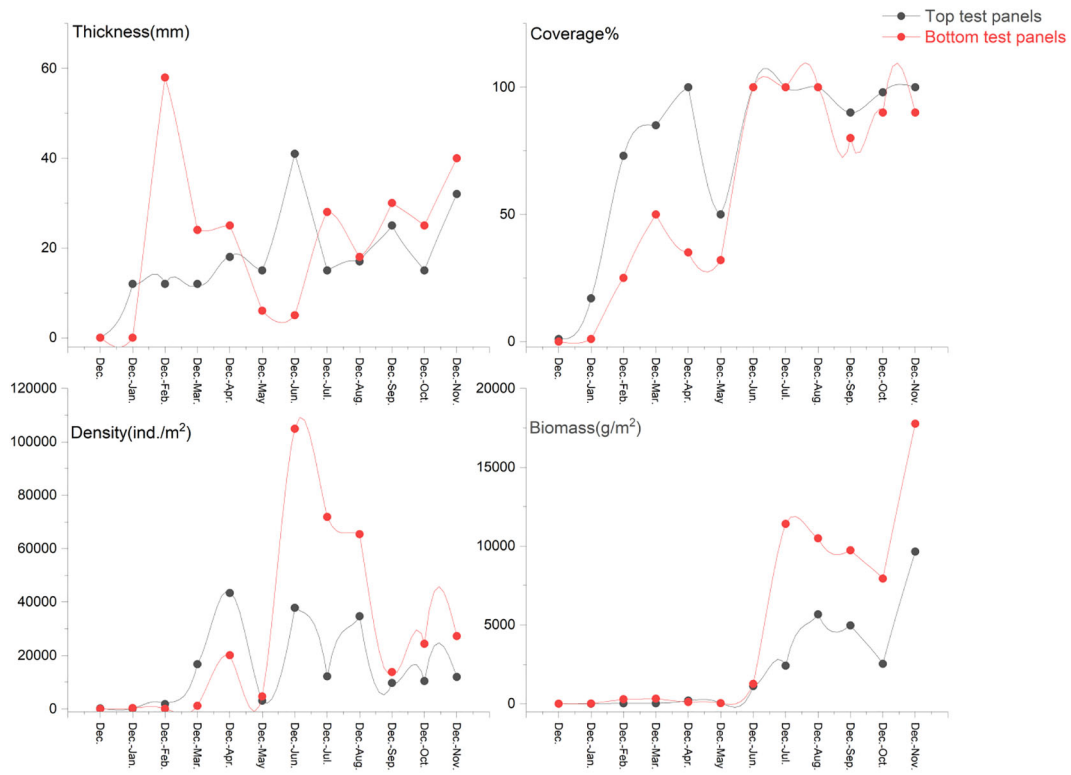

FIGURE 8
The attachment thickness, coverage, density and biomass of MATPs.

fouling organism community reached a relatively stable state (Huang and Cai, 1984). In addition, the attachment substrate provided more diverse and complex habitat spaces, including habitat spaces for organisms with low requirements for attachment space, such as sponges, actiniaria, ascidian, migratory polychaetes, amphipods, and crabs.

4.3 Influencing factors and prevention suggestions

Compared with other facilities, cooling water ystem facilities can significantly strengthen and accelerate the biofouling process. First, the concrete wall of the cooling water system can be an excellent habitat for the attachment and growth of fouling organisms. Second, the continuous flow of water rich in oxygen and food allows for a constant supply of new larvae. Third, the reduction in sediment deposition increases the survival rate of fouling organisms. Fourth, there is a lack of biological competition and predator threat (Huang and Cai, 1984; Huang, 2008; Satpathy et al., 2010; Lin et al., 2012; Lin et al., 2014). Temperature is the most important environmental factor in the geographical distribution of fouling organisms (Yan et al., 2020). The temperature adaptability of organisms is the essential determinant of the spatial differences of fouling organism communities across different climatic zones and is the dominant factor in the seasonal succession of biological communities on a small scale. The seasonal succession pattern in this sea area showed that 24-30°C is a relatively suitable temperature range for fouling organism larvae and that 15°C is the tolerance limit of most larvae (Yan et al., 2020). Light affects the vertical distribution of fouling organisms (Cai and Huang, 1988). Due to the high turbidity and no much light reaches deep-sea areas, almost no algae were observed below a water depth of 5 m in the study waters.

Scientifically effective control plans for fouling organisms need to be based on the environmental conditions and a comprehensive understanding of the composition of the fouling organisms in the sea area and their attachment patterns. We should determine these through targeted preliminary investigations and full research studies, especially on the breeding period, population dynamics, succession pattern, and cumulative effect of the main prevention and control strategies. Targeted and differentiated prevention and control strategies should be implemented at the initial stage of larval attachment, and the frequency and intensity of prevention

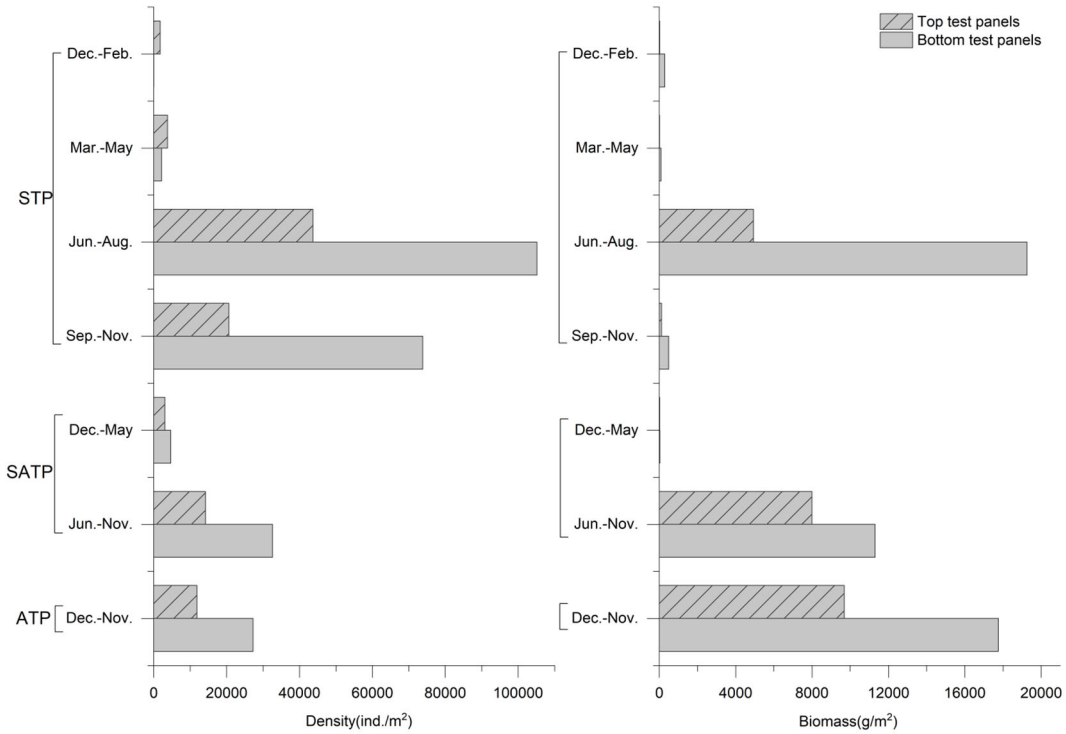

FIGURE 9
The attachment density and biomass of STPs, SATPs and ATPs.

and control should be increased during the peak attachment season. Only in this way can a cost-effective treatment effect be achieved. The biological control of fouling should be avoided in the adult phase to reduce the use of biological control agents and avoid secondary blockage caused by a large number of broken shells.

The focus months of the prevention and control of fouling organisms in this sea area are June to October, when both the frequency and intensity of prevention and control need to be strengthened. To ensure the continuity of prevention and control, targeted prevention and control measures can be started in late May. The focus species of prevention and

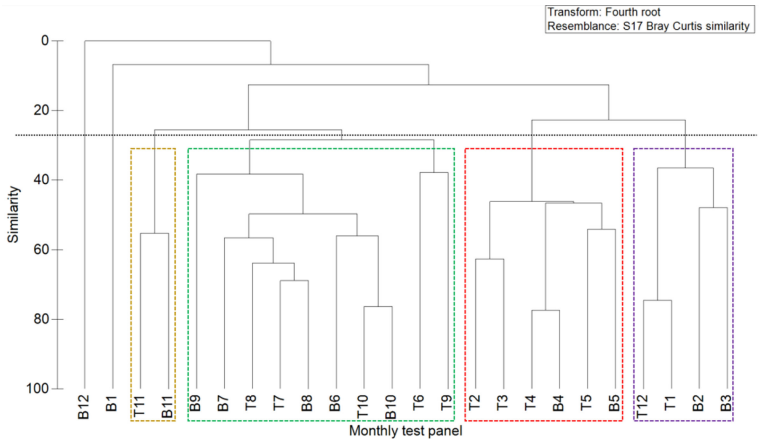

FIGURE 10
Clustering of the Bray–Curtis similarity of the marine fouling communities on monthly test panels.

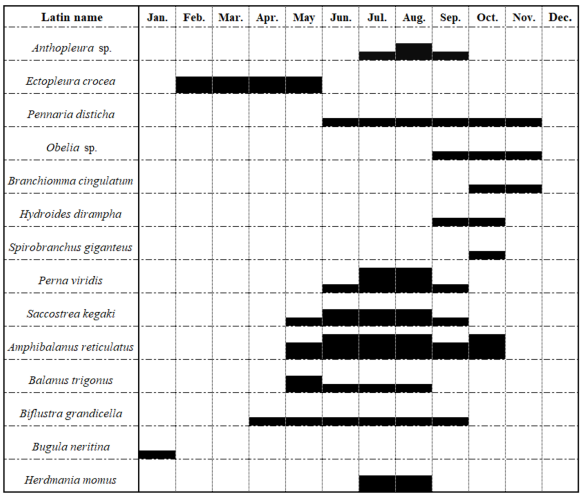

FIGURE 11
The attachment period of the major species.

control are *A. reticulatus* and *P. viridis*. The larvae of the two species have roughly the same peak season and the largest proportions of the attachment amount. In addition, their bodies can create a broader three-dimensional space for the attachment of other fouling species. *A. reticulatus* is superior to *P. viridis* in its short-term attachment strength, but the long-term threat of *P. viridis* is greater. The attachment intensity is low from November to early the following May, so a less strict prevention and control measure can be adopted for this period.

After decades of development of antifouling technologies for coastal power plants, a variety of prevention and control measures have been devised, including physical isolation, the high flow rate method, heat treatment, mechanical removal, chlorine production from seawater by electrolysis, and so on. The methods can be used alone or in combination. In addition, we must also better understand the life history and physiological characteristics of fouling organisms, explore the influencing factors of fouling organism attachment (temperature, water depth, flow rate, light, water quality, and attachment substrate), and establish scientific and effective early-warning models for fouling organisms. To provide scientific basis for inhibiting the attachment of fouling organisms, the formation of mucous membrane and disinfection and sterilization.

5 Conclusions

Fully understanding the composition of fouling organisms and their attachment patterns (especially the breeding periods, population dynamics, succession patterns, and cumulative effects of the main control species) is a prerequisite for the scientific prevention and control of biofouling. The research shows that the biofouling in Xinghua Bay is approximately classified into four stages, of which the attachment peak of fouling organisms is from June to October, with a large attachment density and biomass. The dominant species include *A. reticulatus*, *P. viridis*, *S. kegaki*, *Anthopleura*, *Branchiomma cingulatum*, *B. grandicella* and *H. momus*, etc. Of them *A. reticulatus* is the pioneer of fouling community, but with the extension of the immersion cycle of the test panels, *P. viridis* gradually replaced the dominant position and even occupied most of the surface of the attachment substrate. To implement targeted prevention and control strategies in the prosperous period of larvae of fouling organisms, and to increase the frequency and intensity of prevention and control during this period, is the key to achieve economic and efficient treatment effect. Better understanding the life history and ecological characteristics of the main control species of fouling organisms, clarifying the effects of the influencing factors on fouling organisms (such as temperature, water depth, flow rate, light, water quality, and attachment substrate), and establishing scientific and effective early-warning models are future directions for the development and implementation of scientific prevention and control measures for fouling organisms.

Contribution to the field

Fully understanding the composition of fouling organisms and their attachment patterns (especially the breeding periods,

population dynamics, succession patterns, and cumulative effects of the main control species) is a prerequisite for the scientific prevention and control of biofouling. The main dominant species of fouling organisms have relatively stable attachment cycles. Adopting targeted and differentiated prevention and control strategies at the initial stage of larval attachment and increasing the frequency and intensity of prevention and control during the peak attachment period are the keys to economic and efficient control. The biological control of fouling should be avoided in the adult phase to reduce the use of biological control agents and avoid secondary blockage caused by a large number of broken shells. Better understanding the life history and ecological characteristics of the main control species of fouling organisms, clarifying the effects of the influencing factors on fouling organisms, and establishing scientific and effective early-warning models are future directions for the development and implementation of scientific prevention and control measures for fouling organisms.

Data availability statement

The original contributions presented in the study are included in the article/Supplementary Material. Further inquiries can be directed to the corresponding authors.

Author contributions

HL: Investigation and sampling, data analysis and processing, paper writing. YH: Sample identification. YL: Investigation assistance. SZ: Sample identification, data processing. SY: Data processing. KL: Data processing, drafting. JM: Investigation and sampling, sample identification. JL: Investigation and sampling, sample identification. XH: Sample identification. SF: Sample identification. WX: Investigation and sampling. ZL: Proofread and guide. All authors contributed to the article and approved the submitted version.

Acknowledgments

This work was supported by the National Science Foundation of China under contract (No. 42076237), the Scientific Research Foundation of the Third Institute of Oceanography, MNR, (No. 2018023). We thank Qiang Wang, Xiao Fan and Jie Wang from Fujian Fuqing Nuclear Power Co., Ltd. for the assistance of this study.

Conflict of interest

YL is employed by Fujian Fuqing Nuclear Power Co. Ltd.

The remaining authors declare that the research was conducted in the absence of any commercial or financial relationships that could be construed as a potential conflict of interest.

Publisher's note

All claims expressed in this article are solely those of the authors and do not necessarily represent those of their affiliated organizations, or those of the publisher, the editors and the reviewers. Any product that may be evaluated in this article, or claim that may be made by its manufacturer, is not guaranteed or endorsed by the publisher.

Supplementary material

The Supplementary Material for this article can be found online at: https://www.frontiersin.org/articles/10.3389/fmars.2022.1107087/full#supplementary-material

References

Barath Kumar, S., Mohanty, A. K., Das, N. P. I., Satpathy, K. K., and Sarkar, S. K. (2017). Impingement of marine organisms in a tropical atomic power plant cooling water system. *Mar. pollut. Bull.* 124 (1), 555–562. doi: 10.1016/j.marpolbul.2017.07.067

Cai, R. X., and Huang, Z. G. (1988). Studies on the orientation of cirripedes II orientation on hosts and natural habitats. *Oceanol. Limnol. Sin.* 19 (4), 321–328. doi: 10.1300/J496v17n03_02

Callow, M. (1990). Ship fouling: problems and solutions. *Chem. Ind. Lond* 54, 123–127. doi: 10.1016/0033-0655(90)85007-K

Cao, W., Yan, T., Li, Z., Li, J., and Cheng, Z. (2013). Fouling acorn barnacles in China–a review. *Chin. J. Oceanol. Limnol.* 31 (4), 699–711. doi: 10.1007/s00343-013-2275-z

Dixon, D. (2015). *Best management practices manual for preventing cooling water intake blockages* (Palo Alto, CA: EPRI). 3002006735.

Florin, A.-B., Mo, K., Svensson, F., Schagerstrm, E., Kautsky, L., and Bergstrm, L. (2013). First records of conrad's false mussel, mytilopsis leucophaeata (Conrad 1831) in the southern bothnian Sea, Sweden, near a nuclear power plant. *BioInvasions Records* 2 (4), 1–8. doi: 10.3391/bir.2013.2.4.07

George, R. P., Kamachi Mudali, U., and Raj, B. (2016). Characterizing biofilms for biofouling and microbial corrosion control in cooling water systems. *Anti-Corrosion Methods Materials* 63 (6), 477–489. doi: 10.1108/acmm-07-2014-1401

Graham, J. W., Moncreiff, R. W., Benson, P. H., and Stock, J. N. (1975). Heat treatment for the control of marine fouling at coastal electric generating stations. *OCEAN 75 Conference*. IEEE, 926–930. doi: 10.1109/oceans.1975.1154027

Greene, J. K., and Grizzle, R. E. (2007). Successional development of fouling communities on open ocean aquaculture fish cages in the western gulf of Maine, USA. *Aquaculture* 262 (2-4), 289–301. doi: 10.1016/j.aquaculture.2006.11.003

Huang, Z. G. (2008). *Marine fouling and its prevention (II)* (Beijing, China: China Ocean Press).

Huang, Z. G., and Cai, R. X. (1984). *Marine fouling and its prevention (I)* (Beijing, China: China Ocean Press).

Lin, H. S., Wang, J. J., Liu, W., Liu, K., Zhang, S. Y., He, X. B., et al. (2017). Fouling community characteristics in subtropical coastal waters of the southwestern East China Sea. *Acta Oceanol. Sin.* 36 (10), 70–78. doi: 10.1007/s13131-017-1007-1

Lin, H. S., Wang, J. J., Zheng, C. X., Li, R. G., Zheng, F. W., Lin, J. H., et al. (2012). Ecological research of marine fouling in Dongshan Bay, China. *Acta Oceanol. Sin.* 34 (6), 160–169. doi: 0253-4193(2012)06-0160-10

Lin, H. S., Wang, J. J., Zheng, C. X., Lin, J. H., Huang, Y. Q., He, X. B., et al. (2014). Marine fouling in quanzhou bay, China. *Acta Oceanol. Sin.* 36 (4), 100–109. doi: 10.3969/j.issn.0253-4193.2014.04.007

Liu, K., Lin, H. S., Li, Z., He, X. B., Huang, Y. Q., Lin, J. H., et al. (2020). Community structure of macro-fouling organisms in the northeastern waters of the pingtan island, East China Sea. *Haiyang Xuebao* 42 (6), 70–82. doi: 10.3969/j.issn.0253–4193.2020.06.009

Lu, H., Meng, Y., and Duan, Y. (2018). Research on monitoring and early-warning system of marine organisms for the intake of nuclear power plants. *Anim. Husbandry Feed Sci.* 10 (4), 236–240.

Maruzzo, D., Conlan, S., Aldred, N., Clare, A. S., and Høeg, J. T. (2011). Video observation of surface exploration in cyprids of balanus amphitrite: the movements of antennular sensory setae. *Biofouling* 27 (2), 225–239. doi: 10.1080/08927014.2011.555534

Nápoles-Rivera, F., Bin-Mahfouz, A., Jiménez-Gutiérrez, A., El-Halwagi, M. M., and Ponce-Ortega, J. M. (2012). An MINLP model for biofouling control in seawater-cooled facilities. *Comput. Chem. Eng.* 37, 163–171. doi: 10.1016/j.compchemeng.2011.09.008

Peng, Y., Li, Z., Lin, H. S., Liu, K., Huang, Y. Q., Lin, J. H., et al. (2020). Community structure and its spatio-temporal patterns of fouling organism in nearshore waters of putian, China. *J. Appl. Oceanogr.* 39 (1), 35–41. doi: 10.3969/J.ISSN.2095-4972.2020.01.005

Pradhan, N. N., Gohad, N. V., Orihuela, B., Burg, T. C., Birchfield, S. T., Rittschof, D., et al. (2011). Development of an automated algorithm for tracking and quantifying barnacle cyprid settlement behavior. *J. Exp. Mar. Biol. Ecol.* 410, 21–28. doi: 10.1016/j.jembe.2011.10.001

Qvarfordt, S., Kautsky, H., and Malm, T. (2006). Development of fouling communities on vertical structures in the Baltic Sea. *Estuar. Coast. Shelf Sci.* 67 (4), 618–628. doi: 10.1016/j.ecss.2006.01.004

Rajagopal, S., Sasikumar, N., Azariah, J., and Nair, K. V. K. (1991a). Some observations on biofouling in the cooling water conduits of a coastal power plant. *Biofouling* 3 (4), 311–324. doi: 10.1080/08927019109378185

Rajagopal, S., Venugopalan, V. P., Nair, K. V. K., and Azariah, J. (1991b). Biofouling and its control in a tropical coastal power station: A case study. *Biofouling* 3 (4), 325–338. doi: 10.1080/08927019109378186

Sammarco, P. W., Atchison, A. D., and Boland, G. S. (2004). Expansion of coral communities within the northern gulf of Mexico via offshore oil and gas platforms. *Mar. Ecol. Prog. Ser.* 280, 129–143. doi: 10.3354/meps280129

Satpathy, K. K. (1990). Biofouling control measures in power plant cooling systems - a brief overview. In Nair, K. V. K., and Venugopalan, V. P. (eds) *Marine Biofouling and Power Plants, Bhabha Atomic Research Centre, Bombay* (Kalpakkam, India). 153–156.

Satpathy, K. K., Mohanty, A. K., Sahu, G., Biswas, S., and Selvanayagam, M. (2010). Biofouling and its control in seawater cooled power plant cooling water system - a review. *Nuclear power, Pavel Tsvetkov (Ed.), InTech,* 191–242.Available at: http://www.intechopen.com/books/nuclear-power/biofouling-and-its-control-in-seawater-cooled-power-plantcooling-water-system-a-review-

Tang, Z., Cheng, F., Jin, X., Sun, L., Bao, R., and Liu, Y. (2017). An automatic marine-organism monitoring system for the intake water of the nuclear power plant. *Ann. Nucl. Energy* 109, 208–211. doi: 10.1016/j.anucene.2017.05.040

Tasso, M., Conlan, S. L., Clare, A. S., and Werner, C. (2012). Active enzyme nanocoatings affect settlement of balanus amphitrite barnacle cyprids. *Advanced Funct. Materials* 22 (1), 39–47. doi: 10.1002/adfm.201101173

Wood, T. S., and Marsh, T. G. (1999). Biofouling of wastewater treatment plants by the freshwater bryozoans, *Plumatellavaihiriae* (Hastings, 1929). *Water Res.* 33 (3), 609–614. doi: 10.1016/S0043-1354(98)00274-7

Wu, J. W., Li, Z., Lin, H. S., Liu, K., Huang, Y. Q., Lin, J. H., et al. (2019). Community structure and its spatio-temporal patterns of marine fouling organisms in xinghua bay, China. *J. Appl. Oceanogr.* 38 (4), 578–584. doi: 10.3969/J.ISSN.2095-4972.2019.04.013

Xu, Z. M., Jiang, X., Liu, Z. D., Hu, Y. H., and Li, Y. F. (2021). Experimental investigation of microbial fouling and heat mass transfer characteristics on Ni-p modified surface of heat exchanger. *J. Thermal Sci.* 30, 271–278. doi: 10.1007/s11630-020-1304-4

Yan, T., Li, Z. F., Hu, Y. F., Li, X. X., Cao, W. H., Luo, W. J., et al. (2012). A review on the balanomorph barnacles in the coastal waters of China. *Acta Ecol. Sin.* 32 (16), 5230–5241. doi: 10.5846/stxb201202130185

Yan, T., Lin, M., Cao, W., Han, S., and Song, X. (2021). Fouling characteristics of cnidarians (Hydrozoa and anthozoa) along the coast of China. *J. Oceanol. Limnol.* 39, 2220–2236. doi: 10.1007/s00343-021-0242-7

Yan, J., Lin, M. Q., Cao, W. H., Lin, Y. G., and Zou, L. (2020). Influence of temperature on larval development and settlement of the acorn barnacle *Amphibalanus reticulatus*. *J. Trop. Oceanogr.* 39 (5), 55–61. doi: 10.11978/2019124

Yan, T., and Yan, W. X. (2003). Fouling of offshore structures in China-a review. *Biofouling* 19 (sup1), 133–138. doi: 10.1080/0892701021000057927

Yan, T., Yan, W., Dong, Y., Wang, H., Yan, Y., and Liang, G. (2006). Marine fouling of offshore installations in the northern beibu gulf of China. *Int. Biodeterioration Biodegradation* 58 (2), 99–105. doi: 10.1016/j.ibiod.2006.07.007

Yan, T., Yan, W. X., Dong, Y., Wang, H. J., Yan, Y., and Liang, G. H. (2009). Marine fouling on floating installations west of dongsha islands, the northern south China Sea. *Int. Biodeterioration Biodegradation* 63 (8), 1079–1087. doi: 10.1016/j.ibiod.2009.09.003

Zhang, H., Cao, W., Wu, Z., Song, X., Wang, J., and Yan, T. (2015). Biofouling on deep-sea submersible buoy systems off xisha and dongsha islands in the northern south China Sea. *Int. Biodeterioration Biodegradation* 104, 92–96. doi: 10.1016/j.ibiod.2015.05.003

Zhang, Y. F., Wang, G. C., Xu, Y., Sougrat, R., and Qian, P. Y. (2011). The effect of butenolide on behavioural and morphological changes of marine fouling species balanus amphitrite and bugula neritina. *Biofouling* 27 (5), 467–475. doi: 10.1080/08927014.2011.583985

Zhang, Q., Zhou, S., Wang, X. H., and Zhang, J. Q. (2018). Design and implementation of marine biological preparedness monitoring system of nuclear power plant. *DEStech Trans. Comput. Sci. Eng. (wcne)*, 453–457. doi: 10.12783/dtcse/wcne2017/19897

frontiers | Frontiers in Marine Science

TYPE Original Research
PUBLISHED 06 January 2023
DOI 10.3389/fmars.2022.1098232

OPEN ACCESS

EDITED BY
Kaizhi Li,
South China Sea Institute of Oceanology (CAS), China

REVIEWED BY
Song Feng,
Institute of Oceanology (CAS), China
Xuejia He,
Jinan University, China

*CORRESPONDENCE
Xiaocheng Wang
xcwang@nmemc.org.cn
Chunjiang Guan
cjguan@nmemc.org.cn

SPECIALTY SECTION
This article was submitted to Marine Pollution, a section of the journal Frontiers in Marine Science

RECEIVED 14 November 2022
ACCEPTED 08 December 2022
PUBLISHED 06 January 2023

CITATION
Wang X, Jin Q, Yang L, Jia C, Guan C, Wang H and Guo H (2023) Aggregation process of two disaster-causing jellyfish species, *Nemopilema nomurai* and *Aurelia coerulea*, at the intake area of a nuclear power cooling-water system in Eastern Liaodong Bay, China.
Front. Mar. Sci. 9:1098232.
doi: 10.3389/fmars.2022.1098232

Aggregation process of two disaster-causing jellyfish species, *Nemopilema nomurai* and *Aurelia coerulea*, at the intake area of a nuclear power cooling-water system in Eastern Liaodong Bay, China

Xiaocheng Wang*, Qingqing Jin, Lu Yang, Chuan Jia, Chunjiang Guan*, Haining Wang and Hao Guo

National Marine Environmental Monitoring Center, Dalian, China

The intake safety of nuclear power cooling-water systems (NPCSs) is an important aspect of operational safety of nuclear power plants (NPPs). The blockages caused by aberrant outbreaks of various aquatic organisms have seriously affected operational safety. Large jellyfish constitute the main groups of marine organisms responsible for these blockages. The processes of aggregation and the relationships of two major disaster-causing scyphozoan jellyfish species, *Nemopilema nomurai* and *Aurelia coerulea*, with four environmental factors at the intake area of an NPCS in Eastern Liaodong Bay, China, were investigated in 2019 and 2020. The findings revealed that *A. coerulea* ephyrae were present in the surrounding ports in mid-May; however, *N. nomurai* ephyrae were absent during the survey period in this study, and the medusae of *N. nomurai* started appearing from late May. The individual growth and relative biomass (RB) of the jellyfish increased rapidly from late June to July and decreased rapidly thereafter, in September. The RB of *N. nomurai* was highly correlated to the sea surface temperature (SST) and levels of dissolved oxygen (DO) in the region. The RB increased with increasing SST and decreased at increasing DO levels. The RB of *A. coerulea* was significantly negatively correlated with that of *N. nomurai*, and the peak biomass of the two species alternated over time, which could be attributed to the fact that the jellyfish species share similar ecological niches. The bell diameters were significantly positively correlated with the individual wet weights, and the value of one could be inferred from the value of the other. Although the processes of jellyfish aggregation are attributed to several factors, including interactions with environmental factors and human activities, such as fishing, the results obtained in this study would serve as an important reference and provide a basis for the prevention of jellyfish blooms in waters adjacent to NPPs. The prevention and control of jellyfish disasters at the intake area of

NPCSs are not only local concerns. Therefore, remediation from the source combined with the maximum utilization of social resources for monitoring and early warning would immensely improve the efficacy of such preventive strategies.

KEYWORDS

Liaodong Bay, *Nemopilema nomurai*, jellyfish bloom, nuclear power cooling-water system, *Aurelia coerulea*, disaster-causing jellyfish

1 Introduction

Jellyfish constitute one of the most important groups of gelatinous zooplankton and play critical roles in marine ecosystems (Mills, 1995; Hamilton, 2016). Compared with most pelagic metazoans, jellyfishes have a high water content (95% or above) but a low carbon content (Lucas et al., 2011). This explains why they are larger than non-gelatinous animals with comparable carbon contents (Pitt et al., 2013). Jellyfish can grow faster and demonstrate competitive advantages in various marine ecosystems owing to their higher metabolic rate, good adaptability, and lack of natural enemies, among other characteristics (Schneider, 1992; Dawson and Hamner, 2009; Berwald, 2017).

Blooms caused by jellyfish, especially those of the class Scyphozoa, which have metagenic life cycles, have become a common phenomenon in recent years owing to various environmental pressures, including global climate change and anthropogenic activities (Purcell et al., 2007; Richardson et al., 2009; Purcell, 2012; Dawson et al., 2015; Quinones et al., 2018; Goldstein and Steiner, 2020; Rekstad et al., 2021; Riyas et al., 2021). The sudden or aberrant increase in jellyfish biomass has caused jellyfish disasters in several parts of the globe's oceans, affecting fisheries, and damaging the safety of nuclear power cooling-water systems (NPCSs), especially in Europe, Asia, and North America (Lucas and Dawson, 2014; Schiariti et al., 2015). Jellyfish blooms were responsible for the blockage of the cooling water intakes of the Madras Atomic Power Station, in the south-western Bay of Bengal at Kalpakkam, which led to the shutdown of the power station in 1995–1996 (Masilamoni et al., 2000). An unusually large flow of jellyfish caused the shutdown of the filtering equipment in reactors 1, 2, and 3 of the Kashiwazaki Kariwa Nuclear Power Station in Japan, which forced it to reduce power output on 7 July 1999 (Takizawa, 2005). Jellyfish blooms have been appearing frequently in Korean waters since 2003 and have clogged coastal power plant cooling-water intakes (Yoon et al., 2014). In 2011, while jellyfish outbreaks in the United States, Japan, Israel, and Scotland led to the shutdown of nuclear power plants (NPPs) in these countries (Schrope, 2012).

Nemopilema nomurai is a common species of jellyfish belonging to class Scyphozoa. It has a widespread distribution and is responsible for frequent blooms in East Asian marginal seas. This jellyfish is primarily observed in the waters of China, Korea, and Japan from late spring to autumn (Dong et al., 2018). The northern parts of the East China Sea (ECS), Yellow Sea (YS), and Bohai Sea (BS) in China are considered to be the main habitats of *N. nomurai* (Kawahara et al., 2006; Dong et al., 2010). Although the origin of this large jellyfish remains controversial, field surveys and physical modeling studies have demonstrated that the Yangtze River Estuary and adjacent sea areas are possible sources of *N. nomurai* (Yoon et al., 2008; Moon et al., 2010; Sun et al., 2015). Previous studies reported that the benthic polyps of *N. nomurai* develop into medusae and are released between April and June in the Yangtze River Estuary and the adjacent sea areas (Moon et al., 2010; Dong et al., 2018). The medusae subsequently migrate to the northern side of the YS, eastern side of the ECS, and the East Sea (ES) (Moon et al., 2010; Dong et al., 2018). It has been reported that their biomass increases at rising temperatures and peaks by August (Zhang et al., 2012; Sun et al., 2015). Various environmental factors shape the distribution characteristics of jellyfish to a certain extent. Previous studies have demonstrated that the temperature and salinity of water significantly affect the distribution and abundance of *N. nomurai*, and that there is a positive relationship between the abundance of *N. nomura* and the low salinity of Changjiang Diluted Water (Yoon et al., 2008; Kitajima et al., 2020). Juvenile jellyfishes have been found in Liaodong Bay (LDB), where the waters have low salinity and high temperatures (Dong et al., 2018). During development, the juveniles and small medusae drift to the central and southern regions of the LDB, where the waters have lower temperatures and higher salinity (Dong et al., 2018).

Aurelia coerulea is one of the most common species of jellyfish living in offshore regions, and is widely distributed in tropical, subtropical, and temperate marine areas. *A. coerulea*

outbreaks have been reported in China, Japan, and Korea (Mills, 2001). The outbreaks of *A. coerulea* are different from those of *N. nomurai*, and *A. coerulea* blooms primarily occur in coastal and estuarine areas, where anthropogenic activities are higher (Sun et al., 2012). Outbreaks and aggregation of *A. coerulea* are primarily observed in the bays and temperate areas of YS and BS in China (Dong et al., 2010; Wang et al., 2012). The biomass of *A. coerulea* is particularly high in July and August in the northern coastal sea of China, and this species causes frequent disaster events in Qinhuangdao in the Hebei province, Dalian in the Liaoning province, and in Yantai, Weihai, and Qingdao in the Shandong province (Dong et al., 2010). *A. coerulea* is highly adaptable and can adapt to a wide range of temperature and salinity conditions. For instance, populations of *A. coerulea* can migrate through winter ice caps and survive at an upper temperature range of 31–32°C (Hamner et al., 1982; Hernroth and Gröndahl, 1985). *A. coerulea* can be found in waters with salinity levels of less than 10‰ up to levels of 38‰ (Russell, 1970; Papathanassiou et al., 1987; Olesen and Riisgard, 1994). The previous study had demonstrated that jellyfish outbreaks are primarily mediated by a temporal shift from polyp-dominated to medusa-dominated populations (Goldstein and Steiner 2020). The temperature and variations in temperature are key factors that control the initiation and cessation of strobilation, and an optimal increase in temperature facilitates the release of larvae and the reproduction of polyps (Kroiher et al., 2000; Ishii and Takagi, 2003; Han and Uye, 2010; Prieto et al., 2010; Wang et al., 2014). Low levels of salinity can delay or inhibit the reproduction of polyps (Purcell et al., 2009). Nutrient availability can be another important ecological driver of jellyfish blooms because it facilitates a shift in the population structure from a polyp-dominated to a medusa-dominated population (Goldstein and Steiner 2020).

The Hongyanhe Nuclear Power Plant (HYHNPP) is located in the eastern part of LDB and is currently the only operational NPP in the northern seas of China. Six units of HYHNPP, with a total installed capacity of 6.7 million kilowatts, have been fully completed and put into operation in 2022, making HYHNPP the largest operational NPP in China and the third largest operational NPP in the world. However, the intake area of the NPCS of HYHNPP has been troubled by jellyfish blooms, primarily caused by *N. nomurai* and *A. coerulea* since 2014, and this has affected the normal operation of the HYHNPP. In July 2014, a large jellyfish population entered the inlet region of the recirculating water filtration system, resulting in the shutdown of units 1 and 2 of the HYHNPP. In July 2015, a large jellyfish population flooded the inlet as a result of the rupture of the first and third barrier nets. Although massive human and material resources have been used for coping with jellyfish disasters to date, the approaches have met with limited success. The distribution characteristics of dominant disaster-causing jellyfish at the intake area of NPCSs have been reported in few studies. In addition, the regions from which these jellyfish species originate have always been a concern for managers and researchers. The sudden gathering of jellyfish can block the intake area of NPCSs, which poses as a huge safety risk and causes economic losses to NPPs. Further studies are therefore necessary for obtaining better insights into the patterns of jellyfish blooms for planning targeted measures against jellyfish disasters.

In this study, we investigated the process of aggregation and relationships of the two major disaster-causing scyphozoan jellyfish species, *N. nomurai* and *A. coerulea*, with four environmental factors at the intake area of the NPCS in Eastern LDB in 2019 and 2020. The present study aimed to elucidate the mechanism of distribution of the two jellyfish species, and the findings provide an important reference and supporting data for preventing jellyfish blooms in waters adjacent to NPPs. The study also discussed various measures for predicting and controlling jellyfish outbreaks near the HYHNPP.

2 Materials and methods

2.1 Sample collection

A total of 61 surveys were conducted at the intake area of HYHNPP in the eastern part of LDB from May to September of 2019 and 2020. Five sampling stations were set up at the intake area (Figure 1), of which the central station was set up at the inlet area of the NPCS (HYH03), two stations (HYH01 and HYH02) were located at the north-eastern side of the central station, and two stations (HYH04 and HYH05) were set up at the south-western side of the central station. The distance between two stations was approximately 2 km. Large jellyfish species were sampled using a plane anchor drift net (mesh size: 10 mm, length: 110 m, width: 15 m; Figure 2). The direction of net casting was perpendicular to the direction of the flow, and the nets were hauled with the current. The soak time usually lasted from 30 minutes to 1 hour and was adjusted according to the size of the catch. As individual *N. nomurai* and *A. coerulea* jellyfish are highly fragmented and difficult to count accurately at high density, the relative biomass (RB) was used for expressing the abundance of jellyfish in this study. The crane of the fishing vessel was used for lifting large numbers of jellyfish, which were weighed using a large hanging hook scale. Small numbers of jellyfish and individuals were placed into sample bags and weighed using a small hanging hook scale. The precision of wet weight weighed by the large and small scale was 1 kg and 0.1 g, respectively. The RB of the jellyfish was expressed in kg net^{-1} h^{-1}. The numbers, bell diameters (BDs), and wet weights (WWs) of individual jellyfish were noted; the BD was measured with a straight edge. The surface environmental parameters, including the sea surface temperature (SST), dissolved oxygen (DO), surface salinity (SS), and pH, were measured *in situ* using a YSI ProQuatro water quality meter. Ephyrae and juveniles

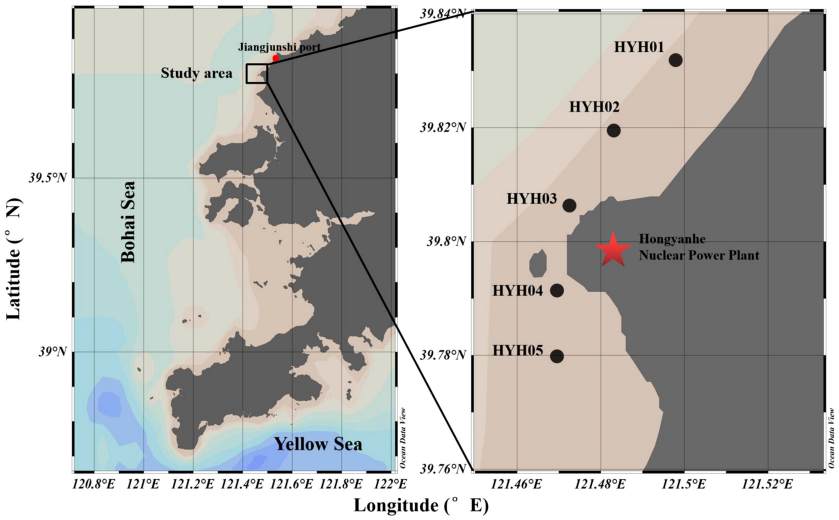

FIGURE 1
Location of the study area. The area from where the ephyrae were collected and the HYHNPP are delimited by the red dot and the red pentacle, respectively.

were collected using a shallow-water type II plankton net (mesh size: 160 μm, diameter: 31.6 cm) and the ephyrae collected from Jiangjunshi port, located 22 km from HYHNPP, were investigated (Figure 1).

2.2 Data analyses

The normality and homogeneity of the variance were confirmed using the one-sample Kolmogorov–Smirnov test and Levene's test, respectively. The Kruskal–Wallis H-test was performed when the data did not approach normality or homogeneity of variance. Multiple parametric comparisons were performed as the data were abnormal or exhibited non-homogeneous variance. Simple correlation analyses were performed for evaluating the statistical correlation between the RB and environmental factors (SST, SS, DO, and pH) using Spearman's correlation with SPSS version 16.0. The graphs were prepared with Microsoft 2016 and R version 4.2.2.

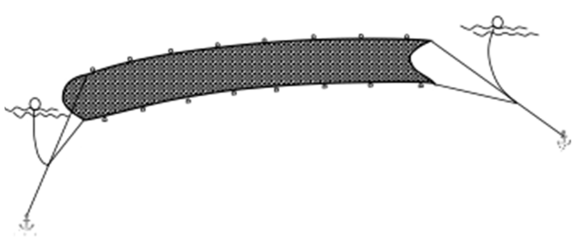

FIGURE 2
A working sketch of the plane anchor drift net.

3 Results

3.1 Occurrence and distribution of large jellyfish

In this study, the first ephyrae of *A. coerulea* appeared at Jiangjunshi port on 15 May 2019 and were collected for further analyses. However, *N. nomurai* ephyrae were absent during the entire period of the survey. The first juvenile medusae of *N. nomurai* appeared on 31 May 2019, with a BD of 4–10 cm. The medusae grew rapidly thereafter and reached a maximum BD of 76 cm at the beginning of September. Medusae of *A. coerulea* were first collected on 8 July, and these had BDs of 12–21 cm and had reached the size of adult organisms. The size of the medusae did not alter much thereafter (Figure 3). The time of appearance of *A. coerulea* ephyrae in 2020 was the same as that in 2019, and no ephyrae of *N. nomurai* were detected in 2020. The first juvenile medusae of *N. nomurai* appeared on 11 June with a BD of 4–6 cm, which was comparable to the BD observed in 2019; however, the medusae appeared at a later period in 2020. There was a difficulty in measuring the BD of the subsequent samples, as the majority of samples were fragments. The results of available survey data revealed that the BD had increased rapidly since the first appearance of juvenile medusa. In this study, the BDs reached a maximum of 130 cm in mid-August 2020, which was significantly greater than the observations in 2019. Compared with 2019, the medusae of *A. coerulea* appeared

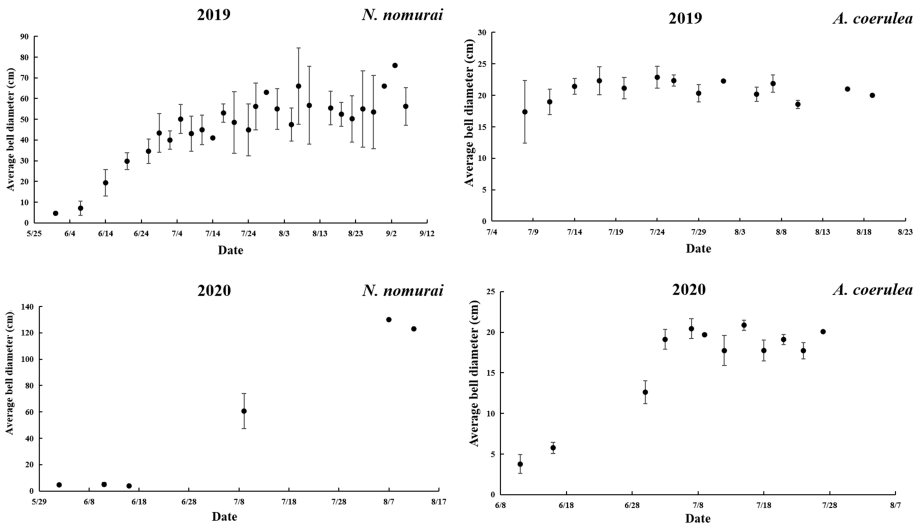

FIGURE 3
The BDs of *N. nomurai* and *A. coerulea* in 2019 and 2020.

earlier the following year, on 11 June 2020. The BDs of *A. coerulea* medusae collected in 2020 were 3–10 cm. The BDs increased rapidly and were similar to the BDs observed in the same period in 2019 (Figure 3).

The RB of the two large jellyfish species, *N. nomurai* and *A. coerulea*, are depicted in Figure 4. N. *nomurai* and *A. coerulea* populations alternated at the intake area of the NPCS, and the RB was not high during the period when they appeared simultaneously. In 2019, large numbers of *N. nomurai* began appearing in late June, and the average relative biomass (ARB) peaked in early July. The RB was highest on 2 July, when it reached a value of 2,806.00 kg net^{-1} h^{-1}, and decreased rapidly thereafter. The ARB of *A. coerulea* increased subsequently and *A. coerulea* gradually became the dominant species from mid-July to mid-August. In 2020, large numbers of large jellyfish started appearing in July, and *A. coerulea* remained the dominant jellyfish species during the whole of July. The abundance of *A. coerulea* was highest on 7 July, when the ARB reached 2,234.40 kg net^{-1} h^{-1}. *A. coerulea* decreased rapidly thereafter and *N. nomurai* gradually dominated from August, during which the RB remained continually low. The abundance of *N. nomurai* was highest on 22 August, when the RB reached 412.50 kg net^{-1} h^{-1}. There were no significant patterns in the abundance of the large jellyfish species across the five stations. Overall, the RB of both species remained consistently lower at HYH04 than at the other stations (Figure 5).

The relationship between the BD of the individual jellyfish species (BD_a for *A. coerulea*, BD_n for *N. nomurai*) and the WW

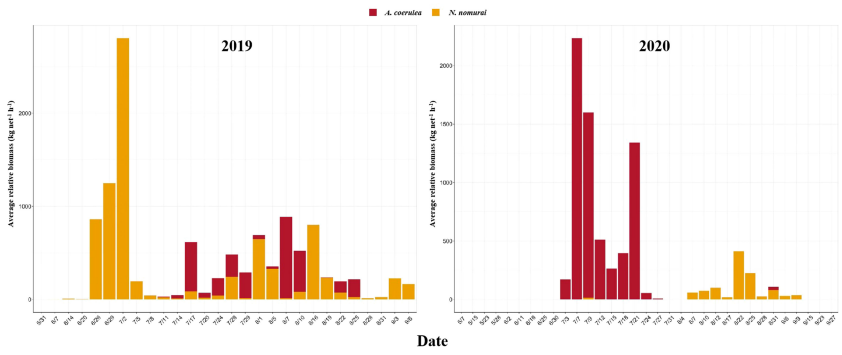

FIGURE 4
The ARB of *N. nomurai* and *A. coerulea* at the intake area of the NPCS in 2019 and 2020.

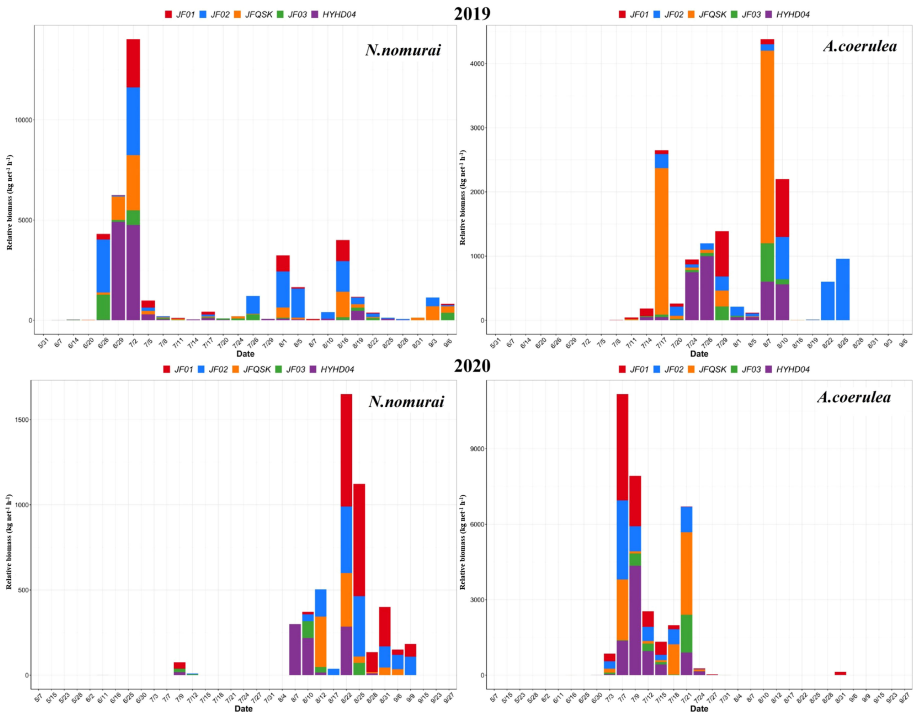

FIGURE 5
The RB of *N. nomurai* and *A. coerulea* at the five different stations in 2019 and 2020.

(W_a for *A. coerulea*, W_n for *N. nomurai*) could be described using the following equations (Figure 6): $W_a = 0.1774BD_a^{2.5232}$ and $W_n = 0.0916BD_n^{2.8265}$.

3.2 Environmental parameters

The fluctuations in the SST, DO level, SS, and pH at the intake area of the NPCS between 2019 and 2020 are depicted in Figure 7. The SST increased from May to early August, gradually stabilized from August, and decreased from September. The annual SST in 2020 was generally lower than that during the same period in 2019. In contrast, the DO levels exhibited a decreasing trend from May to early August, gradually stabilized from August, and decreased from September. Overall, the annual DO level in 2020 was higher than that during the same period in 2019. In 2019, the SS was relatively stable until August, decreased significantly from the beginning of August, and was subsequently stabilized. In 2020, the SS decreased slightly from late August and increased gradually thereafter. The pH

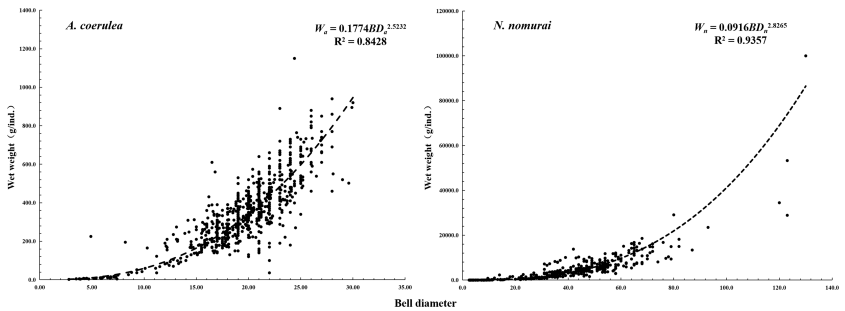

FIGURE 6
Relationship between the BDs and WWs of *N. nomurai* and *A. coerulea*.

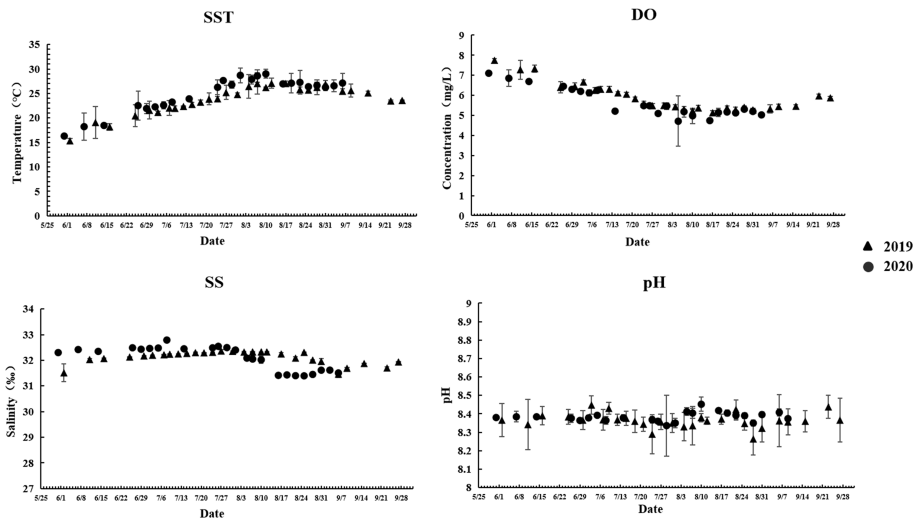

FIGURE 7
Characteristics of the four environmental parameters in 2019 and 2020.

fluctuated and remained relatively stable in 2019 and 2020, with a range of 8.34–8.45. The fluctuations in the DO level, SS, and pH exhibited a similar trend across the five stations; however, the SST fluctuated significantly more at HYH04 than at the other stations and was generally higher than at the other stations (Figure 8).

3.3 Relationships between jellyfish distribution and environmental factors

The survival, SST, DO, SS, and pH range of the two large jellyfish species were similar during the survey period. *A. coerulea* was distributed in waters with SSTs of 16.7–32.2°C, DO levels of 4.37–7.71 mg/l, SS of 31.37–32.82‰, and pH of 8.12–8.50, while *N. nomurai* was distributed in waters with SSTs of 15.6–32.2°C, DO levels of 4.48–7.71 mg/l, SS of 31.27–32.82‰, and pH of 8.12–8.50 (Figure 9). The RB of these two jellyfish species was similar, and greater than 60 kg net^{-1} h^{-1}. The RB of *A. coerulea* was relatively high in waters with SSTs of 20.9–30.9°C, DO levels of 4.37–6.69 mg/l, SS of 31.38–32.61‰, and pH of 8.26–8.50. The RB of *N. nomurai* was relatively high in waters with SSTs of 20.6–32.2°C, DO levels of 4.48–6.69 mg/l, SS of 31.27–32.79‰, and pH of 8.26–8.50 (Figure 9).

The results of simple correlation analyses demonstrated a highly significant negative correlation between the RB of *A. coerulea* and the RB of *N. nomurai* (Figure 9) (r = –0.609, p< 0.01). There was no significant correlation between the RB of *A. coerulea* and the environmental parameters (SST, DO, SS, and pH); however, the RB of *N. nomurai* had a highly significant positive correlation with the SST and a highly significant negative correlation with the DO level (p< 0.01).

4 Discussion

4.1 Determination of the source of jellyfish at the intake area

Determining the sources of jellyfish is essential for deciding appropriate measures for the prevention and control of jellyfish disasters at an early stage; it is currently one of most effective approaches for addressing this concern. A pure waterjet and a scraper have been applied to remove polyps after determining the sources in Korean waters, which proved to be effective (Yoon et al., 2018); however, the sources of large jellyfish at the intake area of the HYHNPP remain to be clearly determined to date.

It has been demonstrated that artificial structures such as ports provide additional habitats for the asexual stage of jellyfish (Feng et al., 2017). Ephyrae of *A. coerulea* were observed at Jiangjunshi port for two consecutive years in this study but were not detected at the intake area. The discovery of ephyrae at Jiangjunshi port indicated that the ephyrae had been released at the region, from where they might have gradually migrated outward to regions around the intake area from mid-May. This finding provides evidence regarding one of the habitats of *A. coerulea*. Moreover, the phenomenon observed at the intake area also coincides with the findings of other studies on the time of appearance of different life history stages of *A. coerulea* (Dong et al., 2008; Dong et al., 2014; Wang and Sun, 2015; Feng et al.,

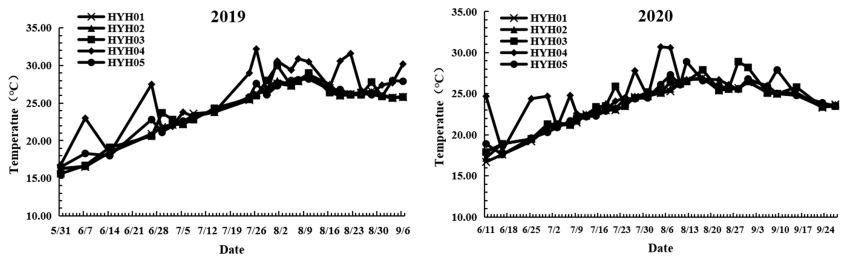

FIGURE 8
Fluctuations in the SST across the different stations in 2019 and 2020.

2018). A previous study indicated that the duration between the release of ephyrae and the development of small medusae of *A. aurita* could be less than 1 month at 18°C (Båmstedt et al., 2001). The newly liberated ephyrae of *A. aurita* developed into young medusae in only 20–28 days in the innermost part of Tokyo Bay (Ishii et al., 2004). In this study, juvenile medusae of *A. coerulea* were collected from the intake area approximately 1.5 and 1 months after the appearance of ephyrae in 2019 and 2020, respectively. Therefore, the findings possibly indicate a potential source of *A. coerulea* around the intake area. However, it is necessary to assess the association between the released ephyrae and the medusae collected at the intake area by continuous monitoring, and to determine whether there are more sources of *A. coerulea*.

Notably, *N. nomurai* ephyrae did not appear at the nearby ports or intake area during the two years of the survey, and the presence of *N. nomurai* ephyrae in this region has not been reported in similar studies (Wang et al., 2013; Dong et al., 2018). These findings indicate that *N. nomurai* did not originate in this region. It has been demonstrated that the northern estuarine

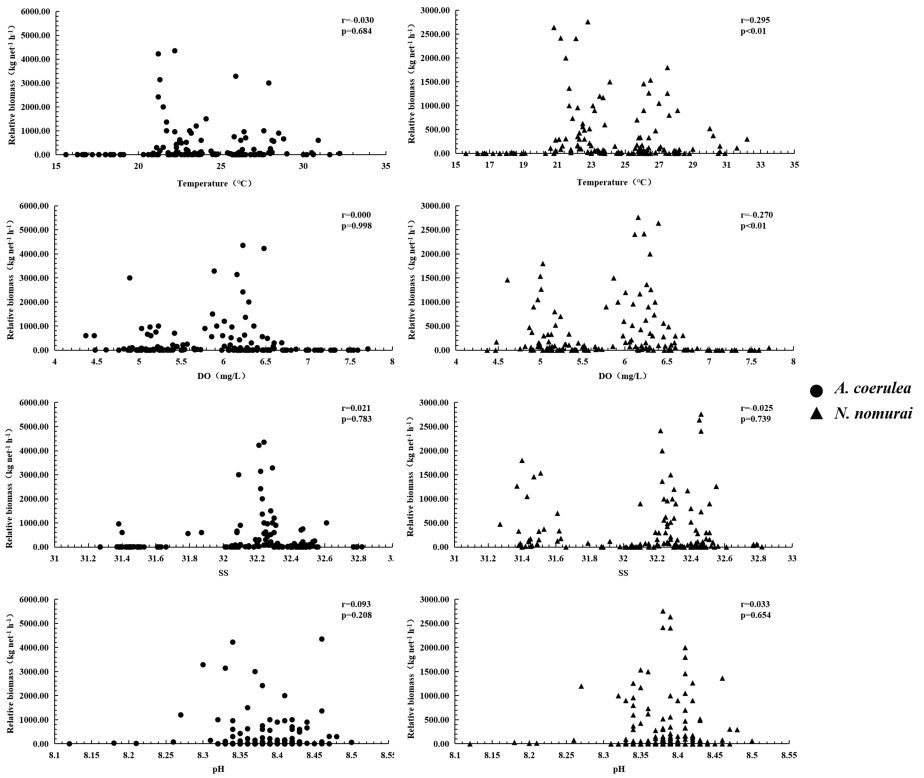

FIGURE 9
Relationship between the RBs of *N. nomurai* and *A. coerulea* and the environmental parameters.

area of LDB is the main habitat of *N. nomurai* in the study area. The ephyrae were possibly produced in mid-spring, and the rapid growth period lasted from late spring to early summer. The juveniles migrate toward the central and southern waters during development, reach maturity, and prepare to spawn in mid-autumn, and the populations decrease rapidly in late autumn (Dong et al., 2018). The intake area was located in the central region of LDB, and the overall timing of each stage was delayed by half a month in the central region, compared with that in the northern area of LDB. It was speculated that, following their release, the ephyrae and some juveniles migrated from the northern region of the LDB and continued to grow during their southward migration, and reached the intake area in early summer, which corresponded to the period of delay discovering juveniles at the study area. The RB increased rapidly in this area during the period of continuous migration, and the individuals grew rapidly, with the BDs reaching more than 50 cm in early July. This situation possibly continued until late autumn, following which the RB declined rapidly owing to the lack of source replenishment and the commencement of fishing activities in early September. The results obtained herein support the findings of previous studies which suggested that the estuarine area is possibly one of the sources of *N. nomurai* in the intake area; however, direct evidence is necessary for confirming the conjecture.

4.2 Distribution patterns of *N. nomurai* and *A. coerulea* in the intake area

Jellyfish feed heavily on plankton, fish eggs, and juveniles, and populations require large quantities of food for supporting the rapid growth period (Greve, 1994; Hansson et al., 2005). Food availability can become a pivotal variable in limiting the viability and fecundity of jellyfish populations when the quantity of food decreases following a rapid increase in the density of large jellyfish species (Goldstein and Steiner 2020; Kitajima et al., 2020). A partial similarity in food composition induced competition between *N. nomurai* and *A. coerulea* (Wang et al., 2021). The study revealed that the RB of large jellyfish increased exponentially at the intake area from late June or early July and reached a plateau thereafter, and finally declined from September. The alternating occurrence and population distribution of these two species with similar niches could indicate passive adaptation and balance under the extremely high biomass and density in a restricted space with limited food availability.

Food composition not only controlled the population size, but also affected the spatial distribution of the two species. The main food for large jellyfish is plankton, which is also the primary species affected by thermal effluents (Bamber and Seaby, 2004; Li et al., 2014). The large influx of thermal effluents in NPPs can alter the hydrodynamic conditions and community structure of local seas (Salgueiro et al., 2015; Lee et al., 2018). In this study, station HYH04 was located near the outlet of the thermal effluents and was characterized by high water velocity and relatively drastic changes in temperature. The SST measured at HYH04 was sometimes higher by 2–3°C or more than that at the other stations during 2019 and 2020, and sometimes there were no differences between the SST at HYH04 and that at other stations. The jellyfish exhibited some, but extremely limited, swimming abilities and migrated actively or passively away from the local seas owing to conditions of strong flow expansion and loss of primary food sources. Comparison of the cumulative RB (CRB) and ARB calculated per hour among different stations revealed that the CRB and ARB were lowest at HYH04, for both *A. coerulea* and *N. nomurai* (Table 1). The findings could be attributed to the characteristics of the local environmental where the station was located.

4.3 Relationship between large jellyfish blooms and environmental factors

The interannual patterns and bloom dynamics of *N. nomurai* were linked to processes of the regional climate (Lee et al., 2021). Temperature is an important factor in influencing the growth and development of jellyfish; temperature affects the production of ephyrae during the asexual stage and the growth of medusae during the sexual stage (Baumsteiger et al., 2018;

TABLE 1 The CRB (kg net^{-1} h^{-1}) and ARB (kg net^{-1} h^{-1}) of *N. nomurai* and *A. coerulea* in 2019 and 2020.

Station	2019				2020			
	N. nomurai		*A. coerulea*		*N. nomurai*		*A. coerulea*	
	ARB	CRB	ARB	CRB	ARB	CRB	ARB	CRB
HYH01	191.60	5,364.82	126.82	2029.13	130.44	1,826.19	573.61	8030.53
HYH02	482.80	13,518.52	202.92	3246.76	92.93	1,301.02	488.14	6834.02
HYH03	275.87	7724.46	356.06	5696.10	56.61	735.90	528.35	7396.84
HYH04	124.66	3,490.50	66.98	1071.67	19.28	231.35	178.33	2496.60
HYH05	396.77	11,109.61	194.65	3114.00	65.18	847.28	586.26	8207.57

Feng et al., 2020). Optimal temperature is beneficial to the growth of juveniles, and previous studies have demonstrated a significant positive correlation between the RB and SST in many waters (Baumsteiger et al., 2018; Dong et al., 2018). In this study, the results of correlation analyses revealed a significant positive correlation between the RB of *N. nomurai* and the SST. The RB and BDs of *N. nomurai* increased rapidly from mid- to late June. The SST decreased slowly after August, while the RB of *N. nomurai* remained relatively stable and gradually decreased thereafter. The rapid warming in late spring and early summer could lead to the rapid growth and development of jellyfish.

In this study, the results of correlation analyses revealed a significant negative correlation between the DO level and the RB of *N. nomurai*, which was consistent with the findings of previous studies (Riyas et al., 2021). The DO level decreased sharply from May to early August, which corresponded with the rapid growth and increased RB, and coincided with a rapid increase in the daily interception and capture of jellyfish. This could be attributed to the increased consumption of DO caused by the rapid increase in RB within a short period of time. The phenomenon could also be attributed to artificial jellyfish control measures at the intake area of the NPCS. The presence of large numbers of fragmented and dead jellyfish could affect the local biogeochemical cycle and rapidly reduce the DO levels owing to the high oxygen consumption by microorganisms during decomposition (Pitt et al., 2009; Condon et al., 2011). The practice of fragmenting and discarding jellyfish pieces into the sea water to avoid the risk of blockages inevitably increases the mass of jellyfish fragments and corpses, which in turn accelerates the consumption of DO. As jellyfish have a low metabolism (Rutherford and Thuesen, 2005), artificial jellyfish control measures could play a more significant role in reducing the DO level.

Salinity is another important factor that affects the RB and distribution of jellyfish, and the effect of salinity was more pronounced in the asexual stage. The ephyrae and juveniles of *N. nomurai* exhibited a preference for low-salinity areas such as estuaries (Yoon et al., 2008; Dong et al., 2018). In this present study, salinity varied in a narrow range, and no significant correlation between SS and RB was detected. Therefore, it is unclear whether distributions of these two species at sexual stages are constrained by salinity. The pH has a limited effect on the RB and distribution of jellyfish, and jellyfish statoliths become significantly smaller at lower pH values (Winans and Purcell, 2010). A reduction in pH affects the pulsing behavior and size of *A. coerulea* ephyrae (Tills et al., 2016); however, it is generally accepted that acidification is not significantly associated with the abundance of medusae (Richardson and Gibbons, 2008). In this study, the pH values fluctuated between 8.26 and 8.50 during the period of investigation, and there was no significant correlation between the pH and RB of both species of jellyfish.

4.4 Recommendations for the intake safety

First, the analysis of environmental factors is an effective strategy for predicting jellyfish blooms (Baumsteiger et al., 2018; Dong et al., 2018; Riyas et al., 2021). Further analyses of metagenic life cycles and real-time online monitoring of environmental indicators would aid in predicting and designing effective measures against the aggregation of different jellyfish species for ensuring the operational safety of NPCSs. Second, ecological theories can provide a theoretical basis for the prevention and control of disasters caused by large jellyfish species. The release of competing species without disturbing the balance of the ecosystem, such as economic fishes, could serve as a suitable strategy for suppressing jellyfish blooms and providing additional economic value. Third, it is necessary to conduct studies on jellyfish blooms in regions beyond the local area of NPCSs. Further efforts are necessary for identifying the sources of jellyfish and understanding their migration patterns for increasing the efficacy of various preventive and control measures. Fourth, the treatment of jellyfish should be enhanced for avoiding negative effects on marine environments (Pitt et al., 2009; Condon et al., 2011), as these would in turn increase the possibility of other related disasters. Fifth, the increased use of unofficial sources or other joint monitoring approaches would increase access to information, provide further evidence for future studies, and aid in ensuring the safety and security of NPCSs (Gutiérrez-Estrada et al., 2021).

5 Conclusion

The distribution patterns of two jellyfish species were investigated during a survey for two consecutive years at the intake area of an NPCS in Eastern LDB, China. The findings revealed that Jiangjunshi port and the northern region of LDB could be the potential sources of *A. coerulea* and *N. nomurai* blooms, respectively. It is necessary to identify the sources of jellyfish species and remove polyps to reinforce the effects. The SST and DO can potentially indicate alterations in *N. nomurai* populations, and the thermal effluents can reshape the community at the local region. The findings also reveal that the interspecific resource competition may lead to variation of abundance in opposite directions in the two jellyfish species. The introduction of some key economic species could provide a solution to the threat of jellyfish blooms. The increased use of other measures for controlling jellyfish blooms in addition to monitoring and early warning measures can enhance the ease and efficacy of preventing jellyfish disasters.

Data availability statement

The raw data supporting the conclusions of this article will be made available by the authors, without undue reservation.

Author contributions

Conceptualization, XW, CG, and HG; data curation, XW, QJ; LY, CJ, and HW; formal analysis, XW and QJ; funding acquisition, XW and CG; investigation, XW, LY, and CJ; methodology, XW, LY, and CJ; validation, XW; writing—original draft, XW; writing—review and editing, XW and CG. All the authors agree to being accountable for the content of this study. All authors contributed to the article and approved the submitted version.

Funding

This work was supported by the National Natural Science Foundation of China (grant number: 42106155), the National Key R&D Program of China (grant number: 2017YFC1404404), and the Doctoral Foundation of National Marine Environmental Monitoring Centre, China (2019-2020 NPCS Safety Guarantee Project).

Acknowledgments

The authors acknowledge Sen Wang and Chunyang Wu for their help during the collection of samples and environmental data. The authors express their gratitude to Junjian Wang, Yi Sun, and Xiaoyu Cui for their help during data analysis.

Conflict of interest

The authors declare that the research was conducted in the absence of any commercial or financial relationships that could be construed as a potential conflict of interest.

Publisher's note

References

Bamber, R. N., and Seaby, R. M. (2004). The effects of power station entrainment passage on three species of marine planktonic crustacean, *Acartia tonsa* (Copepoda), *Crangon crangon* (Decapoda) and *Homarus gammarus* (Decapoda). *Mar. Environ. Res.* 57 (4), 281–294. doi: 10.1016/j.marenvres.2003.08.002

Båmstedt, U., Wild, B., and Martinussen, M. (2001). Significance of food type for growth of ephyrae *Aurelia aurita* (Scyphozoa). *Mar. Biol.* 139 (4), 641–650. doi: 10.1007/s002270100623

Baumsteiger, J., O'Rear, T. A., Cook, J. D., Manfree, A. D., and Moyle, P. B. (2018). Factors affecting distribution and abundance of jellyfish medusae in a temperate estuary: A multi-decadal study. *Biol. Invasions* 20 (1), 105–119. doi: 10.1007/s10530-017-1518-x

Berwald, J. (2017). *Spineless: The science of jellyfish and the art of growing a backbone* Vol. 132 (New York: Riverhead Books), 304.

Condon, R. H., Steinberg, D. K., del Giorgio, P. A., Bouvier, T. C., Bronk, D. A., Graham, W. M., et al. (2011). Jellyfish blooms result in a major microbial respiratory sink of carbon in marine systems. *Proc. Natl. Acad. Sci.* 108, 10225–10230. doi: 10.1073/pnas.1015782108

Dawson, M. N., Cieciel, K., Decker, M. B., Hays, G. C., Lucas, C. H., and Pitt, K. A. (2015). Population-level perspectives on global change: Genetic and demographic analyses indicate various scales, timing, and causes of scyphozoan jellyfish blooms. *Biol. Invasions* 17 (3), 851–867. doi: 10.1007/s10530-014-0732-z

Dawson, M. N., and Hamner, W. M. (2009). A character-based analysis of the evolution of jellyfish blooms: Adaptation and exaptation. *Hydrobiol.* 616, 193–215. doi: 10.1007/978-1-4020-9749-2_13

Dong, Z., Liu, D., and Keesing, J. K. (2010). Jellyfish blooms in China: Dominant species, causes and consequences. *Mar. pollut. Bull.* 60 (7), 954–963. doi: 10.1016/j.marpolbul.2010.04.022

Dong, Z., Liu, D., and Keesing, J. K. (2014). "Contrasting trends in populations of rhopilema esculentum and aurelia aurita in Chinese waters," in *In jellyfish blooms* (Dordrecht: Springer), 207–218.

Dong, J., Sun, M., Wang, B., and Liu, H. (2008). Comparison of life cycles and morphology of *Cyanea nozakii* and other scyphozoans. *Plankton Benthos Res.* 3 (Supplement), 118–124. doi: 10.3800/pbr.3.118

Dong, J., Wang, B., Duan, Y., Yoon, W. D., Wang, A., Liu, X., et al. (2018). Initial occurrence, ontogenic distribution-shifts and advection of *Nemopilema nomurai* (Scyphozoa: Rhizostomeae) in liaodong bay, China, from 2005-2015. *Mar. Ecol. Prog. Ser.* 591, 185–197. doi: 10.3354/meps12272

Feng, S., Lin, J., Sun, S., Zhang, F., Li, C., and Xian, W. (2020). Combined effects of seasonal warming and hyposalinity on strobilation of *Nemopilema nomurai* polyps. *J. Exp. Mar. Biol. Ecol.* 524, 151316. doi: 10.1016/j.jembe.2020.151316

Feng, S., Wang, S. W., Sun, S., Zhang, F., Zhang, G. T., Liu, M. T., et al. (2018). Strobilation of three scyphozoans (*Aurelia coelurea*, *Nemopilema nomurai*, and *Rhopilema esculentum*) in the field at jiaozhou bay, China. *Mar. Ecol. Prog. Ser.* 591, 141–153. doi: 10.3354/meps12276

Feng, S., Wang, S. W., Zhang, G. T., Sun, S., and Zhang, F. (2017). Selective suppression of *in situ* proliferation of scyphozoan polyps by biofouling. *Mar. pollut. Bull.* 114 (2), 1046–1056. doi: 10.1016/j.marpolbul.2016.10.062

Goldstein, J., and Steiner, U. K. (2020). Ecological drivers of jellyfish blooms–the complex life history of a 'well-known'medusa (*Aurelia aurita*). *J. Anim. Ecol.* 89 (3), 910–920. doi: 10.1111/1365-2656.13147

Greve, W. (1994). The 1989 German bight invasion of muggiaea atlantica. *ICES J. Mar. Sci.* 51, 355–358. doi: 10.1006/jmsc.1994.1037

Gutiérrez-Estrada, J. C., Pulido-Calvo, I., Peregrín, A., García-Gálvez, A., Báez, J. C., Bellido, J. J., et al. (2021). Integrating local environmental data and information from non-driven citizen science to estimate jellyfish abundance in Costa del sol (Southern Spain). *Estuar. Coast. Shelf. Sci.* 249, 107112. doi: 10.1016/j.ecss.2020.107112

Hamilton, G. (2016). The secret lives of jellyfish. *Nature* 531, 432–434. doi: 10.1038/531432a

Hamner, W., Gilmer, R., and Hamner, P. (1982). The physical, chemical, and biological characteristics of a stratified, saline, sulfide lake in Palau1. *Limnol. Oceanogr.* 27, 896–909. doi: 10.4319/lo.1982.27.5.0896

Hansson, L. J., Moeslund, O., Kiørboe, T., and Riisgård, H. U. (2005). Clearance rates of jellyfish and their potential predation impact on zooplankton and fish larvae in a neritic ecosystem (Limfjorden, Denmark). *Mar. Ecol. Prog. Ser.* 304, 117—131. doi: 10.3354/meps304117

Han, C. H., and Uye, ,. (2010). Combined effects of food supply and temperature on asexual reproduction and somatic growth of polyps of the common jellyfish Aurelia aurita s.l Plankton. *Benthos. Res.* 5, 98–105. doi: 10.3800/pbr.5.98

Hernroth, L., and Gröndahl, F. (1985). On the biology of *Aurelia aurlta* (L.): 2. major factors regulating the occurrence of ephyrae and young medusae in the gullmar fjord, western Sweden. *B. Mar. Sci.* 37, 567–576.

Ishii, H., Kojima, S., and Tanaka, Y. (2004). Survivorship and production of *Aurelia aurita* ephyrae in the innermost part of Tokyo bay, Japan. *Plankton Biol. Ecol.* 51 (1), 26–35.

Ishii, H., and Takagi, A. (2003). Development time of planula larvae on the oral arms of the scyphomedusa *Aurelia aurita*. *J. Plankton. Res.* 25, 1447–1450. doi: 10.1093/plankt/fbg094

Kawahara, M., Uye, S. I., Ohtsu, K., and Iizumi, H. (2006). Unusual population explosion of the giant jellyfish *Nemopilema nomurai* (Scyphozoa: Rhizostomeae) in East Asian waters. *Mar. Ecol. Prog. Ser.* 307, 161–173. doi: 10.3354/meps307161

Kitajima, S., Hasegawa, T., Nishiuchi, K., Kiyomoto, Y., Taneda, T., and Yamada, H. (2020). Temporal fluctuations in abundance and size of the giant jellyfish *Nemopilema nomurai* medusae in the northern East China Sea 2006–2017. *Mar. Biol.* 167 (6), 1–10. doi: 10.1007/s00227-020-03682-1

Kroiher, M., Siefker, B., and Berking, S. (2000). Induction of segmentation in polyps of *Aurelia aurita* (Scyphozoa, cnidaria) into medusae and formation of mirror-image medusa anlagen. *Int. J. Dev. Biol.* 44 (5), 485–490.

Lee, S. H., Hwang, J. S., Kim, K. Y., and Molinero, J. C. (2021). Contrasting effects of regional and local climate on the interannual variability and phenology of the scyphozoan, aurelia coerulea and nemopilema nomurai in the Korean peninsula. *Diversity* 13 (5), 214. doi: 10.3390/d13050214

Lee, P. W., Tseng, L. C., and Hwang, J. S. (2018). Comparison of mesozooplankton mortality impacted by the cooling systems of two nuclear power plants at the northern Taiwan coast, southern East China Sea. *Mar. pollut. Bull.* 136, 114–124. doi: 10.1016/j.marpolbul.2018.09.003

Li, X. Y., Li, B., and Sun, X. L. (2014). Effects of a coastal power plant thermal discharge on phytoplankton community structure in zhanjiang bay, China. *Mar. pollut. Bull.* 81, 210–217. doi: 10.1016/j.marpolbul.2013.08.006

Lucas, C. H., and Dawson, M. N. (2014). "What are jellyfishes and thalia-ceans and why do they bloom?," in *Jellyfish blooms*. Eds. I. K. A. Pitt and C. H. Lucas (Dordrecht, The Netherlands: Springer), 9–44.

Lucas, C. H., Pitt, K. A., Purcell, J. E., Lebrato, M., and Condon, R. H. (2011). What's in a jellyfish? proximate and elemental composition and biometric relationships for use in biogeochemical studies. *Ecol.* 92, 1704. doi: 10.1890/11-0302.1

Masilamoni, J. G., Jesudoss, K. S., Nandakumar, K., Satpathy, K. K., Nair, K. V. K., and Azariah, J. (2000). Jellyfish ingress: a threat to the smooth operation of coastal power plants. *Curr. Sci.* 79, 567–569.

Mills, C. E. (1995). Medusae, siphonophores, and ctenophores as planktivorous predators in changing global ecosystems. *ICES J. Mar. Sci.: J. Conseil* 52, 575–581. doi: 10.1016/1054-3139(95)80072-7

Mills, C. E. (2001). Jellyfish blooms: Are populations increasing globally in response to changing ocean conditions? *Hydrobiologia* 451, 55–68. doi: 10.1023/A:1011888006302

Moon, J. H., Pang, I. C., Yang, J. Y., and Yoon, W. D. (2010). Behavior of the giant jellyfish *Nemopilema nomurai* in the East China Sea and East/Japan Sea during the summer of 2005: A numerical model approach using a particle-tracking experiment. *J. Marine. Syst.* 80 (1-2), 101–114. doi: 10.1016/j.jmarsys.2009.10.015

Olesen, N. J., and Riisgard, H. U. (1994). Population dynamic, growth and energetics of jellyfish, *Aurelia aurita*, in a shallow fjord. *Mar. Ecol. Prog. Ser.* 105, 9–18. doi: 10.3354/meps105009

Papathanassiou, E., Panayotidis, P., and Anagnostaki, K. (1987). Notes on the biology and ecology of the jellyfish *Aurelia aurita* lam. in elefsis bay (Saronikos gulf, Greece). *Mar. Ecol.* 8, 49–58. doi: 10.1111/j.1439-0485.1987.tb00174.x

Pitt, K. A., Duarte, C. M., Lucas, C. H., Sutherland, K. R., Condon, R. H., Mianzan, H., et al. (2013). Jellyfish body plans provide allometric advantages beyond low carbon content. *PloS One* 8 (8), e72683. doi: 10.1371/journal.pone.0072683

Pitt, K. A., Welsh, D. T., and Condon, R. H. (2009). Influence of jellyfish blooms on carbon, nitrogen and phosphorus cycling and plankton production. *Jellyfish Blooms: Causes Consequences Recent Adv.* 616, 133–149. doi: 10.1007/s10750-008-9584-9

Prieto, L., Astorga, D., Navarro, G., and Ruiz, J. (2010). Environmental control of phase transition and polyp survival of a massive-outbreaker jellyfish. *PloS One* 5, e13793. doi: 10.1371/journal.pone.0013793

Purcell, J. E. (2012). Jellyfish and ctenophore blooms coincide with human proliferations and environmental perturbations. *Annu. Rev. Mar. Sci.* 4, 209–235. doi: 10.1146/annurev-marine-120709-142751

Purcell, J. E., Hoover, R. A., and Schwarck, N. T. (2009). Interannual variation of strobilation by the scyphozoan *Aurelia labiata* in relation to polyp density, temperature, salinity, and light conditions in situ. *Mar. Ecol. Prog. Ser.* 375, 139–149. doi: 10.3354/MEPS07785

Purcell, J. E., Uye, S. I., and Lo, W. T. (2007). Anthropogenic causes of jellyfish blooms and their direct consequences for humans: a review. *Mar. Ecol. Prog. Ser.* 350, 153–174. doi: 10.3354/meps07093

Quinones, J., Chiaverano, L. M., and Ayon, P. (2018). Spatial patterns of large jellyfish chrysaora plocamia blooms in the northern Humboldt upwelling system in relation to biological drivers and climate. *ICES J. Mar. Sci.* 75, 1405–1415. doi: 10.1093/icesjms/fsy004

Rekstad, M. E., Majaneva, S., Borgersen, Å.L., and Aberle, N. (2021). Occurrence and habitat characteristics of *Aurelia* sp. polyps in a high-latitude fjord. *Front. Mar. Sci.* 8. doi: 10.3389/fmars.2021.68463

Richardson, A. J., Bakun, A., Hays, G. C., and Gibbons, M. J. (2009). The jellyfish joyride: Causes, consequences and management responses to a more gelatinous future. *Trends Ecol. Evol.* 24 (6), 312–322. doi: 10.1016/j.tree.2009.01.010

Richardson, A. J., and Gibbons, M. J. (2008). Are jellyfish increasing in response to ocean acidification? *Limnol. Oceanogr.* 53, 2035–2040. doi: 10.4319/lo.2008.53.5.2040

Riyas, A., Dahanukar, N., Krishnan, K. A., and Kumar, A. B. (2021). Scyphozoan jellyfish blooms and their relationship with environmental factors along the south-eastern Arabian Sea. *Mar. Biol. Res.* 17 (2), 185–199. doi: 10.1080/17451000.2021.1916034

Russell, F. S. (1970). *The medusae of the British isles volume II: Pelagic scyphozoa, with a supplement to the first volume of hydromedusae*. (London: Cambridge University Press).

Rutherford, L. D.Jr., and Thuesen, E. V. (2005). Metabolic performance and survival of medusae in estuarine hypoxia. *Mar. Ecol. Prog. Ser.* 294, 189–200. doi: 10.3354/meps294189

Salgueiro, D. V., De Pablo, H., Nevesa, R., and Mateus, M. (2015). Modelling the thermal effluent of a near coast power plant (Sines, portugal). revista de gestão costeira integrada. *J. Integrated Coast. Zone Manage.* 15 (4), 533–544. doi: 10.5894/rgci577

Schiariti, A., Melica, V., Kogovšek, T., and Malej, A. (2015). Density-dependent effects control the reproductive strategy and population growth of *Aurelia aurita* sl scyphistomae. *Mar. Biol.* 162 (8), 1665–1672. doi: 10.1007/s00227-015-2704-y

Schneider, G. (1992). A comparison of carbon-specific respiration rates in gelatinous and non-gelatinous zooplankton: A search for general rules in zooplankton metabolism. *Helgolä nder Meeresuntersuchungen* 46, 377–388. doi: 10.1007/BF02367205

Schrope, M. (2012). Marine ecology: Attack of the blobs. *Nature* 482 (7383), 20–21. doi: 10.1038/482020a

Sun, S., Li, Y., and Sun, X. (2012). Changes in the small-jellyfish community in recent decades in jiaozhou bay, China. *Chin. J. Oceanol. Limnol.* 30, 507–518. doi: 10.1007/s00343-012-1179-7

Sun, S., Zhang, F., Li, C., Wang, S., Wanh, M., Tao, Z., et al. (2015). Breeding places, population dynamics, and distribution of the giant jellyfish *Nemopilema nomurai* (Scyphozoa: Rhizo - stomeae) in the yellow Sea and the East China Sea. *Hydrobiologia* 754, 59–74. doi: 10.1007/s10750-015-2266-5

Takizawa, M. (2005). Countermeasures for jellyfish attacks at kashiwazaki kariwa [Japan] nuclear power station. *Bull. Plankton Soc. Japan* 52 (1), 36–38.

Tills, O., Sun, X., Rundle, S. D., Heimbach, T., Gibson, T., Cartwright, A., et al. (2016). Reduced pH affects pulsing behaviour and body size in ephyrae of the moon jellyfish, aurelia aurita. *J. Exp. Mar. Biol. Ecol.* 480, 54–61. doi: 10.1016/j.jembe.2016.03.014

Wang, N., Li, C., Liang, Y., Shi, Y., and Lu, J. (2014). Prey concentration and temperature effect on budding and strobilation of *Aurelia* sp. 1 polyps. *Hydrobiologia* 754, 125–134. doi: 10.1007/s10750-014-1978-2

Wang, B., Qi, Y. B., Dong, J., Li, Y. L., Wang, W. B., Li, Y. P., et al. (2013). Dynamic distribution of nemopilema nomurai in inshore waters of the northern liaodong bay, bohai Sea. *Acta Ecol. Sin.* 33 (6), 1701–1712. doi: 10.5846/stxb201112081878

Wang, Y. T., and Sun, S. (2015). Population dynamics of *Aurelia* sp. 1 ephyrae and medusae in jiaozhou bay, China. *Hydrobiologia* 754 (1), 147–155. doi: 10.1007/s10750-014-2021-3

Wang, J., Wang, N., Wang, Y., Wang, X., and Li, C. (2021). Food composition of common jellyfish species in hongyanhe area revealed by fatty acid biomarkers and stable carbon and nitrogen isotopes. *Acta Oceanol. Sin.* 52 (1), 132–143. doi: 10.11693/hyhz20200500135

Wang, S., Zhang, G., Sun, S., Wang, Y., and Zhao, Z. (2012). Population dynamics of three scyphozoan jellyfish species during summer of 2011 in jiaozhou bay. *Oceanol. ET. Limnol. Sin.* 43, 471–479.

Winans, A. K., and Purcell, J. E. (2010). Effects of pH on asexual reproduction and statolith formation of the scyphozoan, *Aurelia labiata*. *Hydrobiologia* 645 (1), 39–52. doi: 10.1007/s10750-010-0224-9

Yoon, W., Chae, J., Koh., B. S., and Han., C. (2018). Polyp removal of a bloom forming jellyfish, *Aurelia coerulea*, in Korean waters and its value evaluation. *Ocean. Sci.* 53 (3), 499–507. doi: 10.1007/s12601-018-0015-1

Yoon, W. D., Lee, H. E., Han, C., Chang, S. J., and Lee, K. (2014). Abundance and distribution of nemopilema nomurai (Scyphozoa, rhizostomeae), in Korean waters in 2005–2013. *Ocean. Sci. J.* 49 (3), 183–192. doi: 10.1007/s12601-014-0018-5

Yoon, W. D., Yang, J. Y., Shim, M. B., and Kang, H. K. (2008). Physical processes influencing the occurrence of the giant jellyfish *Nemopilema nomurai* (Scyphozoa: Rhizostomeae) around jeju island, Korea. *J. Plankton. Res.* 30, 251–260. doi: 10.1093/plankt/fbm102

Zhang, F., Sun, S., Jin, X., and Li, C. (2012). "Associations of large jellyfish distributions with temperature and salinity in the Yellow Sea and East China Sea," In: J. Purcell, H. Mianzan and J. R. Frost *Jellyfish Blooms IV. Developments in Hydrobiology* (Dordrecht: Springer), vol. 220. doi: 10.1007/978-94-007-5316-7_7

frontiers | Frontiers in Marine Science

TYPE Original Research
PUBLISHED 10 January 2023
DOI 10.3389/fmars.2022.1089699

OPEN ACCESS

EDITED BY
Huang Honghui,
South China Sea Fisheries Research Institute (CAFS), China

REVIEWED BY
Bin Liu,
Hebei University of Technology, China
Guoliang Wei,
Nuclear and Radiation Safety Center, China
Ma Xin,
Ocean University of China, China

*CORRESPONDENCE
Jian-ling Huo
huo_job@163.Com

SPECIALTY SECTION
This article was submitted to Marine Pollution, a section of the journal Frontiers in Marine Science

RECEIVED 04 November 2022
ACCEPTED 20 December 2022
PUBLISHED 10 January 2023

CITATION
Li C, Huo J-l, Song Y-z, Yang L and Liu S-t (2023) An integrated monitoring system for disaster-causing organisms in the water intake areas of coastal nuclear power plants. *Front. Mar. Sci.* 9:1089699. doi: 10.3389/fmars.2022.1089699

An integrated monitoring system for disaster-causing organisms in the water intake areas of coastal nuclear power plants

Chao Li[1,2,3], Jian-ling Huo[1,2,3]*, Yu-ze Song[1,2,3], Lei Yang[1,2,3] and Song-tang Liu[1,2,3]

[1]Offshore Observation Department, National Ocean Technology Center, Tianjin, China, [2]Key Laboratory of Marine Ecological Monitoring and Restoration Technologies, Ministry of Natural Resources, Shanghai, China, [3]Key Laboratory of Ocean Observation Technology, Ministry of Natural Resources, Tianjin, China

Nowadays, nuclear power plays an important role in the energy structure of many countries. However, A bloom of a disaster-causing organism (DCO) in the cold-water intake area of a coastal nuclear power plant can block the water cooling system and seriously affect the operational safety of the nuclear power unit. Currently, the traditional method of protection is to estimate the DCO abundance by regular manual investigation and sampling, but that method cannot give continuous real-time data. Instead, proposed and implemented here is a seafloor in situ integrated monitoring system for DCOs (known as IMSDCO), which is equipped with an optical microscopic imager (OMI) and hydrometric sensors to monitor automatically the DCO abundance and hydrology. All the data are transmitted to a terminal in the shore station through a photoelectric composite cable for real-time display. When the DCO abundance reaches a preset threshold, software automatically raises an alarm. Since placing IMSDCO at the cold-water intake of the Changjiang nuclear power plant, a six-month field trial has been completed, during which large amounts of hydrology data and DCO images were obtained. IMSDCO successfully identified and estimated the abundances of various DCOs (e.g., *Phaeocystis globosa*, *Acetes chinensis*, and small fish) and predicted their movements based on hydrology data. Based on the analysis of the experimental data, we discussed the reasons for the error in the abundance estimation of DCO and the methods to reduce the error. The experimental results show that the OMI-based IMSDCO can monitor and give early warning of DCOs in the water intake areas of costal nuclear power plants and is worthy of long-term deployment.

KEYWORDS

nuclear power plant, water intake, disaster-causing organism, monitoring system, abundance estimation, optical microscopic imager

1 Introduction

As a high-efficiency, energy-saving, and eco-friendly energy source, nuclear power plays an important role in reducing carbon dioxide emissions, controlling the greenhouse effect, and promoting carbon neutrality (Deng, 2021). To date, more than 30 countries have built nuclear power plants, and nuclear power accounts for an important proportion of the domestic energy structure of the United States, Britain, Russia, and especially France, where it accounts for more than 70% (Chen and Xia, 2017; Xu, 2020; MOC, 2021). By the end of 2020, there were 48 nuclear power units in operation and 17 nuclear power units under construction in mainland China, with nuclear power accounting for ca. 5% of the national cumulative power generation and growing annually (Zhang, 2021; CNEA, 2021).

Most nuclear power plants are built in coastal areas, where the excess heat from the power generation process is taken away by the cyclic seawater to ensure stable operation of the nuclear power units. Therefore, the water quality of its cold-water intake directly affects the operational safety of a nuclear power plant. However, with the over-exploitation of marine resources by humans, the marine ecological environment is deteriorating day by day, and the resulting frequent blooms of algae, jellyfish, fish, shrimp, snails, and other marine organisms can block the intercept net at the water intake of a nuclear power plant, thereby seriously threatening its operational safety (Purcell et al., 2007; Azila and Chong, 2010; Ruan, 2015; Zhang et al., 2019). Since 2000, there have been more than 200 unit outages due to cooling-water blockages in many countries with nuclear power plants, causing major safety hazards and huge economic losses (Han et al., 2018; MEE, 2020), and such incidents are occurring more and more year by year throughout the world.

How to improve the safety of the cold sources of nuclear power plants is now a major common concern of the international nuclear-power community. The United States, France, Japan, South Korea, and other countries have all researched countermeasures for cold-source protection, including strengthening water-quality monitoring, setting up intercept nets, and enhancing the backwashing capacity of drum nets (Meng et al., 2019), which have alleviated the occurrence of such disasters to a certain extent. However, those measures are all based on passive defense and cannot give early warning of an outbreak of a marine disaster-causing organism (DCO). In recent years, some nuclear power plants in China have used sonar detection technology to monitor DCOs at their water intakes, such as the Daya Bay and Hongyanhe nuclear power plants, which have monitored *Creseis acicula* and *Aurelia aurita* (Wang and Fu, 2021; Zeng et al., 2021). However, because sonar echo is particularly vulnerable to near-shore terrain and environment, it is difficult to identify targets, especially tiny plankton.

With the development of optical imaging technology, underwater optical microscopic imagers (OMIs) have been applied to marine-organism monitoring (Jaffe, 2015; Lombard et al., 2019; Liu et al., 2021; Merz et al., 2021). OMIs based on bright-field imaging technology support higher sampling rates, and some research teams in countries other than China have installed them on survey ships and gliders to conduct fish and plankton surveys to obtain images and understand their underwater distribution (Cowen and Guigand, 2008; Picheral et al., 2010; Ohman et al., 2019). However, the disadvantages of a bright-field imager are that its image resolution is poor and its images are easily affected by particles when used in coastal waters (Greer et al., 2016). By contrast, a dark-field imager usually has better resolution but lower sampling rate, making it more suitable for long-term *in situ* observation at fixed points near the shore (Grossmann et al., 2014). Nowadays, benefitting from the rapid development of image processing technology based on machine learning algorithms, OMIs for underwater *in situ* online monitoring can automatically and quickly identify the species, size, and abundance of aquatic organisms (Yang et al., 2022), thereby expanding greatly the application field of OMIs. In China, Bi et al. (Bi et al., 2022) used PlanktonScope to monitor plankton such as copepods, jellyfish, chaetognaths, appendicularians, and meroplanktonic larvae in coastal estuaries, and they researched the primary productivity of estuaries. Also, Li et al. (Li et al., 2022) installed an OMI on a buoy and carried out plankton and water quality monitoring in Dapeng Cove. However, to the best of our knowledge, there have been no reports to date of an OMI being installed on a bottom platform to monitor DCOs at the water intake of a nuclear power plant.

The integrated monitoring system for DCOs (known as IMSDCO) that is reported herein is equipped with an OMI, which can quickly identify marine organisms with sizes of between 500 μm and 20 mm *via* its auto-zoom capability and then generate high-resolution two-dimensional images. Also, IMSDCO is equipped with multiple hydrological and water quality sensors, including an acoustic Doppler current profiler (ADCP), a conductivity–temperature–depth (CTD) sensor, a tidal meter, and two multi-parameter water-quality detectors (pH, dissolved oxygen, temperature, and conductivity).It can monitor DCO quantity, current, temperature, salinity, depth, and water-quality parameters in real time, estimate the abundances of DCOs, and predict their migration tracks algorithmically. The system was placed at the cold-water intake of the Changjiang nuclear power plant in Hainan Province in China, and the monitoring results were displayed in real time *via* PC software to achieve long-term DCO monitoring and quantitative evaluation. The cooling water of Changjiang nuclear power plant is surface water intake from open channel. Three intercept nets are set around the water intake, and IMSDCO is placed on the seabed 800m away from the third net, which is about 1500m away from the water intake.

This distance can ensure that the nuclear power plant has enough time to take countermeasures after discovering the outbreak of the DCOs.

2 Materials and methods

2.1 Design of IMSDCO

IMSDCO comprises a shore station, a photoelectric composite cable, an underwater node, and scientific sensors, as shown in Figure 1. Equivalent to the brain of IMSDCO, the shore station is responsible for power supply, communication, data collection and storage, and human–computer interaction functions to ensure the safe and stable operation of the system. Also, the communication system in the shore station is connected to the public Internet so that authorized users can access IMSDCO from anywhere. The photoelectric composite cable connects the shore station and the seabed monitoring system and is the channel for power supply and communication between them. The underwater node is a platform equipped with scientific sensors, and the electronic cabin thereon provides appropriate power supply and communication interfaces for the sensors. Also, the mooring structure is designed to monitor the sea water profile.

2.2 Power supply system

The submarine environment is complex and changeable, and a reliable power supply for IMSDCO is very important. Alternating current (AC) transmission requires highly insulated cables that form a large equivalent capacitance with seawater and earth, thereby increasing the reactive power loss; therefore, the power loss of long-distance AC transmission is serious without inductance compensation. Compared with AC transmission, although direct current (DC) transmission also has capacitance to ground, its ripple voltage is small, the voltage is stable in the steady state, and the reactive power loss is small; therefore, DC transmission is more economical and stable (Howe et al., 2002; Yu et al., 2013).

The DC power supply of the shore station converts 220-V AC into 375-V DC and then transmits it to the electronic cabin of the underwater node through the photoelectric composite cable. The electronic cabin has one input port and six output ports: the input port can adapt to the voltage range of 275–425 V, while the output ports comprise two 24-V ports and four 12-V ports, each of which is connected to a different scientific sensor. The logic diagram of the power supply system is shown in Figure 2. After the 375-V DC enters the electronic cabin through the input port, it first passes through a surge-protection device to suppress any surge current on the line that would otherwise damage the circuit components. A DC/DC converter converts 375-V DC into 24-V and 12-V DC and supplies power to the communication system, the external scientific sensors, and the internal sensors (temperature, humidity, and water leakage) through the state monitoring and control system.

The surge-protection device is very important for the stable operation of the power supply system. Under the influence of the equivalent capacitance in the circuit, the instantaneous current is very large at the moment of power on; this exposes the circuit components to great potential safety hazards and so must be

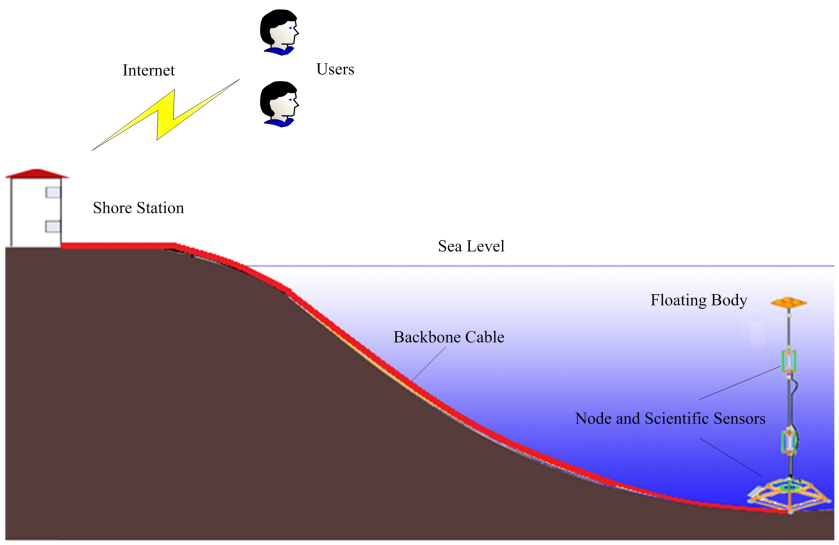

FIGURE 1
Overview of integrated monitoring system for DCOs (IMSDCO).

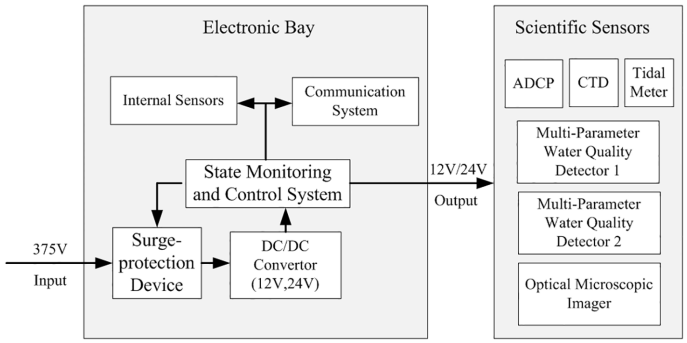

FIGURE 2
Diagram of power supply system of electronic cabin.

limited (Du et al., 2018). The principle of the surge-protection device is shown in Figure 3. Resistor R1 with an appropriate resistance is connected in series in the circuit, and relay KT1 is connected in parallel with R1. After power on, R1 limits the surge current in the circuit within a reasonable range, thereby suppressing it. After a delay of few seconds, a control signal from the state monitoring and control system closes KT1 to short R1, thereby reducing the power loss thereon. The filter and capacitor C1 are used to smooth the peak voltage so that the components can avoid the impact of surge voltage. Also, the monitor behind the surge-protection device monitors the voltage and current in real time and inputs the monitoring data to the state monitoring and control system, which are finally displayed by the PC software in the shore station.

The DC/DC converter has eight outputs that are isolated from each other: two for internal loads and six for the loads of the external scientific sensors. Based on the voltages required by the loads, the output voltages are 12-V and 24-V: the 12-V module (model V375C12T75BL; VICOR Company) has a power of 75-W, and the 24-V module (model V375C24T150BL; VICOR Company) has a power of 150-W. The two power modules are small in size, high in power density, and stable in performance, making them very suitable for use in the narrow confined spaces of underwater monitoring systems. When operating, the power modules generate a lot of heat that must be conducted into the seawater by radiators to ensure stable operation for a long time (Li et al., 2016). The radiators are made of aluminum, which has a high thermal conductivity. As shown in Figure 4, the inner surface of a radiator is planar for fixing power modules, and the outer surface is curved with the same radius as that of the inner wall of the cylindrical pressure vessel. Four symmetrically distributed radiators are connected into a cylindrical shape by a mechanical structure, and a threaded support element is installed in the middle of the cylinder; after the radiators are installed in the pressure vessel, the rotatable part of the threaded support is rotated clockwise manually, and the support element presses two of the symmetrical radiators tightly against the inner wall of the pressure vessel for rapid heat transfer to the seawater. The other two symmetrical radiators are held in place in the same way. For more-effective heat conduction, silicone grease is applied on the outer arc surfaces of the radiators to make them fit more closely.

2.3 State monitoring and control system

The state monitoring and control system has two main functions: (i) monitor the data from the internal sensors and

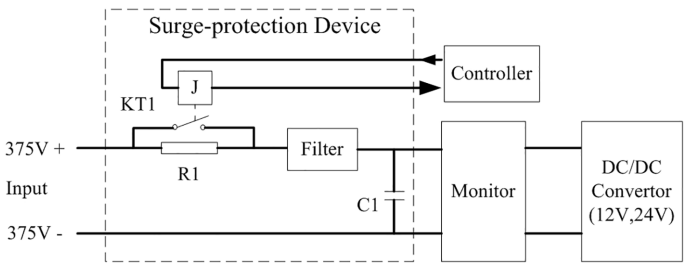

FIGURE 3
Schematic of surge-protection device.

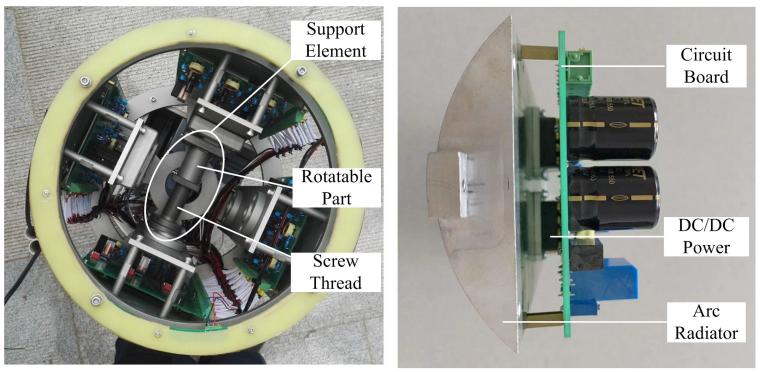

FIGURE 4
Mounting structure for radiator.

the voltage and current of each output port in real time; (ii) control the power outputs of the output ports *via* the PC software, which can automatically isolate local faults in an emergency (e.g., short circuits and reduced insulation performance of an port). The core unit of the state monitoring and control system is a micro-controller chip (MSP430F149; Texas Instruments) with the characteristics of low operating voltage, ultra-low power consumption, flexible expansion, and high reliability (Song et al., 2012). As shown in Figure 5, the MSP430F149 has two RS-232 serial communication ports: one connected to the communication system, the other connected to the load monitoring module. The MSP430F149 has 48 input/output ports in total, but we use only nine of them, with the others being spare. Of the nine used ports, six are connected to the control circuit on the load monitoring module to control the power supply of the external scientific sensors, and the other three are connected to the temperature and humidity sensor, the water-leakage monitoring sensor, and the surge-protection device.

To ensure stable operation of the scientific sensors, the load monitoring module must keep the supply voltage and current within safe and reliable ranges. As shown in Figure 5, the six circuits are isolated from each other, and each circuit is equipped with voltage and current monitoring and over-voltage protection (OVP) and over-current protection (OCP) functions. The voltage and current monitoring monitors the instantaneous voltage and current on the circuit and triggers OVP and OCP if they exceed their preset values; the controller then immediately disconnects the scientific sensor from the power supply through the control actuator, which comprises MOSFET (metal–oxide–semiconductor field-effect transistor) Q1 and electromagnetic relay KT2 in series. The MOSFET has the characteristic of fast switching and can be used as a power

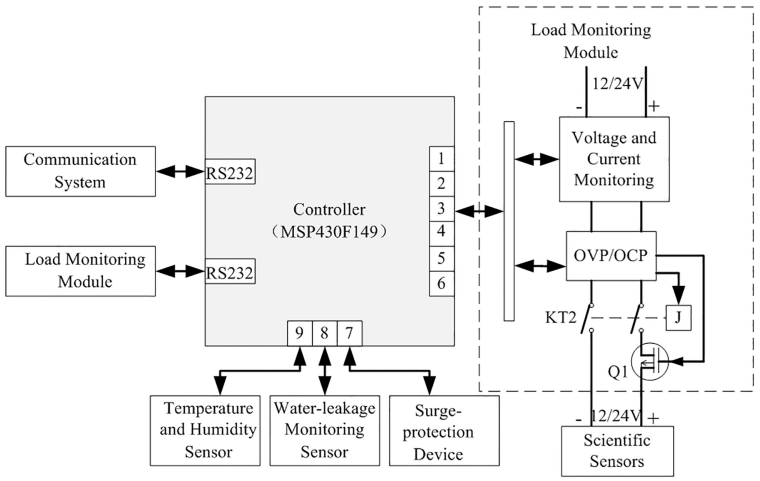

FIGURE 5
Block diagram of state monitoring and control system.

switch to control the load circuit, but it cannot achieve absolute electrical isolation. Although the electromagnetic relay can achieve electrical isolation, the contact is prone to arc discharge when it acts with load; in particular, there is a possibility of action failure in the case of high voltage and current (Lin et al., 2011). Therefore, the MOSFET and electromagnetic relay are connected in series to realize their complementary performance and improve the reliability of the actuator. Their working logic is as follows: under normal conditions, when supplying power to the scientific sensors, KT2 is first connected, then the conduction of Q1 is controlled after a delay of several milliseconds; by contrast, in the case of OVP or OCP, Q1 is stopped, then KT2 is disconnected after a delay of several milliseconds.

2.4 Communication system

The communication system of IMSDCO is *via* optical-fiber Ethernet communication based on TCP/IP (Transmission Control Protocol/Internet Protocol). The communication system architecture is shown in Figure 6. The shore-station communication system comprises a switch and a server running the communication system software. The switch is a network managed industrial optical Ethernet switch (EDS-G509-T; MOXA Company), which supports web management and SNMP (Simple Network Management Protocol) to achieve optimal network settings, and the IP addresses of the ports are set through the configuration software. The communication system in the underwater node comprises a switch and a serial-port server; it realizes communication between the shore station and the controller in the node and serves as a transit station for communication between the shore station and the scientific sensors. The uplink of the switch (EDS-480A-T; MOXA Company) is connected to the shore station through optical fiber, and the downlink is connected to the OMI and the serial-port server based on TCP/IP through twisted-pair cable. The serial-port server (NPort 5650I-8-DT; MOXA Company) connects the scientific sensors based on the RS-232 serial-port communication protocol, which converts the serial-port communication protocol into TCP/IP to achieve bidirectional transparent transmission of data. Also, the serial-port server supports remote configuration, and each of its ports can be set as an independent virtual IP address *via* software, so that each scientific sensor can be accessed remotely at the shore station. Based on the communication system with this architecture, authorized users can access the node and the scientific sensors from anywhere through the Internet.

2.5 Data acquisition and management system

Six scientific sensors are connected to the underwater node: five of them (ADCP, CTD, tidal meter, multi-parameter water-quality detector 1, and OMI) are installed on the bottom platform; the other (multi-parameter water-quality detector 2) is installed on the mooring structure. The specifications of the scientific sensors are given in Table 1.

The hypogynous machine of the data acquisition and management system packages the collected underwater-node operation-status data and scientific-sensor monitoring data and sends them to the PC software in the shore station *via* the communication system. The function of the PC software is to complete data reception, analysis, storage, and visualization. As shown in Figure 7, the PC software is divided into six core service modules: (i) sensor-driven service, (ii) data collection and distribution service, (iii) quality-control service, (iv) time service, (v) data archiving service, and (vi) data application service. The six modules exchange scientific-sensor data, control instructions,

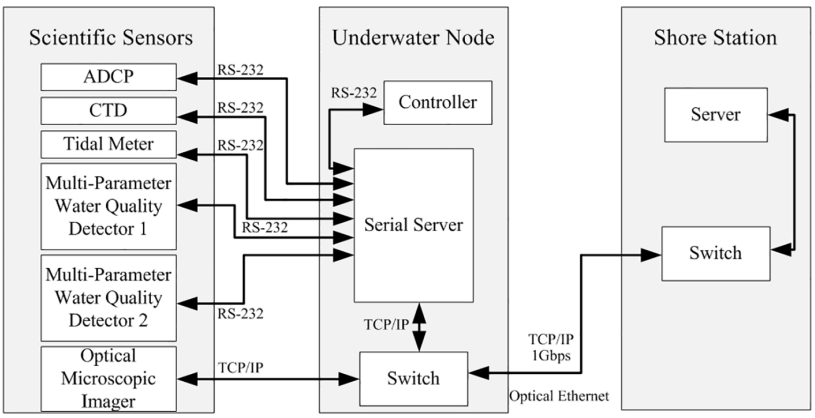

FIGURE 6
Block diagram of communication system.

TABLE 1 Specifications of scientific sensors installed on node.

ADCP	Nortek Signature 500K Max. profiling depth: 60 m (burst mode)/70 m (average mode) Measurement cell range: 0.5–4 m Max. number of cells: 256 (burst mode)/200 (average mode) Max. velocity: 5 m/s (accuracy: ± 0. 3% of measured value ± 3 mm/s; resolution: 1 mm/s) Max. sampling rate: 8 Hz
CTD	SeaBird 37SIP Conductivity range: 0–7 S/m (accuracy: ± 0. 0003 S/m; resolution: 0.00001 S/m) Temperature range: −5°C to 35°C (accuracy: ± 0. 002°C; resolution: 0.0001°C) Pressure range: 0–350 m (accuracy: ± 0. 35 m; resolution: 0.007 m) Acquisition time: 1.0–2.6 s/sample
Tidal meter	RBR virtuoso D (tide) Max. pressure: 100 dbar (accuracy: ± 0. 05%FS; resolution: 0.001%FS) Max. sampling rate: 1 Hz, 2 Hz, 4 Hz, 6 Hz (software selection) Sampling period: 1 s to 24 h
Multi-parameter water-quality detectors 1 and 2	AML P1S4 Derived parameters: pressure, temperature, conductivity, turbidity, and chlorophyll Pressure range: 0–100 dbar (accuracy: ± 0. 05%FS; resolution: 0.02%FS) Temperature range: −5°C to 45°C (accuracy: ± 0. 005°C; resolution: 0.001°C) Conductivity range: 0–90 mS/cm (accuracy: ± 0. 01 mS/cm; resolution: 0.001 mS/cm) Turbidity range: 0–3000 NTU (accuracy: ± 2% of reading or 0. 2 NTU, whichever is greater; resolution: 0.01 NTU) Chlorophyll range: blue excitation (A) 0–50 μg/L (accuracy: no specification provided; min. detection limit: 0.025 μg/L); red excitation (B) > 50 μg/L (accuracy: no specification provided; min. detection limit: 0.5 μg/L)
Optical microscopic imager	IPP05 Particle size measurement range: 500 μm to 20 mm Max. operating depth: 200 m Recognition rate: >80% Operating temperature range: −5°C to 50°C

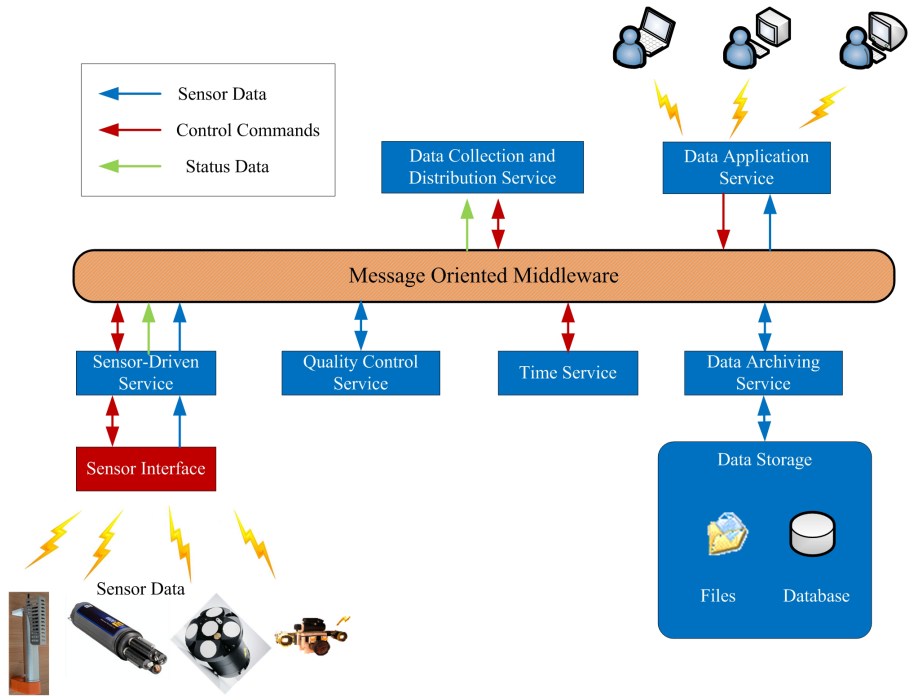

FIGURE 7
Architecture of data acquisition and management system.

andnode operation-status data through message-oriented middleware, and they cooperate to complete the data collection, archiving, distribution, and application. The data acquisition and management system can easily realize various functions, such as user management, permission setting, data query, historical data curve browsing, and instrument maintenance record query, among others.

2.6 Deployment

Having designed IMSDCO, it was tested comprehensively in the laboratory and an indoor pool to confirm that all the design specifications and functions were achieved. On 18 September 2021, with the cooperation of partners, the system was deployed at the cold-water intake of the Hainan Changjiang Nuclear Power Plant. The observation node before deployment is shown in Figure 8. We connected the node and the photoelectric composite cable together on the deck of an engineering ship and used the crane on the ship to place the node on the seabed 800 m from the shore at a depth of 15 m. Next, the engineering ship laid the photoelectric composite cable along a preset path to the intertidal zone. The photoelectric composite cable was pulled by people on the shore to the shore station and was connected with the power supply system and communication system after passing through a photoelectric separation box. After a specially assigned person checked and confirmed that the system was connected correctly, we turned on the power supply, switch, server, and other equipment in the shore station, whereupon IMSDCO began to work. The shore station then received data continuously from the underwater scientific sensors, marking the successful deployment of IMSDCO.

3 Results and discussion

After deploying IMSDCO, by the end of March 2022 all of its functional modules had been running stably for six months and a large amount of data had been obtained. The 12-V and 24-V voltages output by the DC/DC converter were continuously stable, without over-current, short circuit, or other faults. As shown in Figure 9A, the voltage change was less than 1% even when the load step changed. The state monitoring and control system monitored the voltage, current, radiator temperature, and cabin internal humidity and displayed them *via* PC software in real time. The communication system had not been interrupted, and the shore station continuously received monitoring data from the scientific sensors and stored them in the database of the data acquisition and management system. Authorized users could access the data at any time, including temperature, salinity, pH, water depth, tide level, ocean current velocity, and images of DCOs. Temperature and salinity data are shown in Figure 9B, and images of DCOs are shown in Figure 10. Based on the data obtained, we used software algorithms to estimate the changes in DCO abundance with time (Figure 11). As shown in Figure 11, large numbers of *Acetes chinensis* were observed between 00:00 and 09:00, whereas almost none were observed at other times; the reason for this is that the temperature of the sea water near the observation point at night is more appropriate for *Acetes chinensis*, then when the temperature rises in the day, they migrate to the deep-sea area where the temperature is then more appropriate. *Phaeocystis globosa* exhibited a similar situation to that of *Acetes chinensis*, this being because higher temperature is not conducive to forming colonies of *Phaeocystis globosa* cells (Wang et al., 2021).

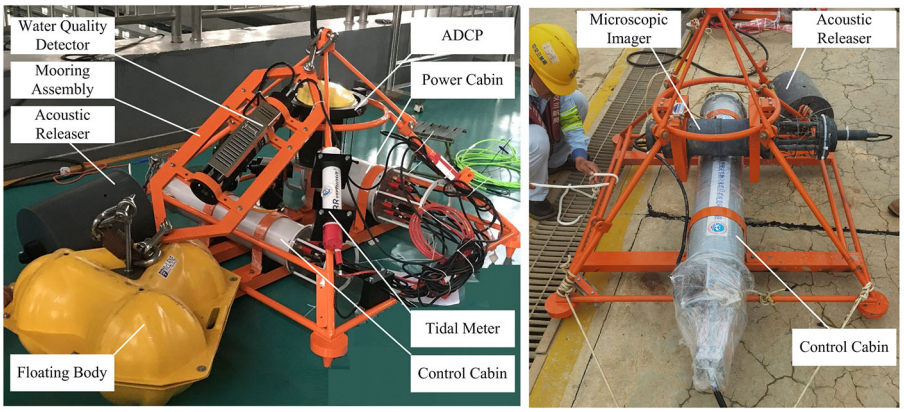

FIGURE 8
Observation node before deployment.

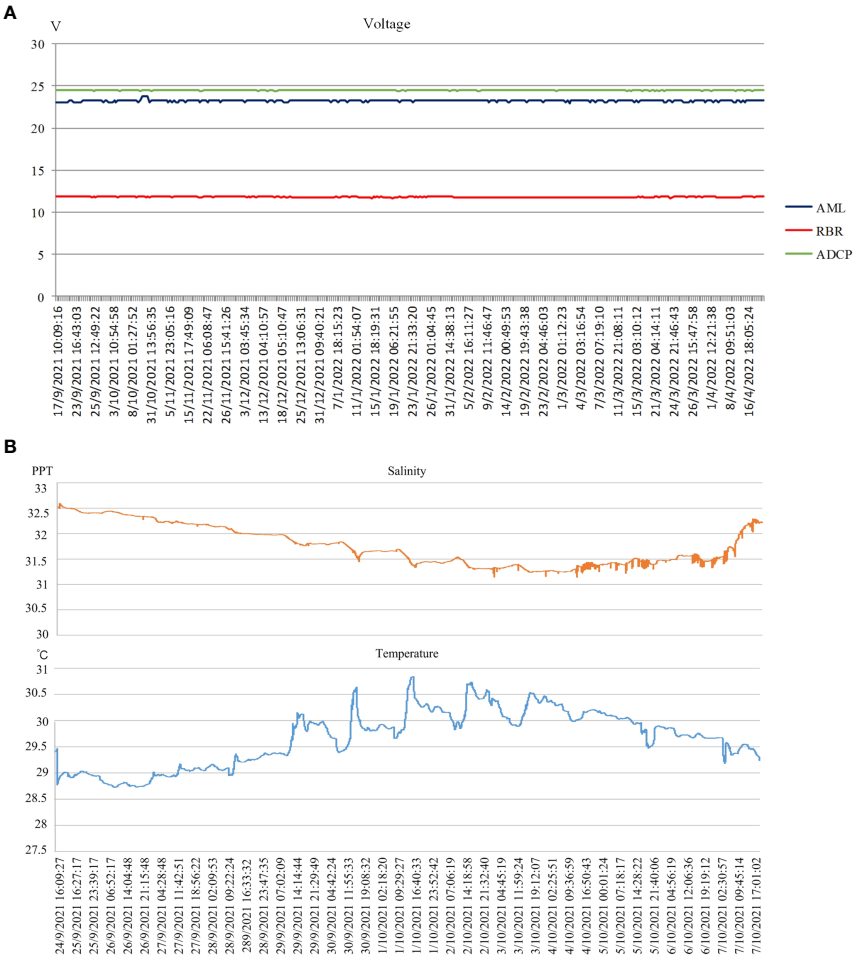

FIGURE 9
Part of monitoring data:**(A)** Sensors voltage data;**(B)** Temperature and salinity data. **Please refer to supplementary material for complete data.*

The theoretical basis for estimating the DCO abundance is as follows:

$$A_{bio} = \frac{Q}{V} \quad , \ (1)$$

$$V = K \times N \quad , \ (2)$$

where A_{bio} is the biological abundance, Q is the total number of identified organisms, V is the total volume of sampled water, K is the water volume corresponding to a single image, and N is the total number of images.

The prediction of DCO trajectories is based on the SCHISM three-dimensional hydrodynamic model, which is established according to the hydrological data of the target sea area, such as tide level, waves, and current. By bringing the number and location information of DCOs at different times into the three-dimensional hydrodynamic model, we can obtain a numerical model of DCO drift and predict the migration trajectories of DCOs. The positions of the DCOs monitored in real time are used as the initial and correction points to continuously modify the trajectory parameters so as to optimize the prediction of DCO trajectories.

The experimental results show that IMSDCO has achieved the design goals, but it still needs to be improved. The estimated DCO abundance is affected by ocean currents, image sampling interval, and biomass of repeated counting in adjacent images, and there will be errors compared with the actual value. The OMI used by IMSDCO can only identify DCOs between 500 μm and 20 mm in size, but large aquatic organisms beyond this range—even aquatic plants and garbage on the sea surface—will also block the water intake; these disaster-causing substances must be monitored by adding sonar, cameras, and radar, which is just one aspect of IMSDCO that needs to be improved. Also, to achieve early warning of a blockage of the water intake of a nuclear power plant, it is necessary to monitor a large sea area near the water intake; however, the spatial distribution of disaster-causing biological data cannot be obtained through only one observation point, which will also result in errors in

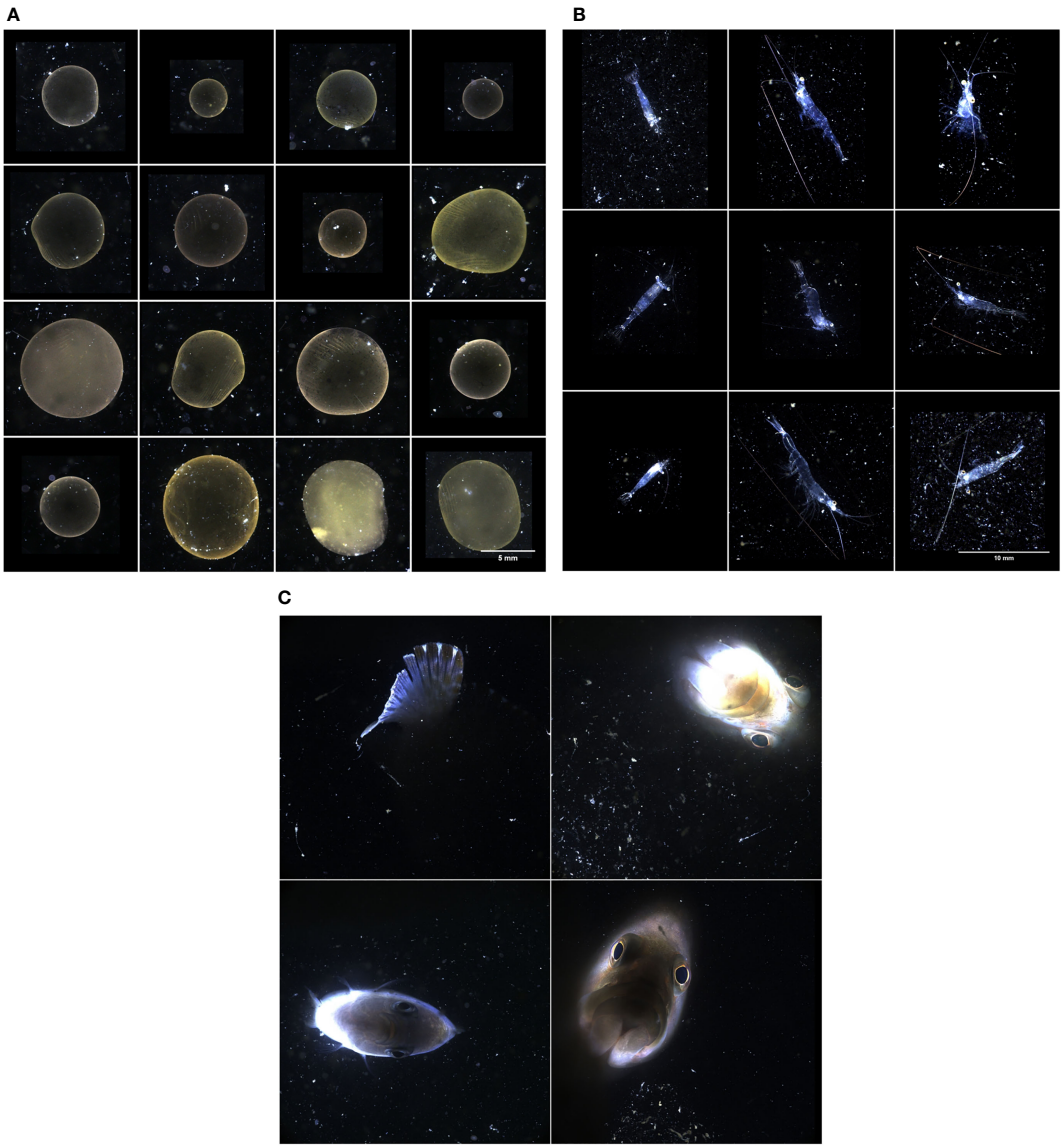

FIGURE 10
Photographs of some disaster-causing organisms (DCOs):**(A)** Phaeocystis globosa;**(B)** *Acetes chinensis*; **(C)** small fish. * These pictures are from the team of Dr. Li Jianping from the Shenzhen Institute of Advanced Technology, Chinese Academy of Sciences, who provided the optical microscopic imager.

DCO abundance estimation and trajectory prediction. In future work, we also need to carry out underwater multi-point observation experiments, enrich the monitoring data by increasing the number of observation points, and reduce errors as much as possible.

4 Conclusions

We have studied and implemented a seafloor *in situ* IMSDCO that provides long-term power and real-time communication for underwater scientific sensors through a cable. The key technologies of power supply, state monitoring and control, multi-protocol communication, and data acquisition and management were proposed and implemented, which improved the reliability and operability of the system. The system was deployed successfully at the cold-water intake of the Hainan Changjiang Nuclear Power Plant. During a six-month sea trial, the system continued to operate stably and obtained long-term hydrological environmental data and a large number of DCO images. Through the software algorithms to analyze the collected images automatically, various DCOs were identified. The monitoring software displayed the DCO abundance in real time, and if it exceeded the alarm threshold, then the software would give a warning. The horizontal movement of the

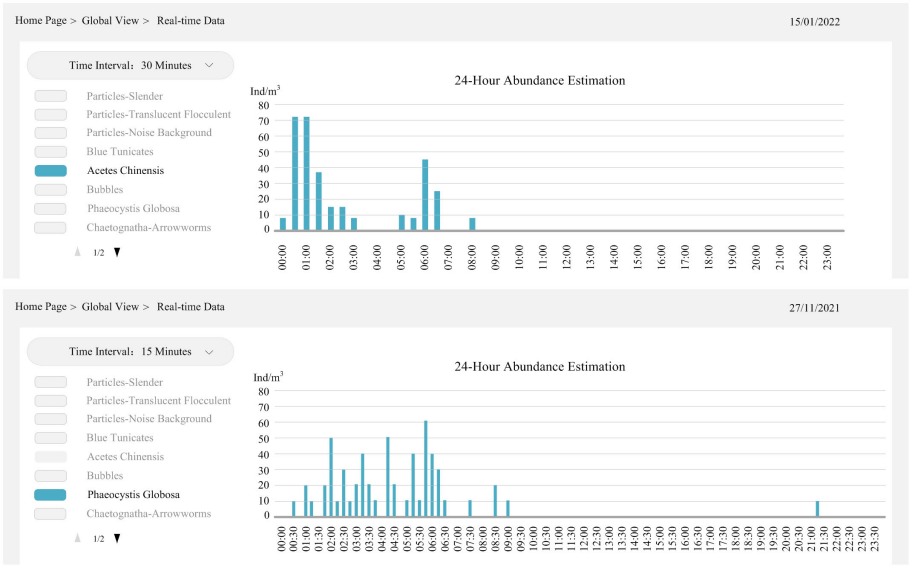

FIGURE 11
24-hDCO abundance estimation of *Acetes chinensis* and *Phaeocystis globosa*.

planktonic DCOs is driven mainly by the ocean currents, and their movement track can be predicted by combining the velocity and direction data. The results of the sea trial show that the optically based IMSDCO is feasible, thereby providing a new idea and scientific guidance for DCO early warning and prevention at the cold-water intakes of nuclear power plants.

Data availability statement

The original contributions presented in the study are included in the article/Supplementary Material. Further inquiries can be directed to the corresponding author.

Author contributions

CL, JH, and S-TL conceived and designed the study. CL, Y-ZS, S-TL, and LY carried out all the experiments. JH and Y-ZS analyzed the data. CL wrote the manuscript. JH, Y-ZS, LY, and S-TL edited the manuscript. All authors contributed to the article and approved the submitted version.

Funding

This project was supported by the Innovation Fund of the National Center for Marine Technology [Grant No. Y1200Z006], the Open Research Fund of the Key Laboratory of Marine Ecological Monitoring and Restoration Technologies [Grant No. MEMRT202116], and the National Key R&D Program of the Ministry of Science and Technology of the People's Republic of China [Grant No. 2018YFC1407506].

Acknowledgments

It was implemented in cooperation with Xiamen University and the Hainan Changjiang Nuclear Power Plant of the China Nuclear Industry Group. The authors sincerely thank the team led by Dr. Li Jianping of the Shenzhen Institute of Advanced Technology of the Chinese Academy of Sciences for their help on the project from the beginning of deployment to the final recovery.

Conflict of interest

The authors declare that the research was conducted in the absence of any commercial or financial relationships that could be construed as a potential conflict of interest.

Publisher's note

Supplementary material

The Supplementary Material for this article can be found online at: https://www.frontiersin.org/articles/10.3389/fmars.2022.1089699/full#supplementary-material

References

Azila, A., and Chong, V. C. (2010). Multispecies impingement in a tropical power plant, straits of malacca. *Mar. Environ. Res.* 70 (1), 13–25. doi: 10.1016/j.marenvres.2010.02.004

Bi, H. S., Song, J. T., Zhao, J., Liu, H., Cheng, X. M., Wang, L. L., et al. (2022). Temporal characteristics of plankton indicators in coastal waters: High-frequency data from PlanktonScope. *J. Sea Res.* 189, 102283. doi: 10.1016/j.seares.2022.102283

Chen, J. C., and Xia, L. S. (2017). The enlightenment of foreign nuclear power development to the development of nuclear power in China. *Value Eng.* 26, 237–241. doi: 10.14018/j.cnki.cn13-1085/n.2017.26.097

CNEA (2021). *China Nuclear energy development report* (Beijing: Social Sciences Academic Press).

Cowen, R. K., and Guigand, C. M. (2008). *In situ* ichthyoplankton imaging system(ISIIS): System design and preliminary results. *Limnol. Oceanogr. Methods* 6 (2), 126–132. doi: 10.4319/lom.2008.6.126

Deng, X. J. (2021). Clean energy cooperation between China and southeast Asia: Opportunities and challenges for nuclear power. *Southeast Asian Stud.* 5, 156–157. doi: 10.19561/j.cnki.sas.2021.05.093

Du, D. P., Lu, X., and Yan, Y. Z. (2018). Design of a surge current suppression circuit on airborne DC/DC. *Microelectronics* 48 (2), 216–221. doi: 10.13911/j.cnki.1004-3365.170374

Greer, A. T., Woodson, C. B., Smith, C. E., Guigand, C. M., and Cowen, R. K. (2016). Examining mesozooplankton patch structure and its implications for trophic interactions in the northern gulf of Mexico. *J. Plankton Res.* 38 (4), 1115–1134. doi: 10.1093/plankt/fbw033

Grossmann, M. M., Gallager, S. M., and Mitarai, S. (2014). Continuous monitoring of near-bottom mesoplankton communities in the East China Sea during a series of typhoons. *J. Oceanogr.* 71 (1), 115–124. doi: 10.1007/s10872-014-0268-y

Han, R., Ji, P., Zhao, Y. J., Liu, Y., and Kang, Z. S. (2018). Investigation and analysis of water intake blockage ofcoastalnuclear power plants. *Water Wastewater Eng.* 44 (S1), 75–80. doi: 10.13789/j.cnki.wwe1964.2018.0265

Howe, B. M., Kirkham, H., and Vorperian, V. (2002). Power system considerations for undersea observatories. *IEEE J. Ocean Eng.* 27 (2), 267–274. doi: 10.1109/JOE.2002.1002481

Jaffe, J. (2015). *In situ* underwater microscopy: A transformative technology for observing small organisms in the sea. *Opt. Optoelectron. Technol.* 13 (4), 1–3.

Li, J. P., Chen, T., Yang, Z. Y., Chen, L. P., Zhang, Y. Z., Yu, G. W., et al. (2022). Development of a buoy-borne underwater imaging system for *In situ* mesoplankton monitoring of coastal waters. *IEEE J. Ocean Eng.* 47 (1), 88–110. doi: 10.1109/JOE.2021.3106122

Li, D. J., Wang, J., Feng, J. S., Yang, C. J., and Chen, Y. H. (2016). Study and design of a heatdissipation system in a junction box for chineseexperimental ocean observatory network. *Mar. Technol. Soc J.* 50 (2), 63–74. doi: 10.4031/MTSJ.50.2.5

Lin, D. D., Li, D. J., Yang, S. J., Jin, B., Chen, Y. H., and Yang, J. C. (2011). Development of power management system based on seafloor observatory network junction box. *Ship Eng.* 33 (2), 77–80. doi: 10.3969/j.issn.1000-6982.2011.02.019

Liu, D.Y., Ke, Z., Cai, Z.H., Huang, H.H., and Bi, H.S. (2021). Outburst of Creseis acicula in southwest Daya bay in July 2020. *Oceanol. Limnol. Sin.* 52 1438–1447. doi: 10.11693/hyhz20210400086

Lombard, F., Boss, E., Waite, A. M., Vogt, M., and Appeltans, W. (2019). Globally consistent quantitative observations of planktonic ecosystems. *Front. Mar. Sci.* 6. doi: 10.3389/fmars.2019.00196

MEE (2020) *Letter on notification of multiple unit shutdown operation events caused by marine organisms affecting the water intake system of nuclear power plant.* Available at: https://www.mee.gov.cn/xxgk2018/xxgk/xxgk07/202003/t20200331_771924.html (Accessed May 18, 2022).

Meng, Y. H., Hu, L. S., Li, J. W., and Zhang, J. F. (2019). Research on marine biological monitoring technology to improve the cold source safety of nuclear power plant. *Electr. Saf. Technol.* 21 (3), 33–39. doi: 10.3969/j.issn.1008-6226.2019.03.010

Merz, E., Kozakiewicz, T., Reyes, M., Ebi, C., Isles, P., Baity-Jesi, M., et al. (2021). Underwater dual-magnification imaging for automated lake plankton monitoring. *Water Res.* 203, 117524. doi: 10.1016/j.watres.2021.117524

MOC (2021) *Utilization of nuclear energy in EU*. Available at: http://at.mofcom.gov.cn/article/jmxw/202112/20211203233311.shtml (Accessed July 15, 2022).

Ohman, M. D., Davis, R. E., Sherman, J. T., Grindley, K. R., and Ellen, J. S. (2019). Zooglider: An autonomous vehicle for optical andacoustic sensing of zooplankton. *Limnol. Oceanogr.Methods* 17 (1), 69–86. doi: 10.1002/lom3.10301

Picheral, M., Guidi, L., Stemmann, L., Karl, D. M., Iddaoud, G., and Gorsky, G. (2010). The underwater vision profiler 5: An advanced instrument for high spatial resolution studies of particle size spectra and zooplankton. *Limnol. Oceanogr. Methods* 8 (9), 462–473. doi: 10.4319/lom.2010.8.462

Purcell, J. E., Uye, S., and Lo, W. (2007). Anthropogenic causes of jellyfish blooms and their direct consequences for humans: A review. *Mar. Ecol. Prog. Ser.* 350, 153–174. doi: 10.3354/meps07093

Ruan, G. P. (2015). Reason analysis and corresponding strategy for cooling water intake blockage at nuclear power plants. *Nucl. Power Eng.* 36 (S1), 151–154. doi: 10.13832/j.jnpe.2015.S1.0151

Song, J. J., Ren, B., and Song, L. (2012). The design and realization of a spectrum acquisition unit based on the MSP430F149 MCU. *Appl. Mech. Mater.* 246–247, 230–234. doi: 10.4028/www.scientific.net/AMM.246-247.230

Wang, K., Chen, B. H., Gao, Y. H., and Lin, H. (2021). Harmful algal blooms caused by phaeocystis globosafrom 1997 to 2018 in Chinese coastal waters. *Mar. pollut. Bull.* 173 (A), 112949. doi: 10.1016/j.marpolbul.2021.112949

Wang, Z., and Fu, Y. Y. (2021). Monitoring of cold source biomass at water intake of hongyanhe nuclear plant by using acoustic methods. *Sci. Technol. Innov.* 36, 169–172. doi: 10.3969/j.issn.1673-1328.2021.36.053

Xu, S. X. (2020). Present situation, problems and countermeasures of nuclear power development in China. *J. North China Electric Power Univ. (Soc. Sci.)* 5, 1–9. doi: 10.14092/j.cnki.cn11-3956/c.2020.05.001

Yang, Z.Y., Li, J.P., Chen, T., Pu, Y.C., and Feng, Z.H. (2022). Contrastive learning-based image retrieval for automatic recognition of in situ marine plankton images. *ICES J. Mar. Sci.* 79 (10), 2643–2655. doi: 10.1093/icesjms/fsac198

Yu, W. J., Li, Z. G., Sun, K., Qin, B. C., Li, M. Z., and Feng, Y. B. (2013). Study on power management and control system for ocean cabled observatory. *Mach. Des. Manuf.* 5, 252–255. doi: 10.3969/j.issn.1001-3997.2013.05.078

Zeng, L., Chen, G., Wang, T., Zhang, S., Dai, M., Yu, J., et al. (2021). Acoustic study on the outbreak of creseise acicula nearby the daya bay nuclear power plant base during the summer of 2020. *Mar. pollut. Bull.* 165, 112144. doi: 10.1016/j.marpolbul.2021.112144

Zhang, Y. (2021). Analysis on the development trend of nuclear energy in China under the dual carbon target. *Nucl. Sci. Eng.* 41 (6), 1347–1351. doi: 10.3969/j.issn.0258-0918.2021.06.034

Zhang, C. W., Guan, C. J., Xu, P., Liu, G. Z., Xu, Q. M., Ye, J. Q., et al. (2019). Analysis on risk organisms for the cold source water of nuclear power plant in the eastern waters of liaodong bay. *Mar. Environ. Sci.* 38 (1), 41–45. doi: 10.13634/j.cnki.mes.2019.01.030

frontiers | Frontiers in Marine Science

TYPE Original Research
PUBLISHED 10 January 2023
DOI 10.3389/fmars.2022.1016074

OPEN ACCESS

EDITED BY
Wei Wu,
University of Southern Mississippi,
United States

REVIEWED BY
Xiaohong Sun,
Shandong University, China
Xuejia He,
Jinan University, China

*CORRESPONDENCE
Fuwu Xie
xfw1021900977@163.com
Xingyu Song
songxy@scsio.ac.cn

SPECIALTY SECTION
This article was submitted to Marine Pollution, a section of the journal Frontiers in Marine Science

RECEIVED 10 August 2022
ACCEPTED 12 December 2022
PUBLISHED 10 January 2023

CITATION
Liu H, Li J, Wang H, Huang H, Xie F and Song X (2023) High-temperature thermal discharge inhibits plankton community metabolism in a partly eutrophicated bay in China. *Front. Mar. Sci.* 9:1016074. doi: 10.3389/fmars.2022.1016074

High-temperature thermal discharge inhibits plankton community metabolism in a partly eutrophicated bay in China

Huaxue Liu[1], Jiajun Li[1], Huijuan Wang[1], Honghui Huang[1], Fuwu Xie[1,2,3]* and Xingyu Song[2]*

[1]South China Sea Fisheries Research Institute, Chinese Academy of Fishery Sciences, Guangzhou, China, [2]Key Laboratory of Tropical Marine Bio-resources and Ecology, South China Sea Institute of Oceanology, Chinese Academy of Sciences, Guangzhou, China, [3]Hainan Eco-Environmental Monitoring Center, Haikou, China

Managing the marine ecosystem effectively requires studying the response of plankton community metabolism to warming. Moreover, warming caused by thermal discharge is known to significantly raise the water temperatures in the nuclear power plants. However, effects of thermal discharge on planktonic community metabolic characteristics, especially net community production, in surrounding waters remain poorly understood. Therefore, in this study, we aimed to analyze the characteristics of plankton community metabolism in thermal discharge area of the Daya Bay, China. The investigations were conducted in August 2016 and January 2017. Our results showed that the plankton community metabolism was promoted in moderately warm regions (29.4-30 °C), with higher gross primary production and community respiration than in high- and extremely high-temperature regions; meanwhile, plankton community metabolism was evidently inhibited in high (31.4 °C in winter) or extremely high (36°C in summer) temperature regions, thereby exhibiting heterotrophic metabolism state. Our findings indicate that warming could affect plankton community carbon metabolism in the Daya Bay, thereby declining the stability of the marine ecosystem.

KEYWORDS

plankton community metabolism, thermal discharge, warming, gross primary production, community respiration

1 Introduction

Plankton metabolism is a fundamental property of marine ecosystem driving the flux of gases and the transference of organic matter to the food web (Agusti et al., 2018). Marine plankton metabolic processes mainly include the gross primary production(GPP) and community respiration (Del Giorgio and Williams, 2005; Ducklow and McAllister, 2005), and directly affect the oceanic carbon cycle (Xiang et al., 2022).The key ecological processes affecting the carbon budget in marine ecosystems remain unknown, and related studies primarily focus on the response of plankton community metabolism to warming due to global climate change (Nguyen et al., 2012; Wang, 2014). Warming caused by thermal discharge could raise the adjacent water temperature in the nuclear power plant by over 8°C (Kim et al., 2007; Choi, 2008). However, effects of thermal discharge on planktonic community metabolic characteristics, especially net community production (NCP), have rarely been reported in surrounding waters.

The Daya Bay is an important subtropical semi-enclosed bay located in southern China. With the increasing number and scale of nuclear power plants in the Daya Bay, heating effect by thermal discharge is gaining attention (Teixeira et al., 2012), but the effects of thermal discharge on planktonic community metabolic characteristics in the Daya Bay remain unknown. In this study, we aimed at demonstrating the response mechanism of plankton community metabolism and carbon metabolism balance to thermal discharge.

2 Materials and methods

2.1 Samples collected and analysis

Sampling and *in situ* experiments were carried out in thermal discharge area from August 1 to 10, 2016, and January 4 to 13, 2017, respectively. Six sampling stations (It was named as S1-S6 in summer and W1-W6 in winter) were set along the actual temperature gradient in the adjacent area around thermal discharge outfall (Figure 1), and water depth ranged from 5 to 7m.

Water samples were collected using a 5L niskin bottle at the surface layer, and environmental factors (temperature, salinity and pH) were measured simultaneously using a YSI 6600 multi-parameter water quality monitor (Yellow Springs Instrument Co., USA) at each sampling site. After collection, the water samples (0.5L) for inorganic nutrients and chlorophyll a (Chl-*a*) determination were filtered on GF/F filters (Whatman). Moreover, the water and filters were preserved at -20°C in the darkness before further processing in the laboratory. The nutrient (nitrate, nitrite, ammonia, and phosphate) concentrations were analyzed using a nutrients-analyzer (Quickchem 8500, USA) according to Kirkwood et al. (1996). Chl-*a* concentration was also measured using a Turner Design 10-AU fluorometer according to Parsons et al. (1984).

2.2 *In situ* plankton metabolism experiment

The planktonic community metabolic rates (GPP; NCP; and community respiration, CR) were estimated from the changes in dissolved oxygen concentrations in the light–dark bottles over a 24-h incubation period following Serret et al. (1999). Each temperature gradient has three duplicate samples, and DO was measured at the 0 h and 24 h of incubation period by Presens precision sensing Microx 4 Oxygen meter with a detection limit of 0.01 mg/L and detection accuracy of ±0.025 mg/L.

2.3 Data analysis

Pearson analysis was also performed to detect the relationships between metabolic rates and Chl-*a* using the SPSS software. The metabolic rates and their responses to biotic and/or abiotic factors were elucidated with canonical correspondence analysis (CCA). The CCA analysis was conducted using the statistical program, CANOCO version 4.5 (Chen et al., 2011).

3 Results

3.1 Environmental characteristics

Environmental parameters in both seasons are shown in Table 1. In summer, sea surface temperature decreased along the transect and ranged from 29.5 to 36°C in summer, with a temperature difference of 6.5°C. Sea surface salinity exceeded the value of 33 in the entire study area. Dissolved inorganic nitrogen (DIN) concentration ranged from 6.15 to 8.72 μmol·L^{-1}, and dissolved inorganic phosphate (DIP) concentration ranged from 0.05 to 0.18 μmol·L^{-1}. Chl-*a* concentration ranged from 0.66 to 1.72 μg·L^{-1}, and Chl-*a* was highly concentrated at S4 and S5.

In winter, the sea surface temperature decreased from 23.2 to 31.2 °C, with a temperature difference of 8°C. The value of sea surface salinity was found to be < 28 in the entire study area. DIN concentration ranged from 13.05 to 22.90 μmol·L^{-1}, whereas DIP concentration ranged from 0.15 to 0.26 μmol·L^{-1}. Chl-*a* concentration ranged from 0.16 to 0.51 μg·L^{-1}, with high concentrations at stations W5 and W6. The atomic ratio of DIN/DIP in thermal discharge area between summer and winter was 16:1, suggesting a potential phosphorus limitation.

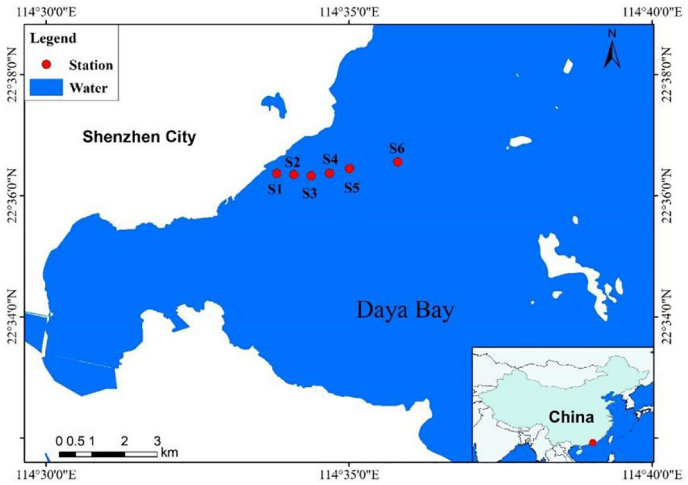

FIGURE 1
Maps of sampling stations in Daya Bay.

3.2 Plankton community metabolism

In summer, CR increased slightly with increasing temperature. Moreover, GPP and NCP increased with warming (Figure 2). GPP and CR were highest in the temperature range of 30.0-31.0°C, with values of 641.25 and 78.75 mgC·m^{-3}·d^{-1}, respectively, and the metabolic balance of the plankton community was in the positive state. In contrast, GPP and CR were lowest in extremely high temperature regions(34.0-36.0°C), declining to 7.50 and 52.50 mgC·m^{-3}·d^{-1} respectively, and the community metabolic rate was in a state of negative metabolic balance.

In winter, CR and GPP increased firstly and then decreased with warming (Figure 3), with maximum values of 300.00 and 112.50 mgC·m^{-3}·d^{-1}, respectively. Plankton community metabolism was in a negative metabolic balance state.

The study areas showed autotrophic metabolic characteristics in summer, except for the extremely high temperature water regions (34–36°C), and plankton community production was higher in summer than in winter. On the contrary, the entire study area showed heterotrophic negative metabolic trend in winter, and respiration rates of communities in winter were higher than those in summer.

3.3 Relationship between plankton community metabolism and environmental parameters

The results of CCA are illustrated in Figure 4. In summer, GPP and Chl-*a* were positively related to salinity (PSU) and temperature (T), respectively. In winter, CR and Chl-*a* were positively correlated with temperature (T) and salinity (PSU), respectively. CCA showed that changes in temperature and salinity affected GPP and CR. Moreover, Pearson analysis

TABLE 1 Environmental parameters of study area during summer and winter in Daya Bay.

Station	Summer						Winter					
	S1	S2	S3	S4	S5	S6	W1	W2	W3	W4	W5	W6
T (°C)	36	34	32.1	31	30	29.5	31.2	29	27.1	26.3	24.6	23.2
PS (‰)	33	33.3	34.1	33.6	33.7	33.3	27.5	27.1	27.6	27.5	27.6	27.6
Chl-*a* (μg·L^{-1})	0.92	0.66	0.85	1.22	1.72	0.9	0.16	0.19	0.26	0.25	0.39	0.51
DIP (μmol·L^{-1})	0.06	0.05	0.08	0.05	0.18	0.06	0.23	0.2	0.26	0.25	0.15	0.25
DIN (μmol·L^{-1})	6.95	6.15	6.2	8.72	8.6	6.43	18.03	18.34	17.61	17.79	22.9	13.05
DIN/DIP	115.83	123	77.5	174.4	47.78	107.17	78.39	91.7	67.73	71.16	152.67	52.2

Chl-a, chlorophyll a; DIP, dissolved inorganic phosphate; DIN, dissolved inorganic nitrogen.

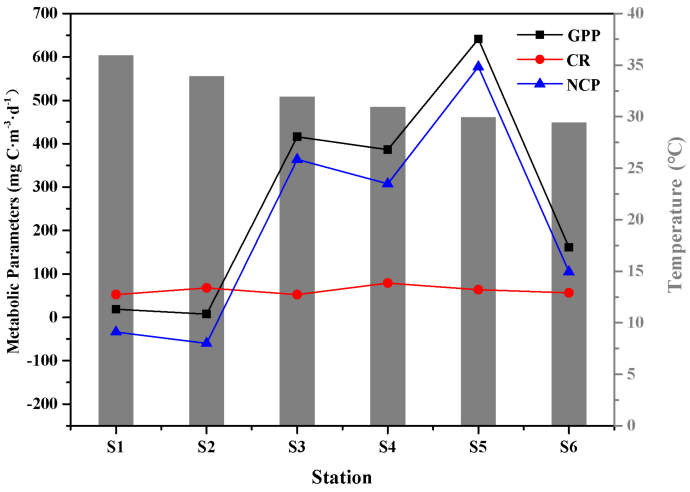

FIGURE 2
Features of plankton community metabolism during summer.Changes in CR are shown in red line and symbols, in NCP in blue line and symbols, and in GPP in black line and symbols, over time. CR, community respiration; GPP, gross primary production; NCP, net community production.

showed that Chl-*a* concentration was positively related to GPP and NCP (Figure 5).

4 Discussion

4.1 Effect of warming on plankton community metabolism

When NCP > 0, primary productivity was higher than the respiratory rate, and the ecosystem exhibited an autotrophic state, acted as a CO_2 sink, and stored or exported the organic matter. In contrast, when NCP < 0, respiratory consumption exceeded primary productivity, and the ecosystem exhibited a heterotrophic state and acted as a CO_2 source that required storage or demineralization by exogenous organic matter input to maintain carbon source (Duarte and Regaudie-de-Gioux, 2009; Duarte et al., 2013). Ecological metabolism theory states that warming could regulate GPP and CR of plankton community. Primary production and respiratory metabolism are evidently impacted by temperature (Brown et al., 2004; Wang, 2014; Vaquer-Sunyer et al., 2015). Warming accelerates the levels of plankton GPP and CR to some extent (Aurore, 2010). In our present study, the result indicated tha plankton community metabolic rates were significantly inhibited and GPP was lower at extremely high temperatures (36 °C in summer or 31.4 °C in winter) than at moderate warm temperatures, indicating a

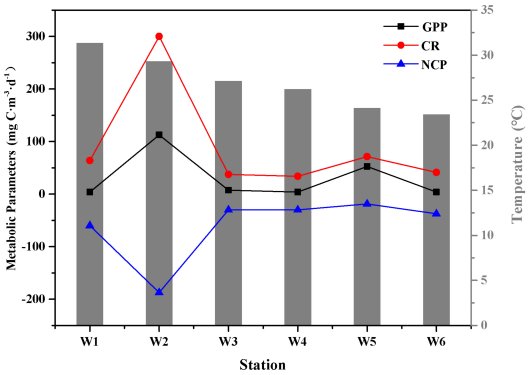

FIGURE 3
Features of plankton community metabolism during winter. Changes in CR are shown in red line and symbols, in NCP in blue line and symbols, and in GPP in black line and symbols, over time. CR, community respiration; GPP, gross primary production; NCP, net community production.

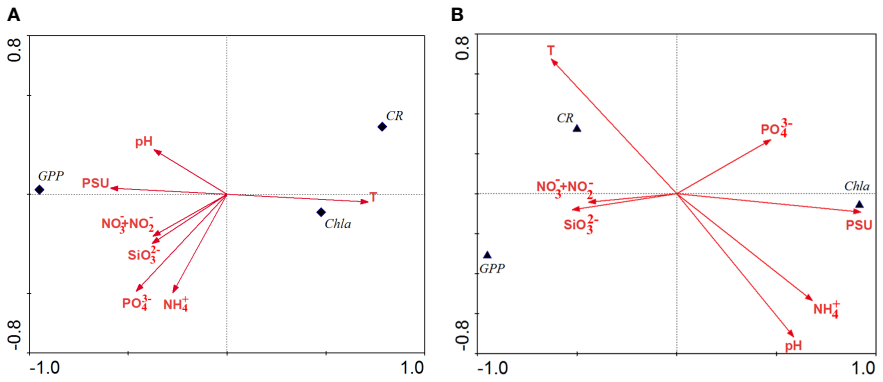

FIGURE 4
Canonical correspondence analysis between ecological parameters and environmental factors. **(A)** summer. **(B)** winter. Chl-*a*, chlorophyll *a*; CR, community respiration; GPP, gross primary production.

heterotrophic metabolic state. To the best of our knowledge, this is the first study to report the phenomenon of inhibiting community metabolism in extremely high-temperature conditions.

The primary mechanism results from a rise in warming that facilitates the enzyme activity in plankton or accelerates the recycling of dissolved organic matter, thereby speeding up community metabolic rate. Extremely high temperature could inhibit enzyme activity and destroy the structure of thylakoid, thereby leading to suffocation of phytoplankton photosynthesis, growth inhibition of zooplankton, and declination in plankton community metabolic rate (Wohlers et al., 2009). Response of

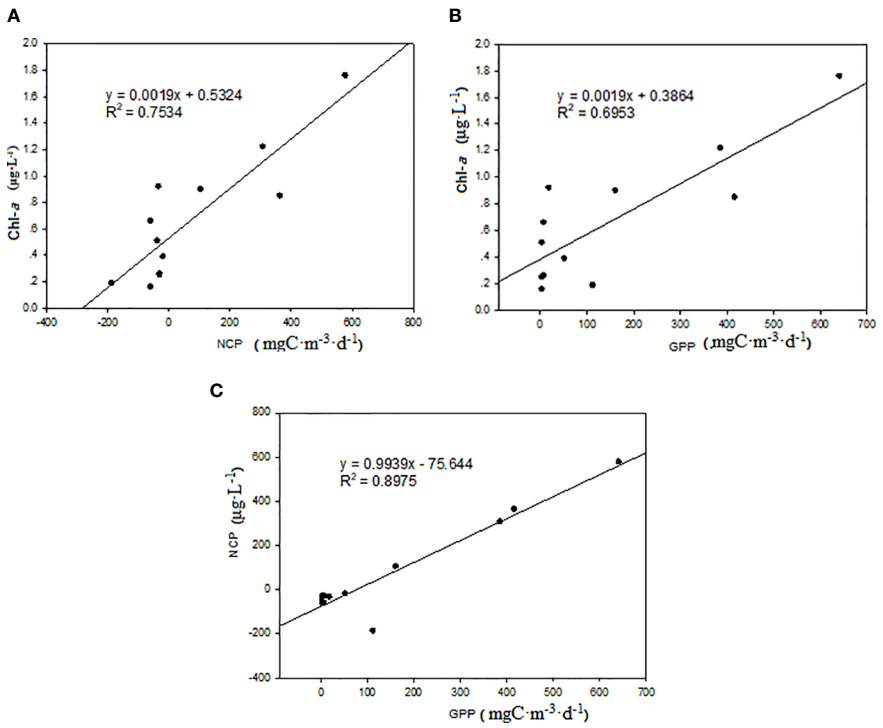

FIGURE 5
Pearson analysis between ecological parameters and environmental factors **(A)** Chl-*a*-NCP. **(B)** Chl-*a*-GPP. **(C)** NCP-GPP). Chl-*a*, chlorophyll *a*; GPP, gross primary production; NCP, net community production.

community metabolic process to warming is consistent with the results of previous reports in the range of optimum temperature, as community metabolic rate between summer and winter was strongest in optimum temperature areas (29–30°C), and the ecosystem showed a autotrophic metabolism state. In general, results of *in situ* investigation showed that planktonic community metabolism exhibited regularly varied characteristics along with variations of temperature gradient. In the field thermal discharge areas, regional distribution and driving mechanism of plankton community metabolism are relatively complex due to the existence of dynamic processes between thermal discharge outward flowing and the external water mixing and the potential impact of the entrainment effect on nuclear power plant prior to discharge.

4.2 Seasonal variation of plankton community metabolism

Temperature and nutrients are key factors affecting the planktonic community metabolic levels, as well as incidence on gross primary production and respiratory metabolism (García-Martín et al., 2014). The potential variation of the environmental factors is related to seasonal differences in the environmental background of the Daya Bay. Seasonal variation, mainly attributed to the high temperature in summer, easily results in stratification, leading to the formation of a high-temperature–high salinity stable water mass, with low contents of phosphate and DIN. At extremely high temperature conditions, dramatic warming could impact physiological processes such as enzymatic reactions or respiratory reaction intensity of photosynthesis and inhibit GPP levels in short term (Regaudie-de-Gioux and Duarte., 2012). However, plankton exhibited rapid propagation and growth trend with sufficient nutrients that were adapted to the high-temperature environment. In winter, seawater temperature was low, vertical mixing of seawater was drastic, and nutrients in the upper waters were replenished and accumulated constantly by vertical mixing. In the context of low temperature and high nutrients, concentrations of CR and GPP were influenced by warming. Therefore, the effects of warming on plankton community metabolism were more significant than those of nutrient input in winter, giving rise to seasonal differences of the two environmental factors between temperature and nutrients on planktonic community metabolism.

Our results showed that seasonal effects of warming and nutrients input on planktonic community metabolic levels were evident. Warming facilitated the rise in GPP and CR concentrations, and this rise was inhibited by thermal effect in the extremely high temperature conditions; Compared with that in winter, there were significant restrained effect of extremely high temperatures (36°C) on the growth of plankton. thus, plankton community showed heterotrophic metabolism state. Warming could affect planktonic community metabolism balance, weaken its stability, and accelerate vulnerability of marine ecosystem in the Daya Bay. In present study, warming impacted the stability of aquatic ecosystem by affecting planktonic community metabolism and weakening the stability of the planktonic ecosystem. In addition, environmental factors such as warming and eutrophication played crucial roles in altering the food web structure and food chain transmission pathways in planktonic ecosystems (Culler, 2013; Lewandowska et al., 2014; Song et al., 2015). The integrated ecological effects had further negative effects on ecosystem function and biological resource output.The results also revealed that there were instability and fragility on ecosystem affected by thermal discharge in the Daya Bay Nuclear Power Station; moreover, plankton primary production and respiratory metabolism were easily affected by high temperatures.

Data availability statement

The original contributions presented in the study are included in the article/supplementary material. Further inquiries can be directed to the corresponding authors.

Author contributions

HL and FX wrote the article and did the field analysis. XS contributed to the laboratory analysis. HW, HH, and JL provided conceptual and editorial inputs on the manuscript and discussed field methodology. All authors contributed to the article and approved the submitted version.

Funding

This research work was supported by General Programs of the National Natural Science Foundation of China (Grant Number: 41706138) and the National Basic Research Program (Grant Number: 2015CB452904)

Acknowledgments

This is a short text to acknowledge the contributions of specific colleagues, institutions, or agencies that aided the efforts

of the authors. We thank the two reviewers whose comments/ suggestions helped improve and clarify this manuscript.

Conflict of interest

The authors declare that the research was conducted in the absence of any commercial or financial relationships that could be construed as a potential conflict of interest.

Publisher's note

References

Agusti, S., Vigoya, L., and Duarte, C. M. (2018). Annual plankton community metabolism in estuarine and coastal waters in Perth (Western Australia). *PeerJ* 6, e5081. doi: 10.7717/peerj.5081

Aurore, RDG, and Carlos M, Duarte (2010). Plankton metabolism in the Greenland Sea during the polar summer of 2007[J]. *Polar Biology* 33:1651.

Brown, J. H., Gillooly, J. F., Allen, A. P., Savage, V. M., and West, G. B.. (2004). Toward a metabolic theory of ecology. *Ecology* 85 (7), 1771–1789.

Chen, M. R., Chen, B. Z., Harrison, P., and Liu, H. B. (2011). Dynamics of mesozooplankton assemblages in subtropical coastal waters of Hong Kong: A comparative study between an eutrophic estuarine and a mesotrophic coastal site. *Cont. Shelf. Res.* 31, 1075–1086. doi: 10.1016/j.csr.2011.03.011

Choi, H. G. (2008). Effects of thermal effluents from wolseong nuclear power plant on macroalgal composition and community structure. *Algae.* 23, 151–162. doi: 10.4490/ALGAE.2008.23.2.151

Culler, L. E. (2013). *Temperature effects on consumer-resource species interactions: Integrating thermal physiology and community ecology*. Thesis (Ph.D.)–Dartmouth College, 2013.

Del Giorgio, P. A., and Williams, P. J. (2005). *Respiration in aquatic ecosystems* (Oxford: Oxford University Press).

Duarte, C. M., and Regaudie-de-Gioux, A. (2009). Thresholds of gross primary production for the metabolic balance of marine planktonic communities. *Limnol. Oceanogr.* 54, 1015–1022. doi: 10.4319/lo.2009.54.3.1015.

Duarte, C. M., Regaudie-de-Gioux, A., Arrieta, J. M., Delgado-Huertas, A., and Agustí, S. (2013). The oligotrophic ocean is heterotrophic. *Ann. Rev. Mar. Sci.* 5, 551–569. doi: 10.1146/annurev-marine-121211-172337.

Ducklow, H. W., and McAllister, S. L. (2005). "The biogeochemistry of carbon dioxide in the coastal oceans," in *The Sea*, vol. 13 . Eds. A. R. Robinson and K. H. Brink (Cambridge, MA: Harvard University Press), 269–315.

García-Martín, E. E., Serret, P., and Leakey, R. J. G. (2014). Plankton community and bacterial metabolism in Arctic sea ice leads during summer 2010. *Deep Sea Res. I.* 92, 152–161. doi: 10.1016/j.dsr.2014.06.007

Kim, Y. H., Ahn, J. K., Yoon, H. D., and Jang, M. A. (2007). Effects of heated effluents on the intertidal macroalgal community near gori nuclear power plant. *Algae.* 22, 297–304. doi: 10.4490/ALGAE.2007.22.4.297

Kirkwood, D. S., Aminot, A., and Carlberg, S. R. (1996). The 1994 quasimeme laboratory performance study: Nutrients in seawater and standard solutions. *Mar. pollut. Bull.* 32, 640–645. doi: 10.1016/0025-326X(96)00076-8

Lewandowska, A. M., Boyce, D. G., Hofmann, M., Matthiessen, B., Sommer, U., and Worm, B. (2014). Effects of sea surface warming on marine plankton. *Ecol. Lett.* 17, 614–623. doi: 10.1111/ele.12265

Nguyen, D., Maranger, R., Tremblay, J. E., and Gosselin, M. (2012). Respiration and bacterial carbon dynamics in the amundsen gulf, Western Canadian Arctic. *J. Geophys. Res.*, C00G16. doi: 10.1029/2011JC007343

Parsons, T. R., Maita, Y., and Lalli, C. M. (1984). *A manual of chemical and biological methods for seawater analyses* (Oxford, UK: Pergamon Press), 173. doi: 10.1016/C2009-0-07774-5

Regaudie-de-Gioux, A., and Duarte, C. M. (2012). Temperature dependence of planktonic metabolism in the ocean. *Global Biogeochem. Cycles.* 26, GB1015. doi: 10.1029/2010GB003907

Serret, P., Fernández, E., Sostres, J. A., and Anadón, R. (1999). Seasonal compensation of microbial production and respiration in a temperate sea. *Mar. Ecol. Prog. Ser.* 187, 43–57. doi: 10.3354/meps187043

Song, X. Y., Liu, H. X., Zhong, Y., Tan, Y. H., Qin, G., Li, K. Z., et al. (2015). Bacterial growth efficiency in a partly eutrophicated bay of south China Sea: Implication for anthropogenic impacts and potential hypoxia events. *Ecotoxicology.* 24, 1529–1539. doi: 10.1007/s10646-015-1497-6

Teixeira, T. P., Neves, L. M., and Araújo, F. G. (2012). Thermal impact of a nuclear power plant in a coastal area in southeastern Brazil: Effects of heating and physical structure on benthic cover and fish communities. *Hydrobiologia.* 684, 161–175. doi: 10.1007/s10750-011-0980-1

Vaquer-Sunyer, R., Conley, D. J., Muthusamy, S., Lindh, M. V., Pinhassi, J., and Kritzberg, E. S. (2015). Dissolved organic nitrogen inputs from wastewater treatment plant effluents increase responses of planktonic metabolic rates to warming. *Environ. Sci. Technol.* 49, 11411–11420. doi: 10.1021/acs.est.5b00674

Wang, N. (2014). *Community and bacterial respiration in the South China Sea and fujian coastal waters* (Xiamen University). Thesis (M.S.)–Xiamen University, 2014.

Wohlers, J., Engel, A., Zöllner, E., Breithaupt, P., Jürgens, K., Hoppe, H. G., et al. (2009). Changes in biogenic carbon flow in response to sea surface warming. *Proc. Natl. Acad. Sci. U. S. A.* 106, 7067–7072. doi: 10.1073/pnas.0812743106

Xiang, C. H., Li, Y., Ke, Z. X., Li, G., Huang, Y. D., Su, X. Y., et al. (2022). Effects of daily nitrogen and phosphorus input on planktonic community metabolism in a semi-enclosed bay by mesocosm experiment. *Acta Oceanologica Sin.* 41 (8), 99–110. doi: 10.1007/s13131-022-1986-4

frontiers | Frontiers in Marine Science

TYPE Original Research
PUBLISHED 12 January 2023
DOI 10.3389/fmars.2022.1093468

OPEN ACCESS

EDITED BY
Kaizhi Li,
South China Sea Institute of Oceanology (CAS), China

REVIEWED BY
Xingyu Song,
South China Sea Institute of Oceanology (CAS), China
Bangping Deng,
MNR, China

*CORRESPONDENCE
Lizhe Cai
cailizhe@xmu.edu.cn

SPECIALTY SECTION
This article was submitted to Marine Pollution, a section of the journal Frontiers in Marine Science

RECEIVED 09 November 2022
ACCEPTED 23 December 2022
PUBLISHED 12 January 2023

CITATION
Cai L, Rao Y, Zhao X, Yang D, Zhou X, Wang D and Yue X (2023) Spatial and seasonal distributions of ten species of benthic macrofauna and twelve water environmental factors in a subtidal zone near the Daya Bay nuclear power plant.
Front. Mar. Sci. 9:1093468.
doi: 10.3389/fmars.2022.1093468

Spatial and seasonal distributions of ten species of benthic macrofauna and twelve water environmental factors in a subtidal zone near the Daya Bay nuclear power plant

Lizhe Cai[1]*, Yiyong Rao[2], Xiaoyu Zhao[1,3], Deyuan Yang[1], Xiping Zhou[3], Deli Wang[4] and Xinli Yue[4]

[1]College of the Environment and Ecology, Xiamen University, Xiamen, China, [2]South China Sea Fisheries Research Institute, Chinese Academy of Fishery Sciences, Guangzhou, China, [3]School of Environmental Science and Engineering, Xiamen University Tan Kah Kee College, Zhangzhou, China, [4]College of Ocean and Earth Science, Xiamen University, Xiamen, China

In this study, we analyzed the spatial and seasonal distributions of ten species of benthic macrofauna and 12 water environmental parameters at thirty-six sampling stations in the subtidal zone near the Daya Bay Nuclear Power Plant. The results showed that there were four types of distribution characteristics for 10 species of macrobenthic animals and 12 water environmental factors near the Daya Bay nuclear power plant: (1) three species of benthic macrofauna, namely *Apionsoma (Apionsoma) trichocephalus*, *Amphioplus (Lymanella) laevis*, and *P. bidentata*, and six water environmental parameters, including water depth, salinity, dissolved oxygen, suspended solids, chromium, and lead increased from inside the bay to outside the bay. (2) Three species of benthic macrofauna, *P. cristata*, *T. lata*, and *T. scabra*, and four water environmental parameters, including oils, arsenic, total phosphorus, and silicate, decreased from inside to outside the bay. (3) Two species of benthic macrofauna, *A. dibranchis,* and *P. undulatus* and one water environmental parameter, pH, were higher in the central bay than inside and outside the bay. (4) One species of benthic macrofauna, *Sigambra hanaokai*, and one water environmental parameter, total nitrogen, were lower in the central bay than inside and outside the bay. Correlation and BIO-ENV analyses confirmed that water depth was the main environmental factor affecting the ten species of benthic macrofauna. Understanding the distributions of the dominant benthic macrofauna could help protect nuclear cold source systems from benthic macrofaunal blockage and explore marine ecosystem connectivity.

KEYWORDS

benthic macrofauna, environmental factor, nuclear power plant, subtidal zone, Daya Bay

1 Introduction

Daya Bay is located in the eastern Guangdong Province between Red (Honghai) Bay and Mirs Bay, with a total area of 650 km^2. The Daya Bay coast contour twists and turns, with smaller bays set into the larger bay. The main bays inside Daya Bay include Chimney (Yancong) Bay, Xunliao Port, Fanhe Port, Aotou Port, and Xiaogui Bay. Daya Bay Nuclear Power Base encompasses two nuclear power stations: Daya Bay and Ling'ao.

Construction of the Daya Bay Nuclear Power Plant began in 1987 and was put into commercial operation in 1994. Subsequently, the Lingao Nuclear Power Plant was built near the Daya Bay Nuclear Power Plant, and the two nuclear power plants jointly formed a nuclear power base.

Benthic macrofauna and water environmental factors in the subtidal zone of Daya Bay were surveyed before the construction of the Daya Bay Nuclear Power Plant and have been continuously monitored since 1986. Over the past 35 years, the most dominant species have remained the same. These include *T. scabra*, *P. undulatus*, *L. brevirostris*, and *Amphioplus (Lymanella) laevis* (Jiang et al., 1990a; Jiang et al., 1990b; Du et al., 2008a; Du et al., 2008b; Du et al., 2009; Du et al., 2011; Yuan et al., 2017; Rao et al., 2020a). *Terebellides stroemii*, *Paucibranchia belli*, and *Glycera alba* were the dominant species in macrozoobenthic communities in the cage culture area (Huang et al., 2005), and *Paraprionospio cristata* was the dominant macrozoobenthic community species in the mariculture area (Rao et al., 2021). *Timoclea scabra*, *P. undulatus*, *L. brevirostris*, and *A. (Lymanella) laevis* were the dominant species of macrozoobenthic communities in the sea area around the Daya Bay Nuclear Power Station (Zhang et al., 2007) and from benthic trawling in Daya Bay (Zhang et al., 2017).

Most previous studies have divided benthic macrofauna into several communities according to the dominant species in different regions. The benthic macrofauna from 50 sampling stations in Daya Bay in 1988 and 1989 were divided into six communities (Jiang et al., 1990b). According to the survey data from four voyages in 2004, three communities of benthic macrofauna were identified (Du et al., 2009).

Some studies have focused on the effects of warm drainage in nuclear power plants on benthic macrofauna (Zhang et al., 2007), and the effects of sewage discharge and mariculture on benthic macrofauna (Huang et al., 2005; Rao et al., 2021), while others have focused on the ecological environmental changes in Daya Bay (Wang et al., 2004; Wang et al., 2008).

Although many benthic macrofaunal communities have been monitored before and after the construction of the Daya Bay nuclear power plant, little research has been conducted on the spatial and seasonal distribution of common benthic macrofauna and their relationships with the water environment. The main goals of this study were to (1) analyze the spatial and temporal distribution characteristics of common benthic macrofauna in the subtidal zone near the Daya Bay Nuclear Power Plant, (2) analyze the spatial and temporal distribution characteristics of some water environmental factors in the subtidal zone near the Daya Bay Nuclear Power Plant, (3) analyze the relationships between common benthic macrofauna and water environmental factors in the subtidal zone near the Daya Bay Nuclear Power Plant. To achieve these goals, we simultaneously sampled benthic macrofauna and measured environmental parameters in the subtidal zone near the Daya Bay Nuclear Power Plant.

2 Materials and methods

2.1 Sampling and treatment of benthic macrofauna

Sixty-five grid-based sampling stations were established and divided into three sectors (inner, middle, and outer) according to their relative geographic locations and environmental conditions (Rao et al., 2020a; Rao et al., 2021). Sampling surveys were conducted in the autumn (November 2017), winter (January 2018), spring (April 2018), and summer (July 2018). However, in this study, we only selected data from 36 sampling stations, namely, 12 sampling stations in the inner bay, 12 sampling stations in the middle of the bay, and 12 sampling stations outside the bay (Figure 1).

Benthic macrofauna were collected using a 0.05 m^2 van Veen grab at each station. The sediments were washed through a 0.5 mm mesh sieve, and the residues were transferred to sample containers with 5% formalin buffer *in situ* for further identification. In the laboratory, benthic macrofauna were identified to the lowest possible taxon and enumerated under a dissecting microscope. They were then weighed using an electronic balance (0.1 mg, FA1204) after blotting surface water off with clean absorbing paper (Rao et al., 2020a; Rao et al., 2021).

2.2 Selection of 10 macrozoobenthic species

There are many benthic animals in the Daya Bay subtidal zone (Jiang et al., 1990a; Jiang et al. 1990b; Du et al., 2008a; Du et al., 2008b; Du et al., 2009; Du et al., 2011; Rao et al., 2020a; Rao et al., 2021). In this study, ten species of benthic animals were considered based on the following three points: (1) according to the relative importance index (IRI) value (Zhang et al., 2017), based on four surveys in 2017 and 2018 that found *Aglaophamus dibranchis, P. undulatus*, *L. brevirostris*, *A. laevis* and *P. cristata* to be the top five species for average IRI values, and *Sigambra*

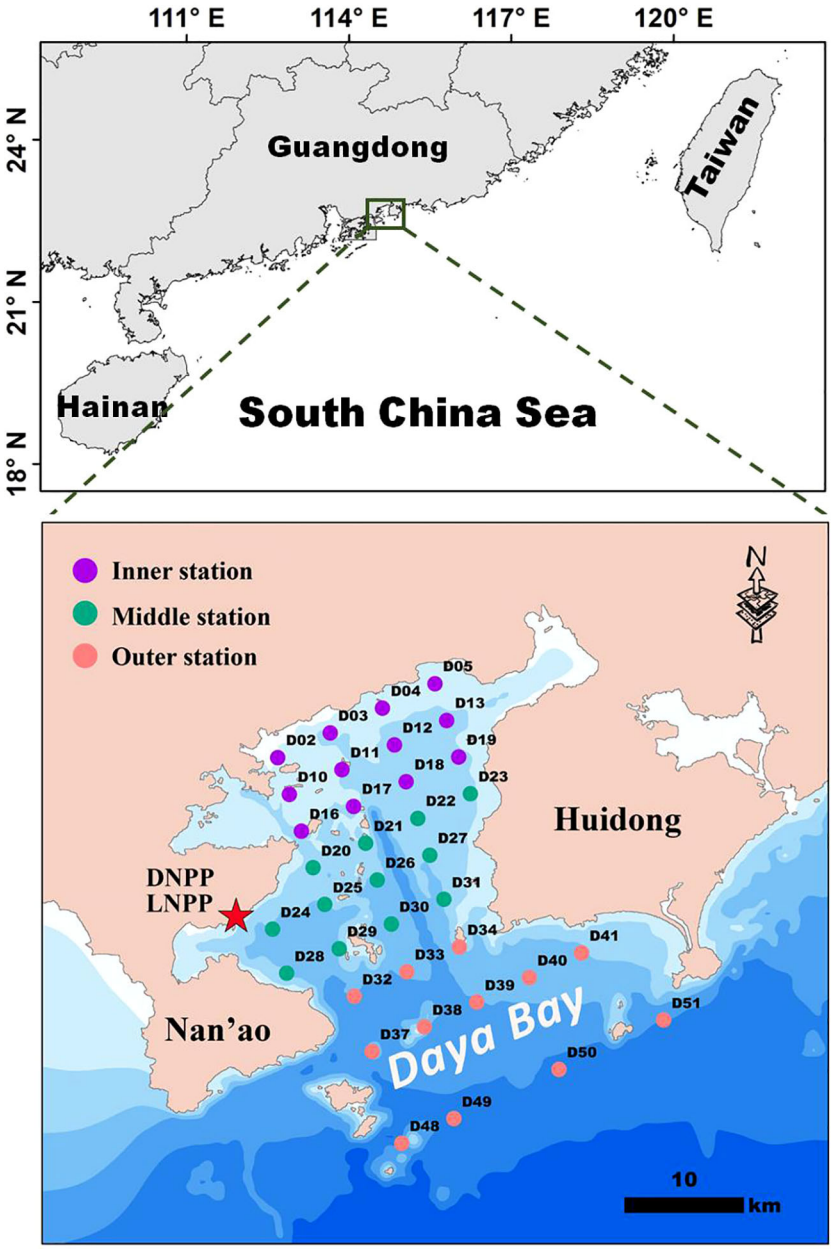

FIGURE 1
Schematic diagram of benthic macrofaunal sampling stations in the Daya Bay Subtidal zone. Stations are divided into three sectors: inner (purple circle, n = 12), middle (green circle, n = 12) and outer (orange circle, n = 12). DNPP, Daya Bay Nuclear Power Plant; LNPP, Ling'ao Nuclear Power Plant.

hanaokai and *T. lata* to be the first seven and the first 20, respectively; (2) potential disaster-causing animals in the nuclear power coldsource system, including *A. dibranchis*, *P. cristata, P. undulatus*, *L. brevirostris*, *Apionsoma (Apionsoma) trichocephalus*, and *P. bidentata* (Cai et al., 2022b); (3) historically recorded dominant species, including *T. scabra*, *P. undulatus*, *L. brevirostris*, and *A. laevis* (Jiang et al., 1990a; Jiang et al., 1990b; Du et al., 2008a; Du et al., 2008b; Du et al., 2009; Du et al., 2011; Yuan et al., 2017; Rao et al., 2020a; Rao et al., 2021).

2.3 Determination of water environmental factors

Water depth was determined using portable bathymetry (SPEEDTECH SM-5A, USA). Salinity and dissolved oxygen (DO) were measured using a portable water quality analyzer (WTW Multi 3430, Germany). Oils were extracted with n-hexane and measured using UV spectrophotometry procedures (Ehrhardt and Burns, 1993). The metal

concentrations of Cr (chromium), As (arsenic), and Pb (lead) were determined using inductively coupled plasma mass spectrometry (Agilent 7700x, Agilent Technologies, USA). Quality assurance was performed using the procedure described by Wang et al. (2019). The samples for analyzing total nitrogen (TN) and total phosphorus (TP) were measured using the method of Varol and Şen (2012). Total nitrogen was measured by converting all nitrogen forms to nitrate *via* alkaline persulfate oxidation and subsequent analysis of nitrate was performed using spectrophotometric procedures. The total phosphorus was determined spectrophotometrically using the ascorbic acid method after persulfate digestion. The silicate content was measured using standard silicon molybdenum blue spectrophotometric procedures. Samples were filtered with 0.45 μm polycarbonate filters and analyzed later using the method of Dai et al. (2008). The samples for analyzing suspended solids (SS) were collected using 0.45 μm polycarbonate filters and were subsequently measured gravimetrically (Wang et al., 2015).

2.4 Statistical analysis

Variance analysis (ANOVA) and correlation analyses were performed using SPSS v25 software. ANOVA was used to determine whether there were significant differences in the ten species of benthic macrofauna and the 12 water environmental parameters in different seasons and regions. Correlation analysis was used to determine whether the densities and biomasses of the common benthic macrofauna were significantly correlated with the 12 water environment parameters. BIO-ENV analyses were performed using PRIMER v7 (Anderson et al., 2008). Similarities in benthic macrofauna between each pair of sites were determined using the Bray-Curtis similarity measure based on the fourth root transformed abundance data. Nonmetric multidimensional scaling (NMDS) ordination based on Bray-Curtis similarity was performed to explore the seasonal and site variation of the macrofaunal community. BIO-ENV analyses were used to examine the major environmental factors affecting the ten species of benthic macrofauna.

3 Results

3.1 The spatial and seasonal distributions of ten species of benthic macrofauna

From the spatial distributions of ten species of benthic macrofauna in the subtidal zone near the Daya Bay Nuclear Power Plant, the densities of *A. trichocephalus*, *A. laevis*, and *P. bidentata* increased from inside the bay to outside the bay. The densities of *P. cristata*, *T. lata*, and *T. scabra* decreased from inside to outside the bay. The densities of *A. dibranchis,* and *P. undulatus* were higher in the middle bay than in the inner bay and outside the bay. The densities of *S. hanaokai* and *L. brevirostris* were lower in the middle bay than in the inner bay and outside the bay (Figure 2). In addition, the density distribution of *L. brevirostris* was inconsistent with the biomass distribution, while the density and biomass distributions of the other nine macrobenthic species were consistent (Figure 3).

Two-way ANOVA results indicated that the densities of *A. trichocephalus*, *A. laevis*, *P. bidentata*, *P. cristata*, *A. dibranchis*, and *P. undulatus* showed significant regional variation (Table 1). The biomasses of *A. trichocephalus*, *A. laevis*, *P. cristata*, *P. undulatus*, and *L. brevirostris* showed significant regional variation (Table 2). The densities of *A. laevis*, *P. cristata*, *A. dibranchis*, *P. undulatus*, and *T. lata* showed significant seasonal variation (Table 1). The biomass of *A. laevis*, *A. dibranchis*, *P. undulatus*, and *T. lata* showed significant seasonal variation (Table 2).

3.2 The spatial and seasonal distributions of twelve environmental parameters

From the spatial distributions of 12 water environmental parameters in the subtidal zone near the Daya Bay Nuclear Power Plant, water depth, salinity, DO, suspended matter, Cr, and Pb increased from inside the bay to outside the bay. Oils, TP, and silicate decreased from the inside to the outside of the bay. The pH was higher in the central bay than in the inner bay and outside the bay. The TN was lower in the central bay than in the inner bay and outside the bay (Figure 4).

A two-way ANOVA indicated that water depth, salinity, Cr, silicate, and pH showed significant regional variation. Salinity, DO, suspended matter, Cr, Pb, silicate, oils, TP, pH, and TN showed significant seasonal variation (Table 3).

3.3 The relationship between ten species of benthic macrofauna and twelve environmental parameters

In terms of water environmental parameters, water depth was significantly correlated with the densities of six species of benthic macrofauna. There was a significant positive correlation between the densities of *A. trichocephalus*, *A. laevis*, *P. bidentata*, and *A. dibranchis* and water depth. There was a significant negative correlation between the densities of *P. cristata* and *T. lata* and water depth. Regarding benthic macrofaunal density, *A. laevis* and *T. lata* were significantly correlated with the five water environmental parameters. There was a significant positive correlation between the density of *A. laevis* and water depth, salinity, and Pb. There was a significant negative correlation between the densities of *A. laevis*, silicate, and TP. There was a

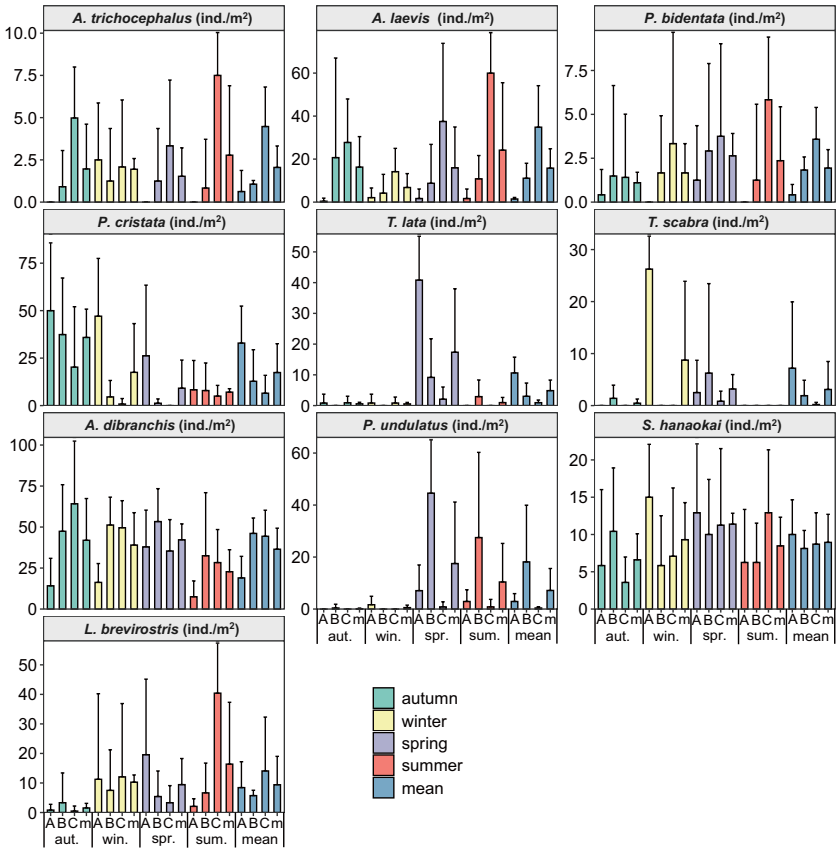

FIGURE 2
The density spatial and temporal distributions of ten species benthic macrofauna in subtidal zone near the Daya Bay Nuclear Power Plant. (A: represent the inner bay; B: represent the middle bay; C: represent the outside bay; m: represent the mean value).

significant positive correlation between the densities of *T. lata*, silicate, and TP. There was a significant negative correlation between the density of *T. lata* and water depth, salinity, and pH (Table 4).

In terms of environmental parameters, water depth was significantly correlated with the biomass of six species of benthic macrofauna. There was a significant positive correlation between the biomass of *A. trichocephalus*, *A. laevis*, and *P. bidentata* and water depth. There was a significant negative correlation between the biomass of *P. cristata*, *T. lata*, *S. hanaokai* and water depth. Among the benthic macrofaunal biomass, *A. laevis* and *T. lata* were significantly correlated with the five water environment parameters. There was a significant positive correlation between the biomass of *A. laevis* and water depth, salinity, As, and Pb. A significant negative correlation was observed between the biomass of *A. laevis* and silicate. There was a significant positive correlation between the biomass of *T. lata* and silicate and TP. There was a significant negative correlation between the biomass of *T. lata* and water depth, salinity, and pH (Table 5).

The BIO-ENV analysis showed that water depth was the first factor affecting 10 macrobenthic species, with a correlation coefficient of 0.191. The second factor affecting 10 macrobenthic species was salinity, with a correlation coefficient of water depth + salinity of 0.215.

4 Discussion

4.1 Effect of environmental factors on three species of polychaetes

This study involved three polychaetes: *P. cristata*, *A. dibranchis*, and *S. hanaokai*. Three species of polychaetes were the dominant species of macrozoobenthic communities in Daya Bay (Jiang et al., 1990a; Jiang et al., 1990b; Du et al., 2008a; Du et al., 2008b; Du et al., 2009; Du et al., 2011; Yuan et al., 2017; Cai et al., 2022b), and they were also the dominant species along the coast of China (Cai and Zheng, 1994; Huang et al., 2012; Chen et al., 2020; Rao et al., 2020b). *Sigambra hanaokai* is the

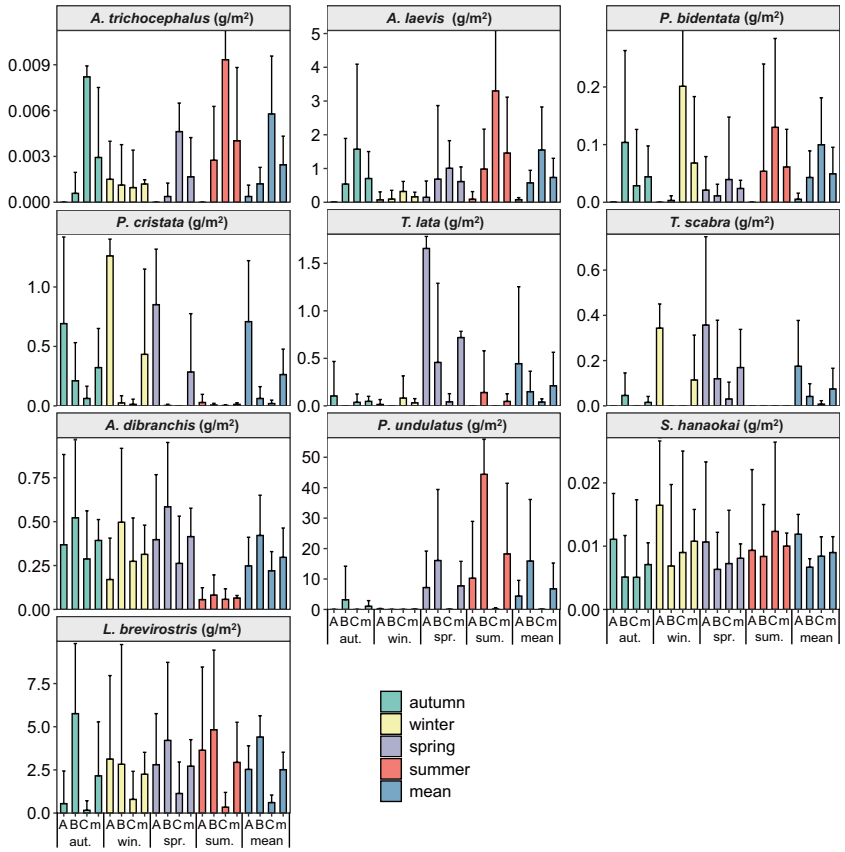

FIGURE 3
The biomass spatial and temporal distributions of ten species benthic macrofauna in subtidal zone near the Daya Bay Nuclear Power Plant. (A: represent the inner bay; B: represent the middle bay; C: represent the outside bay; m: represent the mean value).

TABLE 1 The F and P values between seasons and regions for density of ten benthic macrofauna species in subtidal zone near the Daya Bay Nuclear Power Plant.

Density	Region		Season		Region × Season	
	F	*P*	*F*	*P*	*F*	*P*
Apionsoma (Apionsoma) trichocephalus	12.874	<0.001[c]	1.324	0.269	1.795	0.105
Amphioplus (Lymanella) laevis	26.615	0.045[a]	3.406	0.020[a]	3.048	0.008[b]
P. bidentata	4.863	0.009[b]	0.696	0.556	0.667	0.677
P. cristata	11.699	<0.001[c]	7.935	<0.001[c]	1.767	0.111
T. lata	2.550	0.082	5.121	0.002[b]	2.668	0.018[a]
T. scabra	1.834	0.164	1.679	0.175	2.136	0.053
A. dibranchis,	16.334	<0.001[c]	4.536	0.005[b]	2.276	0.045[a]
P. undulatus	7.895	0.001[b]	4.522	0.005[b]	2.961	0.010[a]
Sigambra hanaokai	0.393	0.676	1.256	0.292	1.780	0.108
L. brevirostris	0.865	0.423	1.324	0.269	1.795	0.105

a: significant at the 0.05 level; [b]: significant at the 0.01 level; [c]: significant at the 0.001 level.

TABLE 2 The F and P values between seasons and regions for biomass of ten benthic macrofauna species in subtidal zone near the Daya Bay Nuclear Power Plant.

Density	Season		Region		Season × Region	
	F	*P*	*F*	*P*	*F*	*P*
A. trichocephalus	9.085	<0.001[c]	1.316	0.272	1.498	0.184
A. laevis	13.126	<0.001[c]	5.111	0.002[b]	2.644	0.019[a]
P. bidentata	1.867	0.159	0.241	0.868	0.795	0.576
P. cristata	15.105	<0.001[c]	2.418	0.069	2.264	0.041[a]
T. lata	2.565	0.081	5.049	0.002[b]	2.644	0.019[a]
T. scabra	2.549	0.082	1.593	0.194	1.005	0.425
A. dibranchis	4.409	0.014[a]	7.171	<0.001[c]	0.650	0.690
P. undulatus	6.102	0.003[b]	4.783	0.003[b]	2.545	0.023[a]
S. hanaokai	1.674	0.192	0.515	0.672	0.369	0.897
L. brevirostris	3.323	0.039[a]	0.096	0.962	0.364	0.901

a: significant at the 0.05 level; [b]: significant at the 0.01 level; [c]: significant at the 0.001 level.

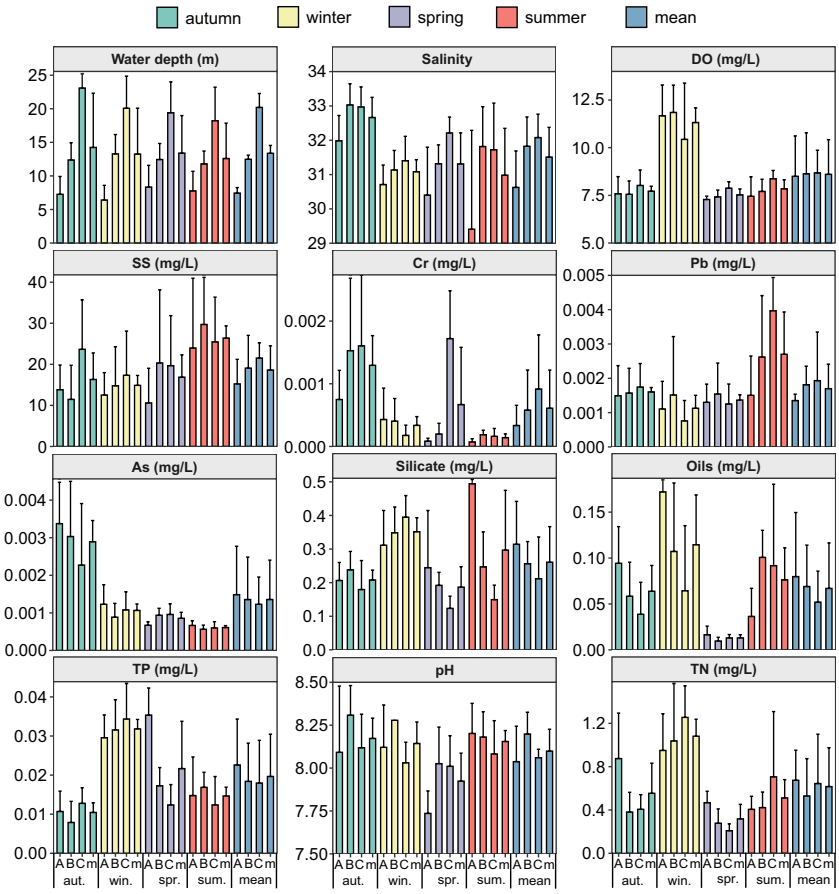

FIGURE 4
The spatial and temporal distributions of twelve environment factors in subtidal zone near the Daya Bay Nuclear Power Plant. (A: represent the inner bay; B: represent the middle bay; C: represent the outside bay; m: represent the mean value).

TABLE 3 The F and P values between seasons and regions for twelve environment factors in subtidal zone near the Daya Bay Nuclear Power Plant.

Environmental factor	Region		Season		Region × Season	
Density	*F*	*P*	*F*	*P*	*F*	*P*
Water depth	132.242	<0.001[c]	1.104	0.350	1.591	0.155
Salinity	21.144	<0.001[c]	16.079	<0.001[c]	2.181	0.049[a]
DO	0.196	0.822	56.125	<0.001[c]	1.797	0.104
Suspended solids	2.327	0.102	4.780	0.003[b]	0.879	0.512
Cr	3.685	0.028[a]	8.282	<0.001[c]	2.666	0.018[a]
As	1.872	0.158	2.011	0.115	1.868	0.091
Pb	1.827	0.165	7.022	<0.001[c]	2.155	0.051
Silicate	18.011	<0.001[c]	30.436	<0.001[c]	15.576	<0.001[c]
Oils	2.168	0.118	14.508	<0.001[c]	3.826	0.002[b]
TP	2.053	0.132	20.537	<0.001[c]	3.587	0.003[b]
pH	5.561	0.005[b]	7.569	<0.001[c]	1.838	0.096
TN	1.674	0.191	23.000	<0.001[c]	3.003	0.009[b]

a: significant at the 0.05 level; [b]: significant at the 0.01 level; [c]: significant at the 0.001 level.

TABLE 4 Correlation analysis between densities of ten species benthic macrofauna and water environmental factors in subtidal zone near the Daya Bay Nuclear Power Plant.

Species	Depth	Salinity	DO	SS	Cr	As	Pb	Silicate	Oils	TP	pH	TN
A. trichocephalus	0.233**	0.160	0.035	0.041	0.006	-0.052	0.140	-0.198*	-0.070	-0.064	-0.100	0.043
A. laevis	0.418**	0.200*	-0.083	0.033	0.130	0.159	0.205*	-0.292**	-0.069	-0.191*	<0.001	-0.137
P. bidentata	0.249**	-0.173	0.277**	0.141	-0.014	-0.044	0.107	-0.112	-0.105	-0.025	-0.019	0.079
P. cristata	-0.372**	-0.032	0.008	-0.178*	0.060	-0.019	-0.037	0.085	0.186*	0.155	-0.141	0.076
T. lata	-0.181*	-0.291**	-0.114	-0.035	-0.060	-0.015	0.019	0.235**	-0.085	0.669**	-0.300**	-0.080
T. scabra	0.115	-0.294	0.187*	-0.109	-0.055	-0.018	-0.073	0.014	0.041	0.067	0.050	0.002
A. dibranchis	0.473**	0.214*	-0.066	-0.056	0.114	0.173*	0.053	-0.196*	0.012	0.039	0.039	0.012
P. undulatus	-0.064	-0.033	-0.118	-0.003	-0.099	-0.031	0.043	-0.115	-0.066	-0.043	-0.045	0.079
S. hanaokai	-0.089	0.037	-0.027	0.011	0.012	-0.074	-0.002	-0.106	0.050	-0.023	-0.004	-0.063
L. brevirostris	0.080	-0.083	0.052	0.017	-0.098	-0.033	0.011	0.138	0.020	0.306**	-0.090	0.315**

*: significant at the 0.05 level; **: significant at the 0.01 level.

dominant species in the macrobenthic community in the southern Yellow Sea (Xu et al., 2021).

P. cristata (It was previously identified as *Paraprionospio pinnata* in China and Korean, therefore, the *P. pinnata* reported in Chinese waters should be *P. cristata*) collected in Jiaozhou Bay and the Yellow Sea may be *P. inaequibranchia* and *P. coora* (Zhou et al., 2008). *P. cristata* has been widely reported in Korean waters (Yokoyama and Choi, 2010). *P. cristata* is considered an opportunistic species (Ji et al., 2022). In coastal waters along the Arabian Sea, *Cossura coasta*, the dominant species during the pre-monsoon period, was replaced by the surface deposit feeder *P. pinnata* during the monsoon and post-monsoon periods (Rehitha et al., 2019). *Paraprionospio pinnata* is only located in low-oxygen habitats in the Humboldt upwelling ecosystem (Fajardo et al., 2018) and it is the dominant species of the macrobenthic community in winter in the cage culture area of Daya Bay (Huang et al., 2005). The results of this study showed that the density of *P. cristata* was

TABLE 5 Correlation analysis between biomass of ten species benthic macrofauna and water environmental factors in subtidal zone near the Daya Bay Nuclear Power Plant.

Species	Depth	Salinity	DO	SS	Cr	As	Pb	Silicate	Oils	TP	pH	TN
A. trichocephalus	0.249**	0.108	0.010	0.030	-0.003	-0.039	0.110	-0.197*	-0.018	-0.120	-0.063	0.022
A. laevis	0.298**	0.177*	-0.081	0.105	-0.034	0.435**	0.271**	-0.224*	-0.088	-0.133	-0.022	-0.155
P. bidentata	0.232**	-0.013	0.350**	0.050	0.008	-0.023	0.050	0.051	-0.054	-0.006	0.037	0.198*
P. cristata	-0.385**	-0.199*	0.049	-0.123	-0.051	-0.032	-0.044	0.133	0.221**	0.394**	-0.243**	0.093
T. lata	-0.177*	-0.289**	-0.120	-0.047	-0.066	-0.016	0.062	0.173*	-0.072	0.586**	-0.284**	-0.086
T. scabra	0.107	-0.065	0.079	-0.144	-0.062	-0.022	-0.070	-0.045	-0.028	0.052	-0.042	-0.036
A. dibranchis	0.061	0.105	-0.108	-0.173*	0.079	-0.044	-0.071	-0.118	-0.097	-0.005	0.004	-0.031
P. undulatus	-0.093	-0.113	-0.125	0.118	-0.099	-0.031	0.046	-0.039	-0.019	-0.054	-0.025	-0.074
S. hanaokai	-0.167*	0.001	-0.003	-0.032	-0.076	0.038	-0.017	<0.001	0.053	0.011	-0.036	0.098
L. brevirostris	-0.119	0.024	0.032	0.005	-0.043	-0.039	0.152	0.055	-0.014	0.044	0.127	-0.100

*: significant at the 0.05 level; **: significant at the 0.01 level.

significantly negatively correlated with water depth and suspended solids, and significantly positively correlated with oil, whereas the biomass of *P. cristata* was significantly negatively correlated with water depth, salinity, and pH, and significantly positively correlated with oils and TP.

The relationship between *S. hanaokai* and the environmental factors in Chinese sea waters has been rarely reported, only a correlation analysis showed that there were significant negative correlations between the density of *S. hanaokai* and the content of organic carbon and nitrogen in the intertidal zone of Xiamen Crocodile Island (Cai et al., 2022c).

In winter and spring, the grappler method risk index (GMRI) of *A. dibranchis* is more than 50%, the risk of blocking the nuclear cold source system is at a medium-risk level. In summer and autumn, the GMRI of *A. dibranchis* is less than 50%, the risk of blocking the nuclear cold source system is at a medium-risk level. The risks of blocking the nuclear cold source system *P. cristata* and *S. hanaokai* are both at a low-risk level in Daya Bay in four seasons (Cai et al., 2022b).

4.2 Effect of environmental factors on *Apionsoma (Apionsoma) trichocephalus* and Listriolobus brevirostris

Apionsoma trichocephalus was not the dominant species in previous surveys in Daya Bay (Jiang et al., 1990a; Jiang et al., 1990b; Du et al., 2008a; Du et al., 2008b; Du et al., 2009; Yuan et al., 2017), but it poses a potential risk of blocking nuclear cooling source systems (Cai et al., 2022b). Although the average density of *A. trichocephala* was low in all four seasons in Daya Bay (below 4 ind./m^2), it was the dominant species in the subtidal zone of the East China Sea during all four seasons (Shou et al., 2018) and in the subtidal zone of the Chinese islands (Huang et al., 2012). However, there are few reports on the relationship between *A. trichocephala* and environmental factors. Our study found that *A. trichocephala* showed a significant positive correlation with water depth and a significant negative correlation with silicate.

L. brevirostris is one of the dominant species in macrozoobenthic communities in Daya Bay (Jiang et al., 1990a; Jiang et al., 1990b; Du et al., 2011; Yuan et al., 2017; Cai et al., 2022b). The results of this study showed that the density of *L. brevirostris* was significantly positively correlated with TN and TP. The density of *L. brevirostris* was high in sea areas with high organic matter content in Daya Bay (Jiang et al., 1990b).

Although the individual weight of *L. brevirostris* is large, its density is low and the distribution range is small; therefore, the risk of blocking the nuclear power cold source system is also low. Except for the GMRI in summer, which is over 50%, the risk of blocking is less than 50% in the other three seasons in Daya Bay (Cai et al., 2022b).

4.3 Effect of environmental factors on three species of bivalves

P. undulatus and *T. scabra* are the dominant species in macrozoobenthic communities in Daya Bay (Jiang et al., 1990a; Jiang et al., 1990b; Du et al., 2009; Du et al., 2011; Yuan et al., 2017; Cai et al., 2022a). The undulated surf clam, *Paphia undulata* (the new revised name in WoRMS is *P. undulatus*), is commercially cultured on the southern coast of China (Zhang et al., 2022a). Therefore, there have been many studies on the relationship between *P. undulatus* and environmental factors. *P.*

undulatus showed a significant positive correlation with the DO, clay, and chlorophyll-a content in the Beibu Gulf (Ye et al., 2010). Mud substrates with ≥ 40% water content in the temperature range of 20–30°C and salinity range of 20–40 psu were appropriate for *P. undulatus* burrowing and may be appropriate for its culture (Zhang et al., 2022a). *P. undulatus* is not only a cultured species but also a common dominant species in the macrozoobenthic community along the southeast coast of China (Ye et al., 2010; Du et al., 2011; Shu et al., 2015; Yuan et al., 2017; Rao et al., 2021; Cai et al., 2022a).

T. scabra is not an economically important species, but it is also a common dominant species in the macrozoobenthic community along the coast of Guangdong (Du et al., 2011; Li et al., 2016). *T. lata* is neither an economically important nor a dominant species on the southeast coast of China (Jiang et al., 1990a; Jiang et al., 1990b; Zhang et al., 2007; Du et al., 2008a; Cai et al., 2022a). Why do heavy metals have less impact on the Daya Bay bivalves? That is, there is no significant correlation between bivalves and heavy metals. This is because the sediment quality radically improved after the late-2000s, and heavy metals in nearshore sediments of Daya Bay were all closely related to the import of anthropogenic and/or terrestrial material, whereas those offshore were likely to be related to the joint influence of anthropogenic activities and natural processes (Du et al., 2008; Qu et al., 2018).

The GMRI of *P. undulatus* in all four seasons was less than 50%; therefore, the risk of blocking the nuclear power cold source system was low in Daya Bay (Cai et al., 2022b).

4.4 Effect of environmental factors on two species of echinoderms

Amphioplus (Lymanella) laevis has been a dominant species in Daya Bay for over 30 years (Jiang et al., 1990a; Jiang et al., 1990b; Zhang et al., 2007; Du et al., 2008a; Du et al., 2008b; Du et al., 2009; Huang et al., 2012; Zhang et al., 2017; Cai et al., 2022b). It is also a common dominant species on the coast and in the Gulf of China (Cai and Zheng, 1994; Chen et al., 2020). The genus *Amphioplus* is also dominant in some open-sea areas. *Amphioplus sinicus* was not only the dominant species of macrozoobenthic communities in Hailing Bay, western Guangdong, but also outside the bay, in addition to being the annual dominant species (Li et al., 2018). *A. laevis* is the dominant species in subtidal amphioxus habitats in Xiamen Bay (Chen et al., 2020; Rao et al., 2020b). BIO-ENV analysis revealed significant seasonal variations in environmental factors affecting community structure (including *A. laevis*) in semi-enclosed waters in Bohai Bay, China (Shi et al., 2022). This study found that the density of *A. laevis* showed a significantly positive correlation with water depth, salinity, and Pb and a significantly negative correlation with silicate and TP.

P. bidentata has not been the dominant species in previous surveys in Daya Bay (Jiang et al., 1990a; Jiang et al., 1990b; Du et al., 2008a; Du et al., 2008b; Du et al., 2009; Zhang et al., 2017; Yuan et al., 2017; Rao et al., 2020a), but it was a common species in the sea area near the nuclear power plant (Cheng et al., 2018; Li et al., 2020; Zhang et al., 2022b), It was a dominant species on the northern coast of Zhejiang Province (Yan et al., 2020) and in the surrounding waters of Qinshan Island (Mao et al., 2022). This study found that the density and biomass of *P. bidentata* were significantly positively correlated with water depth and DO.

The GMRI of *P. bidentata* in all four seasons was less than 50%, so the risk of blocking the nuclear power cold source system was low in Daya Bay (Cai et al., 2022b).

4.5 Effect of environmental factors on the zoobenthic community in Daya Bay

The main sources of pollution near the Daya Bay nuclear power plant were the warm drainage from the power plant and the shallow aquaculture area of Dapeng Ao, but the warm drainage from the power plant had less effect on benthic macrofauna in nearby waters (Zhang et al., 2007). From 1982 to 2004, the ecological environment of Daya Bay changed from 237 species in 1987 to 194 species in 1997 (Wang et al., 2004), and the mean biomass and species of benthic animals near power plants ranged from 317.9 g/m^2 in 1991 to 45.24 g/m^2 in 2004, and from 250 species in 1991 to 177 species in 2004 (Wang et al., 2008). The correlation analysis between the macrobenthos community and environmental factors indicated that secondary productivity was significantly affected by the content of inorganic nitrogen, phosphorus, dissolved oxygen of seawater, and organic carbon content of sediment (Liu et al., 2018). Changes in the ecological environment in Daya Bay are related to sewage discharge and mariculture. Small body size, short longevity, and high tolerance species are more abundant in industrial sewage discharge areas and mariculture areas (Rao et al., 2021). We believe that to accurately identify the main environmental factors affected, long-term monitoring and sufficient comparable data are needed.

Data availability statement

The original contributions presented in the study are included in the article/supplementary materials. Further inquiries can be directed to the corresponding author.

Author contributions

LC conceived of the study and obtained funding. LC, YR, XYZ, DY, DW, XPZ, and XY were responsible for field and laboratory work. LC, YR, and DY conducted the identification of benthic macrofauna. The manuscript was reviewed by LC. YR and XYZ helped analyzing the data and plotting the figures. All authors contributed to the article and approved the submitted version.

Funding

This work was supported by the National Key Research and Development Program of China [2018YFC1407501] and the Coordinate Oil Subsidy Project of Huizhou [F2017-01-4].

Acknowledgments

We sincerely grateful to the Huizhou Ocean Technology Center for providing us with environmental data. We would like to thank Director Haoliang Liang, Junxing Wang, Binglin Chen, Sujing Fu and Bingwen Chen for their support in sample collection. All members involved in this project are to be acknowledged here.

Conflict of interest

The authors declare that the research was conducted in the absence of any commercial or financial relationships that could be construed as a potential conflict of interest.

Publisher's note

References

Anderson, M. J., Gorley, R. N., and Clarke, K. R. (2008). *PERMANOVA + for PRIMER: Guide to software and statistical methods* (Plymouth, UK: PRIMER-E).

Cai, L., Rao, Y., Zhao, X., Yang, D., Lin, J., Fu, S., et al. (2022b). Two risk indices for benthic macrofauna entrapment evaluation on the water intake systems in coastal nuclear power plants. *J. Appl. Oceanography* 41, 655–662. doi: 10.11759/hykx20211003001

Cai, L., Yang, D., Zhao, X., Lin, J., Chen, X., Zhou, X., et al. (2022a). Progress and prospects of mollusk community and population ecology in daya bay. *Mar. Sci.* 46, 124–134. doi: 10.3969/J.ISSN.2095-4972.2022.04011

Cai, L., Zhao, X., Peng, W., Lin, J., Yang, D., Rao, Y., et al. (2022c). Comparison of the macrozoobenthic community and sedimentary environment with and without horseshoe crab presence in the crocodile island intertidal zone, xiamen, China. *J. Oceanology Univ. China* 21, 573–582. doi: 10.1007/s11802-022-5206-9

Cai, L., and Zheng, T. (1994). Macrobenthic communities and evaluation of their environmental affection in subtidal zone, dongshan islands. *J. Xiamen Univ. (Natural Science)* 33, 37–42.

Chen, B., Cai, L., Rao, Y., Li, W., Chen, X., and Fu, S. (2020). Effects of sediment fining on benthic macrofaunal community in subtidal amphioxus habitats in xiamen. *Oceanologia Limnologia Sin.* 51, 494–505. doi: 10.11693/hyhz20191200245

Cheng, H., Wang, J., Tang, Y., Zheng, B., and Lu, C. (2018). Research on community characteristics of macrozoobenthos and environmental quality of offshore north fujian in spring. *J. Shanghai Ocean Univ.* 27, 238–249. doi: 10.12024/jsou.20170902125

Dai, M., Zhai, W., Cai, W., Callahan, J., Huang, B., Shang, S., et al. (2008). Effects of an estuarine plume-associated bloom on the carbonate system in the lower reaches of the pearl river estuary and the coastal zone of the northern south China Sea. *Cont. Shelf Res.* 28, 1416–1423. doi: 10.1016/j.csr.2007.04.018

Du, J., Mu, H., Song, H., Yan, S., Gu, Y., and Zhang, J. (2008). 100 years of sediment history of heavy metals in daya bay, China. *Water Air Soil pollut.* 190, 343–351. doi: 10.1007/s11270-007-9593-8

Du, F., Wang, X., Jia, X., Yang, S., Ma, S., Chen, H., et al. (2011). Species composition and characteristics of macrobenthic fauna in daya bay, south China Sea. *J. Fishery Sci. China* 18, 877–892. doi: 10.3724/SP.J.1118.2011.00877

Du, F., Wang, X., Li, C., Zhang, H., and Jia, X. (2008a). Study species diversity of macrobenthos in daya bay, south China Sea. *South China Fishery Sci.* 4, 33–41.

Du, F., Wang, X., Li, C., Zhang, H., and Jia, X. (2009). Macrobenthic community structure in daya bay, south China Sea. *Acta Ecologica Sin.* 29, 1091–1098.

Du, F., Zhang, H., Li, C., Wang, X., and Jia, X. (2008b). Species composition and diversity of macrobenthic fauna in daya bay. *J. Fishery Sci. China* 15, 252–259.

Ehrhardt, M. G., and Burns, ,. K. A. (1993). Hydrocarbons and related photo-oxidation products in Saudi Arabian gulf coastal waters and hydrocarbons in underlying sediments and bioindicator bivalves. *Mar. pollut. Bull.* 27, 187–197. doi: 10.1016/0025-326X(93)90024-E

Fajardo, M., Andrade, D., Bonicelli, J., Bon, M., Gomez, G., Riascos, J., et al. (2018). Macrobenthic communities in a shallow normoxia to hypoxia gradient in the Humboldt upwelling ecosystem. *PloS One* 13, e0200349. doi: 10.1371/journal.pone.0200349

Huang, H., Chen, B., Chen, G., Ma, Z., and Yu, W. (2012). Spatial and temporal distribution characteristics of macrobenthos at subtidal zone in islands, China. *China Environ. Sci.* 32, 1888–1894.

Huang, H., Lin, Q., Lin, Y., Jia, X., Li, C., and Wang, W. (2005). Spatial-temporal variation of large macrobenthic animals in cage culture sea area in daya bay. *China Environ. Sci.* 25, 412–416.

Jiang, J., Cai, E., Wu, Q., Xu, H., Li, R., Zheng, F., et al. (1990a). Species composition and quantitative distribution on benthic animals in daya bay. *Collections papers Mar. Ecol. Daya Bay (II)*, 237–247.

Jiang, J., Li, R., Zheng, F., Lu, L., Wu, Q., Xu, H., et al. (1990b). Analysis of benthic community structure in daya bay. *Collections papers Mar. Ecol. Daya Bay (II)*, 282–289.

Ji, Y., Wang, J., Zhang, N., Sun, B., Su, K., and Wang, Z. (2022). Community structure and biodiversity of macrobenthos in the coastal waters of rizhao. *J. Shanghai Ocean Univ.* 31, 119–130. doi: 10.12024/jsou.20210103269

Li, Y., Du, F., Gu, Y., Ning, J., and Wang, L. (2016). Relationship between macrobenthic fauna community and environmental factors in southeast leizhou peninsula of the south China Sea. *South China Fisheries Sci.* 12, 33–41. doi: 10.3969/j.issn.2095-0780.2016.06.005

Li, Y., Du, F., Wang, L., Ning, J., and Li, C. (2018). Ecology of microbenthic fauna community in aqualture zones of hailing bay and adjacent waters along the western guangdong coast, China. *Oceanologia Limnologia Sin.* 49, 1294–1307. doi: 10.11693/hyhz20180300058

Li, Y., Shi, Z., Fan, L., Huang, W., Zheng, B., and Xia, Y. (2020). Changes of population on microbenthic and its pollution index evaluation in the adjacent sea area of XX nuclear power plant. *Ocean Dev. Manage.* 2, 66–73. doi: 10.20016/j.cnki.hykfygl.2020.02.012

Liu, K., Du, F., Li, Y., Wang, X., Chen, H. , Zhang, J., et al. (2018). Variation characteristics of microbenthic secondary productivity in daya bay of south China Sea for nearly 30 years. *South China Fisheries Sci.* 14 (2), 1–9. doi: 10.3969/j.issn.2095-0780.2018.02.001

Mao, C., Wei, A., Zhang, Y., Yuan, G., Jiao, X., Cui, C., et al. (2022). Health status evaluation of the macrobenthos community in surrounding waters of qinshan island. *Environ. Monit. Forewarning* 14, 72–78. doi: 10.3969/j.issn.1674-6732.2022.01.013

Qu, B., Song, J., Yuan, H., Li, X., Li, N., and Duan, L. (2018). Intensive anthropogenic activities had affected daya bay in south China Sea since the 1980s: Evidence from heavy metal contaminations. *Mar. pollut. Bull.* 135, 318–331. doi: 10.1016/j.marpolbul.2018.07.011

Rao, Y., Cai, L., Chen, B., Chen, X., Zheng, L., and Lin, S. (2020a). How do spatial and environmental factors shape the structure of a coastal macrobenthic community and meroplanktonic larvae cohort? evidence from daya bay. *Mar. pollut. Bull.* 157, 111242. doi: 10.1016/j.marpolbul.2020.111242

Rao, Y., Cai, L., Chen, X., Zhou, X., Fu, S., and Huang, H. (2021). Responses of functional traits of macrobenthic communities to human activities in daya bay (a subtropical semi-enclosed bay), China. *Front. Environ. Sci.* 9, 766580. doi: 10.3389/fenvs.2021.766580

Rao, Y., Cai, L., Li, W., Chen, X., and Yang, D. (2020b). Spatiotemporal variations of benthic macrofaunal community in the xiamen amphioxus nature reserve, eastern south China Sea. *Acta Oceanologica Sin.* 39, 10–18. doi: 10.1007/s13131-020-1587-z

Rehitha, T., Madhu, N., Vineetha, G., Vipindas, P., Resmi, P., and Revichandran, C. (2019). Spatio-temporal variability in macrobenthic communities and trophic structure of a tropical estuary and its adjacent coastal waters. *Environ. Monit. Assess.* 191, 341. doi: 10.1007/s10661-019-7460-x

Shi, Y., Zhang, G., Zhang, G., Wen, Y., Guo, Y., Peng, L., et al. (2022). Species and functional diversity of marine macrobenthic community and benthic habitat quality assessment in semi-enclosed waters upon recovering from eutrophication, bohai bay, China. *Mar. pollut. Bull.* 181, 113918. doi: 10.1016/j.marpolbul.2022.113918

Shou, L., Liao, Y., Tang, Y., Chen, J., Jiang, Z., Gao, A., et al. (2018). Seasonal distribution of macrobenthos and its relationship with environmental factors in yellow Sea and East China Sea. *J. Oceanology Limnology* 36, 772–782. doi: 10.1007/s00343-018-6271-1

Shu, L., Chen, P., Li, X., Yu, J., and Feng, X. (2015). Species composition and seasonal variation of microbenthic fauna in zhelin bay and adjacent waters. *J. Appl. Oceanography* 34, 124–132. doi: 10.3969/J.ISSN.2095-4972.2015.01.016

Varol, M., and Şen, B. (2012). Assessment of nutrient and heavy metal contamination in surface water and sediments of the upper Tigris river, Turkey. *Catena* 92, 1–10. doi: 10.1016/j.catena.2011.11.011

Wang, Q., Mei, D., Chen, J., Lin, Y., Lu, H., and Yan, C. (2019). Sequestration of heavy metal by glomalin-related soil protein: implication for water quality improvement in mangrove wetlands. *Water Res.* 148, 142–152. doi: 10.1016/j.watres.2018.10.043

Wang, Y., Lou, Z., Sun, C., and Sun, S. (2008). Ecological environment changes in Daya Bay, China, from 1982 to 2004. *Mar. Pollut. Bull.* 56, 1871–1879. doi: 10.1016/j.marpolbul.2008.07.017

Wang, Y., Wang, Z., and Huang, L. (2004). Environment changes and trends in daya bay in recent 20 years. *J. Trop. Oceanography* 23 (5), 85–95.

Wang, D., Yang, X., Zhai, W., Li, Y., and Hong, H. (2015). Spatial distribution of dissolved cadmium in the jiulong river–estuary system: Relevance of anthropogenic perturbation. *Cont. Shelf Res.* 111, 279–285. doi: 10.1016/j.csr.2015.10.008

Xu, J., Xin, L., and Liu, X. (2021). Patterns of species and functional diversity of macrofaunal assemblages and the bioassessment of benthic ecological quality status in the southern yellow Sea. *Mar. pollut. Bull.* 171, 112784. doi: 10.1016/j.marpolbul.2021.112784

Yan, R., Feng, M., Wang, X., and Han, Q. (2020). Temporal and spatial distribution of dominant macrozoobenthos species in the sea area off northern zhejiang province. *Oceanologia Limnologia Sin.* 51, 1162–1174. doi: 10.11693/hyhz20191200253

Ye, J., Cai, L., Huang, R., Zhou, X., Fu, S., Lin, H., et al. (2010). Species composition of trawling mollusk in beibu gulf and its environmental effect. *Mar. Sci. Bull.* 29, 617–622.

Yokoyama, H., and Choi, J. (2010). New records of three *Paraprionospio* species (Polychaeta: Spionidae) from Korean waters. *Ocean Sci. J.* 45, 55–61. doi: 10.1007/s12601-010-0005-4

Yuan, T., Li, H., Li, L., Wang, H., and Yang, C. (2017). Community structure on macrobenthos in summer in daya bay. *J. Trop. Oceanography* 36, 41–47. doi: 10.11978/2016040

Zhang, J., Gao, Y., Shi, X., and Lü, X. (2017). Species composition and diversity of marine organisms from benthic trawling in daya bay of the northern south China Sea. *Biodiversity Sci.* 25, 1019–1030. doi: 10.17520/biods.2017103

Zhang, W., Sun, W., Xu, X., Wang, H., Zheng, B., Lu, C., et al. (2022b). Ecological environment and the potential hazard-causing organisms in the sea area near the nuclear power plant. *Mar. Sci.* 46, 32–43. doi: 10.11759/hykx20211101001

Zhang, J., Xiao, Y., Wang, H., Lin, D., and Dong, Y. (2007). Analysis of community structure on macrobenthos in sea area around daya bay nuclear power station. *Mar. Environ. Sci.* 26, 561–564.

Zhang, P., Yongo, E., Feng, H., Pan, S., Sun, A., Zhou, L., et al. (2022a). Effects of substrate, temperature, salinity, size and transportation on burrowing capacity of juvenile undulated surf clam *Paphia undulata*. *Aquaculture Res.* 53, 2796–2805. doi: 10.1111/are.15794

Zhou, J., Yokoyama, H., and Li, X. (2008). New records of *Paraprionospio* (Annelida: Spionidae) from Chinese waters, with the description of a new species. *Proc. Biol. Soc. Washington* 121, 308–320. doi: 10.2988/08-10.1

frontiers | Frontiers in Marine Science

TYPE Methods
PUBLISHED 26 January 2023
DOI 10.3389/fmars.2023.1100396

OPEN ACCESS

EDITED BY
Huang Honghui,
South China Sea Fisheries Research Institute (CAFS), China

REVIEWED BY
Jianbing Sang,
Hebei University of Technology, China
Li Hongyuan,
Peking University, China

*CORRESPONDENCE
Chao Li
superman5867@163.com

SPECIALTY SECTION
This article was submitted to Marine Pollution, a section of the journal Frontiers in Marine Science

RECEIVED 16 November 2022
ACCEPTED 11 January 2023
PUBLISHED 26 January 2023

CITATION
Huo J, Li C, Liu S, Sun L, Yang L, Song Y and Li J (2023) Biomass prediction method of nuclear power cold source disaster based on deep learning.
Front. Mar. Sci. 10:1100396.
doi: 10.3389/fmars.2023.1100396

Biomass prediction method of nuclear power cold source disaster based on deep learning

Jianling Huo[1,2,3], Chao Li[1,2,3]*, SongTang Liu[1,2,3], Lei Sun[4], Lei Yang[1,2,3], Yuze Song[1,2,3] and Jun Li[2]

[1]Department of Sea Test Site Management,National Ocean Technology Center, Tianjin, China, [2]Key Laboratory of Marine Ecological Monitoring and Restoration Technologies, Ministry of Natural Resources, Shanghai, China, [3]Key Laboratory of Ocean Observation Technology, Ministry of Natural Resources, Tianjin, China, [4]Department of Communication Systems, Toec Technology Co., Ltd, Tianjin, China

Given the insufficient early warning capacity of nuclear cold source biological disasters, this paper explores prediction methods for biomass caused by nuclear cold source disasters based on deep learning. This paper also uses the correlation analysis method to determine the main environmental factors. The adaptive particle swarm optimization method was used to optimize the depth confidence network model of the Gaussian continuous constrained Boltzmann machine (APSO-CRBM-DBN). To train the model, the marine environmental factors were used as the main input factors and the biomass after a period of time was used as the output for training. Optimal prediction results were obtained, and thus, the prediction model of biomass caused by the nuclear cold source disaster was established. The model provides an accurate scientific basis for the early warning of cold source disasters in nuclear power plants and has important practical significance for solving the problem of biological blockage at the inlet of cold source water in nuclear power plants.

KEYWORDS

nuclear power cold source, disaster warning, biomass prediction, deep confidence network, adaptive particle swarm method

1 Introduction

In recent years, with the change of marine ecological environment, the water inlet blockage of nuclear power source caused by marine organisms has become more and more serious (Tang et al., 2017). The nuclear safety accident and economic loss caused by it have been paid more and more attention by all countries in the world. Since 2004, there have been nearly 200 clogged intakes at nuclear power plants around the world, the vast majority of which are caused by jellyfish, seaweed, aquatic plants, shellfish, fish, and other marine organisms. These blockages lead to power reduction or reactor shutdown of units, which seriously affects the safe operation of nuclear power plants (Ruan, 2015; Tang et al., 2017). In the winter of 2014 and 2015, the phaeocystis red tide in the coastal waters of Guangxi covered

the waters near Fangchenggang, and the phaeocystis (2–3 cm) clogged the filter apparatus, posing a threat to the safety of the cold source system of nuclear power facilities. In December 2009, a large number of water weeds invaded and blocked the filtration system of the pump station of unit 4 of the CRUAS nuclear power plant in France, resulting in the loss of cold source of the unit (Tang et al., 2017). In 2012, a large number of jellyfish invaded the cooling water system of a nuclear power plant in California, USA (Tang et al., 2017). In July 2014, a large number of jellyfish flooded into the intake of the circulating water filtration system of the Hongyanhe Nuclear Power Plant, leading to the shutdown of Unit H1/2. In August 2015, a large number of Haitian melons rushed into the water inlet of Ningde No. 3 unit, resulting in unit shutdown operation. In January 2016, the No. 2 unit of the Lingao Nuclear Power Plant was in emergency shutdown due to the influx of shrimp into the water intake (Meng et al., 2018; Meng et al., 2019; Zhang et al., 2020). In April 2018, just at the critical time of the Boao Forum for Asia, a large amount of seaweed flooded into the Changjiang Nuclear Power Plant in Hainan Province, blocking the drum filter screen and causing the circulating water pump to trip. Two units of the Changjiang Nuclear Power Plant were shut down, and the whole plant lost power supply to the outside world. Marine biological disaster is an urgent problem facing the safety of our coastal nuclear power operation.

In order to prevent or reduce the impact of marine disaster-causing organisms, domestic and foreign nuclear power plants have also taken active defense measures. The main approach is to develop a marine disaster biological monitoring system, in order to give early warning before the disaster-causing organisms reach the grid and filter drum network. Kim and Myung, (2018); Kim et al. (2016) collected jellyfish videos on the water surface with cameras mounted on drones, identified and calculated the density of jellyfish in the video frame images, monitored the biomass of disaster-causing organisms in real time, and made track prediction in combination with meteorological and hydrodynamic environment, which could play an early warning role to a certain extent and gain the response time to take measures such as fishing and interception. Meng et al. (2018) established underwater acoustic detection and optical imager for real-time monitoring of marine organisms in the waters near the nuclear power intake. When the biomass reaches a certain threshold, the system software starts to give an early warning. Martin-Abadal et al. (2020) proposed a jellyfish real-time monitoring system based on the deep learning method. The deep learning model processes underwater monitoring videos to realize jellyfish identification and quantitative estimation. A number of scholars (Yang et al., 2018; French et al., 2019; Han et al., 2022) have developed a real-time monitoring system of underwater sonar image, which, combined with hydrodynamic elements, and based on algorithms such as neural networks, gives early warning to marine organisms. However, in many cases, the accumulation rate of disaster-causing organisms is very fast. When the biomass is detected to increase sharply, the response time left for nuclear power plants is very short. Therefore, relying only on real-time monitoring system cannot fundamentally solve the problem. The most effective approach is to develop an early warning system for marine catastrophes to realize early warning before the catastrophes arrive at the grid and filter drum network. At this time, the establishment of an accurate biomass prediction model is an important scientific basis for the system to realize early warning.

A highly nonlinear model between marine environmental parameters and disaster-induced biomass is needed to predict the biomass of nuclear cold sources. Highly nonlinear models are usually constructed by training on traditional artificial neural networks or machine learning methods, such as deep learning. Many biological prediction models for red tide algal blooms have been built by scholars from various countries based on marine environmental data (Zohdi and Abbaspour, 2019), but few prediction models for organisms are caused by nuclear cold sources. Based on the analysis of marine environmental data, this paper uses the mixed APSO-CRBM-DBN deep learning algorithm to study a prediction method that can accurately predict disaster-induced biomass of nuclear power cold sources. We have built an accurate prediction model for the disaster-induced biomass of nuclear power cold sources.

2 Methodology

In this paper, the correlation analysis of marine environmental monitoring data and disaster-causing biomass data was carried out by using the multi-factor correlation analysis method, and the main influencing parameters were determined. Nuclear disaster-causing organisms are affected by a variety of marine environmental factors, and the mapping relationship is nonlinear; thus, it is difficult to predict using the regression model. Therefore, this paper builds a deep confidence network model, trains marine environmental data and pointed pen cap data, and obtains a prediction model suitable for predicting the disaster-causing biomass of nuclear cold source.

2.1 Model input influence factor determination

Organisms that cause nuclear disasters are comprehensively affected by marine environmental parameters. These environmental impact parameters vary for different organisms. Therefore, to improve the accuracy of the model, it is necessary to more accurately determine the environmental parameters affecting the proliferation and aggregation of relevant organisms. In this study, the input environmental impact parameters were selected as comprehensively as possible. The autocorrelation coefficient method was then used to calculate the contribution of each parameter to the biomass, and the correlation coefficients between the parameters were used to calculate the correlation between the parameters. The range of environmental parameters was refined as well.

The correlation coefficient between parameters denotes the covariance of the multivariate parameter matrix. In multivariate probability statistics, the spread matrix is a statistic used to estimate the covariance of a multidimensional normal distribution. An n-dimensional sample represents the adoption of n different environmental parameters, where each dimension represents the time series of one parameter. The matrix X of m x n represents the data matrix of the above n parameters, where $X=[x_1,x_2, ,x_n]$. The sample mean is

$\overline{x} = \frac{1}{n}\sum_{j=1}^{n} x_j$, where x_j is the jth column in X. The semi-positive definite matrix of the dispersion matrix is as follows:

$$S = \sum_{j=1}^{n}(x_j - \overline{x})(x_j - \overline{x})^T = \left(\sum_{j=1}^{n} x_j x_j^T\right) - n\overline{x}\overline{x}^T \quad (1)$$

In the formula, the dispersion matrix $S=XC_nX^TC_nX^T$, where C_n is the centering matrix. The equation to calculate C_n is as follows:

$$C_n = I_n - \frac{1}{n}O \quad (2)$$

where O represents the matrix with all the elements equal to 1. In maximum likelihood estimation, given n data samples, the covariance C_{ML} of a multidimensional normal distribution can be expressed as a normalized divergence matrix, and the correlation coefficient between multiple parameters can be obtained.

$$C_{ML} = \frac{1}{n}S \quad (3)$$

In this paper, the autocorrelation coefficient method was adopted to calculate the contribution of environmental parameters to biomass. The time series of biomass and other environmental parameters is defined as X and Y, and the number of elements is N (N represents the length of the time series), where x_i and y_i are elements in X and Y, respectively, and $\overline{x},\overline{y}$ are sample means, respectively. The correlation coefficient is defined mathematically as:

$$r = \frac{\sum_{i=1}^{n}(x_i - \overline{x})(y_i - \overline{y})}{\sqrt{\sum_{i=1}^{n}(x_i - \overline{x})^2 \sum_{i=1}^{n}(y_i - \overline{y})^2}} \quad (4)$$

2.2 Model design

The model consists of a visible layer, a hidden layer, and an output layer. The input layer is continuously monitoring data, including ecological, hydrodynamic, and other environmental parameters and biomass. The input layer data are represented by $x(t)$,t=1,2, ,T, where T is the number of samples in the data time series. the output layer is the biomass at time $t + MT$, and M can be flexibly adjusted according to the specific prediction time. Figure 1 shows the biomass prediction model structure of a nuclear cold source disaster.

If the output matrix after model learning is Y, there is the output:

$$Y = u(X) \quad (5)$$

In the formula above, $u(X)$ is the deep learning model function.

2.3 Algorithm design

The algorithm formula based on the CRBM-DBN prediction model is:

$$E(v,h;\theta) = \sum_{i=1}^{n}\frac{(v_i - a_i)^2}{2\delta_i^2} - \sum_{j=1}^{m} b_j h_j - \sum_{i=1}^{n}\sum_{j=1}^{m}\frac{w_{ij}v_i h_j}{\delta_i^2} \quad (6)$$

In Equation (6), $\theta=\{\omega,a,b\} = \{\omega=(\omega_{ij})_{n\times m}, a=(a_i)_m, b=(b_j)_m\}$ is the parameter of CRBM; and are the vectors of visible and hidden elements of CRBM, respectively. ω_{ij} is the weight of symmetric connection between the visible cell, v_i, and the hidden cell, h_j. a_1 is the bias of the visible layer element, v_i, and b_j is the bias of the hidden element, h_j. δ_i^2 is the standard deviation of the Gaussian noise of the visible layer element, v_i. n and m are the numbers of visible element, v_i, and the hidden element, h_j, respectively, and δ_i is the standard variance vector of the visible layer Gaussian.

There is no link in the CRBM layer of the prediction model, and the conditional probability of visible layer and hidden layer elements can be calculated by Equations (7) and (8):

$$P(h_j = 1 \mid v) = \sigma\left(\sum_{i=1}^{n} w_{ij}v_i + b_j\right) \quad (7)$$

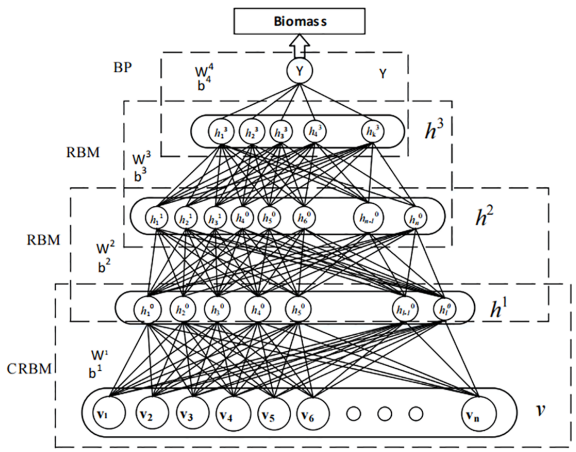

FIGURE 1
Biomass prediction model of nuclear cold source disaster.

$$P(v_i = 1 \mid h) = N\left(\sigma_i \sum_{j=1}^{m} w_{ij} h_j + a_i, \sigma_i^2\right) \tag{8}$$

where $\sigma(x)$ is the sigmoid activation function, and its expression is $\sigma(x)=(1+e^{-x})^{-1}$, $N(\mu,V)$, which represents the Gaussian function with expectation μ and variance V. In order to characterize the complex nonlinear relationship between input and output variables, the prediction model was trained by combining unsupervised and supervised trainings.

2.4 Optimization based on the APSO algorithm

The prediction accuracy of the deep learning model depends mainly on the hyperparameters composed of the learning rate, the number of hidden layer neurons, and the number of hidden layers. However, there is no set of perfect methods to guide the selection of these parameters. This paper uses an adaptive particle swarm optimization algorithm (APSO) to improve the global search ability based on the basic particle swarm optimization algorithm (PSO). This algorithm has fast convergence speed, high precision, and better-optimized performance. Figure 2 shows the flowchart of the optimized model training. Figure 2A shows the training process of the prediction model, which calls the parameters optimized by APSO algorithm for model training. Figure 2B shows the flowchart of the optimization algorithm. The particle swarm optimization algorithm first initializes the hyperparameter according to the empirical value, converts the position into the form of network parameter, and regards the mean square error as the fitness value to calculate the fitness value of each particle in the particle swarm, and update it. If the fitness value is reduced to meet the condition of convergence, the optimal particle is outputted as the optimization hyperparameter of the deep learning model. The adaptive PSO algorithm mainly includes the following steps: Set the population size of the particle swarm as N, and set a four-dimensional vector for each particle. Here, X_{i1} represents the learning rate, while X_{i2}, X_{i3}, and X_{i4} represent the number of nodes in the hidden layer.

1 Read the dataset and initialize the APSO;

2 Particle 1, particle 2,… and particle n training model;

3 The reconstruction error is taken as a fitness function, and the fitness training model of each particle is calculated. The particle, X_{pbest}^{k} , with the maximum fitness and the globally optimal particle, X_{gbest}^{k}, are searched in the iteration.

$$F_{fitness} = \frac{\sum_{i=1}^{N}\sum_{j=1}^{m}\left(p_{ij} - t_{ij}\right)^2}{N} \tag{9}$$

Here, N represents the number of samples in the dataset, m represents the dimension of each data, p_{ij} represents the reconstructed value of the j-dimension monitoring data in the ith sample in the dataset, and t_{ij} represents its true value.

④ The velocity and position of each particle are updated by Equations (10) and (11).

$$\begin{aligned} v_{i,t+1}^{d} &= \omega v_{i,t}^{d} + c_1 * r_1 * \left(p_{i,t}^{d} - x_{i,t}^{d}\right) \\ &+ c_2 * r_2 * \left(p_{g,t}^{d} - x_{i,t}^{d}\right) \end{aligned} \tag{10}$$

$$x_{i,t+1}^{d} = x_{i,t}^{d} + x_{i,t+1}^{d} \tag{11}$$

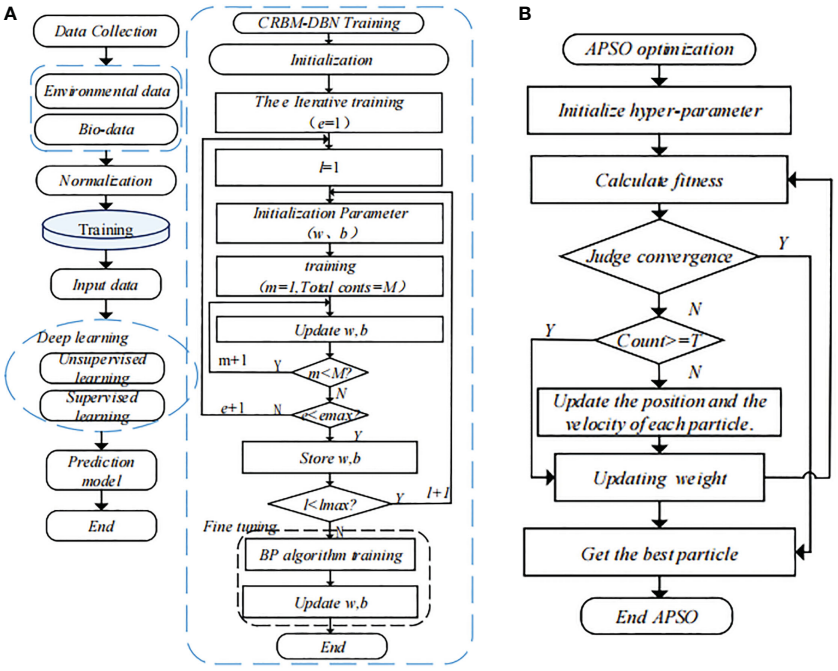

FIGURE 2
Training process of the APSO-CRBM-DBN disaster-induced biomass prediction model. **(A)** Predictive model training process. **(B)** APSO optimization process.

$$\omega = \frac{\omega_{\max} - (\omega_{\max} - \omega_{\max})k}{T} \tag{12}$$

$$\begin{cases} C_1 = \frac{C_{\max} - (C_{\max} - C_{\min})k}{T} \\ C_2 = \frac{C_{\max} + (C_{\max} - C_{\min})k}{T} \end{cases} \tag{13}$$

Above, ω , C_1, and C_2 are the inertial weight and acceleration factor values at the kth iteration.$C_{\max}$ and $C_{\min}$ are the maximum and minimum initial acceleration factor values, respectively, and T is the number of iterations

⑤ Judge whether the fitness function is small enough. If it is small enough, end the algorithm training and select the optimal particle to design the prediction model. Otherwise, go to step 2 to continue the training.

3 Experiments

3.1 Dataset

To effectively verify the accuracy of the prediction model of biomass caused by nuclear power cold source disaster, combined with the training cost of the model, 200 samples were selected as the training set and 40 samples were selected as the test set from the 2,000 continuous and synchronous environmental and biological monitoring data samples obtained from the Changjiang Station of the nuclear power plant in Hainan for 4 months. The environmental parameters in the data samples mainly included temperature, salinity, chlorophyll, dissolved oxygen, flow velocity, flow direction, and wave height. Organisms mainly include nib cap snails, prawns, and phaeocystis. The paper first selected nib cap snails with high biological abundance as research objects, and then used correlation parameter analysis to select environmental parameters closely related to the organisms. Temperature, salinity, chlorophyll, and dissolved oxygen were initially selected as the main influencing parameters and as input parameters of the deep learning model. Figure 3 shows the correlation analysis between input parameters and output biological abundance. Table 1 shows partial tip cap snail abundance and environmental data.

3.2 Data preprocessing

In the prediction model, temperature, salinity, chlorophyll, dissolved oxygen, and the current abundance of nib cap snails were selected as the influence factors in the input layer, and the biological abundance of nib cap snails after an interval of 24 h was selected as the output layer. The frequency of real-time monitoring data is different, and there are invalid data in the monitored data; thus, it is necessary to preprocess the data to obtain high-quality sample data suitable for model training. Therefore, in this paper, the common multiple of frequency is calculated to synchronize the monitoring data elements in the time domain. At the same time, the nonlinear filtering method and correlation analysis between elements are used to remove the noise of environmental data. It is assumed that marine organisms present uniform distribution, and when the monitoring data have a large deviation, the paper calculates the deviation change to judge the anomaly, removes the abnormal value, and finally processes and obtains the synchronized continuous environmental and biological abundance data with an interval of 1 h, which is suitable for model training. The complete dataset is in the supplementary materials.

The formula for median filtering and minimum filtering is:

$$x(k) = \min \quad ium\{x(k-N), \cdots, x(k), \cdots, x(k+N)\} \tag{14}$$

$$\overline{x}(k) = medium\{x(k-N), \cdots, x(k), \cdots, x(k+N)\} \tag{15}$$

where $x(k)$ and $\overline{x}(k)$ represent the monitoring value at moment k and the filtering window of the monitoring data, respectively. The window length was $2N + 1$.

The formula of nearest neighbor interpolation is:

$$x(t) = x_i + \frac{x_{i+1} - x_i}{t_{i+1} - t_i} \mathrm{x}(t - ti) \tag{16}$$

In the above equation, $x(t)$ is the interpolation value at time t; t_i,y and t_{i+1},y_{i+1} are the positions and values of the front and back ends of the missing data segment.

A linear method was adopted to normalize the input layer data. The formula is as follows:

$$x' = 0.1 + \frac{x - x_{\min}}{x_{\max} - x_{\min}} \tag{17}$$

In the above equation, x and x' are the values before and after normalization of the impact factor, respectively; $x_{\max}$ and $x_{\min}$ are the maximum and minimum values of the impact factor sequence, respectively.

3.3 Parameter initialization

Model parameters included model depth, the node number of the model input and output layers, learning rate, weight, and bias. The CRBM-DBN model consisted of one visible layer, two hidden layers, and one output layer. The number of nodes in the input layer was 5, and the number of nodes in the output layer was 1. The weight and bias of the model were initialized by random functions as shown in Equation (18).

$$\begin{cases} W = 0.1 randn(n, m) \\ b = 0.1 \times \mathrm{rand}n(1, m) \\ a = 0.1 \times \mathrm{rand}n(1, n) \end{cases} \tag{18}$$

3.4 Model evaluation

In order to better analyze the prediction effect of the model, two common index parameters, root mean square error (RMSE) and mean absolute error (MAE), are used as the evaluation indexes of the accuracy of the prediction model, which are defined as follows:

$$RMSE = \sqrt{\frac{1}{n}\sum_{i=1}^{n}\left(Y_i - \hat{Y}_i\right)^2} \tag{19}$$

10.3389/fmars.2023.1100396

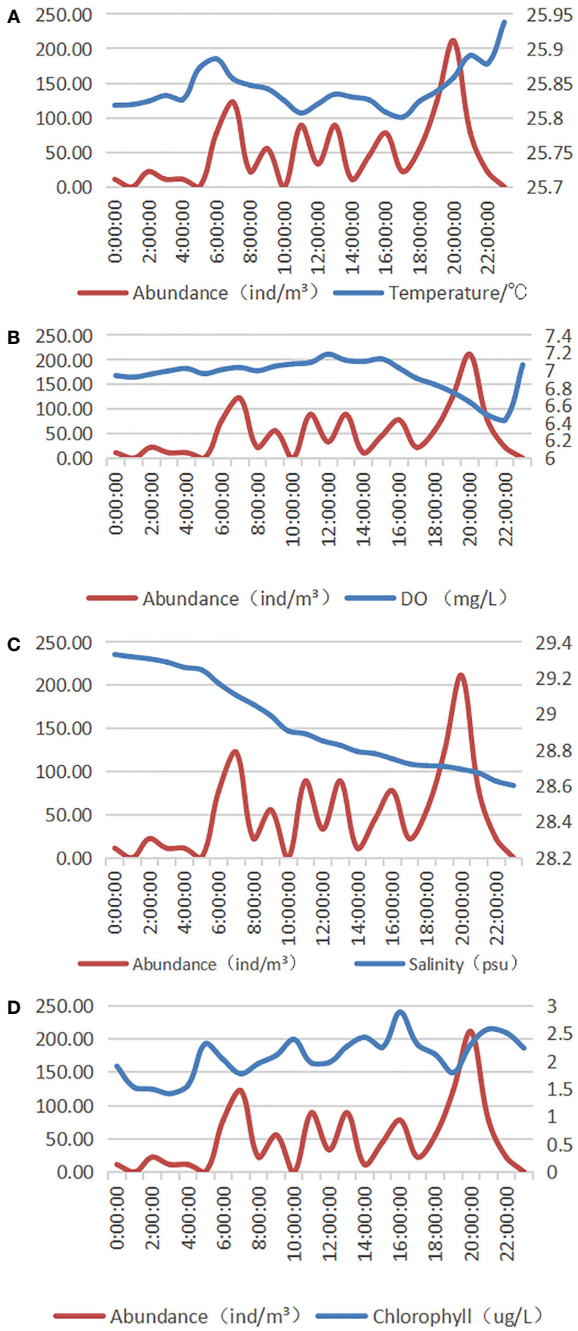

FIGURE 3
Input and output correlation analysis. **(A)** Correlation analysis between the abundance and temperature of tip pen cap snails. **(B)** Correlation analysis between the abundance of tip cap snails and dissolved oxygen. **(C)** Correlation analysis of spikelet abundance and salinity. **(D)** Correlation analysis between the abundance of pointy pen cap snails and chlorophyll.

TABLE 1 Partial tip cap snail abundance and environmental data.

Time	Temperature (°CC)	DO (mg/L)	Chlorophyll (μg/L)	Salinity (psu)	Abundance (ind/m^3)
2021/11/1 0:00	25.818	6.94	1.909	29.33	11.11
2021/11/1 1:00	25.819	6.923	1.521	29.317	16.50
2021/11/1 2:00	25.824	6.958	1.494	29.306	22.22

(Continued)

TABLE 1 Continued

Time	Temperature (°CC)	DO (mg/L)	Chlorophyll (μg/L)	Salinity (psu)	Abundance (ind/m^3)
2021/11/1 3:00	25.832	6.995	1.415	29.288	11.11
2021/11/1 4:00	25.826	7.021	1.559	29.259	11.11
2021/11/1 5:00	25.872	6.962	2.316	29.245	44.40
2021/11/1 6:00	25.885	7.009	2.031	29.169	77.78
2021/11/1 7:00	25.856	7.033	1.775	29.104	122.22
2021/11/1 8:00	25.847	6.996	1.959	29.052	22.22
2021/11/1 9:00	25.842	7.047	2.106	28.99	55.56
2021/11/1 10:00	25.825	7.073	2.393	28.906	66.60
2021/11/1 11:00	25.807	7.09	1.967	28.889	88.89
2021/11/1 12:00	25.82	7.184	1.979	28.85	33.33
2021/11/1 13:00	25.834	7.115	2.267	28.826	88.89
2021/11/1 14:00	25.83	7.102	2.43	28.791	11.11
2021/11/1 15:00	25.826	7.131	2.25	28.779	44.44
2021/11/1 16:00	25.808	7.027	2.884	28.751	77.78
2021/11/1 17:00	25.801	6.91	2.296	28.722	22.22
2021/11/1 18:00	25.824	6.841	2.118	28.712	55.56
2021/11/1 19:00	25.838	6.753	1.792	28.708	122.22
2021/11/1 20:00	25.858	6.639	2.3	28.692	211.11
2021/11/1 21:00	25.89	6.492	2.581	28.671	77.78
2021/11/1 22:00	25.878	6.434	2.513	28.626	22.22
2021/11/1 23:00	25.938	7.063	2.236	28.602	16.50

$$MAE = \frac{1}{n}\sum_{i=1}^{n}\left|Y_i - \hat{Y}_i\right| \tag{20}$$

3.5 Experimental results

The normalized dataset was divided into training and test sets. The model experiment was designed. After model optimization, the model depth was two layers, the learning rate was 0.05, and the number of nodes in the hidden layer was 9 and 11. The fitting curves of predicted and true biomass were drawn, and the root mean square error (RMSE) and mean absolute error (MAE) were used as evaluation criteria to analyze the fitting situation. The performance values in Table 2 clearly confirm the validity of the prediction model and optimization method. Figure 4 is the prediction result. Figure 4A shows the fitting diagram of predicted value and actual monitoring value before and after optimization, and Figure 4B shows the training error loss of the predicted model. It can be seen that the model could effectively fit the changing trend of biomass, and the fitting effect was better after optimization of the algorithm.

4 Conclusion

Based on the real-time monitoring data of the Binhai Nuclear Power Plant, this paper carried out research on the prediction method of disaster-causing biomass of nuclear power plants. The main input environmental parameters were selected by parameter correlation analysis, and the deep learning algorithm of particle swarm optimization was adopted to simulate the nonlinear relationship between marine environmental parameters and typical disaster-causing organisms, taking the tip pen cap snails as an example. The model suitable for nuclear power cold source disaster-induced

TABLE 2 Experimental results.

Model	RMSE	MAE
CRBM-DBN	18.76	15.68
APSO-CRBM-DBN	16.58	14.36

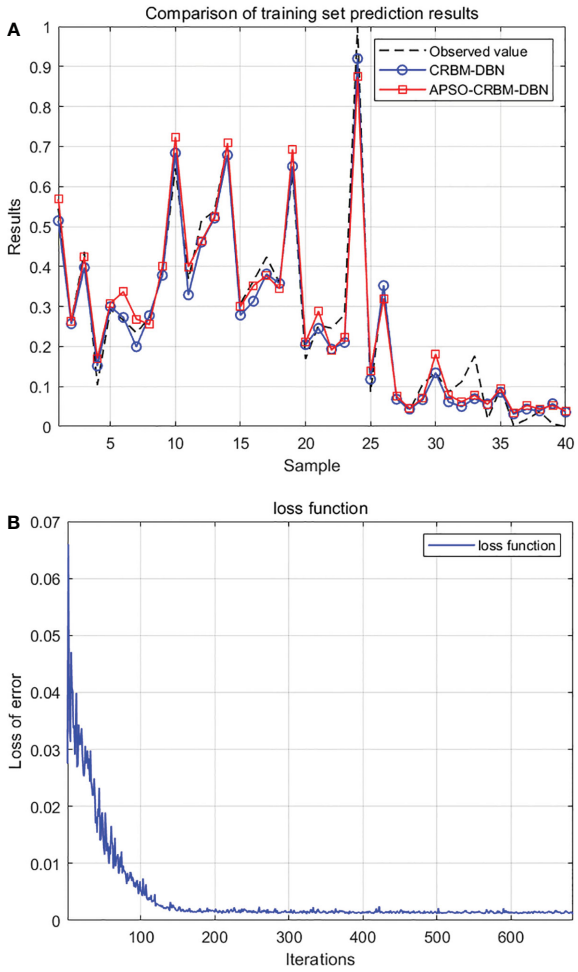

FIGURE 4
Model prediction results. **(A)** Comparison before and after optimization. **(B)** Predict model error losses.

biomass prediction is trained, and the effectiveness of the model is effectively verified by performance indicators, which has important practical significance for solving the problem of biological blockage of cold source water intakes in nuclear power plants.

Data availability statement

The original contributions presented in the study are included in the article/Supplementary Material. Further inquiries can be directed to the corresponding author.

Author contributions

JH and SL designed the model. CL, LY, and JL collected and analyzed the data. YS completed the model test. JH and LS finished the algorithm program writing. JH completed writing the paper. All authors contributed to the article and approved the submitted version.

Funding

This work was supported by the open Research Fund of the Key Laboratory of Marine Ecological Monitoring and Restoration Technology, Ministry of Natural Resources [MEMRT202116], the Innovation Fund of the National Center for Marine Technology [Y1200Z006], and the Key R&D Plan of China [2018YFC1407506].

Acknowledgments

The author wishes to thank senior engineer SL, senior engineer CL, engineer LS, engineer LY, and senior engineer YS for their helpful comments to improve this paper.

Conflict of interest

Author Lei Sun is employed by Toec Technology Co., Ltd, Tianjin, China.

The remaining authors declare that the research was conducted in the absence of any commercial or financial relationships that could be construed as a potential conflict of interest.

Publisher's note

All claims expressed in this article are solely those of the authors and do not necessarily represent those of their affiliated organizations, or those of the publisher, the editors and the reviewers. Any product that may be evaluated in this article, or claim that may be made by its manufacturer, is not guaranteed or endorsed by the publisher.

Supplementary material

The Supplementary Material for this article can be found online at: https://www.frontiersin.org/articles/10.3389/fmars.2023.1100396/full#supplementary-material

References

French, G., Mackiewicz, M., Fisher, M., Challiss, M., Knight, P., Robinson, B., et al. (2019). "JellyMonitor: Automated detection of jellyfish in sonar images using neural networks," in *2018 14th IEEE International Conference on Signal Processing (ICSP)*. (Beijing, China: IEEE) 406–412. doi: 10.1109/ICSP.2018.8652268

Han, Y., Chang, Q., Ding, S., Gao, M., Zhang, B., Li,, et al. (2022). Research on multiple jellyfish classification and detection based on deep learning. *Multimedia Tools Appl.* 14), 81. doi: 10.1007/s11042-021-11307-y

Kim, H., Koo, J., Kim, D., Jung, S., Shin, J. U., Lee, S., et al. (2016). Image-based monitoring of jellyfish using deep learning architecture. *IEEE Sensors J.* 16 (8), 2215–2216. doi: 10.1109/JSEN.2016.2517823

Kim, K., and Myung, H. (2018). Autoencoder-combined generative adversarial networks for synthetic image data generation and detection of jellyfish swarm. *IEEE Access*, 6, 54207–54214. doi: 10.1109/ACCESS.2018.2872025

Martin-Abadal, M., Ruiz-Frau, A., Hinz, H., and Gonzalez-Cid, Y. (2020). Jellytoring: real-time jellyfish monitoring based on deep learning object detection. *Sensors* (Basel, Switzerland) 20 (6), 1708. doi: 10.3390/s20061708

Meng, Y. H., Liu, L., Guo, X. J., Liu, N., and Liu, Y. (2018). An early-warning and decision-support system of marine organisms in a water cooling system in a nuclear power plant. *J. Dalian Ocean Univ.* 33 (01), 108–112. doi: 10.16535/j.cnki.dlhyxb.2018.01.017

Meng, W., Liu, Y., Jian-Wen, L. I., Liu, X. L., Guo, X. J., and Cheng, Z. J. (2019). Early warning model for marine organism detection in a nuclear power plant based on multi-source information fusion technology. *Journal of Dalian Ocean University* 34, 06, 840–845. doi: 10.16535/j.cnki.dlhyxb.2019-020

Meng, W., Liu, Y., Zong, H., Liu, X., Meng, Y., and Li, ,. J. (2018). "Early warning model for marine organism detection in nuclear power stations," in *2018 Chinese control and decision conference (CCDC)*, (Shenyang, China: IEEE) 1999–2004. doi: 10.1109/CCDC.2018.8407454

Ruan, G. (2015). Reason analysis and corresponding strategy for cooling water intake blockage at nuclear power plants. nuclear power engineering. *Nuclear Power Engineer.* 36 (S1), 151–154. doi: 10.13832/j.jnpe.2015.S1.0151

Tang, Z., Cheng, F., Jin, X., Sun, L., Bao, R., Liu, Y., et al. (2017). An automatic marine-organism monitoring system for the intake water of the nuclear power plant. *Ann. Nucl. Energy.* 109, 208–211. doi: 10.1016/j.anucene.2017.05.040

Yang, L., Zong, H., and Wei, M. (2018). "Early warning model for marine organism detection based on BP neural network," in *2018 37th Chinese Control Conference (CCC)*. (Wuhan, China: IEEE) 1909–1914. doi: 10.23919/ChiCC.2018.8483112

Zhang, J., Zhang, S., An, C., Luan, Y., and Li, W. (2020). An effective detection method based on the biological acoustic characteristics of the outlet of nuclear power plant. *IOP Conf. Ser. Mater. Sci. Eng.* 780, 22034. doi: 10.1088/1757-899X/780/2/022034

Zohdi, E., and Abbaspour, M. (2019). Harmful algal blooms (red tide): A review of causes, impacts and approaches to monitoring and prediction. *Int. J. Environ. Sci. Technol.* 16 (3), 1789–1806. doi: 10.1007/513762-018-2108-X

frontiers | Frontiers in Marine Science

TYPE Original Research
PUBLISHED 26 January 2023
DOI 10.3389/fmars.2023.1102686

OPEN ACCESS

EDITED BY
Huang Honghui,
South China Sea Fisheries Research Institute (CAFS), China

REVIEWED BY
Zhengyan Li,
Ocean University of China, China
Zhaohui Wang,
Jinan University, China

*CORRESPONDENCE
Sheng Liu
shliu@scsio.ac.cn

SPECIALTY SECTION
This article was submitted to Marine Pollution, a section of the journal Frontiers in Marine Science

RECEIVED 19 November 2022
ACCEPTED 10 January 2023
PUBLISHED 26 January 2023

CITATION
Hu S, Zhang C, Liu Q, Li T, Huang H and Liu S (2023) Short-term responses of phytoplankton size-fractionated structure and photosynthetic physiology to thermal effluent in a subtropical coastal bay. *Front. Mar. Sci.* 10:1102686. doi: 10.3389/fmars.2023.1102686

Short-term responses of phytoplankton size-fractionated structure and photosynthetic physiology to thermal effluent in a subtropical coastal bay

Simin Hu[1,2,3], Chen Zhang[1,4], Qingxia Liu[5], Tao Li[1,2,3,6,7], Hui Huang[1,2,3,6,7] and Sheng Liu[1,2,3]*

[1]CAS Key Laboratory of Tropical Marine Bio-resources and Ecology, South China Sea Institute of Oceanology, Chinese Academy of Sciences, Guangzhou, China, [2]Guangdong Provincial Key Laboratory of Applied Marine Biology, South China Sea Institute of Oceanology, Chinese Academy of Sciences, Guangzhou, China, [3]Sanya Joint Laboratory of Marine Science Research, Sanya Institute of Ocean Eco-Environmental Engineering, South China Sea Institute of Oceanology, Key Laboratory of Tropical Marine Biotechnology of Hainan Province, Sanya Institute of Ocean Eco-Environmental Engineering, South China Sea Institute of Oceanology, Sanya, China, [4]College of Earth and Planetary Sciences University of Chinese Academy of Sciences, Beijing, China, [5]Guangdong Provincial Key Laboratory of Fishery Ecology and Environment, South China Sea Fisheries Research Institute, Chinese Academy of Fishery Sciences, Guangzhou, China, [6]Sanya National Marine Ecosystem Research Station, Sanya, China, [7]Tropical Marine Biological Research Station in Hainan, Chinese Academy of Sciences, Sanya, China

Elevated water temperature caused by the thermal discharge from power plants can exert multiple ecological impacts on the phytoplankton community in coastal ecosystems. Most recent studies have focused on the reshaping effects on the community structure; however, the short-term response of phytoplankton physiology to thermal discharge remains unclear. This study conducted research on the scope of thermal discharge from the nuclear power plant and the size-fractionated phytoplankton structure combined with photosynthetic physiology in Daya Bay, China. The thermal discharge significantly affected the surface temperature in the outlet regions, and the thermal plume mainly diffused along the northeast coast of the outfall site, resulting in a significant difference in the surface temperature between the inlet and outlet transects (p<0.05). Elevated surface temperatures decreased the total chlorophyll *a* concentrations by 33.19% at the outlet regions, with pico-phytoplankton decreasing the most. Chlorophyll *a* concentrations were higher at sites further away from the outlets, indicating that elevated water temperature might stimulate the rapid growth of phytoplankton, especially nano-phytoplankton which replaced pico-phytoplankton as the dominant group at stations away from the outlets. Significant negative correlations were observed between the photochemical quantum yield (F_v/F_m) and temperature (p<0.05), and the relative electron transport rate (rETR) and temperature (p<0.05). Phytoplankton showed a normal photosynthetic physiological state at most sites with a surface temperature<33°C but was severely affected at the outlet site with a 5°C rise, decreasing from ~0.5 on the inlet transect to 0.07. During the diurnal survey, the high temperatures near the outlet at midday had a compensatory effect on phytoplankton's light suppression. The results indicated that the physiological state of phytoplankton was clearly influenced by the thermal discharge with diurnal variation, and different size-fractionated phytoplankton groups exhibited heterogeneous responses. The

findings may provide further insights into the ecological impacts of thermal discharges as well as global warming in subtropical regions.

KEYWORDS

thermal discharge, phytoplankton, size-fractionated structure, photosynthetic physiology, elevated temperature

1 Introduction

In recent years, with the growth of the nuclear power industry in coastal areas, the thermal effects of circulating cooling water from nuclear power plants have become a major source of heat pollution worldwide (Poornima et al., 2006; Li et al., 2011; Jiang et al., 2019; Xu et al., 2021). According to the World Energy Outlook (2017) (WEO 2017), it is estimated that between 2016 and 2040 more than 90% of new nuclear power resources will come from China and India. Currently, there are 44 sets of nuclear power plant units in operation in China, accounting for 9.73% of the world's total, and 13 sets are under construction, accounting for 23.21% of the world's total (Khttab, 2021). Most of these nuclear power plants are distributed in the coastal areas of China, and elevated seawater temperatures resulting from their circulating cooling water is expected to directly or indirectly affect the physiology of all organisms, the interactions between them, and the dynamic processes and biogeochemical cycle of the ecosystem (Shiah et al., 2006; Lewandowska et al., 2014). In summer, the surface water temperature near the outfall from nuclear power plants could increase by an average of 9.5–10°C compared with that of the inlet area, and the temperature in the receiving waters will rise significantly and mainly concentrate on the surface layer (Madden et al., 2013), Therefore, the warming effect of thermal drainage is considered one of the main threats to aquatic ecosystems, especially for the plankton community (Lin et al., 2018).

Phytoplankton is the most important primary producer in the marine food web and contributes nearly half of the global total primary production even though their photosynthetic biomass is less than 1% of terrestrial plants, playing a crucial role in the global biogeochemical cycle of carbon (Falkowski, 2012). Their small size, short reproductive cycles, and weak motility make them sensitive to environmental changes, therefore, their community dynamics can be used as indicators for predicting the ecological effects of elevated seawater temperatures from power plants (Hays et al., 2005). According to previous studies, the species composition of phytoplankton was affected by elevated temperatures near a nuclear power plant, and this effect has a seasonal difference (Li et al., 2013; Lin et al., 2018). The phytoplankton community showed a shift from diatom dominance to dinoflagellate dominance in the outlet regions in summer (Li et al., 2011). Increased temperatures in the cold season accelerated the cell division rate of phytoplankton, increasing its abundance, while in the warm season it was the opposite (Xu et al., 2021). Furthermore, increased temperatures stimulated faster growth of harmful algae species, and accelerated algal blooms near the nuclear power station (Tian et al., 2021). In natural conditions, higher temperatures and enhanced stratification led to the reduction of nutrient concentration and increased the sedimentation rate of medium-sized phytoplankton, leading to an increased biomass of smaller-sized phytoplankton. This was confirmed by long-term observations, which found that the total abundance of phytoplankton decreased with temperature increased, while the abundance of pico-phytoplankton increased (Morán et al., 2010). These changes in the size composition of phytoplankton will influence the bottom-up transmission of the food chain in the marine ecosystem (Lewandowska et al., 2014; Xu et al., 2020), therefore it is necessary to evaluate the thermal response of different size-fractionated phytoplankton.

Temperature can also influence phytoplankton's physiological characteristics such as their photosynthetic ability, which differs between phytoplankton sizes. Significantly positive relationships were found between the photosynthetic rates of<2 μm-sized phytoplankton and temperatures, indicating that smaller phytoplankton was more capable of acclimating to rapid fluctuations in higher temperatures (Kaiblinger et al., 2007; Shiomoto, 2009). The absorbed light energy of the phytoplankton chlorophyll molecule is transferred to the reaction center in Photosystem I (PS I) and Photosystem II (PS II) for photosynthesis, and during this transmission process heat can be released or fluorescence emitted. Previous studies have shown that when phytoplankton was in a normal environment, most of the energy was transferred smoothly to the photosynthesis reaction center, but heat dissipation and fluorescence production increased when phytoplankton was in an unfavorable environment, such as under high-temperature stress (Kaiblinger et al., 2007) or nutrient limitation (Xie et al., 2015). Therefore, the evaluation of phytoplankton chlorophyll fluorescence can reflect the efficiency of photochemical energy conversion in PS II. The pulse-amplitude-modulation (PAM) technique has been widely used in plant physiological ecology research because of its convenience, rapidity, and absence of damage to samples (Schreiber, 2004). The maximum photochemical quantum yield (F_v/F_m) of PS II measured by PAM is often used as an indicator of environmental stress on plants (Schlensog and Schroeter, 2001). The F_v/F_m value under normal conditions for algae is generally between 0.6–0.7 (Franklin et al, 2006). While under thermal stress, the F_v/F_m value was found to decrease accordingly, but recovered when algae were returned to a normal temperature environment, although the recovery capacity differed among species (Wen et al., 2005). Evaluation of photosynthetic activities of the phytoplankton community has been used to reflect the characteristics of different phases of algal blooms (Shen et al., 2019), while the response of

phytoplankton photosynthetic activities to thermal stress near a nuclear power plant remains unclear.

Daya Bay (DYB) is located in the north of the South China Sea and is a typical subtropical bay. In the past 20 years, the ecological environment of Daya Bay has undergone significant changes under the influence of human activities, including shifts in nutrients and plankton communities (Wang et al., 2004; Yu et al., 2007). One of the most influential human activities in Daya Bay is the thermal discharge from nuclear power plants, which can cause a significant increase in the temperature of the receiving waters. There were two nuclear power stations (Daya Bay and Lingao Nuclear Power Station) located on the northwest coast, discharging hot wastewater at a rate of 315 m^3 s^{-1} when the stations were in operation (Li et al., 2011). The temperature of discharged water can be 8-10℃ higher than the background temperature (Zhang and Zhou, 2004). The semi-closed characteristics of the bay, owing to the mountain ranges on three sides, result in a relatively long average residence time of surface seawater and a relatively stable temperature gradient caused by the regular thermal drainage from the nuclear power plants. Therefore, Daya Bay is considered to be under short-term temperature rise stress (Zhang and Zhou, 2004). In the drainage area of the nuclear power plants, the analysis of continuous observation data for nearly 20 years showed that the average temperature of the surface layer in summer rose from 27.8°C in 1982 to 34.8°C in 2005, and the phytoplankton community structure showed a trend of transformation from diatom dominance to dinoflagellate dominance (Li et al., 2011), resulting in a trend of miniaturization (Hao and Tang, 2010). Furthermore, the frequency of harmful algal blooms is significantly positively correlated with the rise in water temperature (Yu et al., 2007; Tian et al., 2021), and the outbreaks of other organisms that could influence the nuclear power plant operation also increased (Liu et al., 2022). Most of the recent studies on the effect of thermal discharge on phytoplankton have focused on the changes in community structure; however, the physiological response of phytoplankton under thermal stress in the outlet regions is rarely reported. Moreover, Daya Bay is located in the subtropical zone, and the temperature in summer might be near the upper tolerance limit of some plankton species, thus any further increase in the ambient water temperature due to the discharge of heated effluents may seriously affect the physiology of phytoplankton. The objectives of this study were to 1) evaluate the effects of thermal discharge on the size-fractionated structure and photosynthetic physiology of phytoplankton communities, 2) investigate the relationship between the increased temperature ranges and the physiological response of phytoplankton in a subtropical region. The results of our study will help to further understand the potential influence of short-term thermal stress caused by the nuclear power plant on the phytoplankton communities and the possible response of phytoplankton to ocean warming.

2 Materials and methods

2.1 Sampling stations

This study was carried out in the northwest coastal waters near DYB nuclear power station (DNPS) and Ling-ao nuclear power station (LNPS) on July 30, 2012 (Figure 1). Five transects (A, C, E, G, and I) with a total of 38 sampling stations were set along the temperature gradient from the thermal pollution originating from the nuclear power stations. Five skiffs were used for sampling of these five transects simultaneously. Transect A (7 stations) began at the inlet station near Dapeng'ao, which was a cove located in the southwest of Daya Bay, and was the control zone, while stations along transect I (8 stations) began at the outlet region and represent the impacted zone. The stations' depths ranged from 2.8 m to 18.7 m. The farthest stations of all transects were approximately 6.5 km to 26.7 km from the nuclear power stations, making it possible to cover all the regions potentially affected by the thermal discharge.

To evaluate the effects of fluctuating surface temperatures on the phytoplankton community and their photosynthetic physiology, a diurnal investigation was also conducted at stations near the inlet (S1 N22°35.374', E114°32.816') and outlet (S2 N22°36.274', E114°34.0') on July 31, 2012, at three sampling times, morning (6:00), midday (12:00), and night (18:00).

2.2 Determination of environmental parameters

Temperature (Temp) and salinity (S) were measured using a YSI-6600 probe (YSI Incorporated, Ohio, USA) at each sampling site in situ. Surface seawater samples were collected using a water sampler (5 L, Watertools, China), preserved in 5 L buckets covered with black bags, and immediately taken to the laboratory. A subsample of 100 mL water was filtered through a 0.45 μm cellulose acetate filter and analyzed with a nutrient flow analyzer (SKALAR San, Netherlands) for determining the concentrations of nitrate (NO_3-N), nitrite (NO_2-N), ammonium salt (NH_4-N), phosphate (PO_4-P), and silicate (SiO_4-Si).

2.3 Measurement of photosynthetic physiology parameters

The field seawater was taken to the laboratory immediately after sampling. Then the water-PAM (Walz, Germany) was used to determine the fluorescence parameters as follows: the water sample was kept in dark for a 10 min adaptation, then transferred to a measuring cup under the measuring light (< 1 μmol m^{-2} s^{-1}) to obtain F_0, and then exposed to the saturated pulse light (4000 μmol m^{-2} s^{-1}) for 0.8 s to obtain F_m. The maximum quantum yield of PS II (F_v/F_m) was determined using the following formula (Han et al., 2003): $F_v/F_m = (F_m\text{-}F_0)/F_m$, where F_0 represents the background fluorescence of phytoplankton and F_m is the maximum fluorescence of the phytoplankton community.

2.4 Determination of phytoplankton community

A 500 mL water sample was obtained and fixed immediately with neutral Lugol's solution (final concentration approximately 2%) to determine the species composition and abundance of phytoplankton at each site. The samples were kept in dark for >24 h settlement. Then, a 1 mL subsample was used for taxonomic determinations and

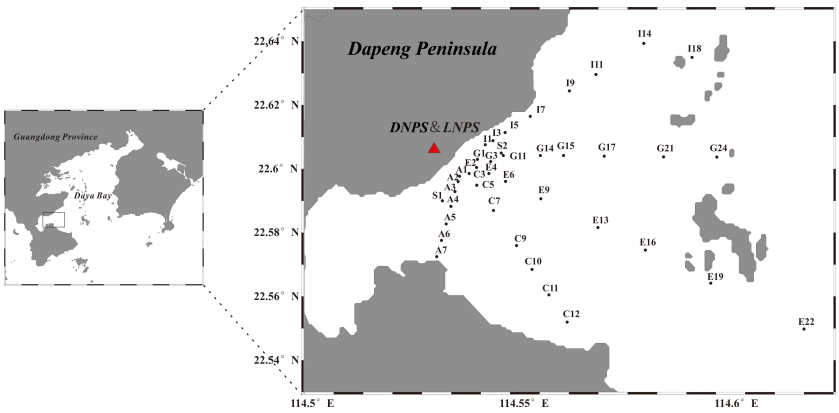

FIGURE 1
Sampling stations near the nuclear power plant area. The red triangles indicate the location of the Daya Bay nuclear power station (DNPS) and Ling-ao nuclear power station (LNPS). Transects A-I were only surveyed in the morning, while S1 and S2 were sites for diurnal investigation at control and outlet sites.

enumeration under a microscope (OLYMPUS CX31, Japan) at 200× or 400× magnification using the Utermöhl settling method.

The size-fractionated chlorophyll *a* concentration was also measured. A subsample of 1000 mL seawater was filtered successively through 20 μm, 3 μm, and 0.2 μm polycarbonate membranes (Millipore, USA) for the calculation of micro-, nano-, and pico-phytoplankton biomass. Then, the pigment was extracted with 90% acetone in a dark environment with a low temperature (4°C), and the concentration was determined using a fluorometer (Turner, USA).

2.5 Data processing and statistical analysis

The abundance of each phytoplankton taxa was calculated by conversion of cell numbers per liter (cells L^{-1}). The Shannon-Weaver diversity index (*H'*) (Shannon, 1948) was used for the calculation of taxonomic diversity:

$$H' = H' = -\sum_{i-1}^{z} P_i log_2 P_i; \quad P_i = N_i/N$$

where *s* is the number of species; *N* is the total number of individuals in the same sample; *Ni* is the number of individuals of species *i*.

Correlation analysis and principal component analysis (PCA) were performed in SPSS 18.0 software. R studio 4.0.3 was also used to implement graphic visualization and data analysis.

3 Results

3.1 Environmental conditions

Temperature variations among different regions were observed (Figure 2A). The outlet region (I1-I3) exhibited the highest temperature while there was a relatively low-temperature area near the inlet area (transect A), ranging from 33.72°C to 36.74°C and 29.03°C to 30.1°C, respectively. Although there was no significant difference in temperatures between water inlet transect A and water outlet section I, the temperature at station I1 near the outlet in the morning and afternoon was as high as 36.7°C and 36.8°C, respectively, while the temperature at station A1 near the water inlet in the morning was only 29.0°C, and the temperature difference between the two stations was as high as 7.7°C. The temperatures along transects C, E, and G were basically stable, and the temperature differences at each station were no more than 2.0°C.

Dissolved inorganic nitrogen (DIN), dissolved inorganic phosphorus (DIP), and silicate (SiO_4-Si) at all stations varied within 1.36–8.48 μmol L^{-1}, 0.03–1.30 μmol L^{-1}, and 6.30–58.00 μmol L^{-1}, respectively. The high-value areas of DIN and DIP were mainly distributed in the aquaculture areas near the nuclear power plants (G15 and G21) (Figures 2B, C). SiO_4-Si was evenly distributed in the nearshore areas except for at stations in transect I, and the highest concentration was observed at G15 (Figure 2D). The ratio of N/P varied from 5.08 to 117.75 with an average value of 23.33, which was slightly higher than the Redfield ratio (Redfield ratio 16:1). Generally, the concentration of nutrients decreased from nearshore sites to offshore areas. Significant differences in the concentration of DIP were only detected between transects C and I, and in the concentration of SiO_4-Si between transects E and G (Table S2, $p<0.05$, one-way ANOVA).

3.2 Distribution of phytoplankton abundance and chlorophyll a concentration

Generally, the phytoplankton abundance was evenly distributed along transects A (except A7), C, E, and G, varying from 6.40×10^4 cells L^{-1} to 3.32×10^6 cells L^{-1} (Figure 3A). Substantial differences were observed in the phytoplankton abundance of transect I and an increasing trend in cell density was observed for sites that were far away from the outlet area. The lowest value was found near the outlet site (I1, I3, and I5) with an average density of $1.32 \pm 0.05 \times10^5$ cells L^{-1}, and the abundance of phytoplankton increased to $7.31 \pm 0.60\times10^5$ cells L^{-1} at I7 and I9. However, at site I11, the abundance was as high as 10^6 cells L^{-1}. Total chlorophyll *a* concentrations varied significantly among the different transects ($p<0.05$, Table S2). Generally, the chlorophyll *a* concentrations at sites of transects I and G (7.35 ± 5.54 μg L^{-1}) were higher than those in transects A, C, and E (2.62 ± 1.25 μg L^{-1}) (Figure 3B). However, the

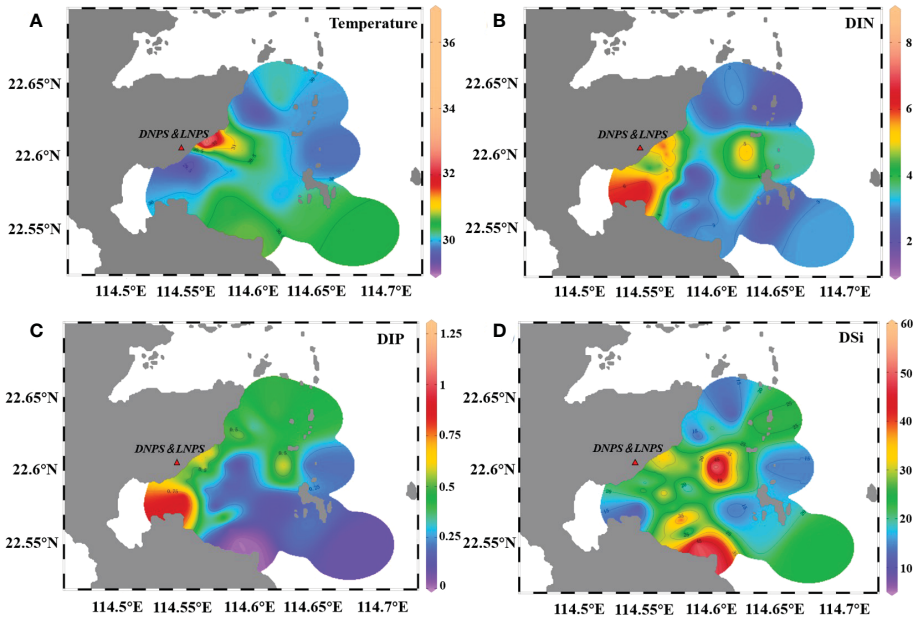

FIGURE 2
Sea surface temperature (**A**, °C) and nutrient (μmol L^{-1}) distribution in the survey area. DIN represents the total concentration of NO_3^- and NO_2^-. **(B)** DIP represents the concentration of PO_4^- **(C)**, and DSi represents the concentration of SiO_4^- **(D)**.

lowest chlorophyll *a* concentration was detected at the outlet site (I1). At sites furthest away from the outlet region (I5 to I18), the chlorophyll *a* concentration gradually increased to a maximum level.

3.3 Phytoplankton composition

A total of 103 phytoplankton species were identified in all the transects, mainly belonging to diatom and dinoflagellate. There were also a few species from Cyanobacteria and others (e.g., Chrysophyceae, Raphidophyceae). The number of dinoflagellate species was higher than that of diatom in transects A, C, and E, while in the transects near the outlet regions (G and I), the number of diatom species was higher than that of dinoflagellate (Figure 4A). Regarding abundance, diatom species were more abundant than dinoflagellates at all stations, ranging from 6.40 $\times 10^4$ cells L^{-1} to 4.6 $\times$ 10^6 cells L^{-1} (Figure 4B). Dinoflagellate species showed a relatively higher abundance (10^5 cells L^{-1}) at I9 and E16. *Thalassionema nitzschiodes* was the most abundant species in almost all sites with a fraction more than 50%, followed by *Skeletonema* spp., *Thalassiosira* spp., *Scrippsiella accuminata*, and *Chaetoceros* spp. Notably, red-tide-forming species such as *S. accuminata* and *Skeletonema costatum* accounted for a much larger proportion in transect I than at other stations. The dominant species in transects A and C were diatom *Thalassionema*, while from transects E to I dinoflagellate species such as *Prorocentrum* and *Scrippsiella* occurred and became abundant. The dominant species in transect I shifted from *Thalassionema nitzschiodes* in I1 (61.39%), I3 (63.80%), and I5 (55.78%) to *Chaetoceros curvisetus* in I7 (48.36%) and I11 (43.79%), and to *Skeletonema costatum* in I14 (37.32%) and I18 (22.13%). The diversity index of the phytoplankton communities in transect I was higher than that of transect A, varying from 0.59 to 3.48, with the highest value recorded at station I9 and the lowest value at station A1.

Pico-phytoplankton occupied more than 50% of the total chlorophyll *a* concentration (average 52.73 ± 3.69%) at most sites in transects A, C, and E, while nano-phytoplankton became the dominant group (average 48.20 ± 5.84%) in transects I and G (Figure 4C). The average proportion of micro-phytoplankton was stable in all the transects, with a percentage of ~14.55% at all stations.

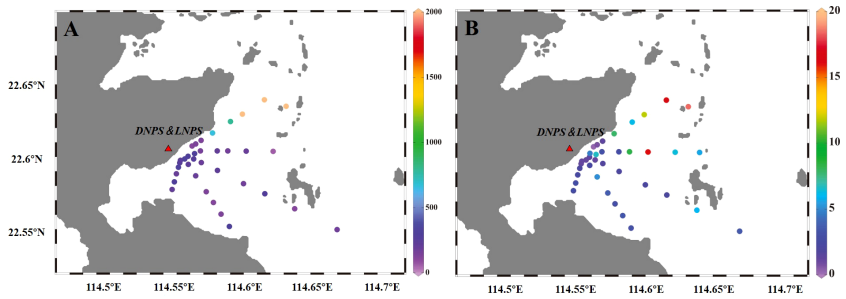

FIGURE 3
Distribution patterns of phytoplankton abundance [**(A)**, cells L^{-1}] and total chlorophyll a concentration [**(B)**, μg L^{-1}] in the survey area.

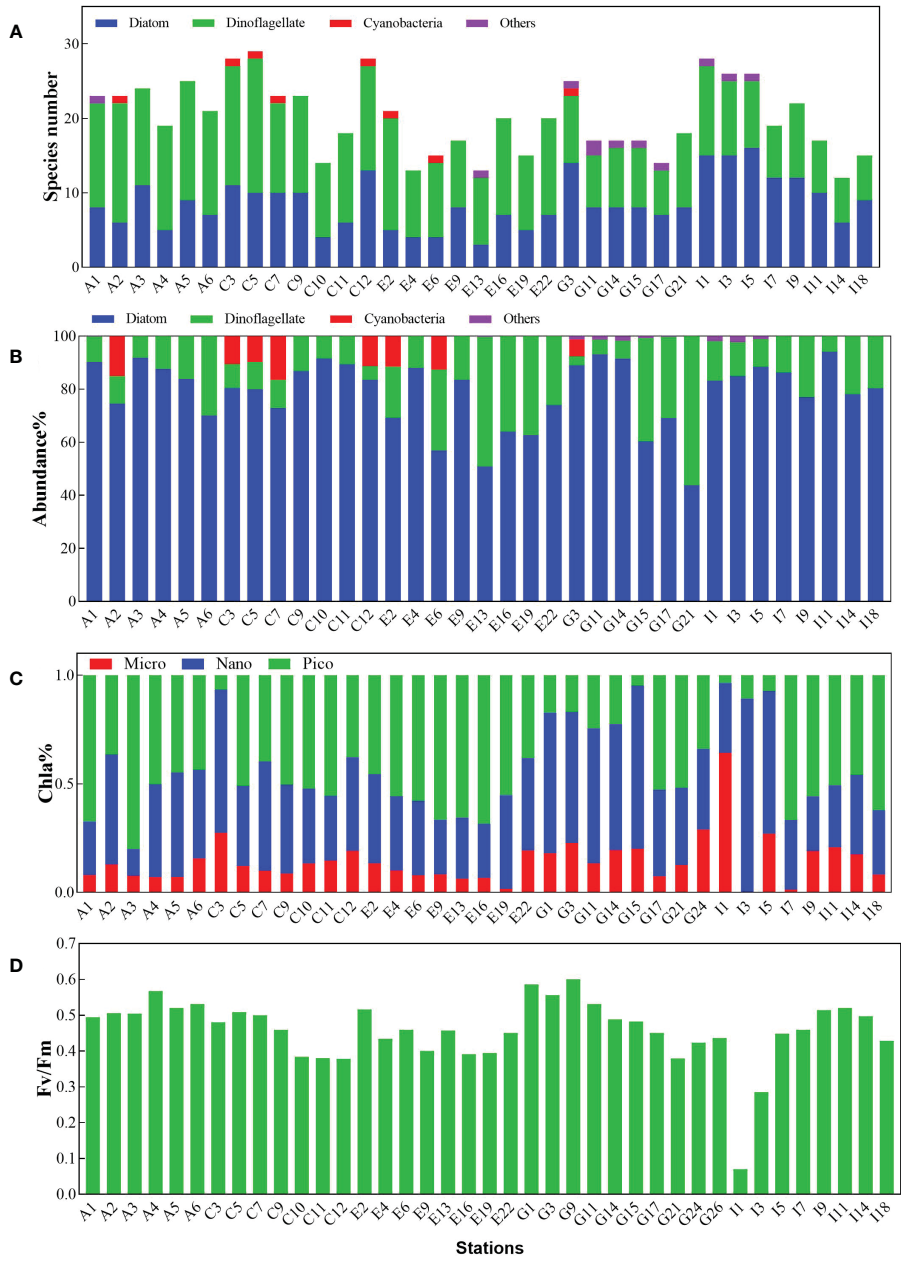

FIGURE 4
Relative characteristics of phytoplankton community in different sampling sites. **(A)** species numbers distributed in different phytoplankton groups. **(B)** the abundance of different phytoplankton groups. **(C)** size-fractionated chlorophyll a concentration. **(D)** the maximum quantum yield of PS II (F_v/F_m). Others represent species belonging to Chrysophyceae and Raphidophyceae.

Pico-phytoplankton was most affected in the outlet site and was hardly detected, but it did recover from 3–10% (I1, I3, I5) to 66% (I7) at sites further away from the outlet station.

3.4 Photosynthetic physiological characteristics of phytoplankton community

The maximum quantum yield of PS II (F_v/F_m) varied within the range of 0.07–0.6 at the sampling sites, with an average value of 0.46 ± 0.09 (Figure 4D). The average F_v/F_m values of transect A were high (0.53 ± 0.03), followed by transects G (0.49 ± 0.06), C (0.44 ± 0.05), and E (0.44 ± 0.04). The photosynthetic physiological state of phytoplankton was significantly impacted at the outlet site (I1), with the F_v/F_m decreasing dramatically to 0.07. However, they did gradually recover to a normal state at sites further away from the outlet site.

3.5 Diurnal variations of environmental parameters and phytoplankton community

The temperature at the outfall station (S2) was significantly higher than that of the control station (S1) (F=24.37, p<0.05), but both of them showed a rising trend from morning to night (Table S3). An average temperature difference of 5.03 ± 0.29°C was observed between

S2 and S1 during the day and the highest difference (5.4°C) occurred at night. The average salinity of station S1 (32.17) was lower than that of S2 (36.57), but the dissolved oxygen (DO) in S1 was higher than that of S2. The total concentration of nitrate at all sampling times in both S1 and S2 showed no significant difference, but the total phosphate concentration in S2 was slightly higher than that in S1, showing a decreasing trend from morning to night. The N:P ratio in S2 was higher than that in S1, reaching as high as 69.6:1 at night.

The species number and abundance of phytoplankton showed no difference between S1 and S2, but the lowest value at both occurred at night (Table S3). The dominant species at S1 and S2 was Bacillariophyta species *T. nitzschiodes* during the sampling time. The total chlorophyll *a* concentration exhibited a trend of midday>morning>night at both S1 and S2, and the micro-phytoplankton group showed the same trend at the two sites (Figure 5A). The chlorophyll *a* concentration of micro-phytoplankton at S2 was substantially lower (decreased about 78%) than that of S1 in the morning and midday but reached a higher value at night. The proportion of nano-phytoplankton at S2 (68.4%) was higher than that of S1 (57.86%) and reached the highest value at midday at both S1 and S2. Meanwhile, the chlorophyll *a* concentration of pico-phytoplankton decreased significantly at S2 compared with S1, especially at midday and night, accounting for 8.61% and 18.07% that of S1, respectively. The maximum quantum yield of PS II (F_v/F_m) of phytoplankton showed a trend of morning >night>midday at both S1 and S2 (Figure 5B). The F_v/F_m at S2 was lower than that at S1 in the morning and night, but higher than S1 at midday.

3.6 Relationships between the environmental parameters and phytoplankton community

The PCA biplot was used to analyze the distribution patterns of both the environmental parameters and the phytoplankton community traits (Figure 6A). The results indicated that 43.3% and 28.9% of the environmental and community variation could be explained by axis 1 and 2, respectively. A significant difference was only detected in temperature between transects A and I ($p<0.05$, Table S2), indicating that temperature acts as the main ecological constraint in the differences between the inlet and outlet sites in the sampling period, especially in I1 and I3. Negative correlations were found between F_v/F_m and temperature, as well as chlorophyll *a* and temperature, but no significant associations with temperature were found for the other parameters. A significant negative correlation was found through correlation analysis of temperature and F_v/F_m at all stations (n = 52, r = -0.6065, $p<0.01$). Generally, F_v/F_m showed a decreasing trend with the increase in temperature, and the highest values of F_v/F_m mainly occurred between 29–33°C but decreased rapidly beyond 33°C (Figure 6B). The relative electron transport rate (rETR) also exhibited a negative relationship with the temperature rise (Figure 6C).

4 Discussion

4.1 Effect regions and influence on the environmental factors of thermal discharge from the nuclear power plant

Daya Bay is a semi-closed bay in subtropical regions with an irregular semi-diurnal tide. In summer, the bottom residual current is a low-speed clockwise circulation system, which is conducive to the transportation of rich nutrients by the open sea and rivers to Dapeng'ao and the circulating cooling of the warm drainage from the nuclear power plants. In summer, the surface current is a counterclockwise circulation, which leads to the right deflection of the warm drainage due to the Coriolis force. The warm drainage is mainly injected into Dapeng Bay, which is difficult to diffuse (Xu, 1989; Yang, 2001). This is consistent with the findings of Lin and Zhan (2000), that is, the impact range of the warm drainage of Daya Bay nuclear power plants is mainly in the coastal waters to the east of the plants, and on the opposite bank of the nuclear power plant, the water inlet region and the middle of Dapeng'ao may also be affected (Lin and Zhan, 2000). In this study, the survey data showed that the thermal effect of warm drainage from the nuclear power plant is mainly concentrated near the plant (mainly transect I), which is consistent with previous research.

In summer, the water in Daya Bay is relatively stable and a thermocline often appears, which makes it difficult to mix and exchange water vertically (Xu, 1989). In summer, the upwelling along the east coast of Guangdong often leads to a further decline of the lowest seawater temperatures (Zhang and Zhou, 2004), which is likely to cause stratification of the seawater. The position of thermal

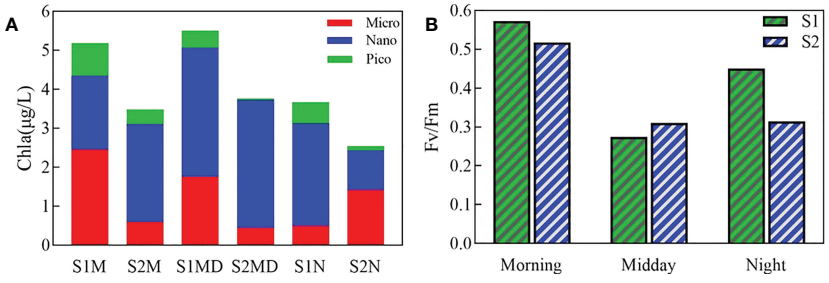

FIGURE 5
Size-fractionated chlorophyll *a* composition **(A)** and the maximum quantum yield (F_v/F_m) **(B)** at the inlet and outlet stations. S1, the inlet site. S2, the outlet site. M represents morning, MD represents midday, and N represents night.

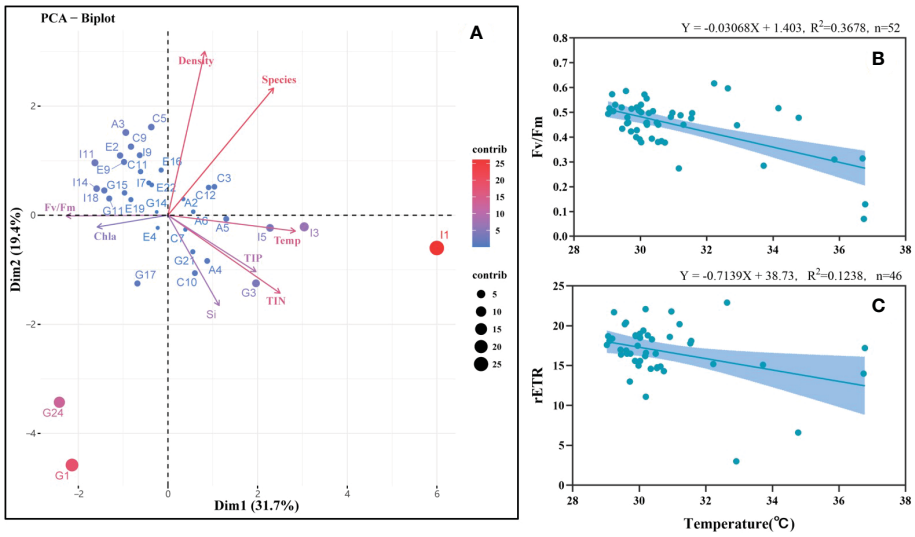

FIGURE 6
Relationships between the environmental parameters and phytoplankton community. **(A)** principal component analysis (PCA) biplot shows the variables for both environmental parameters and phytoplankton characteristics in all sampling stations. **(B)** correlation analysis between the maximal photochemical quantum yield (F_v/F_m) and temperature in the survey area. **(C)** correlation analysis between the relative electron transport rate (rETR) and temperature in the survey area.

drainage from the nuclear power plant further increases the surface water temperature. In this study, the maximum temperature difference between the surface and bottom reaches 10.78°C, and the highest temperature at the surface was recorded near the outlet station, which further expands the temperature difference between the surface and bottom and strengthens the seasonal thermocline. This was not conducive to the vertical convection of the seawater and would intensify the oxygen deficiency and carbon accumulation at the bottom, limiting the biogeochemical cycle of carbon.

The concentrations of the three dissolved inorganic nutrients in this study are consistent with previous studies in Daya Bay (Wang et al., 2011). DIN and DIP were higher near the shore than they were offshore, mainly due to the input of a large number of land-based substances caused by human activities, such as the discharge of aquaculture wastewater (Jiang et al., 2013). The N/P value was greater than 16 in most sites, indicating that the growth limiting factor of phytoplankton in Daya Bay has changed from nitrogen to phosphorus (Wang et al., 2004). Although the nutrient concentration of Daya Bay is lower than that of other bays in China, the total nutrient concentration has developed from an oligotrophic to a mesotrophic level. The water quality in some areas, such as Yaling Bay, Dapeng'ao, and Fanhe port, is poor and shows a trend of eutrophication (Wang et al., 2004). Furthermore, the warm drainage from nuclear power plants promotes the eutrophication process, because increased temperatures accelerate the biogeochemical cycle turnover rate of elements, and the turnover rate of phosphorus is faster than that of nitrogen (Wang et al., 2003). This was confirmed by our study, which found that the DIP concentration at station S1 was significantly higher than that of S2, but there was no significant difference in the DIN concentration.

Principal component analysis found that the dominant factors at different stations were clustered into different categories. Station I1 was in a separate category, and temperature was an influencing factor leading to its separation (Figure 5A). There was a clear temperature gradient with a difference of 3°C from I1 to I5 (~33°C) and the temperature of I1 reached as high as 36.74°C, higher than 35°C. According to long time-series data analysis, 33°C was considered to be the threshold temperature leading to the transformation of phytoplankton community structure from diatom dominance to dinoflagellate dominance, and 35°C was the upper-temperature limit for phytoplankton growth, respectively (Li et al., 2011). Significant differences were found between the temperatures of transect I and the other transects (n=37, F=2.892, p =0.037), indicating that the increased temperature caused by thermal discharge was the most important environmental factor in the outlet regions.

4.2 Effects of thermal discharge on phytoplankton community structure

In this study, the phytoplankton abundance of the outlet site (S2) was lower than that of the inlet station (S1), but the corresponding phytoplankton abundance of stations I11, I14, and I18 near the outlet region, but far away from the outlet site, was one order of magnitude higher than that of other stations. Previous surveys found that the amount of phytoplankton passing through the nuclear power plant cooling device was substantially lower in the seasons with high temperatures, but their abundance recovered quickly in the outlet area and the growth rate of phytoplankton affected by warm drainage increased three-fold (Poornima et al., 2006). The phytoplankton density in the outlet regions within a 2°C temperature rise tended to increase because the relatively higher water temperature was conducive to the rapid recovery of phytoplankton (Tang et al., 2013). On the other hand, the rapid temperature rise over a short period of time may stimulate the cell proliferation of red-tide algal

species (Huang et al., 2002). In this study, a bloom of *S. accuminata* occurred in the afternoon at station I3 (cell density > 10^6 cells L^{-1}; the temperature > 33°C), but in the morning, *S. accuminata* was not a dominant species at I3. In recent years, *S. trochoidea* was one of the species forming high-frequency dinoflagellate blooms in Daya Bay, especially in summer (Li et al., 2011; Tian et al., 2021). *S. accuminata* was found to be more adaptive to high temperatures and still able to grow at >30°C (Xu et al., 2004). Therefore, the frequent occurrence of this kind of harmful algal species in the outlet area is likely due to the rapid growth caused by increased temperatures. In addition, other harmful algae species, such as *Chaetoceros curvisetus* and *Skeletonema costatum*, showed relatively higher abundance in transect I, and the stimulation of warm seawaters may exacerbate the blooms of algal species in optimal hydrodynamic conditions (Tian et al., 2021).

Very few studies have investigated the size-fractioned structure of phytoplankton in Daya Bay, especially in the regions affected by thermal discharge. Li et al. (2013) found that nano-phytoplankton contributed the greatest proportion of phytoplankton chlorophyll *a* concentration in coastal waters along the bay (Li et al., 2013). Previous studies conducted on the phytoplankton community structure found that the concentration of chlorophyll *a* increased or stabilized, but the corresponding cell number of net phytoplankton (mainly micro-phytoplankton species) decreased, indicating a trend of phytoplankton miniaturization (Liu et al., 2006; Hao and Tang, 2010). This was consistent with our results that pico-phytoplankton was abundant at most of our sites except for the outlet regions. While the dominant group changed to nano-phytoplankton at sites near outlet regions and was also abundant at midday at both inlet and outlet sites with higher temperatures. This could be due to the higher sensitivity and lower recovery capability of the pico-phytoplankton group than the micro- and nano-phytoplankton groups under high-temperature conditions (Xie et al., 2015). The concentrations of total chlorophyll *a* in I1, I3, and I5 were very low and at site S2 the pico-phytoplankton chlorophyll *a* could hardly be detected, indicating that high temperatures (>33°C) can exert serious damage to phytoplankton, especially pico-phytoplankton (Li et al., 2011; Tang et al., 2013). The size-fraction structure of phytoplankton changes at the outlet regions due to the discrepant response of different groups, which may affect the trophic transmissions along the food chain.

4.3 Effects of thermal discharge on phytoplankton physiology

Phytoplankton abundance and chlorophyll *a* concentrations can only reflect the current situation of phytoplankton, while F_v/F_m obtained from fluorescence measurements can be used to indicate the primary light energy conversion efficiency of the reaction center of PS II, which can reflect the potential physiological adaptability and predict the trend of community development (Han et al., 2003). Under coercive conditions, F_v/F_m decreases significantly, indicating that the photosynthetic electron transfer of PS II is blocked (Claquin et al., 2008). The F_v/F_m values of the total phytoplankton community in our survey areas were slightly lower than normal values of phytoplankton (0.6–0.7), indicating that the phytoplankton might be stressed by high temperatures and high light intensity in summer. Additionally, the increased temperature in the outlet regions enhanced this effect, with the F_v/F_m at the outlet sites (I1, I3, and I5) being far lower than the normal level. In particular, phytoplankton at station I1 (> 35°C) had basically lost photosynthetic activity (~0.07), but this activity can recover quickly when phytoplankton is far away from the outlet. This was supported by the F_v/F_m value showing an upward trend at the station furthest from the outlet site, which may be caused by the stimulation of phytoplankton by high temperatures (>33°C). During the diurnal investigation of the inlet and outlet sites, the F_v/F_m of S1 was close to 0.6 in the morning and 0.5 in the night but decreased to less than 0.3 at midday, indicating that the high light intensity at noon will affect the photosynthetic activity. The F_v/F_m of S2 was slightly higher than that of S1, indicating that the high temperatures at the outlet site can compensate for the light suppression caused by strong light (Sobrino and Neale, 2007; Halac et al., 2010; Li et al., 2012).

A significant negative relationship was detected between temperature and photosynthetic parameters, and 33 ℃ might be a key temperature level for the change of phytoplankton physiology, which is consistent with a previous research hypothesis on the long-term monitoring data of Daya Bay outlet regions (Li et al., 2011). The effects of temperature on the photosynthetic performance of phytoplankton were influenced by other factors, such as the duration of time and available nutrients. In the laboratory experiment, F_v/F_m of phytoplankton in the first two days was maintained at a normal level but decreased significantly after two days of incubation; adequate nutrients can promote the recovery of phytoplankton at normal temperatures (Xie et al., 2015). Therefore, the short-term stress from thermal discharge will affect the physiological performance of phytoplankton but this damage can be recovered after phytoplankton is carried away from the high-temperature region. Considering the different capabilities of different species or different size groups, the phytoplankton community might change in the long term.

5 Conclusion

In this study, the influence of the warming environment by thermal discharge on the size-fractioned phytoplankton structure and photosynthetic physiological characteristics were surveyed in the potentially affected waters around the nuclear power plants in Daya Bay. The surface water temperature was significantly elevated in the outlet area of the power plants. Moreover, we detected a fast photosynthetic physiological response of phytoplankton to the elevated temperature and a shift in the size-fractioned structure in the outlet regions. Although the photosynthetic physiology could recover when the phytoplankton was taken away from the outlet site, the high-temperature inhibition might change the physiological features and stimulate the stress response of the phytoplankton, such as the high frequency of harmful algae blooms along the coastal regions near the nuclear power plants. Therefore, on the basis of routine monitoring, it is also necessary to pay more attention to physiological changes in phytoplankton communities, especially in

abnormally high temperatures or weather conditions, in order to comprehensively monitor the ecological effects of thermal discharge from the coastal power plants.

Data availability statement

The original contributions presented in the study are included in the article/Supplementary Material. Further inquiries can be directed to the corresponding author.

Author contributions

Conceived and designed the experiments: SH, SL. Field survey and sampling: SH, CZ, TL, SL. Analyzed the data: SH, CZ, QL. Contributed reagents/materials/analysis tools: SL, HH. Wrote the paper: SH. All authors contributed to the article and approved the submitted version.

Funding

This research was funded by the Natural Science Foundation of China (contract No. 42176118); the Science and Technology Planning Project of Guangdong Province (contract No. 2020B1212060058); the Hainan Provincial Natural Science Foundation of China (contract No. 422QN442); and the Science and Technology Program of Guangzhou, China (contract No. 202201010674); Fund of Guangdong Provincial Key Laboratory of Fishery Ecology and Environment (FEEL-2022-6).

Acknowledgments

The authors thank the staff of the Guang Dong Daya Bay National Marine Ecosystem Research Station in Shenzhen for their logistical support. We would also like to thank Dr. Yunxu Liu for assistance with the calculation of environmental parameters and Editage (www.editage.cn) for English language editing.

Conflict of interest

The authors declare that the research was conducted in the absence of any commercial or financial relationships that could be construed as a potential conflict of interest.

Publisher's note

All claims expressed in this article are solely those of the authors and do not necessarily represent those of their affiliated organizations, or those of the publisher, the editors and the reviewers. Any product that may be evaluated in this article, or claim that may be made by its manufacturer, is not guaranteed or endorsed by the publisher.

Supplementary material

The Supplementary Material for this article can be found online at: https://www.frontiersin.org/articles/10.3389/fmars.2023.1102686/full#supplementary-material

References

Claquin, P., Probert, I., Lefebvre, S., and Veron, B. (2008). Effects of temperature on photosynthetic parameters and TEP production in eight species of marine microalgae. *Aquat. Microb. Ecol.* 51 (1), 1–11. doi: 10.3354/ame01187

Falkowski, P. (2012). Ocean science: the power of plankton. *Nature* 483 (7387), S17–S20. doi: 10.1038/483S17a

Franklin, D. J., Cedrés, C. M. M., and Hoegh-Guldberg, O. (2006). Increased mortality and photoinhibition in the symbiotic dinoflagellates of the indo–pacific coral *Stylophora pistillata* (Esper) after summer bleaching. *Mar. Biol.* 149 (3), 633–642. doi: 10.1007/s00227-005-0230-z

Halac, S. R., Villafañe, V. E., and Helbling, E. W. (2010). Temperature benefits the photosynthetic performance of the diatoms *Chaetoceros gracilis* and *Thalassiosira weissflogii* when exposed to UVR. *J. Photochem. Photobiol. B.: Biol.* 101 (3), 196–205. doi: 10.1016/j.jphotobiol.2010.07.003

Han, Z. G., Han, B. P., and Fu, X. (2003). Mechanism and model of algae photosynthesis. *Sci. Press.* Beijing, 72–73.

Hao, Y. J., and Tang, D. L. (2010). Changes in phytoplankton community structure in response to water temperature increases in daya bay, China. *Ecol. Environ. Sci.* 19 (8), 1794–1800. doi: 10.3969/j.issn.1674-5906.2010.08.006

Hays, G. C., Richardson, A. J., and Robinson, C. (2005). Climate change and marine plankton. *Trends Ecol. Evol.* 20 (6), 337–344. doi: 10.1016/j.tree.2005.03.004

Huang, X., Huang, L., Tan, Y., and Zhu, L. (2002). Relationship between red tide and environmental conditions in coastal waters. *Mar. Environ. Science/Haiyang. Huanjing. Kexue.* 21 (4), 63–69. doi: 10.3969/j.issn.1007-6336.2002.04.015

Jiang, L. M., Dong, L. F., Yang, J. F., Xu, Z. H., and Sun, X. X. (2013). Distribution features of nutrients in daya bay. *J. Changzhou. Univ.* 25 (2), 12–15. doi: 10.3969/j.issn.2095-0411.2013.02.003

Jiang, Z., Du, P., Liao, Y., Liu, Q., Chen, Q., Shou, L., et al. (2019). Oyster farming control on phytoplankton bloom promoted by thermal discharge from a power plant in a eutrophic, semi-enclosed bay. *Water Res.* 159, 1–9. doi: 10.1016/j.watres.2019.04.023

Kaiblinger, C., Greisberger, S., Teubner, K., and Dokulil, M. T. (2007). Photosynthetic efficiency as a function of thermal stratification and phytoplankton size structure in an oligotrophic alpine lake. *Hydrobiologia* 578 (1), 29–36. doi: 10.1007/s10750-006-0430-7

Khttab, K. (2021). Nuclear power reactors in the world. *Atom. Dev.* 33 (2), 43–55. doi: 10.1016/0140-6701(95)96544-M

Lewandowska, A. M., Boyce, D. G., Hofmann, M., Matthiessen, B., Sommer, U., and Worm, B. (2014). Effects of sea surface warming on marine plankton. *Ecol. Lett.* 17 (5), 614–623. doi: 10.1111/ele.12265

Li, Y., Gao, K., Villafañe, V. E., and Helbling, E. W. (2012). Ocean acidification mediates photosynthetic response to UV radiation and temperature increase in the diatom *Phaeodactylum tricornutum*. *Biogeosciences* 9 (10), 3931–3942. doi: 10.5194/bg-9-3931-2012

Li, L., Jiang, T., and Lv, S. H. (2013). Size-fractionated biomass of phytoplankton in the coastal waters of daya bay in summer and autumn. *Mar. Environ. Sci.* 32 (2), 185–189. doi: CNKI:SUN:HYHJ.0.2013-02-007

Li, T., Liu, S., Huang, L., Huang, H., Lian, J., Yan, Y., et al. (2011). Diatom to dinoflagellate shift in the summer phytoplankton community in a bay impacted by nuclear power plant thermal effluent. *Mar. Ecol. Prog. Ser.* 424, 75–85. doi: 10.3354/meps08974

Lin, Z., and Zhan, H. (2000). Effects of thermal effluent on fish eggs and larvae in waters near daya bay nuclear plant. *J. Trop. Oceanogr. /Redai. Haiyang. Guangzhou.* 19 (1), 44–51. doi: 10.3969/j.issn.1009-5470.2000.01.007

Lin, J., Zou, X., and Huang, F. (2018). Effects of the thermal discharge from an offshore power plant on plankton and macrobenthic communities in subtropical China. *Mar. pollut. Bull.* 131, 106–114. doi: 10.1016/j.marpolbul.2018.04.005

Liu, S., Huang, L. M., Huang, H., Lian, J. S., Long, A. M., and Li, T. (2006). Ecological response of phytoplankton to the operation of daya bay nuclear power station. *Mar. Environ. Sci.* 25 (2), 9–13.

Liu, Q., Zhou, L., Zhang, W., Zhang, L., Tan, Y., Han, T., et al. (2022). Rising temperature contributed to the outbreak of a macrozooplankton *Creseis acicula* by enhancing its feeding and assimilation for algal food nearby the coastal daya bay nuclear power plant. *Ecotoxicol. Environ. Saf.* 238, 113606. doi: 10.1016/j.ecoenv.2022.113606

Madden, N., Lewis, A., and Davis, M. (2013). Thermal effluent from the power sector: an analysis of once-through cooling system impacts on surface water temperature. *Environ. Res. Lett.* 8 (3), 035006. doi: 10.1088/1748-9326/8/3/035006

Morán, X. A. G., Lopez-Urrutia, Á., Calvo-Diaz, A., and Li, W. K. (2010). Increasing importance of small phytoplankton in a warmer ocean. *Global Change Biol.* 16 (3), 1137–1144. doi: 10.1111/j.1365-2486.2009.01960.x

Poornima, E. H., Rajadurai, M., Rao, V. N. R., Narasimhan, S. V., and Venugopalan, V. P. (2006). Use of coastal waters as condenser coolant in electric power plants: Impact on phytoplankton and primary productivity. *J. Thermal. Biol.* 31 (7), 556–564. doi: 10.1016/j.jtherbio.2006.05.009

Schlensog, M., and Schroeter, B. (2001). A new method for the accurate in situ monitoring of chlorophyll a fluorescence in lichens and bryophytes, in *The lichenologist* 33 (5), 443-452. doi: 10.1006/lich.2001.0340

Schreiber, U. (2004). "Pulse-Amplitude-Modulation (PAM) fluorometry and saturation pulse method: An overview," in *Chlorophyll a fluorescence. advances in photosynthesis and respiration*, vol. Vol 19 . Eds. G. C. Papageorgiou and Govindjee, (Dordrecht: Springer). doi: 10.1007/978-1-4020-3218-9_11

Shannon, C. E. (1948). A mathematical theory of communication. *Bell. System. Tech. J.* 27 (3), 379–423. doi: 10.1002/j.1538-7305.1948.tb01338.x

Shen, A., Ishizaka, J., Yang, M., Ouyang, L., Yin, Y., and Ma, Z. (2019). Changes in community structure and photosynthetic activities of total phytoplankton species during the growth, maintenance, and dissipation phases of a *Prorocentrum donghaiense* bloom. *Harmful. Algae.* 82, 35–43. doi: 10.1016/j.hal.2018.12.007

Shiah, F. K., Wu, T. H., Li, K. Y., Kao, S. J., Tseng, Y. F., Chung, J. L., et al. (2006). Thermal effects on heterotrophic processes in a coastal ecosystem adjacent to a nuclear power plant. *Mar. Ecol. Prog. Ser.* 309, 55–65. doi: 10.3354/meps309055

Shiomoto, A. (2009). Photosynthetic responses to the temperature of size-fractionated phytoplankton in the wintertime north-western pacific. *J. Mar. Biol. Assoc. United. Kingdom.* 89 (2), 265–268. doi: 10.1017/S0025315408003275

Sobrino, C., and Neale, P. J. (2007). Short-term and long-term effects of temperature on photosynthesis in the diatom *Thalassiosira pseudonana* under UVR exposures. *J. Phycol.* 43 (3), 426–436. doi: 10.1111/j.1529-8817.2007.00344.x

Song, X., Huang, L., Zhang, J., Huang, X., Zhang, J. B., Yin, J., et al (2004). ariation of phytoplankton biomass and primary production in Daya Bay during spring and summer. *Mar Pollut Bull* 49 (11), 1036–1044.

Tang, S. M., Yan, Y., and Chen, B. (2013). Impacts of thermal effluent on the phytoplankton community structures nearby dayawan nuclear power station in spring and summer. *J. Appl. Oceanogr.* 32 (3), 373–382. doi: 10.3969/J.ISSN.2095-4972.2013.03.010

Tian, Y., Hu, S., Lin, X., Huang, H., Song, X., Yan, Y., et al. (2021). Mechanisms of high-frequency dinoflagellate blooms of *Scrippsiella trochoidea* in daya bay, south China Sea. *J. Oceanol. Limnol.* 39 (4), 1293–1304. doi: 10.1007/s00343-020-9082-0

Wang, Z. D., Lian, J. S., Hu, J. X., and Wei, G. F. (2003). The characteristics of degraded ecosystem of daya bay. *Ecol. Sci.* 22 (4), 313–320. doi: 10.3969/j.issn.1008-8873.2003.04.006

Wang, Y., Wang, Z., and Huang, L. (2004). Environment changes and trends in daya bay in recent 20 years. *J. Trop. Oceanogr/Redai. Haiyang. Xuebao.* 23 (5), 85–95. doi: 10.3969/j.issn.1009-5470.2004.05.012

Wang, Z., Yang, Y., Song, S., Fu, Y., Deng, B., Wang, Q., et al. (2011). Seasonal changes in nutrients and their accumulation in the surface microlayer in daya bay, south China Sea. *Acta Scientiae. Circumstantiae.* 31 (2), 307–315.

Wen, X., Gong, H., and Lu, C. (2005). Heat stress induces a reversible inhibition of electron transport at the acceptor side of photosystem II in a cyanobacterium *Spirulina platensis*. *Plant Sci.* 168 (6), 1471–1476. doi: 10.1016/j.plantsci.2005.01.015

World Energy Outlook (2017). *Special report: Energy access outlook. outlook for china's energy supply and investment trends: Overview of key supply and investment trends Paris*. (International Energy Agency), 561–603.

Xie, Y. H., Li, T., Jian, W. J., Hu, S. M., Tian, Y., and Liu, S. (2015). Influence of ocean warming on the community structure and photosynthetic efficiency of phytoplankton in daya bay. *J. Trop. Oceanogr.* 34 (2), 24–31. doi: 10.11978/j.issn.1009-5470.2015.02.004

Xu, G. Z. (1989). Environments and resources of Daya Bay. (Anhui Press of Science and technology) p. 11-13.

Xu, C., Hu, S., Guo, Z., Li, T., Huang, H., Chan, L. L., et al. (2020). Flexible feeding patterns of copepod *Centropages tenuiremis* in fluctuating conditions: A possible survival strategy to cope with disturbance. *Acta Oceanolog. Sin.* 39 (2), 59–68. doi: 10.1007/s13131-020-1553-9

Xu, N., Lv, S. H., Chen, J. F., He, L. S., Xie., L. C., and Qi, Y. Z. (2004). The influence of water temperature and salinity on the growth of *Scrippsiella trochoidea*. *Mar. Environ. Sci.* 23 (3), 36–38. doi: 10.3969/j.issn.1007-6336.2004.03.011

Xu, D., Wang, H., Han, D., Chen, A., and Niu, Y. (2021). Phytoplankton community structural reshaping as response to the thermal effect of cooling water discharged from power plant. *Environ. pollut.* 285, 117517. doi: 10.1016/j.envpol.2021.117517

Yang, G. (2001). Characteristics of the tidal current movement in daya bay. *Pear. River.* 1, 30–32.

Yu, J., Tang, D., Wang, S., Lian, J., and Wang, Y. (2007). Changes of water temperature and harmful algal bloom in the daya bay in the northern south China Sea. *Mar. Sci. Bull.* 9 (2), 25–33. doi: 10.3969/j.issn.1000-9620.2007.02.004

Zhang, W., and Zhou, R. (2004). Thermal impact analysis of discharge of circulating cooling water at daya bay nuclear power station (GNPS) and ling'ao nuclear power station (LNPS). *Radiat. Prot. (Taiyuan).* 24 (3-4), 257–262. doi: 10.3321/j.issn:1000-8187.2004.03.014

frontiers | Frontiers in Marine Science

TYPE Original Research
PUBLISHED 27 January 2023
DOI 10.3389/fmars.2023.1100000

OPEN ACCESS

EDITED BY
Huang Honghui,
South China Sea Fisheries Research Institute (CAFS), China

REVIEWED BY
Yun Li,
National Marine Environmental Forecasting Center, China
Shengzhi Wu,
Shengzhi WU, China

*CORRESPONDENCE
Yuwu Jiang
ywjiang@xmu.edu.cn

†These authors contributed equally to this work and share first authorship

SPECIALTY SECTION
This article was submitted to Marine Pollution, a section of the journal Frontiers in Marine Science

RECEIVED 16 November 2022
ACCEPTED 10 January 2023
PUBLISHED 27 January 2023

CITATION
Li J, Xu M, Lin J and Jiang Y (2023) The strategies preventing particle transportation into the inlets of nuclear power plants: Mechanisms of physical oceanography. *Front. Mar. Sci.* 10:1100000. doi: 10.3389/fmars.2023.1100000

The strategies preventing particle transportation into the inlets of nuclear power plants: Mechanisms of physical oceanography

Jintao Li[1,2†], Mengdi Xu[1,2†], Jianwei Lin[3] and Yuwu Jiang[1,2*]

[1]State Key Laboratory of Marine Environmental Science, Xiamen University, Xiamen, China, [2]School of Oceanography and Earth, Xiamen University, Xiamen, China, [3]Fisheries Research Institute of Fujian, Xiamen, China

The formation of aquatic organism aggregations near the inlets of nuclear power plants (NPPs) has become an important global concern, as the aggregated organisms can block the cooling systems of NPPs, and, therefore, threaten their operational safety. In this study we focus on the trajectory of aquatic organisms, that is., how these organisms can be transported to the inlets of NPPs by physical ocean processes related to currents and waves. The Changjiang NPP, located on the west side of Hainan Island in China, is occasionally subject to serious gulfweed blocking events in spring. To study the physical mechanism, with the use of a three-dimensional numerical current–wave-coupled model, the current and wave conditions near the NPP were simulated. Based on the model, several particle-tracking simulations were run to evaluate the extent of the blocking that occurred in the inlet of the NPP's cooling system with different forcings introduced. The results showed that the windage effect and the surface Stokes drift induced by waves were the main causes of blocking events in the Changjiang NPP, with the former transporting surface particles from upstream and the latter transporting surrounding particles onshore, into the NPP's inlet. Further simulations revealed that bending of the inlet and changing the offshore mouth to downstream mouth could limit the blocking greatly, as particles were seldom transported into the mouth by cross-shore transport processes such as the Stokes drift. We suggest that such findings may provide a valuable reference for the development of strategies to prevent aquatic organism aggregation events in other NPPs.

KEYWORDS

nuclear power plant (NPP), schism, surface transport, wave effect, particle tracking

1 Introduction

With the intensive studies and applications of nuclear power, more and more nuclear power plants (NPPs) are being built around the globe. When it comes to the maintenance and management of NPPs, the problem of blockages in NPP cooling systems is particularly serious, because of the high risk it poses to the operational safety of NPPs. The primary cause of NPP blocking events is the formation of aquatic organism aggregations. The rate of growth and aggregation of aquatic organisms is closely bound up with their surrounding environment, and this relationship has been a focus for many researchers (e.g., Li et al., 2011; Zeng et al., 2021; Liu et al., 2022). However, physical ocean processes, such as the tide, ocean circulation, and waves, can also cause blocking events by transporting organisms into the inlets of NPPs, and research into these processes is scarce.

Despite the vertical mixing associated with wind and turbulence, aquatic organisms stay afloat on the ocean surface most of the time owing to their inherent buoyancy and comparatively weak swimming ability, meaning that the surface current has a critical role in the transportation of these organisms. Depending on the dominant forcings, and space or timescales, currents can be divided into different components, including geostrophic currents, and tides and density-driven flows. Surface currents are dominated by wind and wave dynamics, which means that the Ekman current and the Stokes drift are critical to surface particle transport. The Ekman current (Ekman, 1905) is induced by winds; it is strong at the surface and decays with depth. The direction of the Ekman current deviates from the wind direction at a relative angle that changes with depth and shallow topography, being right and left of the wind at surface level in the northern and southern hemispheres, respectively. The Stokes drift (Stokes, 1847) is a material transport mechanism arising from the depth-varying orbital velocities of Stokes's wave motions. The Stokes drift occurs at a much thinner layer than the Ekman current, but it can nevertheless significantly contribute to the surface transport of aquatic organisms: the current magnitude over the upper few centimeters of the water column can be several-fold greater than the average over the upper 10 m (Tamura et al., 2012; Clarke and van Gorder, 2018; Laxague et al., 2018). In open oceans, where waves are mostly generated by local winds, the Stokes drift direction and magnitude are closely related to wind conditions. Meanwhile, in nearshore regions, where waves are generally swell waves that have propagated from afar, the Stokes drift direction changes with water depth. This process is called wave refraction, and can be explained by Snell's law. It results from the decrease in wave phase velocity that occurs in response to reduced water depth as the wave propagates onshore. The wave changes direction, following the direction of the gradient of water depth, leading to the onshore Stokes drift transport. The estimation of the Stokes drift from observational data has been the focus of many articles (e.g., Ardhuin et al., 2009; Ardhuin et al., 2018), in which the wind-dependent proxy approximations, or the more precise calculations using wave spectra, have been used to estimate the Stokes drift. The latter is commonly used as the parameterization in numerical models with different modifications (e.g., Breivik et al., 2014; Breivik et al., 2016).

The use of numerical models is quite practical in studying the trajectory and transport mechanism of surface particles, as it requires fewer human and material resources. The challenges of applying numerical models lies in the accuracy of simulating particle trajectories, which in turn depends on the model resolution as well as the correct expressions of the introduced forcings. Current models calculate current fields by solving the continuity and Navier–Stokes momentum equations; however, the validity of model results is constrained over a certain scale because of limitations related to their computational cost and Courant–Friedrichs–Lewy (CFL) conditions; in other words, such models cannot reproduce real physical processes, such as waves and turbulence, on a small scale. Meanwhile, the generation, propagation, and dissipation of waves are simulated using either phase-resolving or phase-averaged models. Phase-resolving models describe the actual wave motion in great detail, with a resolution that is within the scale of wavelength and wave period, but are seldom used in studies to investigate particle tracking as their computational cost is too high, and they are generally useful only in a laboratory setting, in which detailed analysis is conducted. Phase-averaged models, however, focus on the conservation of wave energy, and are therefore the preferred choice in wave modeling (Holthuijsen, 2007).

The combined use of current and wave models provides us with more accurate data for the calculation of particle trajectories. However, currents and waves are not independent from each other. The theory underlying wave–current interaction (WCI) has been studied and debated in many articles (e.g., McWilliams et al., 2004; Lane et al., 2007; Ardhuin et al., 2008; Mellor, 2008; Bennis et al., 2011). WCI can be divided into two parts: current effects on waves (CEW) and wave effects on currents (WEC). CEW, in most studies, is introduced as the Doppler shifts by currents and elevation changes in the wave dispersion relation; while WEC is a bit more complicated, and includes conservative terms such as wave-induced pressure, material transport by the Stokes drift, and vortex force, as well as non-conservative terms related to wave breaking and bottom drag. In model applications, the inclusion of WEC shows indirect impacts on the current field, especially in the nearshore region, where the wave-breaking processes are intensive (Uchiyama et al., 2009; Uchiyama et al., 2010; Guérin et al., 2018); such impacts are the result of energy transfer and dissipation induced by waves, which link to the physical processes such as the Stokes drift, wave breaking, wave spreading, white bubbles, surface roughness shifting, etc. (Cavaleri et al., 2012; Suzuki and Fox-Kemper, 2016).

Current-wave-coupled models have been adopted in many studies to explore the role of surface current and waves in the transport of floating particles, such as oil, algae, and microplastics (e.g., Drivdal et al., 2014; Fraser et al., 2018; Onink et al., 2019). For example, Fraser et al. (2018) found that kelp could travel over 20,000 km and cross the strong circumpolar currents to reach Antarctica by ocean eddies and the Stokes drift; Onink et al. (2019) found that the accumulation of floating microplastic particles was mainly due to Ekman currents, while the Stokes drift could lead to increased transport to Arctic regions.

Apart from current and wave, windage effect and turbulence movement also play a role in surface particle transport. The term "windage effect" or "leeway" describes the direct forcing effect of wind, pushing surface particles; it is not only dependent on local wind conditions, but it is also associated with the size, shape, and exposed area of particles (Chubarenko et al., 2016). Such inherence makes it difficult to replicate the windage effect in particle-tracking

simulations, as particles have different characteristics, and even a change in the area exposed may change the transport trajectory. To date, the windage effect has most commonly been expressed in particle-tracking simulations as a simplified term, which is proportional to the local wind speed (e.g., Breivik et al., 2011; Duhec et al., 2015). Turbulence movement takes place at such a small scale that it is hard to reproduce it accurately in current models; it is highly random, but could be important to particle transport related to the mixing process (Steinbuck et al., 2011; Grimes et al., 2021). In particle-tracking simulations, turbulence movement is usually parameterized as a random walk term associated with the local diffusivity.

In this paper, we describe the use of a current–wave-coupled model to study the trajectory of aquatic organisms near the Changjiang NPP, which is located on the west side of Hainan Island in China, and occasionally experiences blocking events in spring, when gulfweed outbreaks occur in the nearby area. The goal of this paper is to explore the physical mechanisms that transport gulfweed into the inlet of the NPP, and discuss strategies that could help to prevent subsequent blocking events.

2 Methodology

2.1 Study region

We chose the Changjiang NPP and its surrounding area as our study region (Figure 1A). There are two sites where gulfweed outbreaks commonly occur, about 3 km and 5 km east of the NPP along the coast (Figure 1B). At these sites, large quantities of gulfweed are seen frequently on the ocean surface, particularly in spring, as the gulfweed's rotten roots detach from the ocean floor, causing gulfweed to float upwards. As a result of currents and winds shifting in a southwestward direction during weather events, gulfweed from these two sites comes to be in the NPP's upstream area, and sometimes causes blocking events inside the NPP's inlet. In early November 2021,

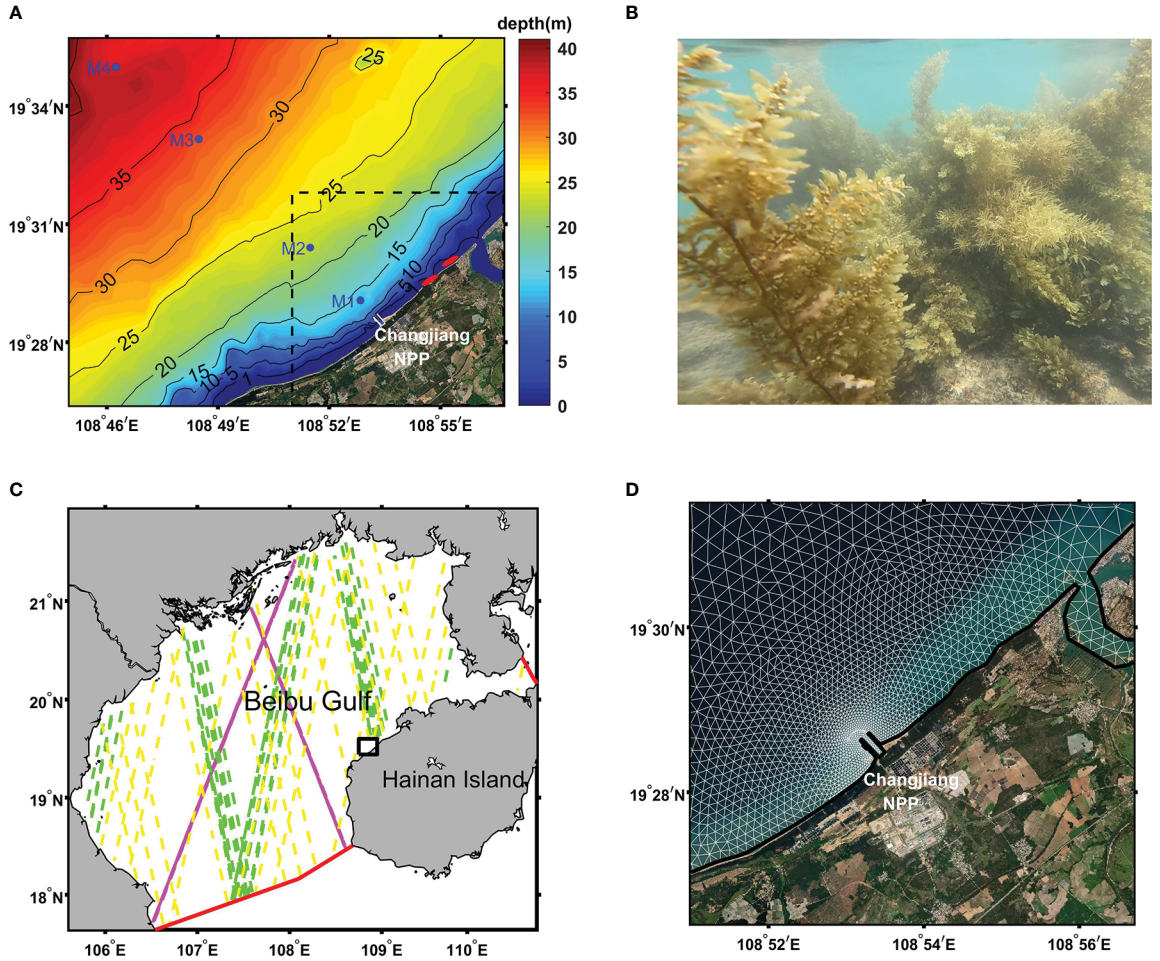

FIGURE 1
(A) The study region with bottom topography (colored shading). The positions of current stations are indicated by blue markers. The two red elliptical markers indicate the locations of two gulfweed source sites near the coast. The dashed rectangular box marks the area of particle release in particle-tracking simulations, whereas the solid white line at the coast outlines the inlet mouth of the Changjiang nuclear power plant (NPP). **(B)** Photograph of gulfweed taken at the source locations. The gulfweed plants in the photograph are approximately 2 m in height. **(C)** Model domain. The two solid red lines are the open boundaries of the model. Dashed lines track the Jason-3 (magenta), SARAL/AltiKa (yellow), and CFOSAT (green) satellite trajectories from late December 2018 to early April 2019. The solid black rectangular box corresponds to the study region. **(D)** Computational grid in the study region (white line). Note that this is only part of the model grid. The entire grid over the model domain is not shown.

a small field campaign was carried out in our study region, with four acoustic Doppler current profilers (ADCPs) deployed at different stations (Figure 1A) to collect current data for 3 days; these data were used for current validation to assess the model performance. Unfortunately, there was a lack of observational station data for waves in our study region. As an alternative, L3-significant wave height data from Jason-3 (NOAA/EUMETSAT/NASA/CNES), SARAL/AltiKa (CNES/ISRO) and CFOSAT (CNSA/CNRS/IFREMER/SHOM/METEOFRANCE) satellites were used to evaluate the wave field calculated by model over the entire model domain (Figure 1C).

2.2 Model description and setting

The semi-implicit cross-scale hydroscience integrated system model (SCHISM) was used to calculate current fields in our study. SCHISM is a three-dimensional (3D), unstructured-grid ocean model that solves the Reynolds-averaged Navier–Stokes equation using the semi-implicit finite-element formulation, which shows enhanced numerical stability and low numerical dissipation (Zhang et al., 2016). The high flexibility of SCHISM makes it appropriate for model applications of cross-scale interactions as well as ocean regions with complex topography and coastlines. As an open source, community-supported model, SCHISM has been adopted worldwide, and it is continually being developed by the embedding of different modules into its model system, such as those for waves, sediment transport, and ecosystem. The wave module embedded in SCHISM is based on the third-generation spectral wind–wave model (WWM) of Roland et al. (2012), which is a phase-averaged model that calculates wave fields by solving the wave action equation (e.g., Komen et al., 1994) as follows:

$$\frac{\partial}{\partial t}N + \nabla_X(\dot{X}N) + \frac{\partial}{\partial \sigma}(\dot{\sigma}N) + \frac{\partial}{\partial \theta}(\dot{\theta}N) = S_{tot}, \quad (1)$$

where ∇_X is the horizontal gradient operator, σ is the relative wave frequency, and θ is the wave direction; $\dot{X}$, $\dot{\sigma}$, and $\dot{\theta}$ are the velocities in the geographical, frequency, and direction phase spaces, respectively; N denotes to E/σ, with E being the variance density of surface elevations; and S_{tot} is the total source term, including energy input from wind and non-linear wave interactions, as well as energy dissipation by whitecapping, wave breaking, and bottom friction. The coupling of SCHISM and WWM is conducted at a source code level by exchanging variables between the two models with the same subdomains in the parallel MPI implementation to ensure efficiency and avoid interpolation. During the exchange, values for water elevation, wet and dry flags, and velocities are passed from SCHISM to WWM to calculate CEW, while the calculated radiation stress or vortex force term, total surface stress, and wave orbital velocity (needed for the calculation of wave-induced bottom stress) from WWM are run through SCHISM to determine WEC.

The entire computational grid we used covered a larger domain (Figure 1C) that included our study region (Figure 1D), with the horizontal spatial resolution ranging from about 3 km in the central area to approximately 30 m at the land boundary. There was a sink being set at the inner side of the Changjiang NPP's inlet, with a constant sucking flux of 100 m^3/s. The discretization of 23 layers in the vertical direction was adopted based on the hybrid S–Z coordinates, with h_c , θ_b , and θ_f set to 10, 0.7, and 5.0, respectively. The model simulation period was from 1 November 2018 to 10 April 2019, and the SCHISM model was run twice—one run was coupled with WWM, whereas the other was not, so that wave effect could be explored from the comparably different outcomes. In early November 2021, an additional run was carried out to compare the model performance with the observational current data from the field campaign. SCHISM and WWM shared the same computational grid and the same time step of 60 s. The boundary data of SCHISM were obtained using a robust operational ocean model simulation of the Taiwan Strait (Liao et al., 2013; Chen et al., 2014; Lin et al., 2016), which provided daily temperature, salinity, and velocity measurements for the linear interpolation at the open boundary. Tidal forcing was calculated from 13 main tidal constituents obtained from the FES2014 tide model (Carrere et al., 2016). The atmospheric data, with a 1-hour time resolution and 0.2° spatial resolution from the weather research and forecast (WRF) model product of the Fujian Marine Forecasts, were used to compute atmospheric forcing in SCHISM and WWM. The five necessary wave parameters (significant wave height, mean wave direction, mean directional spreading, peak frequency, and mean zero-downcrossing wave period) for constructing wave spectra at the open boundary were interpolated using the data from a global hindcast product (Rascle and Ardhuin, 2013). The vortex force formulation was chosen for the coupling in WWM with the wave roller turned off, and both spectral and direction discretization were set to 30 bins. The initial fields for SCHISM were obtained from the same ocean model product for boundary data, whereas the initial fields for WWM were set to zero since the wave field developed quickly enough to remove initial error within hours.

2.3 Particle-tracking simulations

A Lagrangian particle-tracking model is provided inside the SCHISM code package for post processing of the model outputs. In our study cases, we assumed that the gulfweed keeps floating at the ocean surface, and thus only the horizontal movement of particles was calculated. Such assumptions are valid, as gulfweed is buoyant and does not have the ability to move vertically in the way, for example, that dinoflagellate does. When adopting all the forcing terms, the trajectory of each gulfweed particle is calculated independently according to the below formula:

$$\Delta X = (U + W + \nabla K_X + SD)\Delta t + RW, \quad (2)$$

where ΔX is the horizontal position change for each time step, and Δt is the time step interval; U is the water velocity and W is the proxy of windage effect, which is set to 3% of local wind speed at a 10-m height in our study; ∇K_X is horizontal gradient of diffusion coefficient, which is used to calculate the virtual advection term from regions of low to high diffusivity to prevent spurious aggregation (Visser, 1997); SD is the overall surface Stokes drift; and RW is the random walk representing turbulence movement. The SD term is calculated from WWM by summing the surface Stokes drift of each spectral and direction bin with:

$$U_{st} = \sigma\vec{k}\frac{\cosh(2kz + 2kD)}{\sinh^2(kD)}E, \quad (3)$$

where σ and E are the same as in Equation (1), $\vec{k}$ is the horizontal wavenumber vector, D is the water depth, and z equals zero at the surface. Finally, the RW term is calculated with a smaller time step by $R\sqrt{6K_X(\Delta t^*)}$, with R being a uniform random number between −1 and 1, K_X being the turbulent diffusion coefficient, and Δt^* being half of the time step. By alternately adding or removing the W, SD, and RW terms in Equation (2), the corresponding simulation results can be compared to investigate the impacts of windage effect, the Stokes drift, and turbulence movement, respectively.

All the simulations were carried out from 1 to 5 April 2019, as a serious gulfweed blocking event occurred during this period. Particle trajectories were calculated using the outputs at 10-min interval from SCHISM (and WWM in the case of the coupled run). For each model output, the particle positions were upgraded in 100 substeps using Equation (2). By carrying out sensitivity experiments, we found that the variation in results decreased as the number of substeps increased, and at the number of substeps we adopted, 100, approximated to zero. During each simulation, particles were released every hour throughout the first simulation day; thereafter, the simulation was kept running for the last 4 simulation days without any particles being released. In each release, 1,452 particles were placed uniformly on the ocean surface at approximately 200-m intervals throughout the study region (Figure 1A), with the exception of the coastal area, where water depth was less than 0.5 m, to reduce unnecessary computational costs. As a result, each particle release site had 24 trajectories, corresponding to the 24 release times, in the first simulation day for each particle-tracking simulation; the probabilistic intensity of each spot was calculated as the ratio of the number of trajectories that came to be inside the NPP's inlet to the total number (which is exactly 24) of trajectories.

3 Results

3.1 Model validation

Figure 2 shows the current validation results between the 3-day observational station data and the corresponding model outputs in November 2021, which included eastward velocity and northward velocity at three depths: near surface, middle layer, and near bottom. The basic statistics—mean bias (MB), root-mean-square difference (RMSD), and correlation coefficient (CC)—are shown in Table 1. In general, the calculated currents at stations agreed well with observations, with correlation coefficients higher than 0.8 in some station layers. Orbital significant wave heights from atellite data and model outputs over the whole model domain from late December 2018 to early April 2019 are compared in Figure 3, which reveals an overall good model performance for waves, with MB, RMSD, and CC being 0.11 m, 0.41 m, and 0.84, respectively.

3.2 Current, wind, and the Stokes drift fields

Figure 4 shows the time-averaged fields in the study region during the simulation period (1–5 April 2019). The mean surface current field (Figure 4A) reveals that there is a general southwestward velocity higher than 0.1 m/s in the region, with the magnitude dropping near the shore and the current direction slightly shifting toward the west in offshore areas. The wind field at a 10-m height (Figure 4B) showed a nearly homogeneous pattern, with the direction being southwestward over the region, and the magnitude dropping linearly from north to south. As for the surface Stokes drift field (Figure 4C), its direction was more southward than that for the current and wind field offshore, and became perpendicular to the coast as it got near the shore. The Stokes drift velocity was at its highest near the shore, and was at its lowest close to the coastline and inside the NPP's inlet.

3.3 Particle-tracking simulation results

The results of the probabilistic intensity (hereinafter PI) distributions of the different simulations are shown in Figure 5, and the setting for each simulation can be found in Table 2. PI indicates the relevance of the location of released particles to their likelihood of reaching the NPP's inlet. A PI of 100% indicates that all of the particles released in a given location will be transported to the NPP's inlet during the simulation period, whereas a PI of 0% indicates that all of the released particles at a given location will not be transported to the NPP's inlet. For each simulation, a non-zero PI value occurred only at the area upstream of the inlet, near the coast, which indicated that this area accounted for the particle transport into the inlet. When the windage effect was included (Figures 5D–F), the area with a high PI value extended upstream along the coast from the inlet to the outside of the study region, covering the two gulfweed source sites. The pattern of the highest PI value in the simulation was seen when the Stokes drift was included (Figure 5F), with the area with a PI value exceeding 90% occurring approximately 6 km upstream from the inlet and about 500 m offshore. The simulation results of the current model without waves (Figure 5D) showed a slightly different pattern, that is, a high PI value applied to the area at a shorter distance off the coast, but a low PI value extended further offshore. The simulation results of the current–wave model without the Stokes drift included resulted in an area with a high PI value that was smaller than in the case of the other two simulations (Figure 5E), as the area to which a low PI value applied was further offshore than in the simulation including the Stokes drift (Figure 5F), but covered a shorter distance than the simulation without waves (Figure 5D). With the windage effect excluded (Figures 5A–C, the PI distributions of the three simulation results showed obvious shrinking compared with those with the windage effect included (Figures 5D–F), with a high PI value observed only in the area very close to the east side of the inlet and pressed into the coastline as it extended upstream, and no longer covering the two gulfweed source sites. The simulation of current–wave model with the Stokes drift had the highest PI value among the three simulations (Figure 5C), with the area to which its non-zero PI value applied extending about 10 km upstream from the inlet. The impact of turbulence movement on particle trajectories in our study, whether or not included, was negligible in all simulations (not shown in this paper).

4 Discussion

The formation of aquatic organism aggregations can lead to blocking events in NPP inlets, and thus compromise the operational safety of NPPs. In addition to the local growth and

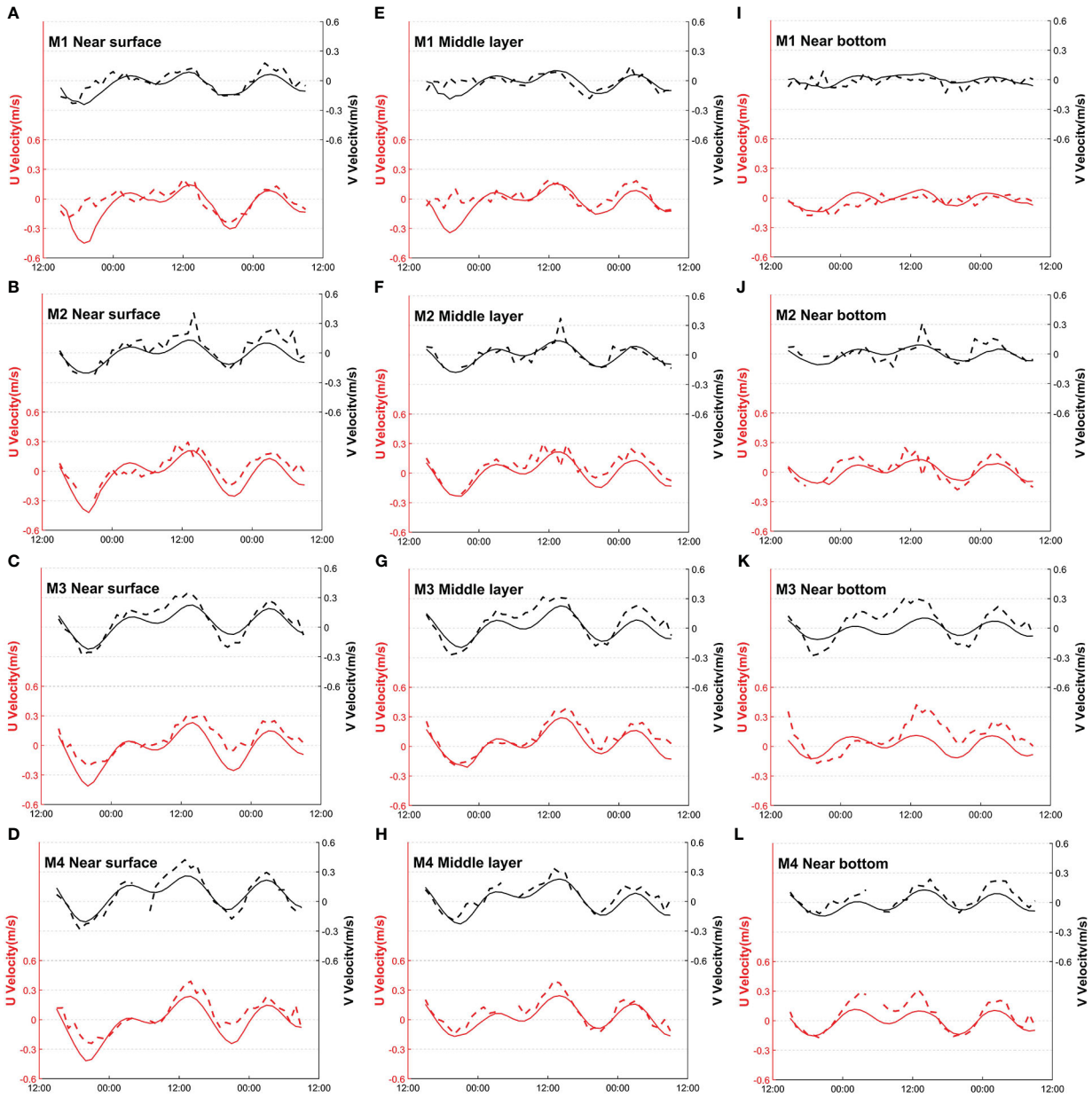

FIGURE 2
(A–L) Current validation between observational data and model outputs at the near surface, middle layer, and near bottom of M1, M2, M3, and M4 stations operating from 2 to 4 November 2021. The black lines at the top indicate northward current velocity (V) at different times (right-hand axis), whereas the red lines below indicate eastward current (U) velocity (left-hand axis). Dashed lines are observational data, and solid lines are model outputs.

aggregation related to environmental disturbances, the transport of aquatic organisms can also be the cause of blocking events. To study the physical processes associated with currents and waves that transport aquatic organisms into the inlets of NPPs, a 3D current–wave-coupled model with high resolution was used to provide current and wave fields for the post-processed particle-tracking simulations (computational resolution should be of a higher standard when wave fields are to be calculated in a numerical model, as wave at the ocean surface is mainly related to wind speed, which in turn has a time period in seconds). With a spatial resolution of 30 m near the coast and a time step of 60 s for solving both currents and waves, the coupled model we used was sufficient to simulate the physical processes of interest for this study. The validation results revealed good model performance, though we used the satellite data to validate modeled wave fields only because of the lack of observational station data for waves in our study region.

Particle-tracking simulations compute the trajectory of virtual particles with the introduced forcings. In this paper, we used the field data of current, wave, and wind provided by model to simulate the gulfweed trajectory, as gulfweeds transported from the nearby area could cause serious blocking events inside the inlet of the NPP in our study region. With probabilistic intensity (PI) calculated from the simulation results, we evaluated the impact of different forcings on the gulfweed transport that could lead to blocking inside the NPP inlet.

Before looking at the simulation results, the time-averaged fields (Figure 4) during the simulation period partly revealed the role of

TABLE 1 Basic statistics for current validation between observational data and model outputs.

Station layer	MB (U)	MB (V)	RMSD (U)	RMSD (V)	CC (U)	CC (V)
M1 surface	−0.05 m/s	−0.04 m/s	0.13 m/s	0.07 m/s	0.67	0.82
M2 surface	−0.09 m/s	−0.07 m/s	0.18 m/s	0.13 m/s	0.44	0.69
M3 surface	−0.10 m/s	−0.03 m/s	0.12 m/s	0.08 m/s	0.88	0.93
M4 surface	−0.09 m/s	−0.01 m/s	0.13 m/s	0.08 m/s	0.85	0.95
M1 middle	−0.06 m/s	−0.01 m/s	0.12 m/s	0.07 m/s	0.57	0.57
M2 middle	−0.08 m/s	−0.02 m/s	0.15 m/s	0.11 m/s	0.54	0.48
M3 middle	−0.05 m/s	−0.05 m/s	0.08 m/s	0.10 m/s	0.92	0.86
M4 middle	−0.06 m/s	−0.05 m/s	0.11 m/s	0.07 m/s	0.80	0.89
M1 bottom	0.02 m/s	0.02 m/s	0.06 m/s	0.06 m/s	0.56	0.28
M2 bottom	−0.04 m/s	−0.04 m/s	0.13 m/s	0.13 m/s	0.43	0.19
M3 bottom	−0.09 m/s	−0.06 m/s	0.16 m/s	0.13 m/s	0.53	0.78
M4 bottom	−0.07 m/s	−0.06 m/s	0.12 m/s	0.08 m/s	0.87	0.88

CC, correlation coefficient; MB, mean bias; RMSD, root-mean-square difference.

current, wind, and the Stokes drift induced by wave action. The surface current (Figure 4A) transported upstream particles near the coast with an increased velocity magnitude, as well as a slightly offshore inclination, which would move particles away from the inlet as they floated downstream. Meanwhile, wind moving in a southwestward direction (Figure 4B), and the associated decrease in velocity magnitude along its direction, would be more likely to cause the accumulation of particles in the downstream area. Finally, the surface Stokes drift showed an onshore velocity overall (Figure 4C). Near the shore, the Stokes drift reached its maximum velocity while

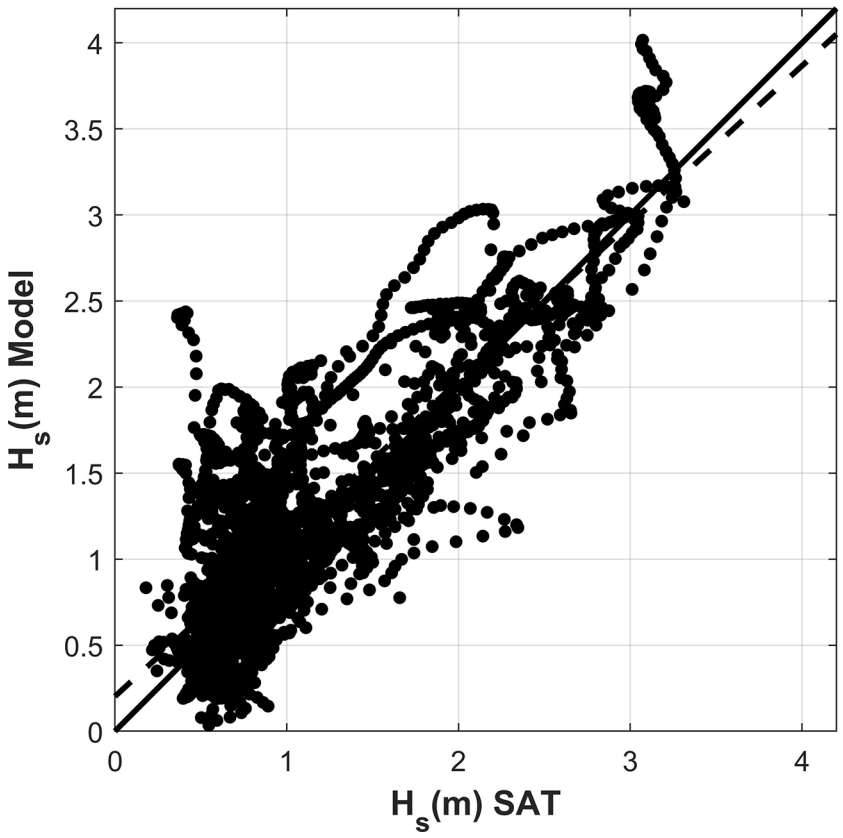

FIGURE 3
Scatter diagram of significant wave height from the satellite data and corresponding model outputs. The solid black line indicates the ideal fit and the black dashed line shows the linear regression for the two datasets, with a slope of 0.92.

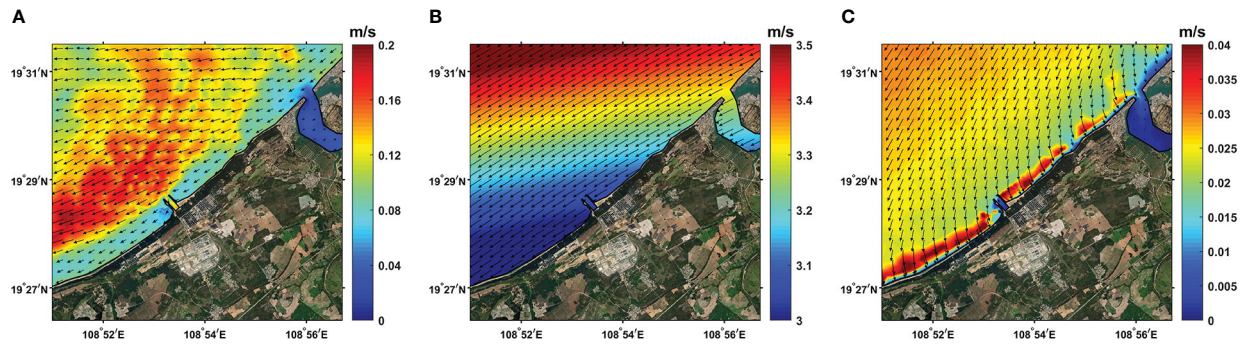

FIGURE 4
Time-averaged horizontal fields during the simulation period (1–5 April 2019), with colored shading showing the vector magnitude. **(A)** Surface current field. **(B)** Wind field at a 10-m height. **(C)** The surface Stokes drift field.

its direction became more perpendicular to the coast, which in turn caused strong cross-shore transport of particles. These field patterns showed that current, wind, and the Stokes drift have different impacts on the transport of particles in different areas. For example, although the current had a higher order of magnitude than the Stokes drift over the study region, the inverse could be true near the shore, where the current is weak and the Stokes drift is strong.

The windage effect is an important forcing in particle-tracking simulations, for it represents the direct wind forcing on surface particles. We used a 3% wind speed at a 10-m height as a proxy for the windage effect to simplify evaluation of its impact on particle tracking. The simulation results showed that the PI value in the upstream area of the inlet increased greatly when the windage effect was introduced (Figures 5D–F), and in most areas, the PI value exceeded 60%, compared with its value of less than 20% without the inclusion of the windage effect (Figures 5A–C). The fact that high PI values at the two gulfweed source sites were observed only when windage effect was included indicates that the windage effect was the main force that transported gulfweed from the gulfweed source sites to the NPP's inlet. Simulations carried out in late December 2018 produced similar results (not shown in this paper). All of these simulation results revealed that windage effect had a significant part in the blocking events in our study region. In fact, cross-shore transport only counts when particles are transported by windage effect from an upstream area to the surrounding of the inlet mouth.

For model calculations, the windage effect, along with the Stokes drift, is generally estimated as being 3% of local wind speed at a 10-m height. However, such rough estimations are clearly not applicable to all scenarios. Haza et al. (2019) evaluated different parameterizations of Lagrangian velocity in the northern Gulf of Mexico using substantial trajectories of the drifters launched during the Lagrangian submesoscale experiment (LASER). The authors found variations in trajectory improvement under different wind and wave conditions, as well as in different geographic regions. As our model adopted only the wind-dependent estimation of the windage effect, without considering other factors, further studies are needed to provide a more comprehensive view.

The highest PI value was observed in the simulation that included both the Stokes drift and the windage effect (Figure 5F), and revealed the significance of the Stokes drift to the transportation of particles to the NPP's inlet in our study region. Because of wave refraction, the Stokes drift shifted in a direction more perpendicular to the coast as it got closer to shore. As a result, stronger cross-shore transport occurred near the shore when the Stokes drift force was included in the simulation, which led in turn to more opportunities for the upstream particles to be transported into the offshore inlet mouth. In addition, this could account for the serious blocking events inside the inlet.

Apart from the Stokes drift, the wave effect could also indirectly have an impact on the current (WEC). Near the shore region, WEC mainly changes the current pattern by two processes: the offshore anti-Stokes flow and the littoral wave-induced current. The anti-Stokes flow results from the onshore Stokes drift, that is, to maintain the water conservation, the onshore Stokes drift would cause an anti-flow to balance the water transport. Guérin et al. (2018) studied the effect of WEC on water setup near the coast and found a typical wave-induced vertical circulation—an onshore flow at the upper layer and an offshore undertow, the magnitude of which changes with the beach slope and wave energy. The study of littoral wave-induced current can be traced back to the works of Longuet-Higgins (1970a, 1970b), which found that the littoral current was the result of the dynamic balance between bottom friction and an introduced wave dissipation term. Uchiyama et al. (2009) found that a strong littoral current occurred at the location where wave breaking was strong, with the bottom drag adjusting the current—broad, weak current with low drag, and narrow, strong current with high drag. From our results, the WEC can be seen in Figures 5D and E—when the Stokes drift transport was excluded from the particle-tracking simulations, the current–wave-coupled model (Figure 5E) indicated that the chance of the particles being transported into the NPP's inlet was, overall, lower than that in the current model without waves (Figure 5D), which might be related to the offshore transport of the anti-Stokes flow, as well as to the strong littoral wave-induced current.

To support the discussions of the transport forcing terms mentioned above, another model simulation was run to provide additional analysis results. The model and post-processed particle-tracking simulations were run using the same settings as the original ones, except for the model computational grid, which used a downstream mouth of the inlet (C2, Figure 6A) instead of the original offshore mouth structure (C1, Figure 1D). The results showed that the PI distributions were the same pattern for all simulations (Figure 6B)—non-zero PI values were observed only

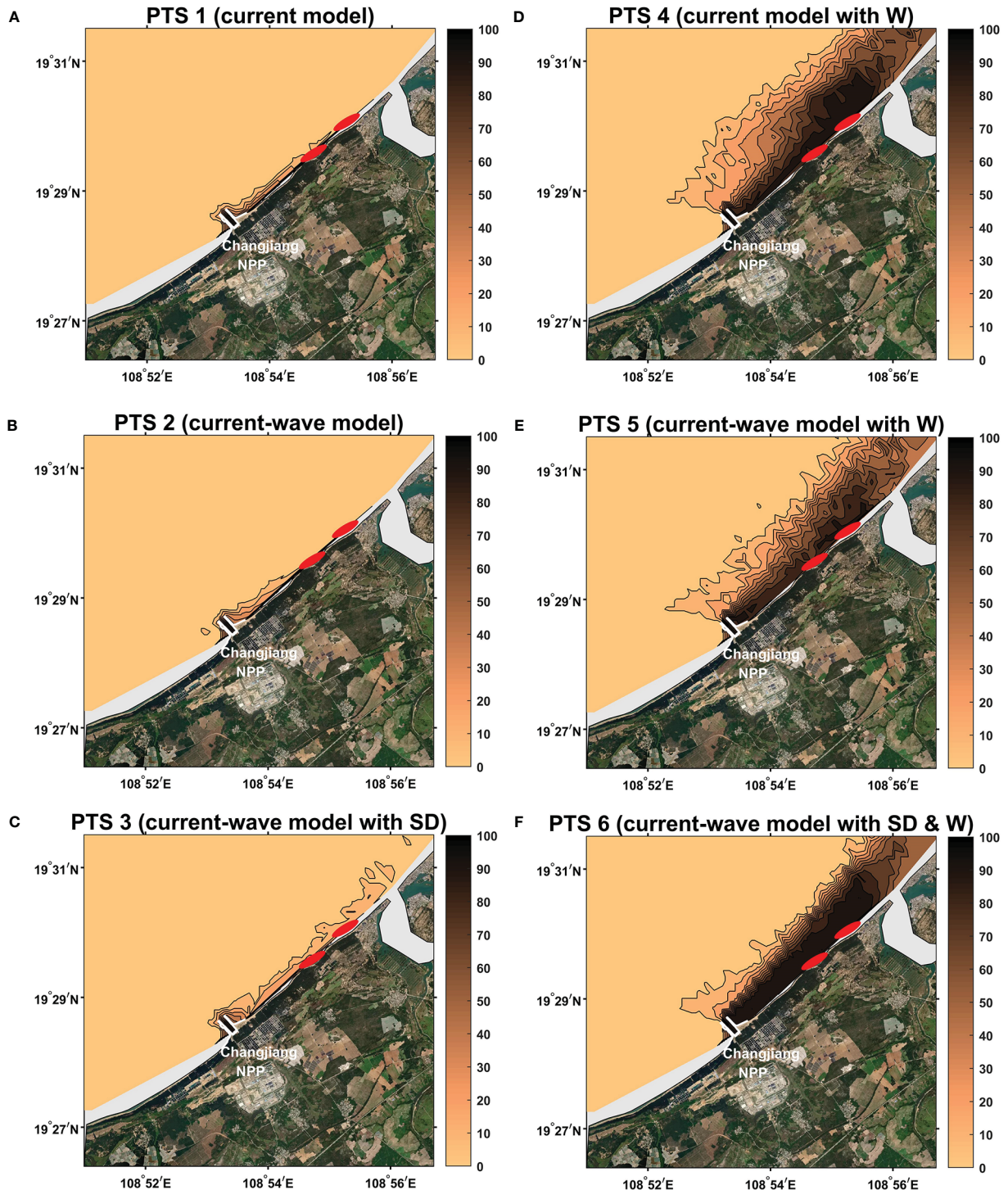

FIGURE 5
(A–F) Probabilistic intensity distributions of different particle-tracking simulation results. Color shading represents the odds (expressed as a percentage) of the particles released in the region being transported into the NPP's inlet. The higher the value, the greater the likelihood that particles released at that location are transported into the inlet during the simulation period. The two red elliptical markers indicate the locations of two gulfweed sources near the coast.

inside the inlet, which revealed an absolute isolation of the inlet for the outside surface particles. These results support our theory that cross-shore means of particle transportation, such as the Stokes drift, have an important impact on blocking events, as it was shown that, when adopting a downstream structure for the NPP inlet, blocking events could be greatly limited through the prevention of the cross-shore transportation of particles from upstream.

The current–velocity profiles of the two model cases were compared. The profile sections selected for the two cases are shown in Figure 7, with two magenta dots marking the section fragment

TABLE 2 Experimental settings for particle-tracking simulations.

Particle-tracking simulation (PTS)	Model	Stokes drift (SD)	Windage (W)
PTS 1	Current	\	Off
PTS 2	Current–wave	Off	Off
PTS 3	Current–wave	On	Off
PTS 4	Current	\	On
PTS 5	Current–wave	Off	On
PTS 6	Current–wave	On	On

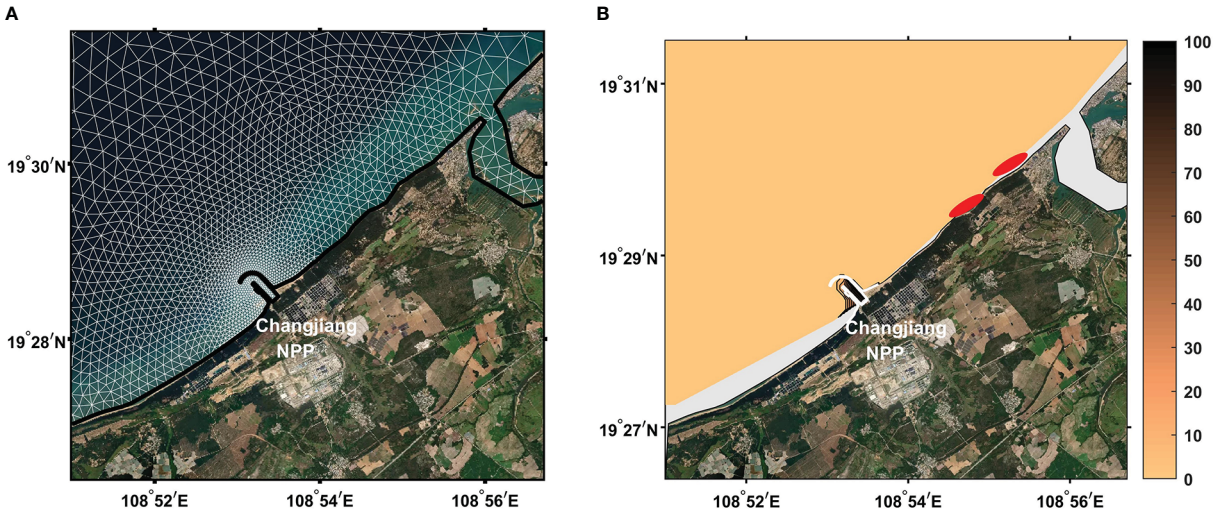

FIGURE 6
(A) Computational grid in the study region (white line) for the new model case. **(B)** Probabilistic intensity distribution calculated from outputs of the new model case, which yields the same result for all particle-tracking simulations. The two red elliptical markers indicate the locations of two gulfweed source sites near the coast.

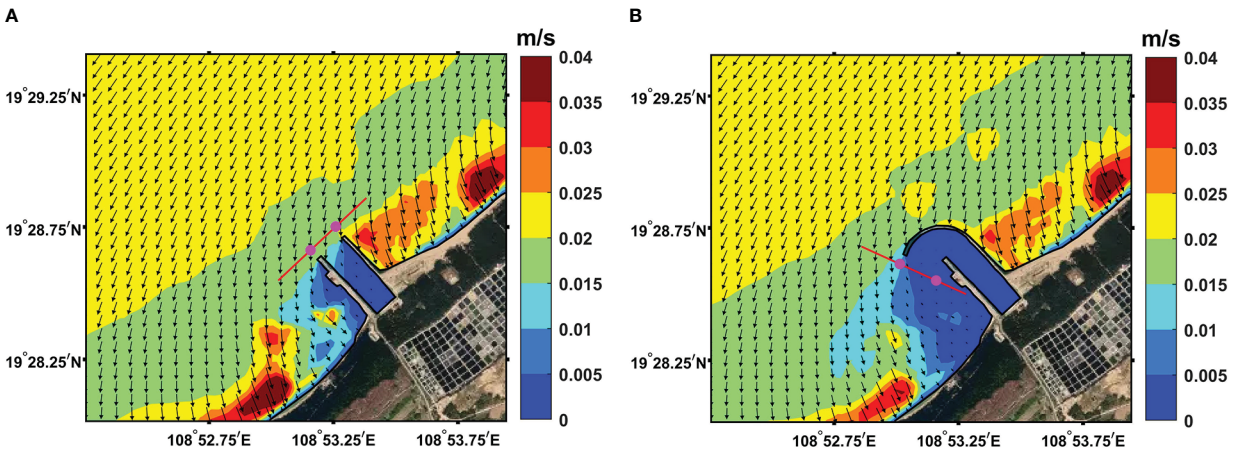

FIGURE 7
The position of current–velocity profile section (red line) for two model cases: **(A)** C1, with an offshore inlet mouth, and **(B)** C2, with a downstream inlet mouth. The two magenta dots in the red line mark the section fragment closest to the inlet mouth. The black vectors indicate the mean surface Stokes drift on 2 April 2019, with color shading representing the vector magnitude.

closest to the inlet mouth. In each case, four velocity profiles at 6-hour intervals were chosen to analyze the current pattern, with a positive value (red) representing inflow to the inlet and a negative value (blue) representing outflow from the inlet (Figure 8). The current profiles of C1 (offshore mouth) showed a relatively stable pattern, with an inflow velocity core maintaining at the middle layer (Figures 8A–D), which reflected the constant sucking flux of the NPP's inlet. The surface current was mostly inflow, and it had a magnitude of approximately 0.02 m/s, which was comparable to those of the surface current and the Stokes drift around the inlet mouth (Figure 7A). In addition, both the surface current and the Stokes drift transported particles into the inlet. Meanwhile, for C2 (downstream mouth), the current profiles were more unstable and without an obvious pattern, which could have strong velocity shear vertically (Figures 8E, F) or horizontally (Figures 8G, H with surface outflow and underneath inflow). The mechanism of such pattern shifts might be due to the interaction between topography and tidal activity in the region, which requires further exploration, and is currently out with the scope of our study. Nevertheless, we did observe that the high current variation, along with the negligible surface Stokes drift near the downstream mouth (Figure 7B), added more uncertainty to particle trajectories, which might account for their reduced inlet-blocking opportunities when compared with C1.

In conclusion, our results suggested that windage effect and the Stokes drift had an important impact on gulfweed blocking events inside the NPP's inlet in our study. With the wind field being appropriate, that is, the two gulfweed sources being upstream of the NPP, the windage effect would transport gulfweed from the gulfweed source sites to the inlet's surroundings, and the Stokes drift would then transport surrounding gulfweed onshore into the inlet. Further simulations revealed that a downstream mouth structure of the inlet could greatly limit the likelihood of blocking by interrupting the cross-shore transport from the Stokes drift, which might be a potential prevention strategy for blocking events in other NPPs.

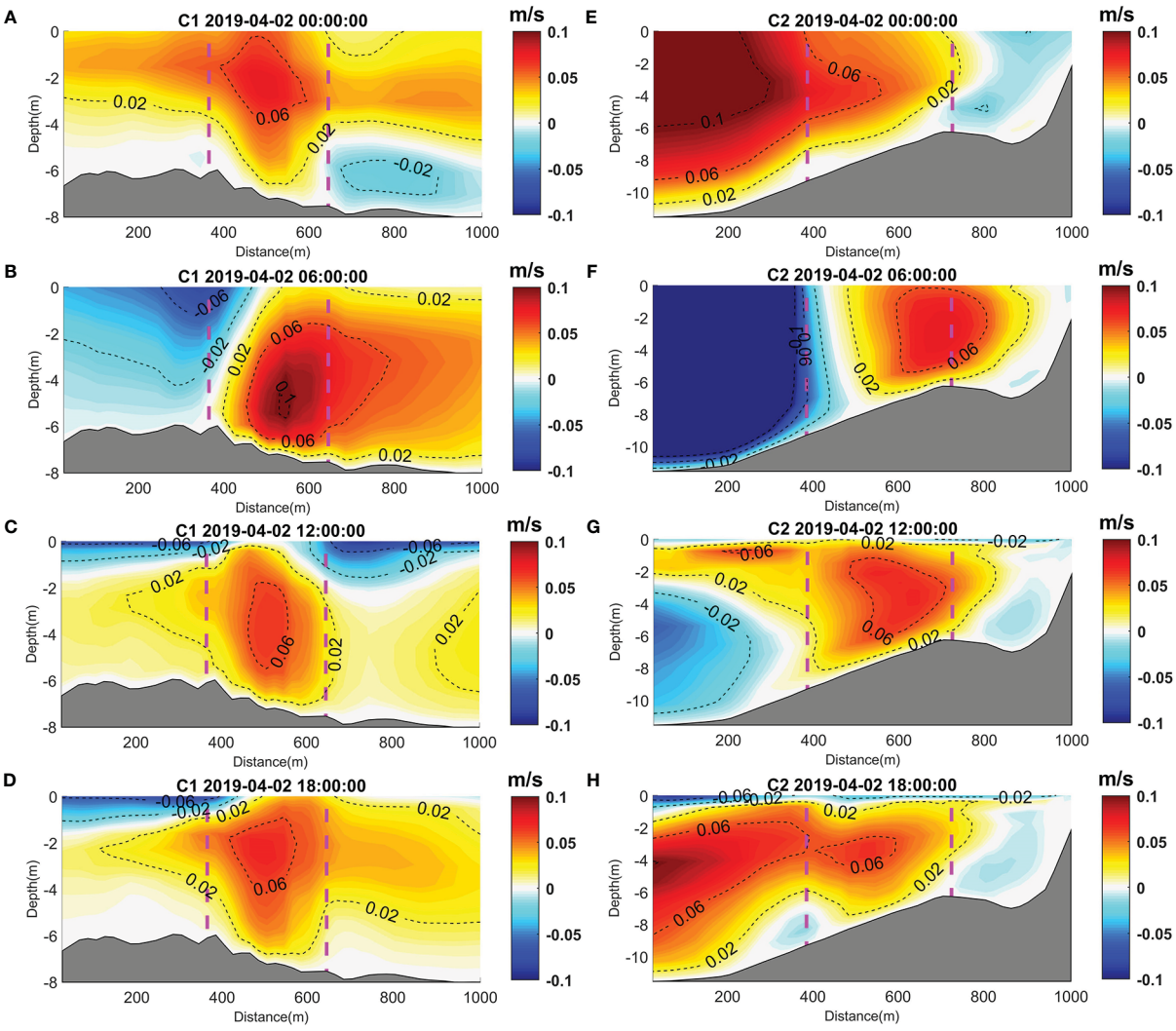

FIGURE 8
Velocity profiles with 6-hour intervals of the two model cases: **(A–D)** C1, with an offshore inlet mouth, and **(E–H)** C2, with a downstream inlet mouth. Colored shading represents the horizontal velocity magnitude perpendicular to the section, with a positive value (red) representing inflow and a negative value (blue) representing outflow near the inlet. The gray patch is the section topography, whereas the two magenta vertical lines correspond to the two magenta dots in Figure 7, which mark the section fragment closest to the inlet mouth.

However, there are some aspects of the research in this paper which are open to improvement and further exploration. For example, the proxy for the windage effect could be improved by considering particle characteristics, as well as considering adjustments under different conditions; the results of different wave model setting should be compared with the study of the role of wave action in dissipation processes, such as wave breaking and wave-induced bottom drag; and the physical mechanism responsible for the current pattern near the inlet requires further dynamic diagnosis.

Data availability statement

The raw data supporting the conclusions of this article will be made available by the authors, without undue reservation.

Author contributions

JLi and MX performed the research and prepared the manuscript. JLin provided necessary support for conducting the field campaign. YJ supervised the work, and provided supportive data and guidance for numerical models. All authors contributed to the article and approved the submitted version.

Acknowledgments

This work was supported by the Chinese Ministry of Science and Technology through the National Key Research and Development Program of China (2022YFA1004404). The field work was supported by grant (U22A20579, 41961144011, 41876004) from Natural Science Foundation of China (NSFC). S. Fang, Y. Yu and Z. Xu from Information and Network Center of Xiamen University are acknowledged for the help with the high-performance computing.

Conflict of interest

The authors declare that the research was conducted in the absence of any commercial or financial relationships that could be construed as a potential conflict of interest.

Publisher's note

All claims expressed in this article are solely those of the authors and do not necessarily represent those of their affiliated organizations, or those of the publisher, the editors and the reviewers. Any product that may be evaluated in this article, or claim that may be made by its manufacturer, is not guaranteed or endorsed by the publisher.

References

Ardhuin, F., Aksenov, Y., Benetazzo, A., Bertino, L., Brandt, P., Caubet, E., et al. (2018). Measuring currents, ice drift, and waves from space: the sea surface kinematics multiscale monitoring (SKIM) concept. *Ocean Sci.* 14, 337–354. doi: 10.5194/os-14-337-2018

Ardhuin, F., Jenkins, A. D., and Belibassakis, K. A. (2008). Comments on "The three-dimensional current and surface wave equations". *J. Phys. Oceanography* 38, 1340–1350. doi: 10.1175/2007JPO3670.1

Ardhuin, F., Marie, L., Rascle, N., Forget, P., and Roland, A. (2009). Observation and estimation of lagrangion, stokes, and eulerian currents induced by wind and waves at the sea surface. *J. Phys. Oceanography* 39, 2820–2838. doi: 10.1175/2009JPO4169.1

Bennis, A. C., Ardhuin, F., and Dumas, F. (2011). On the coupling of wave and three-dimensional circulation models: choice of theoretical framework, practical implementation and adiabatic tests. *Ocean Model.* 40, 260–272. doi: 10.1016/j.ocemod.2011.09.003

Breivik, Ø., Allen, A., Maisondieu, C., and Roth, J. (2011). Wind-induced drift of objects at sea: the leeway field method. *Appl. Ocean Res.* 33, 100–109. doi: 10.1016/j.apor.2011.01.005

Breivik, Ø., Bidlot, J. R., and Janssen, P. A. (2016). A stokes drift approximation based on the Phillips spectrum. *Ocean Model.* 100, 49–56. doi: 10.1016/j.ocemod.2016.01.005

Breivik, Ø., Janssen, P. A., and Bidlot, J. R. (2014). Approximate stokes drift profiles in deep water. *J. Phys. Oceanography* 44, 2433–2445. doi: 10.1175/JPO-D-14-0020.1

Carrere, L., Lyard, F., Cancet, M., Guillot, A., and Picot, N. (2016). FES 2014, a new tidal model–validation results and perspectives for improvements. *ESA Living Planet Conference Prague.*

Cavaleri, L., Fox-Kemper, B., and Hemer, M. (2012). Wind waves in the coupled climate system. *Bull. Am. Meteorological Soc.* 93, 1651–1661. doi: 10.1175/BAMS-D-11-00170.1

Chen, Z. Y., Yan, X. H., and Jiang, Y. W. (2014). Coastal cape and canyon effects on wind-driven upwelling in northern Taiwan strait. *J. Geophysical Res. Oceans* 119, 4605–4625. doi: 10.1002/2014jc009831

Chubarenko, I., Bagaev, A., Zobkov, M., and Esiukova, E. (2016). On some physical and dynamical properties of microplastic particles in marine environment. *Mar. pollut. Bull.* 108, 105–112. doi: 10.1016/j.marpolbul.2016.04.048

Clarke, A., and van Gorder, S. (2018). The relationship of near-surface flow, stokes drift, and the wind stress. *J. Geophysical Res. Oceans* 123, 4680–4692. doi: 10.1029/2018JC014102

Drivdal, M., Broström, G., and Christensen, K. H. (2014). Wave-induced mixing and transport of buoyant particles: application to the statfjord a oil spill. *Ocean Sci.* 10, 977–991. doi: 10.5194/os-10-977-2014

Duhec, A. V., Jeanne, R. F., Maximenko, N., and Hafner, J. (2015). Composition and potential origin of marine debris stranded in the western Indian ocean on remote Alphonse island, Seychelles. *Mar. pollut. Bull.* 96, 76–86. doi: 10.1016/j.marpolbul.2015.05.042

Ekman, V. W. (1905). On the influence of the earth's rotation on ocean currents. *Arch. Math. Astron. Phys.* 2, 1–52.

Fraser, C. I., Morrison, A. K., Hogg, A. M., Macaya, E. C., van Sebille, E., Ryan, P. G., et al. (2018). Antarctica's ecological isolation will be broken by storm-driven dispersal and warming. *Nat. Climate Change* 8, 704–708. doi: 10.1038/s41558-018-0209-7

Grimes, D. J., Feddersen, F., and Giddings, S. N. (2021). Long-Distance/Time surf-zone tracer evolution affected by inner-shelf tracer retention and recirculation. *J. Geophysical Res. Oceans* 126, 1–22. doi: 10.1029/2021jc017661

Guérin, T., Bertin, X., Coulombier, T., and de Bakker, A. (2018). Impacts of wave-induced circulation in the surf zone on wave setup. *Ocean Model.* 123, 86–97. doi: 10.1016/j.ocemod.2018.01.006

Haza, A. C., Paldor, N., Özgökmen, T. M., Curcic, M., Chen, S. S., and Jacobs, G.. (2019). Wind-based estimations of ocean surface currents from massive clusters of drifters in the gulf of Mexico. *J. Geophysical Research: Oceans* 124, 5844–5869. doi: 10.1029/2018jc014813

Holthuijsen, L. H. (2007). *Waves in oceanic and coastal waters* (Cambridge, U. K: Cambridge University Press), 1–7.

Komen, G. J., Cavaleri, L., Donelan, M., Hasselmann, K., Hasselmann, S., and Janssenet, P. A. (1994). *Dynamics and modelling of ocean waves* (Cambridge, U. K: Cambridge University Press), 532.

Lane, E. M., Restrepo, J. M., and McWilliams, J. C. (2007). Wave–current interaction: A comparison of radiation-stress and vortex-force representations. *J. Phys. Oceanography* 37, 1122–1141. doi: 10.1175/JPO3043.1

Laxague, N. J. M., Özgökmen, T. M., and Haus, B. K. (2018). Observations of near-surface current shear help describe oceanic oil and plastic transport. *Geophysical Res. Lett.* 45, 245–249. doi: 10.1002/2017gl075891

Liao, E. H., Jiang, Y. W., Li, L., Hong, H. S., and Yan, X. H. (2013). The cause of the 2008 cold disaster in the Taiwan strait. *Ocean Model.* 62, 1–10. doi: 10.1016/j.ocemod.2012.11.004

Li, T., Liu, S., Huang, L., Huang, H., Lian, J., Yan, Y., et al. (2011). Diatom to dinoflagellate shift in the summer phytoplankton community in a bay impacted by nuclear power plant thermal effluent. *Mar. Ecol. Prog. Ser.* 424, 75–85. doi: 10.3354/meps08974

Lin, X. Y., Yan, X. H., Jiang, Y. W., and Zhang, Z. C. (2016). Performance assessment for an operational ocean model of the Taiwan strait. *Ocean Model.* 102, 27–44. doi: 10.1016/j.ocemod.2016.04.006

Liu, Q., Zhou, L., Zhang, W., Zhang, L., Tan, Y., Han, T., et al. (2022). Rising temperature contributed to the outbreak of a macrozooplankton creseis acicula by enhancing its feeding and assimilation for algal food nearby the coastal daya bay nuclear power plant. *Ecotoxicology Environ. Saf.* 238. doi: 10.1016/j.ecoenv.2022.113606

Longuet-Higgins, M. S. (1970b). Longshore currents generated by obliquely incident sea waves: 2. *J. Geophysical Res.* 75, 6790–6801. doi: 10.1029/JC075i033p06790

Longuet-Higgins, M. S. (1970a). Longshore currents generated by obliquely incident sea waves: 1. *J. Geophysical Res.* 75, 6778–6789. doi: 10.1029/JC075i033p06778

McWilliams, J. C., Restrepo, J. M., and Lane., E. M. (2004). An asymptotic theory for the interaction of waves and currents in coastal waters. *J. Fluid Mechanics* 511, 135–178. doi: 10.1017/S0022112004009358

Mellor, G. L. (2008). The depth-dependent current and wave interaction equations: a revision. *J. Phys. Oceanography* 38, 2587–2596. doi: 10.1175/2008JPO3971.1

Onink, V., Wichmann, D., Delandmeter, P., and van Sebille, E. (2019). The role of ekman currents, geostrophy, and stokes drift in the accumulation of floating microplastic. *J. Geophysical Research: Oceans* 124, 1474–1490. doi: 10.1029/2018JC014547

Rascle, N., and Ardhuin, F. (2013). A global wave parameter database for geophysical applications. part 2: Model validation with improved source term parameterization. *Ocean Model.* 70, 174–188. doi: 10.1016/j.ocemod.2012.12.001

Roland, A., Zhang, Y. J., Wang, H. V., Meng, Y., Teng, Y., Maderich, V., et al. (2012). A fully coupled 3D wave-current interaction model on unstructured grids. *J. Geophysical Research: Oceans* 117, C00J33. doi: 10.1029/2012jc007952

Steinbuck, J. V., Koseff, J. R., Genin, A., Stacey, M. T., and Monismith, S. G. (2011). Horizontal dispersion of ocean tracers in internal wave shear. *J. Geophysical Res.* 116, C11031. doi: 10.1029/2011JC007213

Stokes, G. G. (1847). On the theory of oscillatory waves. *Trans. Cambridge Philos. Soc.* 8, 441–473.

Suzuki, N., and Fox-Kemper, B. (2016). Understanding stokes forces in the wave-averaged equations. *J. Geophysical Research: Oceans* 121, 3579–3596. doi: 10.1002/2015JC011566

Tamura, H., Miyazawa, Y., and Oey, L.-Y. (2012). The stokes drift and wave-induced mass flux in the north pacific. *J. Geophysical Res.* 117, C08021. doi: 10.1029/2012JC008113

Uchiyama, Y., McWilliams, J. C., and Restrepo, J. M. (2009). Wave-current interaction in nearshore shear instability analyzed with a vortex force formalism. *J. Geophysical Res.* 114, C06021. doi: 10.1029/2008jc005135

Uchiyama, Y., McWilliams, J. C., and Shchepetkin, A. F. (2010). Wave–current interaction in an oceanic circulation model with a vortex-force formalism: Application to the surf zone. *Ocean Model.* 34, 16–35. doi: 10.1016/j.ocemod.2010.04.002

Visser, A. W. (1997). Using random walk models to simulate the vertical distribution of particles in a turbulent water column. *Mar. Ecol. Prog. Ser.* 158, 275–281. doi: 10.3354/meps158275

Zeng, L., Chen, G., Wang, T., Zhang, S., Dai, M., Yu, J., et al. (2021). Acoustic study on the outbreak of creseise acicula nearby the daya bay nuclear power plant base during the summer of 2020. *M Mar. pollut. Bull.* 165. doi: 10.1016/j.marpolbul.2021.112144

Zhang, Y. J., Ye, F., Stanev, E. V., and Grashorn, S. (2016). Seamless cross-scale modeling with SCHISM. *Ocean Model.* 102, 64–81. doi: 10.1016/j.ocemod.2016.05.002

frontiers | Frontiers in Marine Science

TYPE Original Research
PUBLISHED 03 February 2023
DOI 10.3389/fmars.2023.1100802

OPEN ACCESS

EDITED BY
Huang Honghui,
South China Sea Fisheries Research Institute (CAFS), China

REVIEWED BY
Yun Li,
National Marine Environmental Forecasting Center, China
Qiang Li,
Tsinghua University, China

*CORRESPONDENCE
Xueqing Zhang
zxq@ouc.edu.cn

SPECIALTY SECTION
This article was submitted to Marine Pollution, a section of the journal Frontiers in Marine Science

RECEIVED 17 November 2022
ACCEPTED 04 January 2023
PUBLISHED 03 February 2023

CITATION
Lou Q, Zhang X, Xiang X, Yu F, Xiong Y and Li Z (2023) Analysis on the dynamic mechanism of *Acetes* aggregation near a nuclear power cooling water system based on the Lagrangian flow network. *Front. Mar. Sci.* 10:1100802. doi: 10.3389/fmars.2023.1100802

Analysis on the dynamic mechanism of *Acetes* aggregation near a nuclear power cooling water system based on the Lagrangian flow network

Qi Lou[1,2], Xueqing Zhang[1,2]*, Xusheng Xiang[1,2], Fan Yu[1,3], Ying Xiong[4] and Zhengyan Li[1,2]

[1]College of Environmental Science and Engineering, Ocean University of China, Qingdao, China, [2]Key Laboratory of Marine Environment and Ecology, Ministry of Education of China, Ocean University of China, Qingdao, China, [3]State Key Laboratory of Nuclear Power Safety Monitoring Technology and Equipment, Shenzhen, China, [4]Marine and Fisheries Research Institute in Jiangsu Province, Nantong, China

The outbreak of nuclear power cooling water system (NPCS) disaster-causing organisms has become more frequent, causing huge economic losses. Therefore, it is necessary to understand the aggregation mechanism of disaster-causing organisms for the risk prevention and control of NPCS. Hence, this study applied the Lagrangian flow network (LFN) to analyze the aggregation mechanism of *Acetes* near NPCS, as such a complex network can describe the interconnections between massive nodes and has already been used for modeling complex nonlinear systems, revealing how the mechanisms of such novel processes emerge. In this study, the degree and probability paths in the network were used to reveal the transport pathway and aggregation area of *Acetes*. The experimental results highlighted that the sea area of the nuclear power plant is the key node with a large in-degree of the LFN, where the material easily accumulated. The *Acetes* near the NPCS mainly originated from the east along two critical paths. Overall, this study demonstrates that the LFN is a feasible approach to predicting the transport and the accumulation of the NPCS disaster-causing plankton.

KEYWORDS

complex flow network, Lagrangian particle tracking, *Acetes chinensis*, nuclear power plant cooling system

1 Introduction

According to the 2022 world nuclear industry status report, in 2021, the world's nuclear power plants generated 2,653 billion kilowatt-hours of electricity, constituting 9.8% of the total electricity generated (Schneider et al., 2016). Most nuclear power plants are located in coastal areas to utilize seawater as the cooling water source, imposing challenges to the safe

operation of seawater intake. In recent years, marine biological outbreaks have blocked the cold source seawater intake of nuclear power plants, affecting the safe and stable operation of such power plants from time to time (Azila and Chong, 2010; Barath Kumar et al., 2017). Blockage of the cold source seawater intake of coastal nuclear power plants mainly involves algae, jellyfish, *Acetes*, seagrass, sand, ice, and crude oil, among others, of which these marine organisms are the main causes, accounting for 84% of the blocking events (An et al., 2021). In China, the nuclear power plants at Hongyanhe, Ningde, Fangchenggang, and Yangjiang have been shut down several times due to the blockage of the cooling water intakes caused by blooms of jellyfish, sea cucumbers, algae, and *Acetes*, respectively (Zeng et al., 2019; An et al., 2021; Wang et al., 2021). Specifically, due to their high biological density, short growth period, fast growth rate, and small size, *Acetes* are the most challenging disaster-causing organisms that should be controlled. Thus, this study focused on the *Acetes* near a nuclear power cooling water system (NPCS) and analyzed their transport, aggregation, and outbreak mechanisms.

Studies on the transport and mechanism of *Acetes* have received more attention in recent years. One of the research approaches is ocean investigation, such as the trawl method, underwater visual census techniques (Edgar et al., 2004; Tessier et al., 2013), acoustic method (Zeng et al., 2019), and the vessel monitoring system (VMS) (Fonseca et al., 2008; Li et al., 2022). An alternative research approach is employing a statistical model in which a species distribution model (SDM), such as BIOCLIM (bioclimatic modeling), DOMAIN (domain environmental envelope), GARP (genetic algorithm for rule-set production), CLIMEX (climate change experiment), and MaxEnt (maximum entropy) (He et al., 2021), utilizes the known species distribution data and relevant environmental variables to determine the spatial niche of species. However, this statistical model cannot reveal the dynamic mechanisms. Therefore, the particle tracking model (Hufnagl et al., 2017) or the individual-based model (IBM) (El Saadi and Bah, 2006; Falcini et al., 2020) is often applied to study the transport of biological particles, but describing the transport pathway and the connectivity between regions from complex particle trajectories is quite difficult.

This work utilized the Lagrangian flow network (LFN) theory to study the transport of *Acetes*. The LFN describes the fluid flow or material exchange among different locations, which is defined as a flow network or transport network. In the LFN, small regions in the fluid domain are interpreted as vertices, and the mass transfer from one of these regions to another defines the weighted links among them (Ser-Giacomi et al., 2015a). Based on the network, the material transport convert to the characteristics of the complex networks. Hence, a lot of powerful tools from the graph theory are available for analysis of the material transport processes. Over the past decade, the LFN theory has been successfully applied to analyze turbulent mixing (Iacobello et al., 2019), ocean transport in the Mediterranean (Ser-Giacomi et al., 2015b), and ocean surface connectivity in the Arctic (Reijnders et al., 2021), etc.

In this study, the prognostic, unstructured grid, finite-volume, free-surface, three-dimensional primitive equation coastal ocean circulation model (FVCOM) was used to obtain the current field of the study area, and the LFN approach was applied to detect the structures of the material transport, including the degrees, betweenness, and connectivity.

This paper is organized as follows. *Section 1* introduces the background of the NPCS disaster-causing organisms. *Section 2* introduces the hydrodynamic model and the LFN approach. *Section 3* shows the results of the distribution, the pathway, and the source of the *Acetes* particles. *Section 4* includes the discussion and conclusion.

2 Materials and methods

The LFN framework requires the calculation of the material transport process in the whole domain and then uses a number of mathematical methods to map the material transport process into the edges of the network. The first step in calculating the material transport process is to obtain the hydrodynamic field with a high spatial and temporal resolution, which can only be derived from the ocean circulation model. Therefore, the FVCOM was introduced in this study.

2.1 Hydrodynamic model

FVCOM was applied to obtain the hydrodynamic field in this study. The hydrodynamic equations were numerically resolved on unstructured grids using the finite-volume method. Because of the advantage of the body-fitted grid, FVCOM is widely used in estuarine and coastal areas. In addition, the finite-volume algorithm guarantees volume and mass conservation of the momentum fluxes. The reader is referred to Chen et al. (2003) for further details on the governing equations.

In this study, the model area is located 111.86°–112.97° E, 21.45°–22.02° N (Figure 1), which comprised 4,505 nodes and 8,172 triangles (elements) with 200 m minimum horizontal grid resolution and five uniform σ layers. Horizontal diffusion was parameterized based on Smagorinsky's formation, and vertical turbulent mixing was calculated with the 2.5-level Mellor and Yamada turbulence model. The tide level data on the boundary were taken from the TMD toolbox (Tidal Model Driver) (Padman, 2005) with the TPXO7 global tide model, which included eight tidal constituents (M_2, S_2, K_1, O_1, P_1, Q_1, N_2, and K_2). The sea surface wind data were extracted from the ERA5 (European Centre for Medium-Range Weather Forecasts) reanalysis dataset. The drainage water of the NPCS was also included in the model, with the flux set as 350 m^3/s (Chen et al., 2013) at a temperature of 8°C higher than natural environment seawater.

FVCOM produced a three-dimensional hydrodynamic field hourly. Subsequently, the surface current field was extracted and interpolated to drive a particle tracking model to simulate the drifting process of *Acetes*, which was then used in the construction of the LFN.

2.2 Construction of the Lagrangian flow network

The network, also called the graph in mathematics, is a set of points joined together in pairs by lines. The points are referred to as vertices or nodes and the lines referred to as edges or links. Many objects of interest in the physical, biological, and social sciences can be considered as networks (Newman, 2010). The adjacency matrix is the

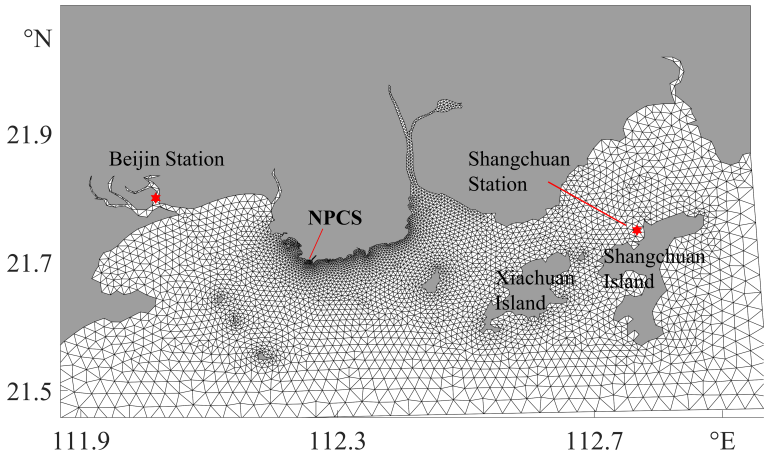

FIGURE 1
Model grid in the study area.

most common representation of a network. The adjacency matrix A is the matrix with elements A_{ij}:

$$A_{ij} = \begin{cases} 1, \text{if there is an edge between vertices } i \text{ and } j \\ 0, \quad \text{otherwise} \end{cases} \tag{1}$$

The network constructed by A_{ij} is unweighted. Similarly, the weight matrix representing the strength of the connection between vertices i and j is denoted as W_{ij}:

$$W_{ij} = \begin{cases} 1, \textit{if the weitht of the link}(\mathrm{i},\mathrm{j}) \textit{ is } W_{ij} \\ 0, \textit{ otherwise} \end{cases} \tag{2}$$

In the ocean, one way to establish the network is to base it on the particle transport dynamics, in which the nodes correspond to discretized domains and the links are defined by the connectivity between the regions (Ser-Giacomi et al., 2015a). The research domain was divided into 831 sub-regions (Figure 2) with an area of 4 km^2. A total of 250,000 particles were seeded in the domain, and all particles were tracked from time t_0 March 1) to time t (March 30). The swimming speed of *Acetes* was far less than the flow velocity, so that they are considered as being passively advected by the sea current:

$$\frac{\mathrm{d}\vec{x}}{\mathrm{d}t} = \vec{v}(\vec{x}(t), t) \tag{3}$$

where $\vec{x}$ is the displacement vector of the particles at time t and $\frac{\mathrm{d}\vec{x}}{\mathrm{d}t}$ the derivative of the displacement vector $\vec{x}$ to time t. The $\vec{v}$ is the velocity of the particle coming from the FVCOM output.

For any particle that moves from V_i to V_j, the connection from V_i to V_j is established defining the edge E_{ij} ($A_{ij} = 1$). However, it should be emphasized that the link in the network is directed, which means that the link from V_i to V_j is not the same as that from V_j to V_i. Moreover, the weight of the links is defined by the transport probability of particles from vertex V_i to V_j:

$$W_{ij}(t_0, \tau) = P_{ij}(t_0, \tau) = \frac{N_{ij}}{N_i}(4) \tag{4}$$

where N_{ij} is the number of particles from V_i to V_j and N_i is the initial number of particles in V_i. $P_{ij}(t_0,\tau)$ is regarded as the weight of the link from node V_i to node V_j. Subsequently, the network described by a transport matrix $P(t_0,\tau)$ as constructed.

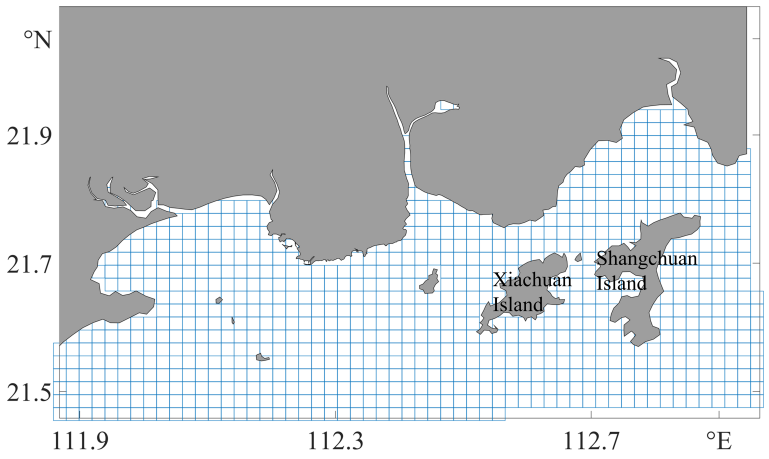

FIGURE 2
Vertices of the Lagrangian flow network (LFN) in the study area.

3 Results

3.1 Model validation

3.1.1 Water level validation

Tide is the most prominent driving factor of the current field offshore. Therefore, we verified the model based on the tidal level. The tide observation data, covering the period from December 20 to December 30, 2019, were obtained from the National Marine Data Center. Figure 1 illustrates the tide stations, while Figure 3 compares the simulation and the observation results, highlighting that the results of the model fitted well with the observations. The mean Pearson's correlation coefficient for the two-site data was 0.9616, and the root mean square error (RMSE) values were 0.18 and 0.10 m for the Beijin and Shangchuan stations, respectively.

3.1.2 Tidal current validation

The M_2 and K_1 tide components dominated the current in the investigated research domain. We calculated the tide current ellipse of these tide components based on the output of the FVCOM, and the observation data were derived from an environmental impact assessment report conducted near the nuclear power plant (Zhang, 2021). The *in situ* investigation started on June 21 and ended on June 23, 2020. The parameters including the major axis length, the minor axis length, and the orientation of the tidal ellipses based on the observation data were provided in this report. The tidal ellipses at three observation stations were calculated from the model output as well for comparison.

As seen in Figure 4, the M_2 tidal current component with a speed of about 20 cm/s contributed the majority of the tidal current, and the average speed of the K_1 tide ellipses was about 10 cm/s. The tide ellipse orientations of the model and the observation were similar, which were both parallel to the coastline, and the difference of the ellipse axis length between the simulated and measured values was not obvious, confirming the validity of the FVCOM from the other side. Quantitatively, for M_2 and K_1, the RMSE values of the tide ellipse major axis length were 3.09 and 2.40 cm/s, respectively, while those of the tide ellipse orientation were 15.26° and 3.72°, respectively. In conclusion, the hydrodynamic model can provide reliable hydrodynamic fields for subsequent analysis.

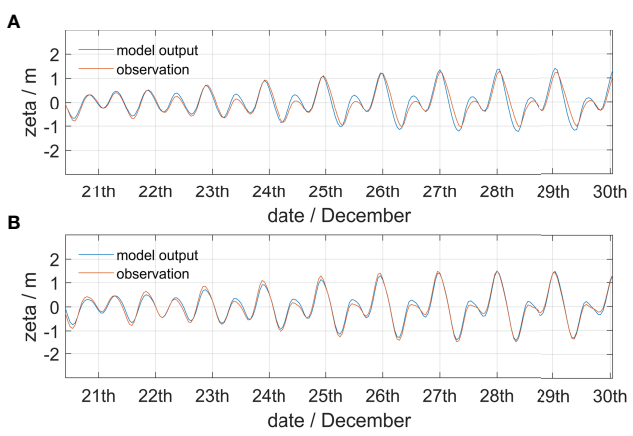

FIGURE 3
Tidal level validation at Beijin station **(A)** and Shangchuan Island station **(B)**.

3.2 Tidal current field

Figure 5 depicts the flow field distribution at ebb time and flood time during the spring tide in the simulated area. At flood time, the current flowed from the southeast to northwest, and at ebb time, the flow direction is in reverse. During flood time, the flow velocity in the whole field was mostly at 0–0.4 m/s, which can reach 0.4–0.8 m/s in the area around the NPCS and Xiachuan Island due to the influence of topography. The velocity during the ebb time was lower than that during flood time.

3.3 Transport of virtual *Acetes* particles

To clearly describe the transport and distribution of *Acetes* near the nuclear power plant, this study utilized a Lagrangian particle tracking model using passive particles to represent the *Acetes*. The particles were seeded in a uniform distance of 200 m and ran for 30 days, with March 1, 2020, as the initial release moment. Figure 6 shows the distribution of the particles for 3, 7, 15, and 30 days after releasing the particles.

The particles were mainly transported offshore for 3 days in the study area. After 7 days, the particles started showing a spatial dispersion near the coast, with some striped distribution structures. Figures 6C, D indicate obvious strips of structures where the aggregation of the particles occurred near the sea entry of three rivers. In contrast, the particles at the estuary spread rapidly, and the number of remaining particles was very small. The particles were mostly in patched aggregates near several islands on the eastern side of the study area. Since *Acetes* are poor swimmers and can be considered as plankton whose transport and distribution are controlled by currents, the particle tracking results can represent their trajectories in this region.

3.4 Out-degree and in-degree

The degree of a vertex in a graph is the number of edges connected to it. In a directed network, the connectivity of each vertex is described by both the in-degree and the out-degree. The in-degree k_i^{in} of vertex i is the number of edges arriving at i while the out-degree k_i^{out} of vertex i is the number of outgoing edges from i. In terms of the adjacency matrix A_{ji} the in-degree and out-degree can be written as:

$$k_i^{\text{in}} = \sum_{j=1}^{n} A_{ji} \tag{5}$$

$$k_i^{\text{out}} = \sum_{j=1}^{n} A_{ij} \tag{6}$$

The degree of a vertex has an immediate interpretation considering centrality, quantifying how well an element is

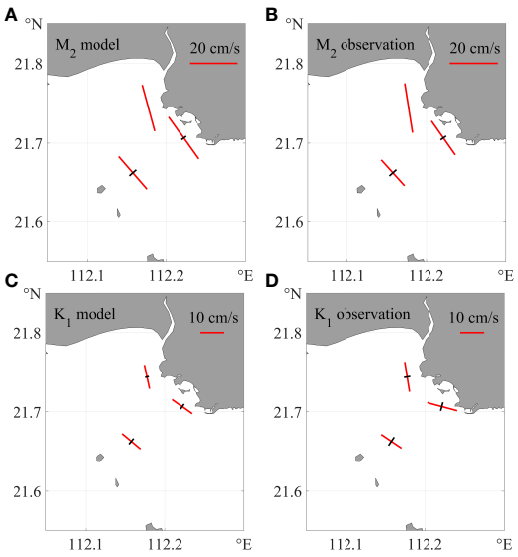

FIGURE 4
Tidal current ellipses obtained through both model simulation and observation. **(A)** Model output of the M_2 tide ellipse. **(B)** Observation of the M_2 tide ellipse. **(C)** Model output of the K_1 tide ellipse. **(D)** Observation of K_1.

connected to the other elements in the graph (Barrat et al.). Regarding the LFN that corresponds to the aggregation and diffusion of materials in the ocean, the vertex with a large in-degree implies that the material easily accumulates there, which is generally considered as a "sink" in the description of ocean material transport; in contrast, a large out-degree indicates that the vertex can be considered as a "source".

Figure 7 illustrates the distribution of the in-degree and out-degree within 30 days. The degrees were mostly less than 10, and vertices with a large degree are likely to be near the coast. Figure 7 also highlights that the in-degree and out-degree were higher at offshore areas, i.e., sea areas where the cooling system is located that act both as a "sink" and as a "source" of the materials around them. From a network's perspective, it is the hub vertex in the material transport process. If any environmental variations influence the nearby material transport, for instance, reducing the diffusion process, the materials will be continuously convected inwards because of the large in-degree, but not outwards due to the limited diffusion process. The NPCS is in an unstable equilibrium condition, and this material transport pattern brings with it a high risk of natural outbreak of these organisms.

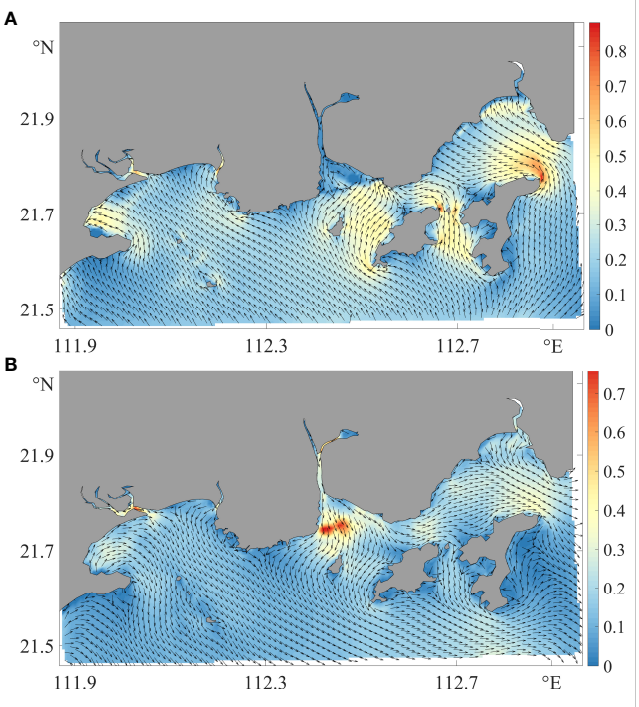

FIGURE 5
Current distribution at flood time **(A)** and ebb time **(B)**.

3.5 The path and source of *Acetes*

A path in a network is any sequence of vertices so that every consecutive pair of vertices in the sequence is connected by an edge in the network (Newman, 2010). The path is often used to analyze the connectivity among vertices, and the path concept depends on the distances among vertices. In the ocean, the distance is not limited to the Euclidean distance, as the shortest time to the fastest path or the most probable path (MPP) is more meaningful in practice. This study applied the MPP to determine the optimum path.

When all paths connected to the location of the nuclear power plant were found, we collected their starting points and labeled them as the source of *Acetes* (red dots in Figure 8). Obviously, the results depend on the integration time. Considering the results within 30 and 90 days, the potential source area was located east of the nuclear power plant, which covered an area of about 120 km^2, and within 90 days, the area was about 475 km^2.

In order to determine the path, we introduced another network metric, the betweenness centrality. Betweenness measures the extent to which a vertex lies on the key paths between other vertices. Mathematically, if N_{jl} s the total number of the MPPs (Ser-Giacomi et al., 2015b) from V_j o V_l and $N_{jl}(i)$ is the number of these MPPs that

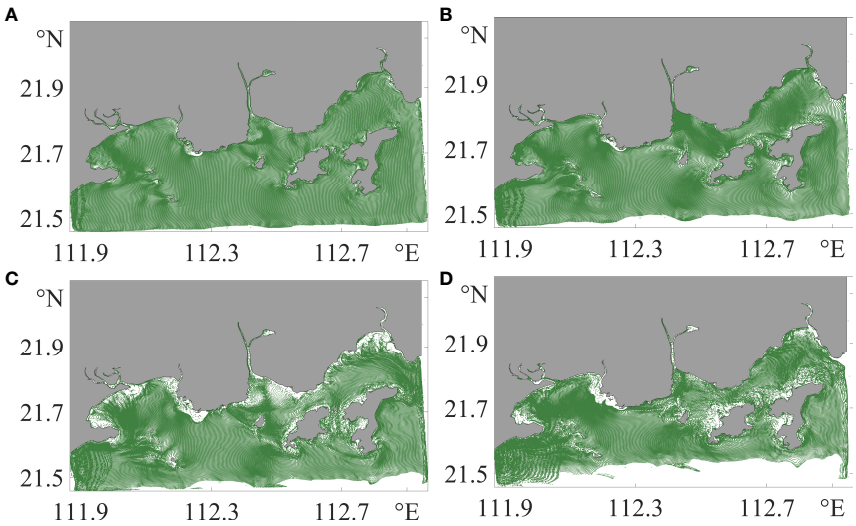

FIGURE 6
Distribution of the virtual *Acetes* particles for integration times of 3 days **(A)**, 7 days **(B)**, 15 days **(C)**, and 30 days **(D)** since March 1, 2020.

pass through the V_i the betweenness of V_i is defined as:

$$B_i = \sum_{\substack{\forall j,l \\ j \neq l \neq i}} \left[N_{jl}(i)/N_{jl}\right] \tag{7}$$

Vertices with high betweenness pose a greater influence within a network. On the other hand, in terms of the ocean, betweenness is a measure of the hidden bottlenecks of the material transport system, and aligned high-betweenness vertices indicate the major material transport pathways (Ser-Giacomi et al., 2021). Hence, the betweenness is critical in the analysis of material transport and in the determination of the ocean's flow structure.

As mentioned above, the *Acetes* near the nuclear power plant originated from the east with a large probability. The betweenness results showed that the organisms were not uniformly or randomly transported to the nuclear power plant's sea area. Instead, two clear transport pathways (Figure 9) passed through the sea area of the nuclear plant. The first pathway goes along the coast that extends to the eastern boundary of the research domain, while the other bypasses the southern edges of Xiachuan Island and merges with the first pathway just near the NPCS. The two pathways formed a "-<"-shaped transport structure, and the intersection of two major material transport pathways was only about 10 km from the NPCS. Most of the time, this "-<"-shaped pathway carries materials westward and works in balance. However, when any environmental interruptions such as coast-pointing winds occur, this fragile system falls into unbalance and the material flow is cut off, which might result in an organism aggregation or even in a harmful outbreak. The effect of wind direction will be discussed in the next section.

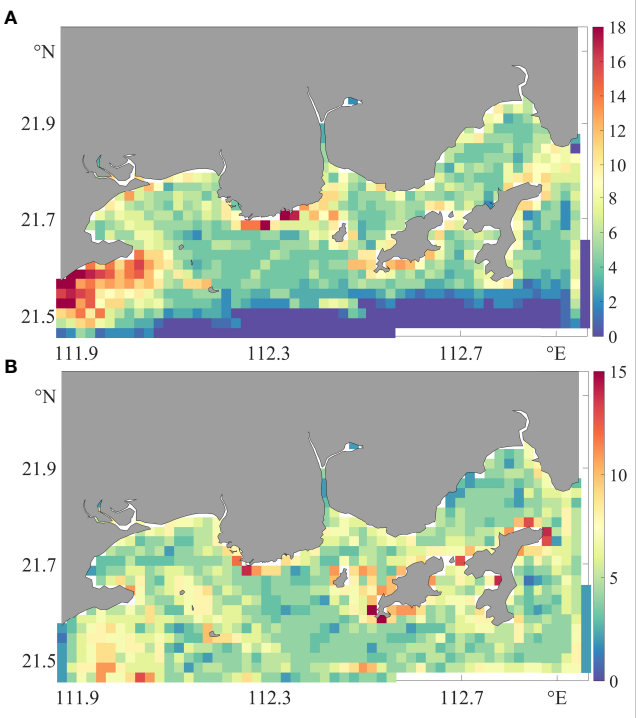

FIGURE 7
Distribution of in-degree **(A)** and out-degree **(B)**.

3.6 Discussion

The distribution of *Acetes* is affected by biological, chemical, and physical factors, with their outbreak mechanism still being poorly understood. In this study, we focused on the dynamic factors. Figure 10 reveals the relationship between wind and the daily catch of *Acetes* from 2020 to 2021. The *Acetes* catch data were provided by the State Key Laboratory of Nuclear Power Safety Monitoring Technology and Equipment, and the wind data around the NPCS were extracted from the ERA5 reanalysis data. An *Acetes* outbreak is most likely to happen in late winter or in early spring, so we aimed to analyze and determine what happens during these periods. We hypothesized that the temperature and the material transport

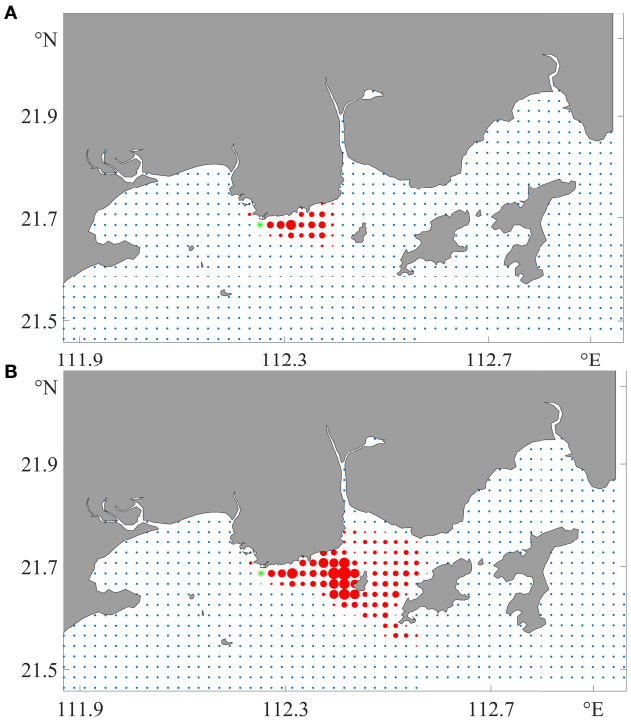

FIGURE 8
Potential source of *Acetes* near the nuclear power plant. **(A, B)** Results within 30 days **(A)** and 90 days **(B)**.

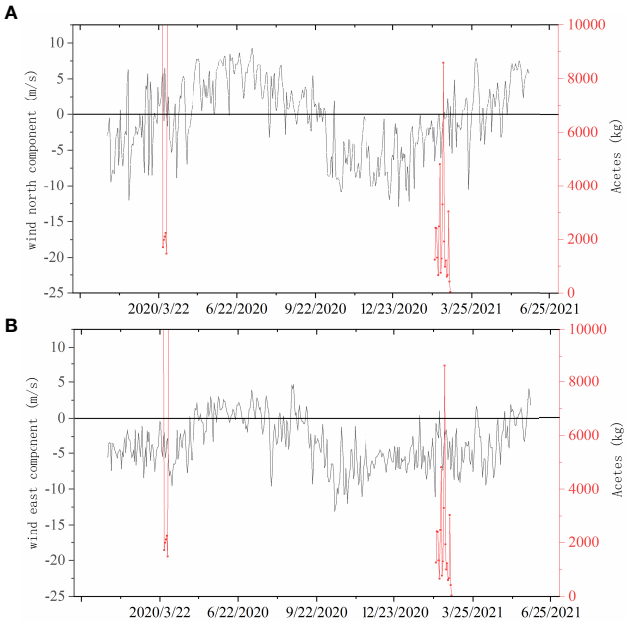

FIGURE 10
Association between wind and the *Acetes* catch. **(A)** The wind north component. **(B)** The wind east component.

pattern are the intrinsic causes, and wind is an acceleration factor. Intriguingly, the outbreak of *Acetes* showed a strong relationship with the time when the winds are turning from northeast to southwest. Wind stress turning from offshore to onshore influenced the material transport pattern; that is, the two major pathways intersected in the cooling system, thus causing the aggregation of *Acetes* around it. Afterward, with the reversed wind direction, the old transport pattern was destructed and the seawater temperature also rose too high for *Acetes* to survive, explaining the reduction in the daily catch of *Acetes*.

Subsequently, we ran a parallel experiment that removed the surface wind on the ocean to clarify the model's sensitivity to wind. The configurations of the hydrodynamic model and the network were the same, except for the removal of the surface wind stress. The two experiments were denoted as the "with-wind" case and the "no-wind" case.

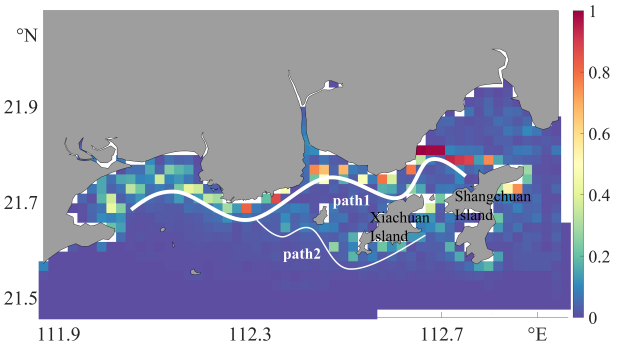

FIGURE 9
Distribution of the betweenness of the vertices.

On the one hand, Figure 11 depicts the betweenness pathways in the no-wind experiment, where the shape of the pathways was similar to that in the with-wind experiment, which is a two-pathway flow from the east to the west conjunct in the middle; however, the pathways in the no-wind experiment were shifted two or three grids to the south and thus staggered the NPCS. Most materials transported westward will not go through the NPCS, if the wind is weak. Therefore, the *Acetes* had a small probability of touching the NPCS or even break out without the assistance of the northwestward winds.

On the other hand, the in-degree and out-degree of the network, which depict the characteristic of the aggregation and diffusion processes of *Acetes*, also made significant changes under the influence of wind. When wind was added to the model, the in-degree, which represents the sink of a material, increased significantly (Figures 12A, B). However, the out-degree, which represents the source of the material, decreased by about 50% when wind was included (Figures 12C, D). To sum up, the extra northwestward wind increased the extent of the material sink and decreased the extent of the material source near the NPCS.

4 Conclusion

This paper applied the LFN theory to study the transport and aggregation mechanism of *Acetes* near a nuclear power plant. The LFN is a feasible and novel method used to predict the spatial and temporal distribution of plankton, such as the pelagic larva and *Acetes*. Particularly, LFN can detect the material transport path and

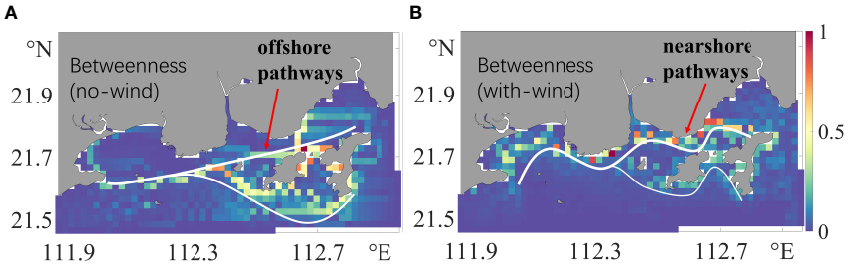

FIGURE 11
The betweenness pathways with wind in March **(B)** and without wind **(A)**.

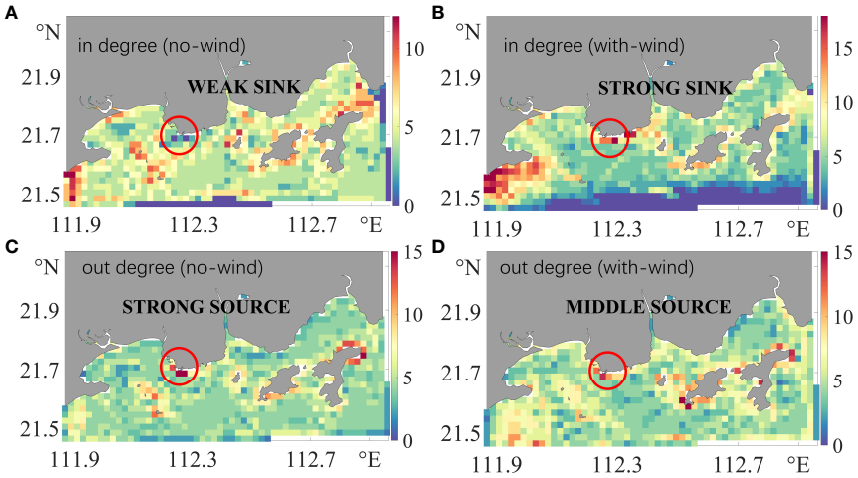

FIGURE 12
In-degree **(A, B)** and out-degree **(C, D)** under the no-wind and with-wind experiments.

trace the origin of disaster-causing organisms, which cannot be achieved using circulation or particle tracking methods.

The degree of LFN illustrates the importance of the vertex in the network, which corresponds to the aggregation or the diffusion characteristic. In this study, the cooling water intake of the nuclear power plant comprised just the high in-degree and high out-degree nodes, representing a large material diffusion ability and accumulation probabilities. Hence, any small perturbation destroys the nearby mass balance, and thus a large amount of material might be immediately accumulated near the area.

From the perspective of betweenness, the cooling water intake of the nuclear power plant was located at the junction of the two pathways. The materials were transported from the east to the west and from the south to the north, forming a "-<"-shaped transport structure (see Figure 9) and passing through the sea area of the nuclear power plant. When the external environment changes, e.g., the wind direction suddenly changes from the offshore wind to the onshore wind, the materials transported from the pathway will accumulate near the coast under the effect of wind. This phenomenon has also been confirmed by observation.

Nevertheless, we suppose that the wind direction might be an important factor causing the outbreak of *Acetes*; that is, at a suitable temperature, the southeast wind will cause the aggregation of *Acetes* in the study area.

Data availability statement

The raw data supporting the conclusions of this article will be made available by the corresponding author, without undue reservation.

Author contributions

XZ proposed the idea of using the Lagrangian flow network on the *Acetes* near the nuclear power cooling water system and wrote the manuscript. QL ran the hydrodynamic model and wrote the context in this paper. XX established the LFN model and plotted the figures in this paper. FY recorded and provided precious long-term observation data on *Acetes*. ZL proposed some valuable suggestions in revising this article. YX provided some important information about the habits of *Acetes* and helped revise the introduction part. All authors contributed to the article and approved the submitted version.

Funding

This work was supported by the Fisheries Ecology and Resource Monitoring Project of Agricultural Ecological Protection and Resource Utilization in Jiangsu Province (2021-SJ-110-02) and the National Natural Science Foundation of China (no.41974085).

Acknowledgments

We would like to express our gratitude to all the reviewers and editors for their valuable comments.

Conflict of interest

The authors declare that the research was conducted in the absence of any commercial or financial relationships that could be construed as a potential conflict of interest.

Publisher's note

All claims expressed in this article are solely those of the authors and do not necessarily represent those of their affiliated organizations, or those of the publisher, the editors and the reviewers. Any product that may be evaluated in this article, or claim that may be made by its manufacturer, is not guaranteed or endorsed by the publisher.

References

An, L., Wang, L., Ou, D., Jia, C., Li, W., Ding, Y., et al. (2021). The ecological mechanisms of acetes blooms as a threat to the security of cooling systems in coastal nuclear power plants. *J. Coast. Conserv.* 25, 55. doi: 10.1007/s11852-021-00845-0

Azila, A., and Chong, V. C. (2010). Multispecies impingement in a tropical power plant, straits of malacca. *Mar. Environ. Res.* 70, 13–25. doi: 10.1016/j.marenvres.2010.02.004

Barath Kumar, S., Mohanty, A. K., Das, N. P. I., Satpathy, K. K., and Sarkar, S. K. (2017). Impingement of marine organisms in a tropical atomic power plant cooling water system. *Mar. pollut. Bull.* 124, 555–562. doi: 10.1016/j.marpolbul.2017.07.067

Barrat, A., Lemy, M. B., and Vespignani, A. (2008). DYNAMICAL PROCESSES ON COMPLEX NETWORKS Cambridge university press. 367.

Chen, C., Liu, H., and Beardsley, R. C. (2003). An unstructured grid, finite-volume, three-dimensional, primitive equations ocean model: Application to coastal ocean and estuaries. *J. Atmospheric Ocean. Technol.* 20, 159–186. doi: 10.1175/1520-0426(2003)020<0159:AUGFVT>2.0.CO;2

Chen, X., Tang, S., and Ou, D. (2013). Assessment report of yangjiang nuclear power plant project on fishery resources and ecology in adjacent waters.

Edgar, G. J., Barrett, N. S., and Morton, A. J. (2004). Biases associated with the use of underwater visual census techniques to quantify the density and size-structure of fish populations. *J. Exp. Mar. Biol. Ecol.* 308, 269–290. doi: 10.1016/j.jembe.2004.03.004

El Saadi, N., and Bah, A. (2006). On phytoplankton aggregation: A view from an IBM approach. *C. R. Biol.* 329, 669–678. doi: 10.1016/j.crvi.2006.05.004

Falcini, F., Corrado, R., Torri, M., Mangano, M. C., Zarrad, R., Di Cintio, A., et al. (2020). Seascape connectivity of European anchovy in the central Mediterranean Sea revealed by weighted Lagrangian backtracking and bio-energetic modelling. *Sci. Rep.* 10, 18630. doi: 10.1038/s41598-020-75680-8

Fonseca, T., Campos, A., Afonso-Dias, M., Fonseca, P., and Pereira, J. (2008). Trawling for cephalopods off the Portuguese coast–fleet dynamics and landings composition. *Fish. Res.* 92, 180–188. doi: 10.1016/j.fishres.2008.01.015

He, Y., Liu, S., Yuan, Y., Jiang, K., Wang, T., Qin, Y., et al. (2021). The potential suitability habitat prediction of acaudina molpadioides based on maxent model. *Haiyang Xuebao* 43, 65–74.

Hufnagl, M., Payne, M., Lacroix, G., Bolle, L. J., Daewel, U., Dickey-Collas, M., et al. (2017). Variation that can be expected when using particle tracking models in connectivity studies. *J. Sea Res.* 127, 133–149. doi: 10.1016/j.seares.2017.04.009

Iacobello, G., Scarsoglio, S., Kuerten, J. G. M., and Ridolfi, L. (2019). Lagrangian Network analysis of turbulent mixing. *J. Fluid Mech.* 865, 546–562. doi: 10.1017/jfm.2019.79

Li, G., Li, D., Xiong, Y., Zhong, X., Tang, J., Song, D., et al. (2022). Changes in the resource distribution of acetes chinensis and patterns of species replacement in haizhou bay in summer based on BeiDou VMS data. *Reg. Stud. Mar. Sci.* 56, 102655. doi: 10.1016/j.rsma.2022.102655

Newman, M. E. J. (2010). *Networks: An introduction* (Oxford, New York: Oxford University Press).

Padman, L. (2005) *Tide model driver (TMD) manual.* Available at: https://svn.oss.deltares.nl/repos/openearthtools/trunk/matlab/applications/DelftDashBoard/utils/tmd/Documentation/README_TMD_vs1.2.pdf.

Reijnders, D., van Leeuwen, E. J., and van Sebille, E. (2021). Ocean surface connectivity in the Arctic: Capabilities and caveats of community detection in Lagrangian flow networks. *J. Geophys. Res. Oceans* 126. doi: 10.1029/2020JC016416

Schneider, M., Froggatt, A., Hosokawa, K., Thomas, S., Yamaguchi, Y., and Hazemann, J. (2016). The world nuclear industry status report. *Mycle Schneider Consult. MSC* 12, 124–128.

Ser-Giacomi, E., Baudena, A., Rossi, V., Follows, M., Clayton, S., Vasile, R., et al. (2021). Lagrangian Betweenness as a measure of bottlenecks in dynamical systems with oceanographic examples. *Nat. Commun.* 12, 1–14. doi: 10.1038/s41467-021-25155-9

Ser-Giacomi, E., Rossi, V., López, C., and Hernández-García, E. (2015a). Flow networks: A characterization of geophysical fluid transport. *Chaos Interdiscip. J. Nonlinear Sci.* 25, 036404. doi: 10.1063/1.4908231

Ser-Giacomi, E., Vasile, R., Hernández-García, E., and López, C. (2015b). Most probable paths in temporal weighted networks: An application to ocean transport. *Phys. Rev. E Stat. Nonlin. Soft Matter Phys.* 92, 12818. doi: 10.1103/PhysRevE.92.012818

Tessier, A., Pastor, J., Francour, P., Saragoni, G., Crec'hriou, R., and Lenfant, P. (2013). Video transects as a complement to underwater visual census to study reserve effect on fish assemblages. *Aquat. Biol.* 18, 229–241. doi: 10.3354/ab00506

Wang, J., Ma, C., and Zou, Q. (2021). Status and suggestions of cold source safety guarantee for nuclear power plants in south China. *Nucl. Saf.* 20, 65–71. doi: 10.16432/j.cnki.1672-5360.2021.03.012

Zeng, L., Chen, G., Wang, T., Yang, B., Yu, J., Liao, X., et al. (2019). Acoustic detection and analysis of acetes chinensis in the adjacent waters of the daya bay nuclear power plant. *J. Fish. Sci. China* 26, 1029–1039.

Zhang, (2021). *Environmental impact assessment report on the rescue and reinforcement project of baishatou revealment of dongping national central fishing port in yangjiang city (Phase III)* (Tianjin: Sea Island Environmental Science and Technology Research Institute (Tianjin).

frontiers | Frontiers in Marine Science

TYPE Original Research
PUBLISHED 13 March 2023
DOI 10.3389/fmars.2023.1110160

OPEN ACCESS

EDITED BY
Ángel J. Gutiérrez Fernández,
University of La Laguna, Spain

REVIEWED BY
Wentao Li,
Ocean University of China, China
Chao Song,
Freshwater Fisheries Research Center (CAFS), China

*CORRESPONDENCE
Yan-Guo Wang
wangyg@tio.org.cn
Hong-Hui Huang
huanghh@scsfri.ac.cn

†These authors have contributed equally to this work and share corresponding authorship

SPECIALTY SECTION
This article was submitted to Marine Pollution, a section of the journal Frontiers in Marine Science

RECEIVED 28 November 2022
ACCEPTED 10 February 2023
PUBLISHED 13 March 2023

CITATION
Wu F-X, Gu Y-G, Liu Q-X, Zhang S-F, Rao Y-Y, Liu H-X, Dai M, Wang Y-G and Huang H-H (2023) Research on the seasonal variation of zooplankton community in Daya Bay, South China Sea. *Front. Mar. Sci.* 10:1110160. doi: 10.3389/fmars.2023.1110160

Research on the seasonal variation of zooplankton community in Daya Bay, South China Sea

Feng-Xia Wu[1], Yang-Guang Gu[1], Qing-Xia Liu[1], Shu-Fei Zhang[1], Yi-Yong Rao[1], Hua-Xue Liu[1], Ming Dai[1], Yan-Guo Wang[2*†] and Hong-Hui Huang[1*†]

[1]Guangdong Provincial Key Laboratory of Fishery Ecology and Environment, South China Sea Fisheries Research Institute, Chinese Academy of Fishery Sciences, Guangzhou, China, [2]Laboratory of Marine Biodiversity, Third Institute of Oceanography, Ministry of Natural Resources, Xiamen, China

Changes in zooplankton composition, abundance, and some species in response to environmental variation were investigated over four seasons (2020) in Daya Bay. In total, 129 taxa of zooplankton (16 groups of planktonic larvae and 20 indeterminate species) were identified. Zooplankton communities exhibited a significant seasonal shift in abundance and taxonomic composition. The maximum number of zooplankton species was recorded in winter (72 species) and the lowest in spring (42 species). However, the abundance was highest in spring (1,372.01 ± 1,071.14 individuals/m^3) and lowest in autumn (50.93 ± 34.05 individuals/m^3). Pearson correlation analyses demonstrated that the zooplankton abundance and the variations of indicator species were obviously correlated with environmental parameters (*e.g.*, salinity, temperature, pH, and chlorophyll-*a*). Based on specificity and occupancy analysis, a total of eight species were selected as indicator species. It is noteworthy that some kollaplankton (such as *Dolioletta gegenbauri* and *Doliolum denticulatum*) could potentially cause disaster to the nuclear power plant cooling system because of their relatively large body size and huge blooms in spring. In addition, *Centropages tenuiremis* blooms in spring and *Penilia avirostris* blooms in summer could attract assemblages of larval or adult pelagic fish, which would also threaten the cooling system security in Daya Bay. In conclusion, our results suggest that zooplankton communities and some species may be considered as favorable indicators of the marine environment.

KEYWORDS

zooplankton, indicator species, Daya Bay, nuclear power, disaster-causing organism

Introduction

Coastal waters, which lie at the transition zones between oceans and continents, are the most relevant to human society. They also support rich fishing grounds and provide economic benefits due to their relatively higher productivity (Herrera-Silveira and Morales-Ojeda, 2009; Lange et al., 2010). Coastal areas support relatively greater

plankton production and degradation and also play a key role in biogeochemical processes. However, their biodiversity and ecological function are threatened by global changes and anthropogenic pressures which cause the degradation of biotopes and biocenosis (Kemp and Boynton, 2012; Zhang, et al., 2021). Increased anthropogenic activities have accelerated the process of eutrophication, leading to dystrophic crises and/or irreversible deterioration—for example, a decrease in the mean size of dominant copepods from the late 1940s to 2012 was detected in the Central Basin of Long Island Sound, Japan (Rice et al., 2015).

Daya Bay is a semi-enclosed, shallow embayment with depths ranging from 5 to 20 m and an area of 650 km^2, which is located in the northern part of the South China Sea (Song et al., 2004). It contains complex habitats, tremendous biological resources, abundant biodiversity, and plentiful marine products, which make it one of the most important treasure houses for sub-tropical aquatic resources. In recent years, rapid social and economic developments have resulted in environmental degradation in Daya Bay. Studies have shown that degradation and habitat modification have significantly increased (Wu et al., 2009; Liu et al., 2018), while eutrophication has reduced the zooplankton species richness by about 50% (Li et al., 2014). Dominant species in the spring have changed because of the rapid increase in water temperature and abundant food supply in Daya Bay (Xiang et al., 2021; Zhao et al., 2022), and Li et al. (2021) reported that the zooplankton community was undergoing great changes, showing tendencies of miniaturization and gelatinization over the past 30 years. Several large-scale zooplankton blooms have occurred in Daya Bay, which were related to changes in water temperature, salinity, and food supply variation (Zeng et al., 2019; An et al., 2021; Zeng et al., 2021; Liu et al., 2022).

Zooplankton are sensitive to chemical, physical, and biological factors in marine systems (Sun et al., 2010; Shi et al., 2015). The composition and abundance of zooplankton are highly dependent on environmental conditions and respond quickly to environmental variations. Consequently, zooplankton are considered as bio-indicators of environmental quality and water mass (Dam, 2013; Carter et al., 2017; Wang et al., 2020; Wang et al., 2022). Zooplankton are not only a key link in energy transfer from primary production to higher trophic levels but also a key factor in controlling the harmful effects of eutrophication and proliferation of microalgae (Rissik et al., 2009)—for example, dinoflagellates and prasinophytes are the most preferred phytoplankton groups by the mesozooplankton in Daya Bay (Li et al., 2018).

Daya Bay Nuclear Power Station and Ling-Ao Nuclear Power Station were built in 1994 and 2002, respectively. They are located in the inner regions of west Daya Bay. The thermal discharge is affected by tidal currents, which depend on the topography of Daya Bay (Yuan et al., 2021). The residual current is relatively small within the bay in summer but is stronger with the stronger current fields in winter, and the self-purification capacity of this area is weak (Wu et al., 2007). In addition, other studies have demonstrated that the thermal discharge has a significant impact on the Daya Bay ecosystem, including levels of nutrients, and zooplankton and phytoplankton (Jiang and Wang, 2020). Therefore, it is vital to monitor the zooplankton composition and variation in Daya Bay.

The aims of this research were to (1) investigate whether there is significant variation in the zooplankton composition in the research area, (2) identify the indicator composition under different environmental conditions, (3) measure the correlation of indicator species with the environmental parameters in the research area, and (4) discuss whether the indicator species caused a potential threat to the safety of the nuclear power plant cooling systems in the research area.

Materials and methods

Field sampling

Twenty-four sampling stations were set up in Daya Bay during winter (January), spring (March), summer (August), and autumn (November) of 2020 (Figure 1). Zooplankton samples were collected at each station during every survey. In total, 96 zooplankton samples were obtained by vertical tow from 1 m above the bottom to the surface at a speed of 0.5 m/s using a plankton net (mesh size, 505 μm; mouth diameter, 50 cm; and net length, 145 cm). A Hydro-Bios flow meter (Hydro-Bios Apparatebau GmbH., Altenholz, Germany) was mounted at the mouth of the net to calculate the filtered water volume. Then, zooplankton samples were immediately preserved with 5% formalin seawater solution on board at each station. Environmental factors, such as temperature, pH, salinity, and dissolved oxygen (DO), were measured *in situ* using a multi-parameter sensor (YSI Professional Plus, Xylem Analytics, Beijing, China) at each station where the zooplankton samples were collected. In addition, 5,000 ml of seawater samples for nutrient analysis was collected from each station with a Niskin water sampler at a depth of 0.5 m and preserved immediately upon collection by placing them at -20°C in the dark. Simultaneously, approximately 500 ml of sampled seawater was filtered through GF/F filters. These filters were frozen and later extracted with 90% acetone at −20°C in the dark for 24 h to determine the concentration of chlorophyll-*a* (Chl-*a*) using a fluorometer (Tuner-10-AU).

Data analysis

In the laboratory, zooplankton samples were split into sub-samples with a Folsom plankton sample splitter until each subsample contained about 200 individuals. All individuals in the subsamples were quantified and identified to species level where possible under a stereomicroscope (Leica MZ95, Leica Microsystems Ltd, Wetzlar, Germany) according to the descriptions of Chen and Zhang (1965), Zheng et al. (1984), Chen (1992); Chihara and Murano (1997), and Lian et al. (2019). Abundance was calculated by the individuals' numbers to be divided by filtered water volume at each station. Total abundance was equal to the sum of all individuals' abundance in that station. Total average abundance means the summation of total abundance in each station to be divided by station numbers in each survey. Relative abundance represents the percentage

of a certain species' average abundance in the total average abundance.

One-way analysis of variance with Tukey's *post-hoc* test was used to estimate the seasonal variation of environmental characteristics, and the correlation of different parameters was analyzed *via* Pearson correlation analysis using SPSS software (IBM SPSS statistics for Windows, Armonk, NY, USA). The dominance (Y) of each species was calculated using the formula $Y=(n_i/N)*f_i$, where n_i represents the mean number of species i, and N represents the total mean number of zooplankton. The specificity and occupancy were calculated using the following formula with reference to Dufrene and Legendre (1997). The figure of specificity–occupancy was finished by ggplot 2 in R language.

$$\text{Specificity} = \frac{N_{\text{individuals}_{i,j}}}{N_{\text{individuals}_i}};$$

$$\text{Occupancy} = \frac{N_{\text{sites}_{i,j}}}{N_{\text{sites}_j}}$$

Where $N_{\text{individuals}i,j}$ means the mean abundance of species i in survey j. $N_{\text{individuals}_i}$ means the sum of the mean abundance of species i in different surveys. Occupancy also means occurrence rate. $N_{\text{sites}_{i,j}}$ means the station numbers of species i occurrence in survey j and N_{sites_j} means all stations in survey j.

Results

Environmental parameters

The year-round mean surface water temperature was 24.59 ± 3.87°C, and the water temperature followed a clear seasonal pattern. The maximum was recorded in summer (30.48 ± 0.48°C), and the minimum was in winter (20.01 ± 0.93°C). The temperature was close to the year-round average surface water temperature in spring and autumn at 23.73 ± 1.00°C and 24.13 ± 0.85°C, respectively (Figure 2A). The values of salinity and pH peaked in spring but were relatively lower in summer (Figures 2B, C). Additionally, the values of DO ranged from 6.32 ± 0.45 mg/L in summer to 7.76 ± 0.67 mg/L in autumn, with a mean of 7.11 ± 0.70 mg/L (Figure 2D). The values of Chl-*a* varied consistently with DO—the maximum value was recorded in autumn, and the minimum value was recorded in summer. There were no obvious differences in Chl-*a* concentration between the spring, summer, and winter surveys (Figure 2E).

Zooplankton composition and seasonal variation

A total of 129 zooplankton species (16 groups of planktonic larvae and 20 indeterminate species) were identified in this study. All species were arranged into cladocera, copepoda, kollaplankton, large crustacean, meroplankton, other crustacean, and other plankton groups, based on the systematics and their function in the marine environment. Kollaplankton included tunicates, cnidaria, ctenophores, and chaetognatha. Mysidacea, euphausiacea, and decapoda were classified as large crustaceans. The other crustaceans included amphipoda and ostracoda. Annelida and petropoda were classified as other plankton in this study. The species composition of zooplankton showed obvious seasonal variation (Figure 3). In winter, 72 species were recorded at the species level. This was followed by autumn, summer, and spring,

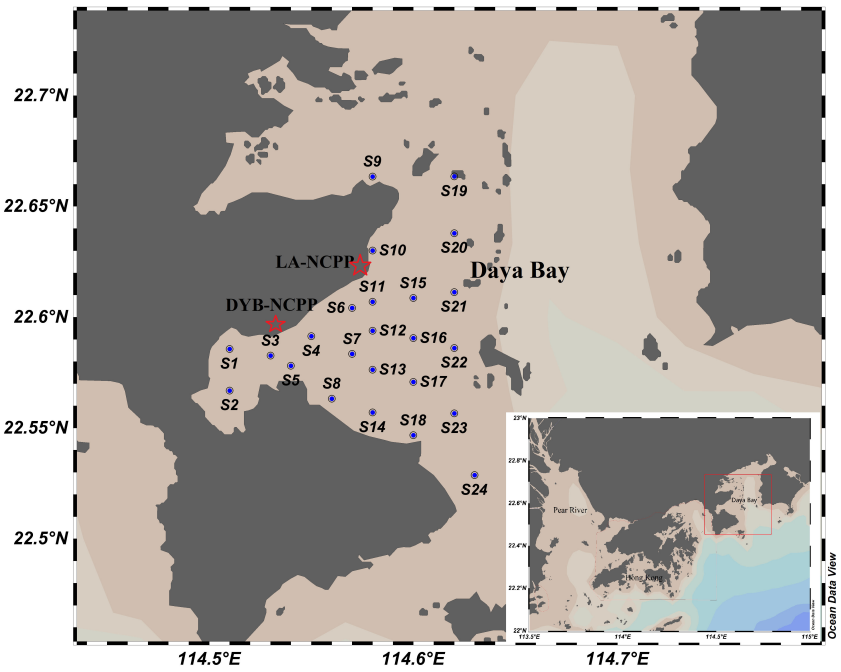

FIGURE 1
Study area and stations located at western Daya Bay. DYB-NCPP, Daya Bay Nuclear Power Plant; LA-NCPP, Ling'ao Nuclear Power Plant.

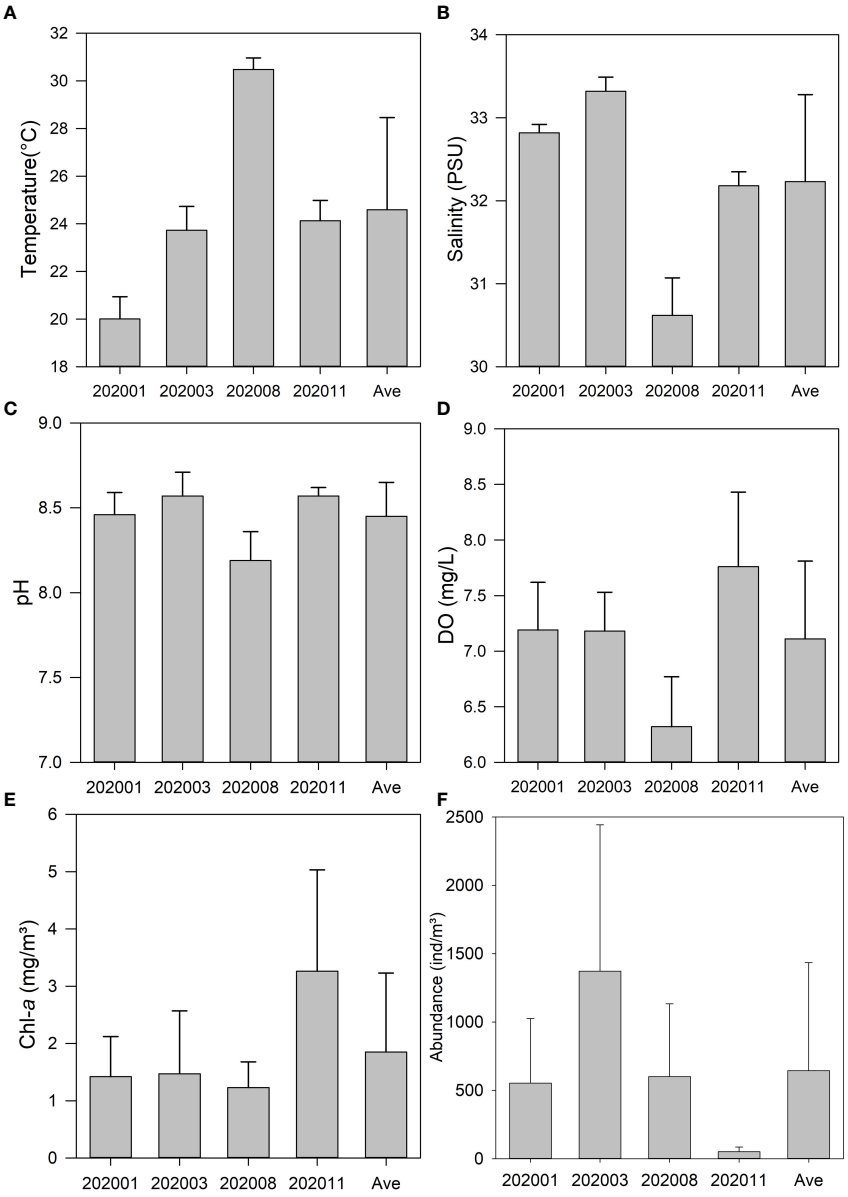

FIGURE 2
Bar plot of the temperature **(A)**, salinity **(B)**, pH **(C)**, dissolved oxygen **(D)**, chlorophyll-a **(E)**, and total average abundance **(F)** in the research area.

with 54 species, 44 species, and 42 species, respectively. Copepods accounted for the highest number of species, and the percentage ranged from 43.18% to 62.96%.

The total average zooplankton abundance showed a significant seasonal variation. The greatest average abundance was in spring, and the lowest in autumn (Figure 2F). In spring, the average abundance of zooplankton was 1,372.01 individuals/m^3, while the zooplankton assemblage was largely dominated by kollaplankton (46.36% of total average abundance), meroplankton (27.04% of total average abundance), and copepods (19.95% of total average abundance). In summer, the average abundance of zooplankton was significantly reduced to 601.10 individuals/m^3, with the average abundance of cladocera (58.21% of total average abundance) being the highest, followed by copepods (28.20% of total average abundance) and meroplankton (10.97% of total average abundance). In autumn, zooplankton average abundance was only 50.93 individuals/m^3, with copepods and meroplankton dominating, accounting for 57.22% and 21.93% of total average abundance, respectively (Figure 3). However, the zooplankton average abundance increased in winter, reaching 553.06 individuals/m^3. The dominant species were cladocera and copepods, with abundance values of 233.14 individuals/m^3 (42.15% of total average abundance) and 225.86 individuals/m^3 (40.84% of total average abundance), respectively.

The Pearson correlation analysis results showed that the total abundance of zooplankton was significantly positively correlated with surface water salinity and markedly negatively correlated with Chl-*a* ($p< 0.01$) (Table 1). In addition, the abundance of cladocera and copepods was significantly negatively correlated with Chl-*a* ($p< 0.01$). Similarly, there was a significant negative correlation between

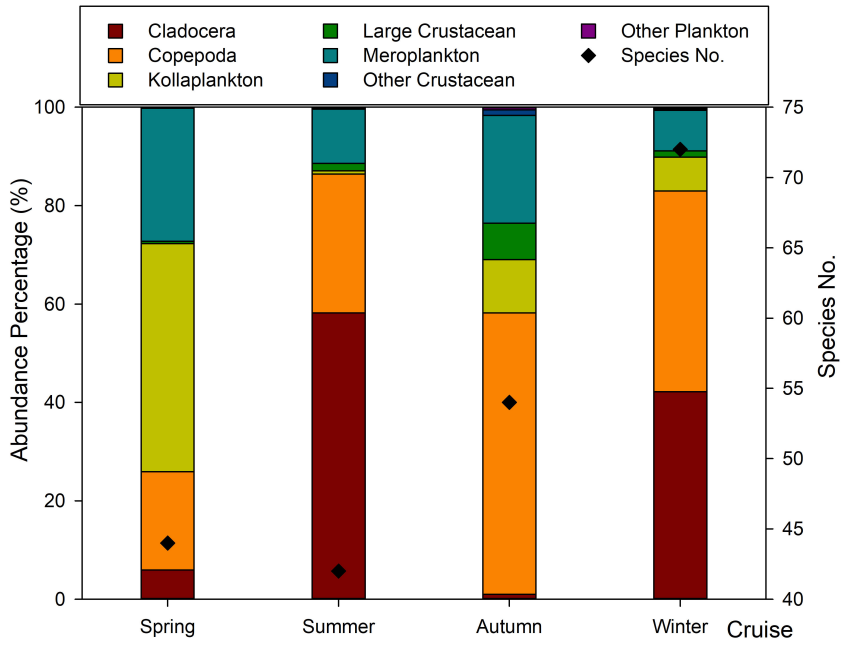

FIGURE 3
Species number and abundance percentage in Daya Bay.

the abundance of kollaplankton, large crustaceans, meroplankton, and Chl-*a* ($p< 0.05$). However, cladocera abundance showed a significantly positive correlation with surface water temperature and a notable negative correlation with DO. The abundance of cladocera showed a notable negative correlation with pH, while kollaplankton abundance was positively correlated with pH ($p< 0.01$). The salinity showed a significantly negative correlation with the abundance of cladocera and a notably positive correlation with abundance of kollaplankton and meroplankton ($p< 0.01$). Both the abundance of other crustaceans and that of other plankton showed

TABLE 1 Correlation analysis of environmental parameters with different functional groups in the research area.

		Temperature	Salinity	pH	DO	Chl-a concentration
Cladocera	Pearson correlation	0.23*	-0.33**	-0.33**	-0.32**	-0.34**
	Significance (two-tailed)	0.03	0.001	0.001	0.002	0.001
Copepoda	Pearson correlation	-0.07	0.16	0.02	-0.11	-0.35**
	Significance (two-tailed)	0.48	0.13	0.83	0.27	0
Kollaplankton	Pearson correlation	-0.08	0.44**	0.27**	0.05	-0.24*
	Significance (two-tailed)	0.50	0	0.008	0.62	0.02
Large crustacean	Pearson correlation	0.13	-0.11	-0.10	-0.17	-0.22*
	Significance (two-tailed)	0.22	0.30	0.33	0.11	0.04
Meroplankton	Pearson correlation	-0.01	0.34**	0.18	-0.007	-0.21*
	Significance (two-tailed)	0.93	0.001	0.09	0.94	0.04
Other crustacean	Pearson correlation	-0.04	0.14	0.14	-0.06	-0.16
	Significance (two-tailed)	0.69	0.18	0.18	0.55	0.13
Other plankton	Pearson correlation	-0.02	-0.07	-0.04	-0.08	-0.18
	Significance (two-tailed)	0.82	0.53	0.67	0.43	0.08
Total abundance	Pearson correlation	0.02	0.25*	0.08	-0.11	-0.40**
	Significance (two-tailed)	0.88	0.01	0.43	0.27	0

*Correlation is significant at the 0.01 level (two-tailed).
**Correlation is significant at the 0.05 level (two-tailed).

no obvious correlation with the environmental parameters in the research area.

Dominance was calculated when the individual was identified to the species level. A total of 13 species were considered as dominant species, with dominance values higher than 0.02 (Table 2). In spring, *Dolioletta gegenbauri* was the most dominant species. Its mean abundance and relative abundance (RA) were 435.10 individuals/m^3 and 44.15%, respectively. It was followed by *Doliolum denticulatum* and *Centropages tenuiremis*, with mean abundance of 177.25 individuals/m^3 and 130.23 individuals/m^3, respectively. In summer, there were three new dominant species—*Peniliaavirostris*, *Evadne tergestina*, and *Acartia clausi*—with *P. avirostris* being the most dominant species in summer. Its abundance was 257.14 individuals/m^3, and its RA was 49.21%. Eight species were defined as dominant species in autumn, and the most dominant species was *A.clausi*, with an average abundance of 8.38 individuals/m^3 and RA of 22.88%. In winter, the dominant species were *E.tergestina* and *Temora turbinata*. Their abundance and RA were 231.48 individuals/m^3 and 46.76%, and 90.84 individuals/m^3 and 18.35%, respectively. In addition, the most dominant species showed an obvious seasonal variation in the research area and was abundant with a relatively high occurrence rate only in one or two surveys. In contrast, both the occurrence rate and the relative abundance of *T. turbinata* showed relatively higher values during the 1-year survey.

Specificity and occupancy of the zooplankton

The specificity and occupancy were calculated and projected onto a plot (Figure 4). In the plot, the x-axis indicates occupancy, which means how the species was distributed across all stations in that survey. As indicated by the spread across the x-axis, zooplankton displayed a highly varied occupancy in all surveys. Fewer species were present in all stations. The y-axis represents the specificity, which means whether that species was found in other surveys. The highest number of habitat-specialist species (20 species) was found in the winter survey, while there were eight, six, and two specialist species in autumn, spring, and summer, respectively.

Species which were specific to a habitat and common in their habitat at most sites were selected as indicator species of each survey when specificity and occupancy were greater or equal to 0.7 (dotted boxes in Figure 4). The number of indicator species differed significantly between different surveys (Table 3). *Dolioletta gegenbauri*, *D. denticulatum*, *Diphyes chamissonis*, *Sagitta bedoti*, and *C. tenuiremis* were selected as indicator species in spring. In summer, the indicator species were *A. clausi* and *P. avirostris*. *Aglaura hemistoma* was the only indicator species in winter. There was no species suitable as an indicator species in autumn.

The Pearson correlation analysis results revealed that zooplankton abundance was negatively associated with Chl-*a* ($p< 0.01$) and positively associated with salinity ($p< 0.05$). Nevertheless, the variations of indicator species were mainly affected by salinity and pH—for example, *D. gegenbauri*, *D. chamissonis*, *S. bedoti*, and *C. tenuiremis* had a significantly positive correlation with salinity ($p< 0.01$), whereas *A. clausi* and *P. avirostris* showed a significantly negative correlation with salinity ($p< 0.01$). Simultaneously, other significantly positive correlations included those between *D. denticulatum* and salinity and between *D. chamissonis*, *S. bedoti*, *C. tenuiremis*, and *D. gegenbauri* and pH. However, *A. clausi* and *P. avirostris* showed negative correlations with pH. In addition, the water temperature was significantly negatively correlated with *A.*

TABLE 2 The average abundance (AA), relative abundance (RA), and occurrence rate (OR) of dominant species in the research area.

Species	Spring			Summer			Autumn			Winter		
	AA	RA	OR	AA	RA	OR	AA	RA	OR	AA	RA	OR
Acartia clausi	7.20	0.01	0.54	**81.39**	**0.16**	**0.96**	**8.38**	**0.23**	**1.00**	12.34	0.02	0.54
Acartia danae	3.58	0.00	0.33	1.16	0.00	0.21	**3.13**	**0.09**	**0.88**	13.49	0.027	0.67
Canthocalanus pauper	19.60	0.02	0.75	0.95	0.00	0.25	**2.84**	**0.08**	**0.75**	9.22	0.02	0.58
Centropages tenuiremis	**130.23**	**0.13**	**1.00**	4.31	0.01	0.58	0.69	0.02	0.58	**20.00**	**0.04**	**0.88**
Doliolum denticulatum	**177.25**	**0.18**	**1.00**	0.04	0.00	0.04	0.00	0.00	0.00	1.27	0.00	0.46
Dolioletta gegenbauri	**435.10**	**0.44**	**1.00**	0.00	0.00	0.00	0.00	0.00	0.00	10.37	0.02	0.88
Evadne tergestina	12.01	0.01	0.83	**92.75**	**0.18**	**1.00**	0.18	0.00	0.25	**231.48**	**0.47**	**1.00**
Lucifer intermedius	0.87	0.00	0.38	6.24	0.01	0.88	2.33	0.06	0.96	1.60	0.00	0.46
Penilia avirostris	**69.11**	**0.07**	**0.92**	**257.14**	**0.49**	**1.00**	0.32	0.01	0.29	1.66	0.00	0.25
Sagitta enflata	4.01	0.00	0.83	0.67	0.00	0.42	**2.84**	**0.08**	**0.88**	4.32	0.01	0.92
Subeucalanus subcrassus	12.03	0.01	0.71	10.39	0.02	0.83	**1.22**	**0.03**	**0.63**	**13.10**	**0.03**	**0.88**
Temora turbinata	26.92	0.03	0.88	36.50	0.07	0.92	**3.60**	**0.10**	**0.96**	**90.84**	**0.18**	**1.00**
Tortanus gracilis	0.39	0.00	0.08	7.58	0.01	0.79	**1.76**	**0.05**	**0.92**	5.03	0.01	0.75

Bold values is that species was the dominant species on that survey.

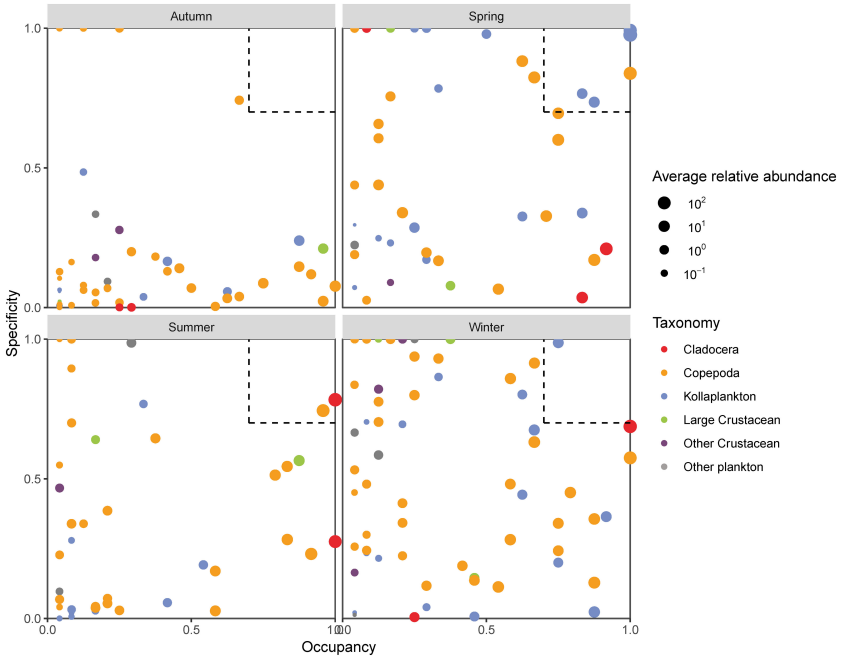

FIGURE 4
SPEC-OCCU plots of zooplankton.

hemistoma but positively correlated with *A. clausi* and *P. avirostris*. The DO showed a significantly negative correlation with *A. clausi* and *P. avirostris*. The Chl-*a* concentration was significantly negatively correlated with *D. gegenbauri*, *D. chamissonis*, *S. bedoti*, C. *tenuiremis*, and *P. avirostris*.

Discussion

Daya Bay, which is located in a subtropical zone, is a semi-closed bay. Due to the influence of the monsoon, there is plenty of rainfall from May to October and less from November to April (Wu and Wang, 2007). In the dry season (winter), the northeast monsoon prevails, with low temperatures and precipitation. In contrast, in the wet season (summer), the southwest monsoon predominates, with relatively high levels of precipitation and temperature. Spring and autumn are the monsoon transition seasons in the research area (Xu, 1989; Wu et al., 2009; Wu et al., 2010, Wu et al., 2011, Wu et al., 2012; Wu et al., 2016). The highest surface water temperature was observed during summer in this study. Owing to the precipitation and runoff, the surface water was diluted, resulting in relatively low salinity, pH, DO, and Chl-*a* concentration in summer. The correlation analysis showed that there was a significantly positive correlation between salinity, DO, and pH. Nevertheless, a significantly negative correlation was observed between DO and Chl-*a* in summer (Supplementary), which was consistent with the results reported for the northern region of the South China Sea during autumn (Long et al., 2006). Shen et al. (2017) reported that a significantly negative correlation was also observed between salinity and Chl-*a* in Daya Bay. In contrast, we found a notably positive correlation between Chl-*a* and salinity in autumn and a negative correlation in spring. However, no

TABLE 3 Mean abundance (MA), specificity, and occupancy of indicator species.

Species	Specificity (%)	Occupancy (%)	MA (individuals/m^3)	Cruise
Dolioletta gegenbauri	97.67	100.00	435.10	Spring
Doliolum denticulatum	99.27	100.00	177.25	Spring
Diphyes chamissonis	76.62	83.33	3.48	Spring
Sagitta bedoti	73.59	87.50	5.47	Spring
Centropages tenuiremis	83.90	100.00	130.23	Spring
Acartia clausi	74.45	95.83	81.39	Summer
Penilia avirostris	78.34	100.00	257.15	Summer
Aglaura hemistoma	98.78	75.00	4.41	Winter

obvious correlation was detected between Chl-*a* and salinity in summer or winter in this study. During the dry and monsoon transition seasons, the values of surface water salinity, pH, and DO remained fairly constant without the effects of rainfall dilution in the research area.

Zooplankton species composition and abundance are known to change seasonally in the marine environment (Sammacro and Crenshaw, 1984). Zooplankton diversity and abundance are also greatly affected by environmental parameters (Wang et al., 2018; Aguilera, 2020; Wang et al., 2020; Wang et al., 2022). In this study, there was a significantly negative correlation between the total zooplankton abundance and Chl-*a* concentration. This finding was in accordance with the result of Jiang and Wang (2020). They found that the seasonal change of zooplankton had its own characteristic pattern, which did not coincide with the phytoplankton but lagged behind by nearly 1 month (Jiang and Wang, 2020). Similarly, in our research, there was a significant seasonal variation in zooplankton composition, and the highest species number was observed in winter. Interestingly, many warm temperature species appeared in winter. This warm temperature species intrusion could be carried by the China Coastal Current—for instance, *Salpa fusiformis* has been defined as a warm temperature indicator species in California and displays a massive occurrence in the Southern Yellow Sea during summer (Silver, 1975; Liu et al., 2012). *Calanus sinicus* is the indicator species of the China Coastal Current in the Taiwan Strait and was collected only during winter in the research area (Hwang and Wong, 2005; Wang et al., 2020). In addition, the zooplankton abundance was highest in spring. *Dolioletta gegenbauri* is a warm-water species which was the most dominant species in spring. It commonly appears in productive subtropical neritic regions worldwide. The abundance of *D. gegenbauri* is usually at bloom concentrations, which could consume a large fraction of daily primary production (Paffenhöfer and Köster, 2011; Walters et al., 2019).

Temora turbinata is regarded as the predominant species in mesozooplankton communities in various environments around the world. It is able to adapt to various habitats, such as eutrophic lagoons, polluted and eutrophicated waters, outfall areas, and nuclear power plant discharge areas (Hsu et al., 2008; Tseng et al., 2011; Wang et al., 2021). In particular, *T. turbinate* and *Karenia brevis* can co-occur in the Gulf of Mexico. *Karenia brevis* is a toxic dinoflagellate, which often causes blooms (Lester et al., 2008). Copepodites and adults of *T. turbinata* are often found in upwelled water masses which are usually preferred by *D. gegenbauri* (Paffenhöfer and Köster, 2011). Li et al. (2018) reported that *T. turbinanta* ranges in abundance from 1 individual/m^3 to 1,185 individuals/m^3 in Daya Bay, and the highest abundance was recorded during a winter survey in 2017. Consistent with previous results, *T. turbinata* was the only dominant species present throughout the year. *Temora turbinanta* was recorded during our 1-year survey, and the average abundance ranged from 3.60 individuals/m^3 (autumn) to 90.84 individuals/m^3 (winter) in this study. *T. turbinanta* abundance changed significantly with season, but it was the dominant species throughout the year. Thus, we suggest that *T. turbinanta* could be considered as a potential indicator species to monitor its aquatic habitat. Notably, *T. turbinanta* abundance was obviously lower in the research area than in the northeast coastal area of Taiwan (Tseng et al., 2011; Wang et al., 2021). The seasonal variation characteristics of *T. turbinanta* abundance were also different. Undoubtedly, these differences could be due to differences in sampling method, local conditions, or the thermal discharge from the nuclear power plant in Daya Bay. Additionally, the other indicator species, *P. avirostris*, is not only a quality live food supply for marine pelagic fish but also an important component of the zooplankton community of many tropical, subtropical, and temperate waters and occurs seasonally with especially high abundance in summertime (Calbet et al., 2001; Fernández de Puelles et al., 2003; Marazzo and Valentin, 2003; Rose et al., 2004). The body length of female *P. avirostris* ranges from 0.70 to 1.09 mm (Zhou et al., 2022). Thus, *P. avirostris* blooms could block the cooling system of a nuclear power plant by attracting huge numbers of larva and adult pelagic fish (such as herring, mackerel, sardine, horse mackerel, *etc.*). *Centropages tenuiremis* is an important common copepod in the neritic mesozooplankton assemblage. It is an obviously omnivorous feeding species and can expand its food spectrum under stressful conditions (Xu et al., 2020). *Dolioletta gegenbauri* and *D. denticulatum* have been reported to form dense blooms in shallow waters of the continental shelf (Paffenhöfer et al., 1995; Nakamura, 1998; Tew and Lo, 2005). Our results are consistent with previous reports (Lian et al., 2011; Li et al., 2011; Li et al., 2021). These species mentioned above have also become the dominant species in Daya Bay. Additionally, our research revealed that *P. avirostris* blooms and *C. tenuiremis* blooms might also threaten the cooling system by acting as the food supply for pelagic fish in spring. It is noteworthy that most of the above-mentioned indicator species in spring belong to kollaplankton. Thus, we suggest that kollaplankton could cause potential disaster to the nuclear power plant cooling system due to their relatively large body size and potential to form huge blooms in spring. Moreover, *C. tenuiremis* blooms in spring and *P. avirostris* blooms in summer could also threaten the cooling system security by attracting larva or adult pelagic fish assemblages into Daya Bay. Therefore, these species should be considered as key species in future ecological studies.

Conclusion

In summary, the zooplankton communities showed a significant seasonal variation in terms of species composition, abundance, and dominant species in Daya Bay. Seasonal variations in the dominant species were observably related to environmental variations, such as thermal discharge, pH, salinity, and Chl-*a*. Thus, zooplankton could be considered as a favorable indicator of the marine environment. In addition, some kollaplankton, cladocera, and copepod species might directly or indirectly affect nuclear power plant cooling systems.

Data availability statement

The original contributions presented in the study are included in the article/Supplementary Material. Further inquiries can be directed to the corresponding authors.

Author contributions

F-XW: conceptualization, data curation, writing—original draft, and writing—review and editing. H-HH: Writing—review and editing and funding acquisition. Y-GW: Writing—review and editing, validation, and visualization. Y-GG: investigation and supervision. Q-XL, S-FZ, Y-YR, H-XL, and MD: investigation and formal analysis. All authors contributed to the article and approved the submitted version.

Funding

We gratefully acknowledge the National Key Research and Development Program of China (2018YFC1407501), Central Public-interest Scientific Institution Basal Research Fund, CAFS (NO.2020TD15), Central Public-interest Scientific Institution Basal Research FundSouth China Sea Fisheries Research Institute, Chinese Academy of Fishery Sciences (2021SD03), Guangdong Basic and Applied Basic Research Foundation (2020A1515010331, 2022A1515110603), Guangzhou Basic and Applied Basic Research Foundation (202201010306) and Fund of Guangdong Provincial Key Laboratory of Fishery Ecology and Environment (FEEL-2022-9).

Acknowledgments

We thank Xian Zhou, Xiao-Qing Qin, Sheng-Qi Du, and Zhi-Hui Zhong for their help in sample collection and Zhen Tan, Gang Hou, and Chuang-Hao Pan for their help in data analysis. In addition, we thank International Science Editing (http://www.internationalscienceediting.com) for editing this manuscript.

Conflict of interest

The authors declare that the research was conducted in the absence of any commercial or financial relationships that could be construed as a potential conflict of interest.

Publisher's note

Supplementary material

The Supplementary Material for this article can be found online at: https://www.frontiersin.org/articles/10.3389/fmars.2023.1110160/full#supplementary-material

References

Aguilera, V. M. (2020). pH and other upwelling hydrographic drivers in regulating copepod reproduction during the 2015 El nino event: A follow-up study. *Estuar. Coast. Shelf S.* 234, 106640. doi: 10.1016/j.ecss.2020.106640

An, L. N., Wang, L., Huang, H., Ou, D. Y., and Li, W. W. (2021). Population dynamics of acetes chiensis and its response to environmental factors in western daya bay. *J. of. Appl. Oceanography.* 40 (3), 403–412.

Calbet, A., Garrido, S., Saiz, E., Alcaraz, M., and Duarte, M. (2001). Annual zooplankton succession in coastal NW Mediterranean waters: The importance of the smaller size fractions. *J. Plankton Res.* 23 (3), 319–331. doi: 10.1093/plankt/23.3.319

Carter, J. L., Schindler, D. E., and Francis, T. B. (2017). Effects of climate change on zooplankton community interactions in an alaskan lake. *Climate Change Responses.* 4 (3), 1–12. doi: 10.1186/s40665-017-0031-x

Chen, Q. C. (1992). *Zooplankton of China seas* Vol. 1 (Beijing, China: Science Press), 1–87.

Chen, Q. C., and Zhang, S. Z. (1965). The planktonic copepods of the yellow Sea and the East China sea. i. calanoida. *Studia Mar. Sin.* 7, 20–131.

Chihara, M., and Murano, M. (1997). *An illustrated guide to marine plankton in Japan* (Tokyo, Japan: Tokai University Press), pp1–1000.

Dam, H. G. (2013). Evolutionary adaptation of marine zooplankton to global change. *Annu. Rev. Mar. Sci.* 5, 349–370. doi: 10.1146/annurev-marine-121211-172229

Dufrene, M., and Legendre, P. (1997). Species assemblages and indicator species: the need for a flexible asymmetrical approach. *Ecological Monographs* 67 (3), 345–366.

Fernández de Puelles, M. L., Pinot, J. M., and Valencia, J. (2003). Seasonal and inter-annual variability of zooplankton community in water off mallorca island (Balearic Sea, Western mediterranean): 1994-1999. *Oceanolog. Acta* 26, 673–686. doi: 10.1016/j.oceact.2003.07.001

Herrera-Silveira, J. A., and Morales-Ojeda, S. M. (2009). Evaluation of the health status of a coastal ecosystem in southeast Mexico: Assessment of water quality, phytoplankton and submerged aquatic vegetation. *Mar. pollut. Bull.* 59, 72–86. doi: 10.1016/j.marpolbul.2008.11.017

Hsu, P. K., Lo, W. T., and Shih, C. T. (2008). The coupling of copepod assemblages and hydrography in a eutrophic lagoon in Taiwan: Seasonal and spatial variations. *Zool. Stud.* 47, 172–184.

Hwang, J. S., and Wong, C. K. (2005). The China coastal current as a driving force for transporting *Calans sinicus* (Copepoda: Calanioida) from its population centers to waters off Taiwan and Hong Kong during the winter northeast monsoon period. *J. Plankton Res.* 27, 205–210. doi: 10.1093/plankt/fbh162

Jiang, R., and Wang, Y. S. (2020). Modeling the ecosystem response of the semi-closed daya bay to the thermal discharge from two nearby nuclear power plants. *Ecotoxicology.* 29, 736–750. doi: 10.1007/s10646-020-02229-w

Kemp, W. M., and Boynton, W. R. (2012). Synthesis in estuarine and coastal ecological research: What is it, why is it important, and how do we teach it? *Estuar. Coast.* 35, 1–22. doi: 10.1007/s12237-011-9464-9

Lange, H. J. D., Sala, S., Vighi, M., and Faber, J. H. (2010). Ecological vulnerability in risk assessment-a review and perspectives. *Sci. Total Environ.* 408 (18), 3871. doi: 10.1016/j.scitotenv.2009.11.009

Lester, K. M., Heil, C. A., Neely, M. B., Spence, D. N., Murasko, S., Hopkins, T. L., et al. (2008). Zooplankton and *Karenia brevis* in the gulf of Mexico. *Cont. Shelf Res.* 28, 99–111. doi: 10.1016/j.csr.2007.04.009

Lian, X. P., Tan, Y. H., Huang, L. M., Chen, Q. C., Li, K. Z., and Liu, Y. H. (2011). Space-time variations and impact factors of macro-meso zooplankton in daya bay (in Chinese). *Mar. Environ. Science.* 30 (5), 640–645.

Lian, G. S., Wang, Y. G., Sun, R. X., and Hwang, J. S. (2019). *Species diversity of marine planktonic copepods in china's seas* (Beijing, China: China Ocean Press), Pp 868.

Li, Y. M., Han, L. Y., Chen, M. R., and Tong, M. M. (2018). The mesozooplankton community structure and their herbivory in daya bay. *Oceanologia Limnologia Sinica.* 49 (4), 839–850. doi: 10.11693/hyhz20180100020

Li, K. Z., Ma, J., Huang, L. M., Tan, Y. H., and Song, X. Y. (2021). Environmental drivers of temporal and spatial fluctuations of mesozooplankton community in daya bay, northern south China Sea. *J. Ocean. U. China.* 20 (4), 1013–1026. doi: 10.1007/s11802-021-4602-x

Liu, J. J., Ni, Z. X., Diao, Z. H., Hu, Y. X., and Xu, X. R. (2018). Contamination level, chemical fraction and ecological risk of heavy metals in sediments from daya bay, south China Sea. *Mar. pollut. Bull.* 128, 132–139. doi: 10.1016/j.marpolbul.2018.01.021

Liu, Y. Q., Sun, S., and Zhang, G. T. (2012). Seasonal variation in abundance, diel vertical migration and body size of pelagic tunicate *Salp fusiformis* in the southern yellow Sea. *Chin. J. Oceanology Limnology.* 30 (1), 92–104. doi: 10.1007/s00343-012-1048-4

Liu, Q. X., Zhou, L. B., Zhang, W. R., Zhang, L., Tan, Y. H., Han, T. T., et al. (2022). Rising temperature contributed to the outbreak of macrozooplankton *Creseis acicula* by enhancing its feeding and assimilation for algal food nearby the coastal daya bay nuclear power plant. *Ecotox. Environ. Safe.* 238, 113606. doi: 10.1016/j.ecoenv.2022.113606

Li, K. Z., Yin, J. Q., Huang, L. M., Zhang, J. L., Lian, S. M., and Liu, C. W. (2011). Distribution and abundance of thaliaceans in the northwest continental shelf of south China Sea, with response to environmental factors driven by monsoon. *Cont. Shelf Res.* 31 (9), 979–989. doi: 10.1016/j.csr.2011.03.004

Li, K. Z., Yin, J. Q., Tan, Y. H., Huang, L. M., and Song, X. Y. (2014). Short-term variation in zooplankton community from daya bay with outbreaks of *Penilia avirostris*. *Oceanologia.* 56, 583–602. doi: 10.5697/oc.56-3.583

Long, A. M., Chen, S. Y., Zhou, W. H., Xu, J. R., Sun, C. C., Zhang, F. Q., et al. (2006). Distribution of macro-nutrients, dissolved oxygen, pH and chl *a* and their relationships in northern south China Sea. *Mar. Sci. Bulletin.* 25 (5), 9–16.

Marazzo, A., and Valentin, J. L. (2003). *Penilia avirostris* (Crustacea, ctenopoda) in a tropical bay: variations in density and aspects of reproduction. *Acta Oecologica.* 24, 251–257. doi: 10.1016/S1146-609X(03)00019-5

Nakamura, Y. (1998). Blooms of tunicates oikopleura spp. and *Dolioletta gegenbauri* in the seto inland Sea, Japan, during summer. *Hydrobiogia.* 385 (1-3), 183–192.

Paffenhöfer, G. A., Atkinson, L. P., Lee, T. N., Verity, P. G., and Bulluck, L. R. (1995). Distribution and abundance of thaliaceans and copepods off the southeastern USA during winter. *Cont. Shelf Res.* 15 (2-3), 255–280. doi: 10.1016/0278-4343(94)E0004-6

Paffenhöfer, G. A., and Köster, M. (2011). From one to many: On the life cycle of *Dolioletta gegenbauri* uljanin (Tunicata, thaliacea). *J. Plankton Res.* 33 (7), 1139–1145. doi: 10.1093/plankt/fbr001

Rice, E., Dam, H. G., and Stewart, G. (2015). Impact of climate change on estuarine zooplankton surface water warming in long island sound is associated with changes in copepod size and community structure. *Estuar. Coast.* 38, 13–23. doi: 10.1007/s12237-014-9770-0

Rissik, D., Shon, E. H., Newell, B., Baird, M. E., and Suthers, I. M. (2009). Plankton dynamics due to rainfall, eutrophication, dilution, grazing and assimilation in an urbanized coastal lagoon. *Estuar. Coast. Shelf S.* 84, 99–107. doi: 10.1016/j.ecss.2009.06.009

Rose, K., Roff, J. C., and Hopcrof, R. R. (2004). Production of *Penilia avirostris* in Kingston harbour, Jamaica. *J. Plankton Res.* 26 (3), 1–11. doi: 10.1093/plankt/fbh059

Sammacro, P. W., and Crenshaw, H. (1984). Plankton community dynamics of the central great barrier reef lagoon: analysis of data from ikeda et al. *Mar. Biol.* 82 (2), 167–180.

Shen, C. Y., Chen, H. S., and Zhao, H. (2017). The satellite remotely-sensed analysis of temporal and spatial variation of surface chlorophyll in the daya bay. *J. Guangdong Ocean University.* 37 (6), 57–64.

Shi, Y. Q., Sun, S., Zhang, G. T., Wang, S. W., and Li, C. L. (2015). Distribution pattern of zooplankton functional groups in the yellow Sea in June: A possible cause for geographical separation of giant jellyfish species. *Hydrobiologia.* 754 (1), 43–58. doi: 10.1007/s10750-014-2070-7

Silver, M. W. (1975). The habitat of *Salpa fusiformis* in the California current as defined by indicator assemblages. *Limnol. Oceanogr.* 20 (2), 230–237. doi: 10.4319/lo.1975.20.2.0230

Song, X. Y., Huang, L. M., Zhang, J. L., Huang, X. P., Zhang, J. B., Yin, J. Q., et al. (2004). Variation of phytoplankton biomass and primary production in daya bay during spring and summer. *Mar. pollut. Bull.* 49 (11-12), 1036–1044. doi: 10.1016/j.marpolbul.2004.07.008

Sun, S., Huo, Y., and Yang, B. (2010). Zooplankton functional groups on the continental shelf of the yellow Sea. *Deep-Sea Res. PT. II.* 57 (11), 1006–1016. doi: 10.1016/j.dsr2.2010.02.002

Tew, K. S., and Lo, W. T. (2005). Distribution of thaliacea in SW Taiwan coastal water in 1997, with special reference to *Doliolum denticulatum*, *Thalia democratica* and *T. orientalis*. *Mar. Ecol. Prog. Ser.* 292, 181–193. doi: 10.3354/meps292181

Tseng, L. C., Kumar, R., Chen, Q. C., and Hwang, J. S. (2011). Faunal shift between two copepod congeners (*Temora discaudata* and *T. turbinata*) in the vicinity of two nuclear power plants in southern East China Sea: Spatiotemporal patterns of population trajectories over a decade. *Hydrobiologia.* 666, 301–315. doi: 10.1007/s10750-011-0616-5

Walters, T. L., Gibson, D. M., and Frischer, M. E. (2019). Cultivation of the marine pelagic tunicate *Dolioletta gegenbauri* (Uljanin 1884) for experimental studies. *Jove.-J. Vis. Exp.* 9, 150.

Wang, Y. G., Chen, X. Y., Xing, B. P., Sun, R. X., Fitria, N., Xiang, P., et al. (2018). Zooplankton composition and distribution in the lembeh strait of north sulawesi, Indonesia. *Acta Oceanol. Sin.* 37 (12), 35–44. doi: 10.1007/s13131-018-1286-1

Wang, Y. G., Tseng, L. C., Sun, R. X., Chen, X. Y., Xiang, P., Wang, C. G., et al. (2022). Copepods as indicators of different water masses during the northeast monsoon prevailing period in the northeast Taiwan. *Biology.* 11, 1–16, 1357. doi: 10.3390/biology11091357

Wang, Y. G., Tseng, L. C., Xing, B. P., Sun, R. X., Chen, X. Y., Wang, C. G., et al. (2021). Seasonal population structure of the copepod *Temora turbinata* (Dana 1849) in the kuroshio current edge, southeastern East China Sea. *Appl. Sci.* 11, 7545. doi: 10.3390/app11167545

Wang, Y. G., Zeng, L. C., Sun, R. X., Liu, Z. Y., Lin, M., and Hwang, J. S. (2020). Effects of the China coastal current on the community structure of planktonic copepods in early spring, with note on eurytemora pacifica sato 1913 in the Western Taiwan strait. *Crustaceana.* 93 (3-5), 487–506. doi: 10.1163/15685403-00004010

Wu, R. H., Cai, S. Q., Wang, S. A., and Zhang, W. J. (2007). Three-dimensional numerical simulation of tidal current and residual current at daya bay. *J. Trop. Oceanography.* 26 (3), 18–23.

Wu, M. L., and Wang, Y. S. (2007). Using chemometrics to evaluate anthropogenic effects in daya bay, china. estuar. *Coast. Shelf Sci.* 72, 732–742. doi: 10.1016/j.ecss.2006.11.032

Wu, M. L., Wang, Y. S., Dong, J. D., Sun, C. C., Wang, Y. T., Sun, F. L., et al. (2011). Investigation of spatial and temporal trends in water quality in daya bay, south China Sea. *Int. J. Environ. Res. Public Health* 8, 2352–2365. doi: 10.3390/ijerph8062352

Wu, M. L., Wang, Y. S., Sun, C. C., Sun, F. L., Cheng, H., Wang, Y. T., et al. (2012). Monsoon-driven dynamics of water quality by multivariate statistical methods in daya bay, south China sea. *Oceanol. Hydrobiol. Stud.* 41, 66–76. doi: 10.2478/s13545-012-0040-0

Wu, M. L., Wang, Y. S., Sun, C. C., Wang, H., Dong, J. D., and Han, S. H. (2009). Identification of anthropogenic effects and seasonality on water quality in daya bay, south China Sea. *J. Environ. Manage.* 90 (10), 3082–3090. doi: 10.1016/j.jenvman.2009.04.017

Wu, M. L., Wang, Y. S., Sun, C. C., Wang, H. L., Dong, J. D., Yin, J. P., et al. (2010). Identification of coastal water quality by statistical analysis methods in daya bay, south China Sea. *Mar. pollut. Bull.* 60, 852–860. doi: 10.1016/j.marpolbul.2010.01.007

Wu, M. L., Wang, Y. S., Wang, Y. T., Sun, F.-L., Sun, C. C., Cheng, H., et al. (2016). Seasonal and spatial variations of water quality and trophic status in daya bay, south China Sea. *Mar. pollut. Bull.* 112, 341–348. doi: 10.1016/j.marpolbul.2016.07.042

Xiang, C. H., Ke, Z. X., Li, K. Z., Liu, J. X., Zhou, L. B., Lian, X. P., et al. (2021). Effects of terrestrial inputs and seawater intrusion on zooplankton community structure in daya bay, south China Sea. *Mar. pollut. Bull.* 167, 112331. doi: 10.1016/j.marpolbul.2021.112331

Xu, G. Z. (1989). *Environments and resources of daya bay* (HeFei, China: Anhui Science Publishing House).

Xu, C. J., Hu, S. M., Guo, Z. L., Li, T., Huang, H., Chan, L. L., et al. (2020). Flexible feeding patterns of copepod *Centropages tenuiremis* in fluctuating conditions: A possible survival strategy to cope with disturbance. *Acta Oceanol. Sin.* 39 (2), 59–68. doi: 10.1007/s13131-020-1553-9

Yuan, K. R., Wang, J. J., Lin, J. Y., Han, Y., Wang, K. M., Xu, Y. C., et al. (2021). Analysis of the seasonal variation of the residual currents by HF surface wave radar data in adjacent waters of daya bay. *J. Appl. Oceanography.* 40 (2), 271–283.

Zeng, L., Chen, G. B., Wang, T., Yang, B. Z., Yu, J., Liao, X. L., et al. (2019). Acoustic detection and analysis of *Acetes chinensis* in the adjacent waters of the daya bay nuclear power plant. *J. fishery Sci. China.* 26 (6), 1029–1039.

Zeng, L., Chen, G. B., Wang, T., Zhang, S. F., Dai, M., Yu, J., et al. (2021). Acoustic study on the outbreak of *Creseise acicula* nearby the daya bay nuclear power plant base during the summer of 2020. *Mar. pollut. Bull.* 165, 112144. doi: 10.1016/j.marpolbul.2021.112144

Zhang, L., Xiong, L., Li, J., and Huang, X. (2021). Long-term changes of nutrients and biocenoses indicating the anthropogenic influences on ecosystem in jiaozhou bay and daya bay, China. *Mar. pollut. Bull.* 168, 112406. doi: 10.1016/j.marpolbul.2021.112406

Zhao, J. J., Zhang, H. C., Liu, J. X., Ke, Z. X., Xiang, C. H., Zhang, L. M., et al. (2022). Role of jellyfish in mesozooplankton community stability in a subtropical bay under the long-term impacts of temperature changes. *Sci. Total Environ.* 849, 157627. doi: 10.1016/j.scitotenv.2022.157627

Zheng, Z., Li, S. J., and Xu, Z. Z. (1984). *Marine planktology (In Chinese)* (Beijing: China Ocean Press), 1–653.

Zhou, X. N., Zhao, W., and Yin, D. P. (2022). Research progress of ecological distribution and cultivation utilization in cladoceran *Penilia avirostris*: A review. *J. Dalian Ocean University.* 37 (2), 345–351.

frontiers | Frontiers in Marine Science

TYPE Original Research
PUBLISHED 15 March 2023
DOI 10.3389/fmars.2023.1075059

OPEN ACCESS

EDITED BY
Paulo João Vieira Vale,
Portuguese Institute for Sea and Atmosphere (IPMA), Portugal

REVIEWED BY
Pengbin Wang,
Ministry of Natural Resources, China
Sun Cuici,
South China Sea Institute of Oceanology (CAS), China

*CORRESPONDENCE
Honghui Huang
huanghh@scsfri.ac.cn

SPECIALTY SECTION
This article was submitted to Marine Pollution, a section of the journal Frontiers in Marine Science

RECEIVED 20 October 2022
ACCEPTED 02 March 2023
PUBLISHED 15 March 2023

CITATION
Shi R, Qi Z, Han T, Dai M, Zhang S and Huang H (2023) Responses of bacterioplankton, particle- and colony-attached bacterial communities to *Phaeocystis globosa* blooms in Mirs Bay, China. *Front. Mar. Sci.* 10:1075059. doi: 10.3389/fmars.2023.1075059

Responses of bacterioplankton, particle- and colony-attached bacterial communities to *Phaeocystis globosa* blooms in Mirs Bay, China

Rongjun Shi, Zhanhui Qi, Tingting Han, Ming Dai, Shufei Zhang and Honghui Huang*

Guangdong Provincial Key Laboratory of Fishery Ecology and Environment, Key Laboratory of Open-Sea Fishery Development, Ministry of Agriculture and Rural Affairs of China, South China Sea Fisheries Research Institute, Chinese Academy of Fishery Science, Guangzhou, China

Microalgae blooms are a frequent occurrence in coastal waters worldwide. It is reasonable to assume that these blooms have various influences on bacterial communities, which in turn may affect the development and dissipation of the bloom. However, the bacterial community characteristics, particularly of attached bacteria, associated with microalgae blooms remain unclear. In this study, we investigated the community profiles of bacteria using high-throughput sequencing during a *Phaeocystis globosa* bloom in Mirs Bay, southern China, in January 2021. Bacteria living in three habitats, i.e., bacterioplankton, particle-attached bacteria, and colony-attached bacteria, were studied from the exponential growth phase to the decline growth phase of the bloom. Distinct variations in bacterial community composition existed among the three habitats. Bacteroidota, Proteobacteria, and Cyanobacteria were the dominant phyla of bacterioplankton, particle–attached bacteria, and colony-attached bacteria, respectively. Richness and diversity were significantly highest ($p < 0.01$) in particle-attached bacteria, followed by bacterioplankton, and lowest in colony-attached bacteria. The community diversities of bacterioplankton and particle-attached bacteria decreased significantly ($p < 0.05$) as the bloom shifted from the exponential to the decline phase. During the decline growth phase of the bloom, Bacteroidota and Verrucomicrobiota were the dominant remarkably abundant bacteria in the bacterioplankton community, whereas Verrucomicrobiota was dominant in the particle-attached bacteria community. No significant difference was observed in the colony-attached bacterial community between the exponential and decline phases of the *P. globosa* bloom owing to their complex network. The results of this study suggest that *P. globose* bloom has a profound impact on marine bacteria, particularly species that can decompose organic matter, which could play a crucial role in the dissipation of algal blooms.

KEYWORDS

***Phaeocystis globosa* bloom, bacterioplankton, particle-attached bacteria, colony-attached bacteria, Mirs Bay**

Introduction

The formation and dissipation of algal blooms, which are caused by the rapid growth of one or more phytoplankton species, are known to be affected by various environmental factors, such as temperature, salinity, eutrophic conditions, and light intensity (Higashi et al., 2016). The interactions between algae and other organisms, such as marine bacteria that rely on the organic matter secreted by algae, are crucial for algal growth (Anderson et al., 2002; Higashi et al., 2016). The community compositions of bacteria, which play critical roles in the marine ecosystem by participating in biochemical reactions and associate with chemical transformations of almost all elements, are sensitive to environmental changes (Arrigo, 2004; Comte and Del Giorgio, 2010; Ruiz-Gonzalez et al., 2013; Sun et al., 2017; Xia et al., 2020). Previous studies have suggested that bacterial communities can be significantly influenced by algal blooms, such as diatom blooms (Liu et al., 2019; Sun et al., 2020), dinoflagellate *Karenia brevis* blooms (Meyer et al., 2014), and dinoflagellate *Noctiluca scintillans* blooms in marine waters (Xia et al., 2020). Therefore, it is hypothesized that the occurrence of *Phaeocystis globosa* bloom in this study is likely to have a substantial impact on bacteria.

A wide range of interactions between bacteria and phytoplankton determine the composition of bacterial communities (Cole, 1982; Sher et al., 2011; Delmont et al., 2014). Most marine bacteria in seawater are free-living (bacterioplankton), while some are attached bacteria with sophisticated interactions with their hosts (Worden et al., 2015). Bacteria can decompose organic matter such as microalgae cells and use algal polysaccharides as a carbon source (Teeling et al., 2016), making attached bacteria more important in the dissipation of bloom due to their interaction with their attached host. However, most research has focused on bacterioplankton and its interaction with algae, neglecting information on community structures of attached bacteria and their temporal variations with bloom development, which is essential for understanding the complex interactions between microalgae and bacteria, quite limited (Meyer et al., 2014; Li et al., 2020).

In January 2021, a bloom of *P. globosa*, which alternates between solitary cells (3–10 μm in diameter) and gelatinous colonies (3 cm in maximal diameter), occurred for the first time in Mirs Bay, southern China (Wang et al., 2021a; Wang et al., 2021b). Of the seven identified colony-forming *Phaeocystis* species, *P. globosa* is the most widespread, and its bloom could affect the bacterioplankton community by environmental filtering of specific taxa (Li et al., 2020). The gelatinous colonies of *P. globosa* may also favor the attachment of specific bacteria, further affecting the blooming process. To understand the effects of *P. globosa* bloom, it is necessary to consider not only bacterioplankton but also attached bacteria, may play an important role in the outbreak and dissipation of algal blooms.

In this study, we investigated the community profiles of bacteria during a *P. globosa* bloom in Mirs Bay, southern China. Bacteria living in three habitats, i.e., bacterioplankton, particle-attached bacteria, and colony-attached bacteria, were studied from the exponential growth phase to the decline growth phase of the bloom. This study aimed to investigate the differences in bacterial communities among three habitats and their temporal variations during blooming, as well as the interactions between microalgae and bacteria.

Materials and methods

Study sites and sampling protocols

Mirs Bay, located between Dapeng Peninsula in Shenzhen and Kowloon Peninsula in Hong Kong, is a semi-enclosed subtropical bay with a high frequency of HABs due to the rapid development of marine aquaculture, tourism, and commercial shipping (Chan et al., 2008). In 2021, a *P. globosa* bloom occurred in Mirs Bay along the Shenzhen coast from 23 January to 3 February. During the bloom, triplicate surface water samples were collected daily from January 22 to 28, and every second day from January 30 to February 3 at stations S1 and S2 (Figure 1).

For bacterial DNA, three kinds of bacteria (bacterioplankton, particle-attached bacteria, and colony-attached bacteria) were collected. Specifically, 1 L of water was pre-filtered with a 20-μm-pore-size bolting cloth to remove debris and larger organisms and then filtered sequentially through 3-μm-pore-size and 0.2-μm-pore-size membranes (Merck Millipore, Bedford, MA, USA). Bacteria retained on the 3-μm-pore-size membranes and 0.2-μm-pore-size membranes were particle-attached bacteria and bacterioplankton, respectively. Additionally, 40 P. *globosa* colonies were absorbed by pipette, washed twice with sterile seawater, and filtered with a 3-μm-pore-size polycarbonate membrane. Bacteria retained on the 3-μm-pore-size membranes were colony-attached bacteria. The bacteria retained on the membranes were all stored at −80°C for DNA extraction.

Environmental factor analysis

Water temperature, salinity, dissolved oxygen (DO), and pH were measured using multiprobe sonde (Yellow Springs Instrument Co., Dayton, OH, USA), and the density of *P.* globosa colony was counted directly *in situ* to evaluate the different growth stages of *P. globosa*. The density of *Akashiwo sanguinea* was measured using FlowCAM8400 (Yokogawa Fluid Imaging Technologies, Inc., Scarborough, Maine, USA). The concentrations of Chl *a*, NO_3^-, NH_4^+, NO_2^-, PO_4^{3-}, and chemical oxygen demand (COD) were measured according to marine monitoring specifications (GB/T 12763.4-2007, 2007). 0.5 L seawater was filtered through a pre-combusted GF/F membrane, and the concentrations of dissolved inorganic carbon (DIC) and dissolved total carbon (DTC) were measured according to the method of Chen et al. (2020), with dissolved organic carbon (DOC) being the difference value between DTC and DIC.

DNA extraction, sequencing, and analysis

DNA extraction was based on the manufacturer's instructions of the E.Z.N.A. Water DNA Kit (Omega Bio-Tek, Inc., Norcross, GA, USA). The concentration and quality of DNA were determined

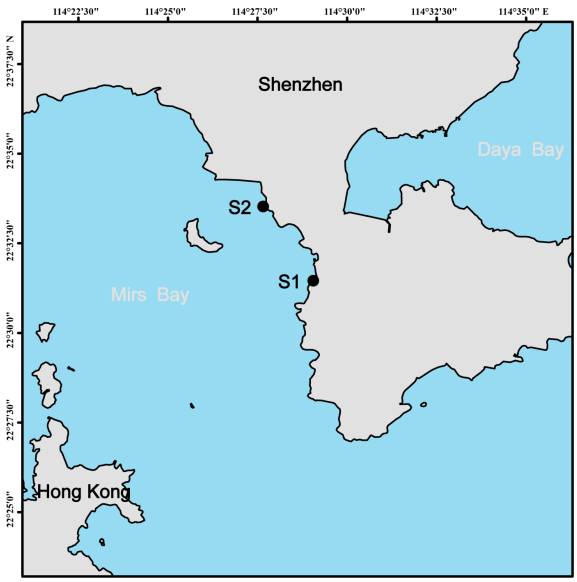

FIGURE 1
Sampling stations (●) in Mirs Bay during the *phaeocystis globosa* bloom.

by NanoDrop 2000 UV-vis spectrophotometer (Thermo Scientific, Wilmington, USA) and 1% agarose gel electrophoresis, respectively. The PCR amplification primers of bacterial V4-V5 regions were 515F (5′-GTGYCAGCMGCCGCGGTAA-3′) and 926R (5′-CCGYCAATTYMTTTRAGTTT-3′) (Parada et al., 2015). PCR reactions, further processing, and sequencing of PCR products were performed following a method described in Shi et al. (2022). In addition, demultiplexed, quality-filtered, and merged methods of raw 16S rRNA gene sequencing reads were described in Shi et al. (2022). The high-quality sequences were then clustered into operational taxonomic units (OTUs) with 97% similarity using UPARSE (Edgar, 2013), with a minimum number of sequences (27106) as the rarefied criterion to standardize uneven sequence depth. The taxonomy of each OTU was analyzed by RDP Classifier based on the 16S rRNA database (Silva v138) with a confidence threshold of 0.7 (Wang et al., 2007).

The calculation and multiple comparisons of α-diversity indices (Chao 1, Pielou's evenness, and Shannon-Wiener indices) were performed by packages "mother" and "multcomp" of R (Hothorn et al., 2008; Schloss et al., 2009; R Core Team, 2018). The bacterial analysis of similarities (ANOSIM), Non-metric multidimensional scaling (NMDS) based on Bray-Curtis distance and Redundancy analysis (RDA) were conducted in package "vegan" of R (Oksanen et al., 2019) with forward selection used to avoid collinearity of environmental factors and a parsimonious set of significant environmental variables selected using a permutation test. Co-occurrence network and Network topological features (degree and network density) were drawn and calculated using packages "psych" and "igraph" of R (Benjamini et al., 2006; Csárdi and Nepusz, 2006; Ma et al., 2016; Revelle, 2021). The difference significance tests (ANOVA) of bacterial community and adjusted p-values (Benjamini and Hochberg false discovery rate) were calculated using STAMP between the exponential and decline growth phase of *P. globosa* bloom (Parks et al., 2014).

Results

Density of *P. globosa*

Changes in *P. globosa* colony density are shown in Figure 2. Colony density increased from 4.41 to 16.80 colonies L^{-1} from January 23 to 25 and decreased sharply to 2.53 colonies L^{-1} on January 27 and fluctuated until February 3. The growth phase of the *P. globosa* bloom was divided into an exponential growth phase (January 23 to 26) and a decline growth phase (January 27 to February 3) based on colony density. It is worth noting that the concentration of chl a (representing solitary cells) on January 26 was still in high value, and thus the growth of *P. globosa* bloom on January 26 was classified as in the exponential growth phase, although colony density had begun to decrease.

Composition of bacterial communities

16S rRNA sequences obtained from samples were clustered into 7235 OTUs, assigned to 54 different phyla. Large variations in bacterial community compositions were observed among the three kinds of bacteria, particularly between colony-attached bacteria and the other two (Figure 3). Specifically, the dominant phyla of bacterioplankton were Bacteroidota (percentages of the total OTUs ranged from 16.80 to 76.30%), Proteobacteria (16.05–58.43%, mainly belonging to Alphaproteobacteria and Gammaproteobacteria) and Cyanobacteria (0.82–31.37%). The

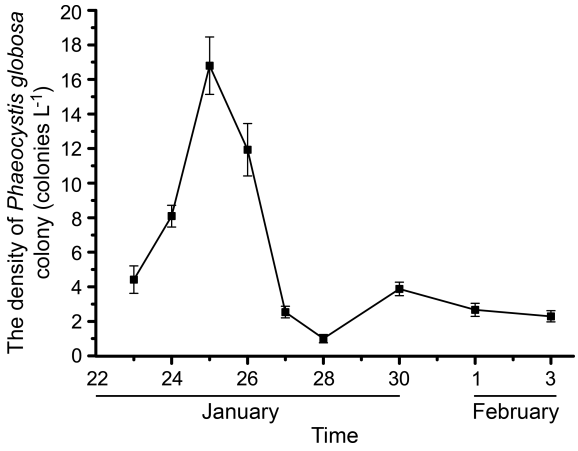

FIGURE 2
Changes of the *phaeocystis globosa* colony density (colonies L^{-1}). The error bars represent standard errors of the *P. globosa* colonies density.

dominant phyla of particle-attached bacteria were Proteobacteria (12.97–75.44%, mainly belonging to Alphaproteobacteria and Gammaproteobacteria), Bacteroidota (4.94–48.47%), Verrucomicrobiota (0.91–59.72%) and Cyanobacteria (1.04–55.33%). The community compositions of colony-attached bacteria were simple, with the dominant phyla of Cyanobacteria (26.97–98.90%) and Proteobacteria (0.63–65.91%).

α-diversity of bacterial communities

The differences in α-diversity indices among bacterioplankton, particle-attached bacteria and colony-attached bacteria during the *P. globosa* bloom were extremely significant ($p < 0.01$). Particle-attached bacteria had the highest α-diversity indices, followed by bacterioplankton, and colony-attached bacteria had the lowest (Figure 4A). In the decline growth phase of the bloom, Shannon-Wiener and Pielou's evenness indices decreased significantly in bacterioplankton and increased significantly in colony-attached bacteria ($p < 0.05$), but Chao1 indices showed no significant differences between the exponential and decline growth phases in those two groups ($p > 0.05$). However, the Chao1 index of particle-attached bacteria increased significantly ($p < 0.05$), while the Shannon-Wiener and Pielou's evenness indices decreased extremely significantly ($p < 0.01$) when the bloom entered the decline growth phase (Figure 4B).

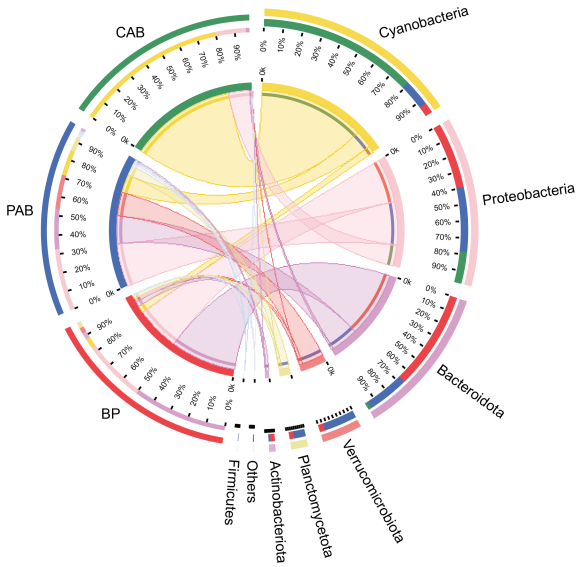

FIGURE 3
Dominant bacterial lineages (top 7 phyla) of BP (bacterioplankton), PAB (particle-attached bacteria), and CAB (colony-attached bacteria).

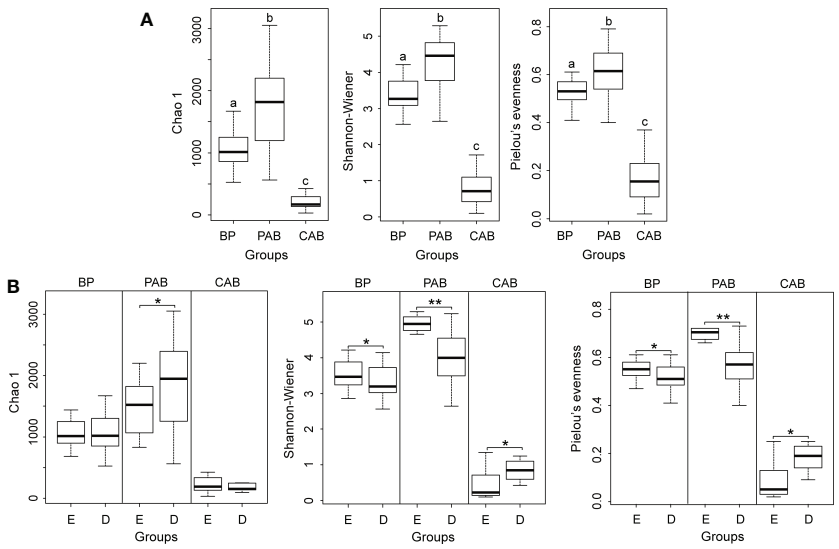

FIGURE 4
Boxplot of α-diversity indices on genus level among three kinds of bacteria **(A)** Different lowercase letters represent significant differences, $p < 0.01$ and between exponential and decline growth phases of *Phaeocystis globosa* bloom **(B)**. BP, bacterioplankton; PAB, particle-attached bacteria; CAB, colony-attached bacteria; D, exponential growth phase of bloom; E, decline growth phase of bloom. *$p< 0.05$; **$p< 0.01$.

Bacterial community structure

During the *P. globosa* bloom, the bacterial community structures of the three kinds of bacteria were markedly different, and the differences among groups were greater than those within groups (Figures 5A, B). The community compositions of colony-attached bacteria showed smaller variations compared to bacterioplankton and particle-attached bacteria and did not change much throughout the *P. globosa* bloom (Figure 5C). However, obvious distinctions were observed between the exponential and decline growth phases in bacterioplankton and particle-attached bacteria (Figure 5C). In particular, members of Bacteroidota and Verrucomicrobiota in bacterioplankton and Verrucomicrobiota in particle-attached bacteria were notably higher during the decline growth phase of the *P. globosa* bloom (Figure 6). Furthermore, the bacterial community structures of bacterioplankton and particle-attached bacteria on January 28 were distinct from the other groups (Figure 5A).

Bacterial inter-taxa relationship network

The co-occurrence networks of bacterioplankton, particle-attached bacteria, and colony-attached bacteria had much higher positive correlations than negative correlations (Figure 7). The network of bacterioplankton had 574 nodes and 2603 edges, of which 2565 were positive and 38 were negative correlations. The network of particle-attached bacteria had 893 nodes and 4514 edges, of which 4495 were positive and 19 were negative correlations. The network of colony-attached bacteria had 510 nodes and 6808 edges, of which 6798 were positive and 10 were negative correlations (Figure 7). The network densities of bacterioplankton, particle-attached bacteria, and colony-attached bacteria were 0.016, 0.011 and 0.052, respectively, and their average degrees were 9.07, 10.11 and 26.70, respectively.

Relationships between bacteria and environmental factors

As exhibited in Figure 8, the relationships between the community structures of the three kinds of bacteria and the environmental factors varied between the growth phases of the bloom. During the exponential growth phase of the bloom, the community structures of bacterioplankton were positively correlated with COD and PO_4^{3-} concentrations in seawater, whereas, when the bloom shifted to the decline phase, the structures were positively correlated with temperature, salinity, and pH. For particle-attached bacteria, their community structures were positively correlated with DOC, NO_3^- and DO during the exponential growth phase of the bloom, and shifted to salinity during the decline growth phase. Whereas, the community structures of colony-attached bacteria were correlated with seawater temperature, salinity, DO, and COD throughout the bloom, with no obvious bacterial difference observed between the exponential and decline phases.

Discussion

The bacterial communities harbored in the three habitats were influenced by the inhabited niches and the growth phases of microalgae bloom. We found marked variations in bacterial community structures among the three types of bacteria, potentially due to the diverse lifestyles of bacterioplankton and attached bacteria (Acinas et al., 1999; Fuchsman et al., 2011; Li et al.,

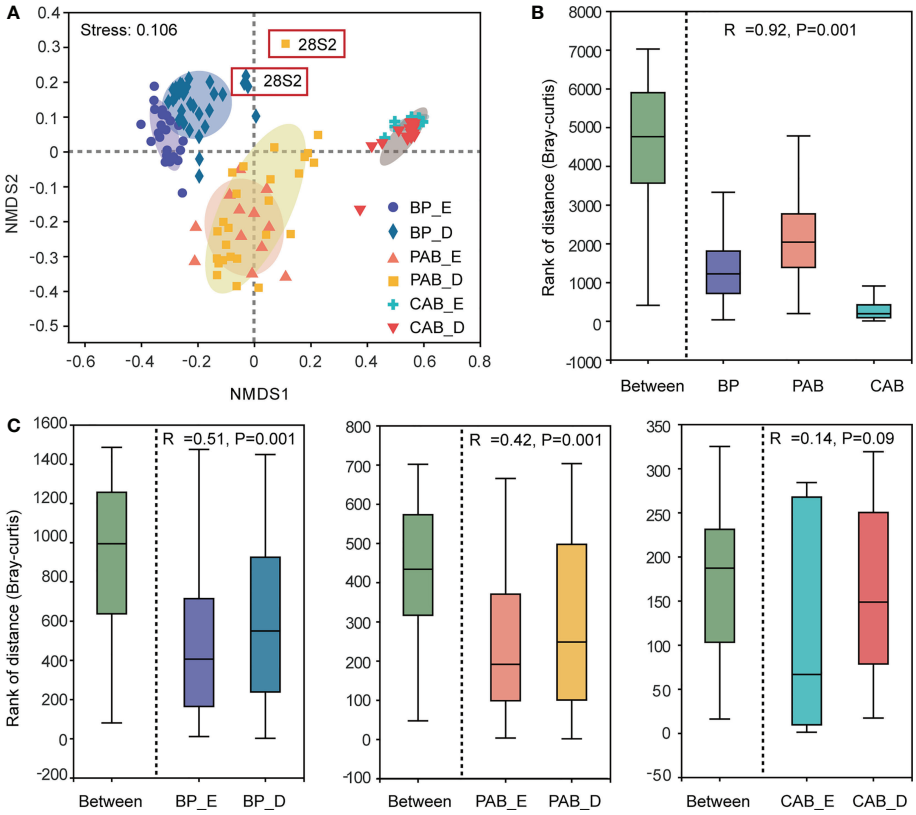

FIGURE 5
NMDS on genus level **(A)**, distances boxplot among three kinds of bacteria **(B)** and between exponential and decline growth phase of *Phaeocystis globosa* bloom **(C)**. BP, bacterioplankton; PAB, particle-attached bacteria; CAB, colony-attached bacteria; E, exponential growth phase of bloom; D, decline growth phase of bloom.

2015). The physical and biochemical characteristics of bacterial hosts impact their diversity, with particle-attached bacteria exhibiting greater diversity than bacterioplankton and colony-attached bacteria, consistent with the findings in the Black and Beaufort Seas (Fuchsman et al., 2011; Ortega-Retuerta et al., 2013). In contrast, a lower taxonomic richness of particle-attached bacterial communities compared with bacterioplankton was reported by Li et al. (2015) in the South China Sea, which may be attributed to the *P. globosa* bloom outbreak in the present study. Further research is required to gain a better understanding of the mechanisms involved.

The present study showed that the characteristics of bacterial communities were related to the growth phases of microalgae bloom, likely due to the varying availability of substrates. Exopolysaccharides were the most available polysaccharides at the beginning of the bloom and were utilized first by most bacteria species. As the bloom progressed, recalcitrant substrates such as sulfated polysaccharides in cellular substrates become dominant, allowing specific bacteria to

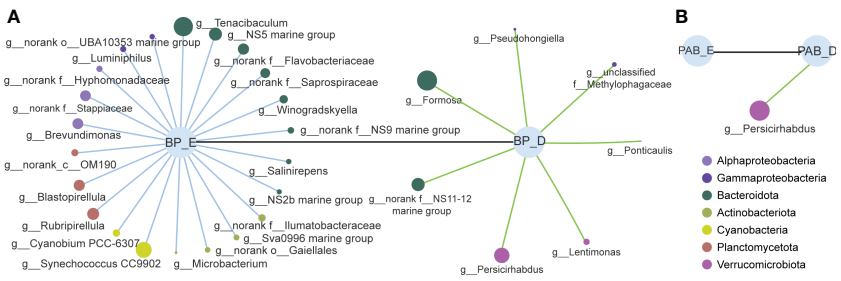

FIGURE 6
The abundance of bacterioplankton **(A)** and particle-attached bacteria **(B)** with significantly differences between exponential and decline growth phase of *Phaeocystis globosa* bloom. Radiating dots represent bacterial genus, and the dots size and color represent their abundance and phylum they belong to. BP, bacterioplankton; PAB, particle-attached bacteria; E, exponential growth phase of bloom; D, decline growth phase of bloom. ($p < 0.01$).

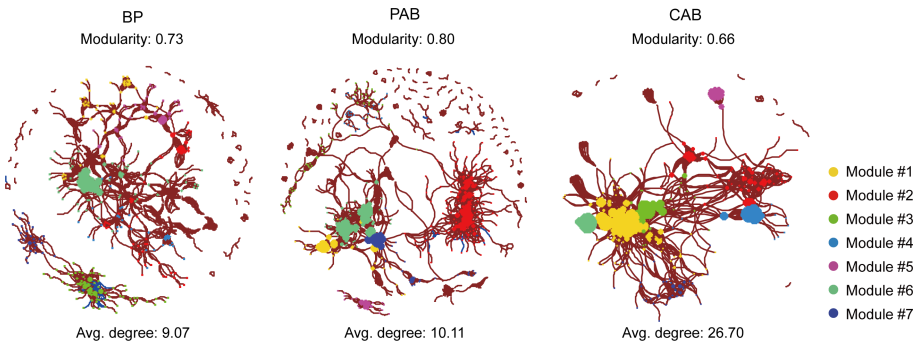

FIGURE 7
Co-occurrence network of bacterial relationship from BP (bacterioplankton), PAB (particle-attached bacteria), and CAB (colony-attached bacteria) created with a Spearman's coefficient threshold of ± 0.7 and an adjusted *p*-value threshold of 0.01. Each node represents bacterial genus and the node size is proportional to the value of degree, lines connecting two nodes indicated the interactions between them. Red lines represent a positive significant correlation and blue lines represent negative significant correlation. Node color represents the bacterial distribution modules.

acquire a dominant position (Teeling et al., 2016). These differences in substrate availabilities at different growth phases of *P. globosa* bloom likely caused the variations in dominant species and the richness of bacterial communities. Additionally, the change of bloom species also influenced the bacterial community. The *A. sanguinea* bloom at station S2 on January 28 caused a marked shift in the bacterial communities of bacterioplankton and particle-attached bacteria (Figure S1). For example, *Candidatus puniceispirillum*, a member of the SAR11 clade of Alphaproteobacteria, increased significantly compared to station S1 on January 28 and station S2 on January 26. *C. pelagibacter*, another member of the SAR11 clade, is known to be a dominant genus in the bacterial community and plays a crucial role in carbon cycling during *A. sanguinea* blooms (Yang et al., 2012). Therefore, the explosive growth of *C. puniceispirillum* during the *A. sanguinea* bloom in this study may be attributed to their similar abilities to *C. pelagibacter*.

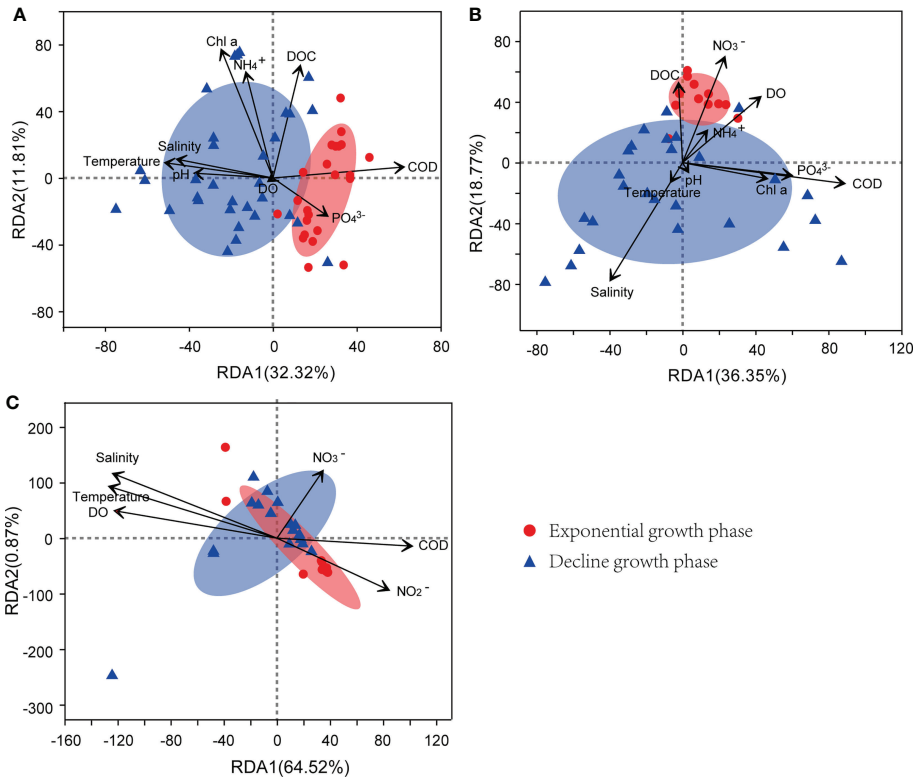

FIGURE 8
RDA of environmental factors and bacterial community structure from bacterioplankton **(A)**, particle-attached bacteria **(B)**, and colony-attached bacteria **(C)**. E, exponential growth phase of *Phaeocystis globosa* bloom; D, decline growth phase *P. globosa* bloom.

It has been reported that the dominant phyla of bacterioplankton in the South China Sea are Proteobacteria and Cyanobacteria (Shi et al., 2018; Sun et al., 2021; Ren et al., 2022). However, the present study found that Bacteroidota was the most abundant bacterioplankton, likely due to the high concentrations of nutrients (e.g. PO_4^{3-}) that favor these organisms during bloom periods, as well as their ability to degrade complex proteins and mucopolysaccharides released by *P. globosa* (Cottrell and Kirchman, 2000; Janse et al., 2000; Brussaard et al., 2005; Lamy et al., 2009; Almutairi, 2015). Remarkable differences in bacterial community structure and diversity were also observed between the exponential and decline growth phases of the bloom, likely due to the increased proportion of recalcitrant polysaccharides (e.g., fucose-containing sulfated polysaccharides) derived from algal fragmentation, which favored specific bacteria such as *Persicirhabdus* sp. of Verrucomicrobiota (Martinez-Garcia et al., 2012; Sichert et al., 2020; Orellana et al., 2021). On the other hand, the dominant bacterioplankton that differed significantly between the exponential and the decline growth phases of bloom were all belonged to Bacteroidota, indicating their important role in the degradation of complex organic carbon, particularly in the forms of polysaccharides and hydrocarbons (Bauer et al., 2006; Wolińska et al., 2017). The amounts of organic matter which served as electron donors for organic matter-degrading bacteria such as denitrifying bacteria and sulfate-reducing bacteria can be evaluated by the COD value. In the present study, the community structures of bacterioplankton were positively correlated with COD during the exponential growth phase of the bloom. Notably, the COD value decreased drastically as the bloom developed into the decline phase due to algal cell death or sinking to the bottom, yet the bacterioplankton community did not change accordingly that much. This suggested that the bacterioplankton community was regulated not only by the quantity of organic matter but also by its quality, i.e., biological and chemical composition and form characteristics (Stelzer et al., 2014). Furthermore, environmental factors such as temperature, salinity, and pH were also essential in shaping the community profiles of bacterioplankton.

Particle-attached bacteria possess a critical capability of attaching to particulate matters including *Phaeocystis* aggregates, providing them many advantages including increased nutrient acquisition, reduced predation risk, and enhanced interactions among populations (Dang et al., 2008). The aggregates of particles or microalgae cells serve as organic-rich microhabitats with abundant substrates, harboring large amounts of bacteria (Alldredge et al., 1986; Li et al., 2015). In the present study, Proteobacteria (Alphaproteobacteria and Gammaproteobacteria) was the dominant phylum of particle-attached bacteria due to their great adhesion ability, as reported by Li et al. (2015). As the bloom shifted from the exponential phase to the decline phase, the homogeneity of their hosts (dominated by algal fragments) caused a significant decrease in the community diversity of particle-attached bacteria (Kiørboe and Jackson, 2001; Azam and Malfatti, 2007; Fang et al., 2015). In addition, the dissolved organic matter released into ambient waters was further utilized by bacterioplankton, such as *Persicirhabdus* sp. of Verrucomicrobiota, whose abundance significantly increased in the decline growth phase of the bloom, resulting in the complex relationship among organic particles, phytoplankton, particle-attached bacteria, and bacterioplankton, and further studies are needed to explore this.

The formation and enlargement of gelatinous colony is a defense strategy for *Phaeocystis*, allowing them to avoid predation and become cosmopolitan marine phytoplankton (Wang et al., 2015; Wang et al., 2021a). These colonies are capable of maintaining their position in the euphotic zone by regulating their buoyancy based on light intensity and water flow (Wang et al., 2010). Correspondingly, the majority of colony-attached bacteria were species belonging to autotrophic cyanobacteria, which require light absorption for photosynthesis. Intensive host selection pressure (unique host) resulted in the lowest diversity of colony-attached bacteria, but this could also be an advantage in maintaining the stability of symbiotic relationships between colony-associated bacteria and their hosts (Edwards et al., 2015). A more complex microbial ecosystem with greater connectivity is more stable and robust during environmental changes, as indicated by the high network density, average degree, and the number of edges with the least nodes in colony-attached bacteria (Santolini and Barabási, 2018; Huang et al., 2022). This complex network may explain why there was no significant difference in colony-attached bacterial communities between the exponential and decline growth phases of the *P. globosa* bloom.

Conclusion

Our study reveals the profound impacts of *P. globosa* bloom on marine bacteria, with the bacterioplankton and particle-attached bacterial communities varying as the bloom progressed. Bacteria, particularly those with organic decomposing abilities (e.g., Verrucomicrobiota and Bacteroidota), could play a key role in the dissipation of *P. globosa* blooms. Our findings emphasize the importance of studying the intricate connections between bacteria and microalgae blooms.

Data availability statement

The datasets presented in this study can be found in online repositories. The names of the repository/repositories and accession number(s) can be found below: https://www.ncbi.nlm.nih.gov/genbank/, PRJNA776989.

Author contributions

RS and HH conceived the original ideas and collected samples during the outbreak of *P. globosa* bloom for the manuscript. RS developed the outline and analyzed the data, prepared the manuscript with some contributions to drafting from SZ, MD,

and TH and critical refinement by ZQ. All authors contributed to the article and approved the submitted version.

Funding

This work was supported by the National Natural Science Foundation of China (31900094, 41976149), Guangdong Basic and Applied Basic Research Foundation (2021A1515011377), Guangzhou Basic and Applied Basic Research Foundation (202201010306), Central Public-interest Scientific Institution Basal Research Fund, CAFS (2020TD15), Central Public-interest Scientific Institution Basal Research Fund, South China Sea Fisheries Research Institute, CAFS (2021SD03).

Acknowledgments

We are thankful for the comments and suggestions of the reviewers and the editor that helped to improve the manuscript.

Conflict of interest

The authors declare that the research was conducted in the absence of any commercial or financial relationships that could be construed as a potential conflict of interest.

Publisher's note

Supplementary material

The Supplementary Material for this article can be found online at: https://www.frontiersin.org/articles/10.3389/fmars.2023.1075059/full#supplementary-material

References

Acinas, S. G., Anton, J., and Rodriguez-Valera, F. (1999). Diversity of free-living and attached bacteria in offshore western Mediterranean waters as depicted by analysis of genes encoding 16S rRNA. *Appl. Environ. Microbiol.* 65, 514–522. doi: 10.1128/AEM.65.2.514-522.1999

Alldredge, A. L., Cole, J. J., and Caron, D. A. (1986). Production of heterotrophic bacteria inhabiting macroscopic organic aggregates (marine snow) from surface waters. *Limnol. Oceanogr.* 31, 68–78. doi: 10.4319/lo.1986.31.1.0068

Almutairi, A. (2015). Spatial–temporal variations and diversity of the bacterioplankton communities in the coastal waters of Kuwait. *Mar. pollut. Bull.* 100 (2), 699–709. doi: 10.1016/j.marpolbul.2015.09.016

Anderson, D. M., Glibert, P. M., and Burkholder, J. M. (2002). Harmful algal blooms and eutrophication: nutrient sources composition, and consequences. *Estuaries* 25, 704–725. doi: 10.1007/BF02804901

Arrigo, K. R. (2004). Marine microorganisms and global nutrient cycles. *Nature* 437, 349–355. doi: 10.1038/nature04159

Azam, F., and Malfatti, F. (2007). Microbial structuring of marine ecosystems. *Nat. Rev. Microbiol.* 5, 782–791. doi: 10.1038/nrmicro1747

Bauer, M., Kube, M., Teeling, H., Richter, M., Lombardot, T., Allers, E., et al. (2006). Whole genome analysis of the marine bacteroidetes 'Gramellaforsetii' reveals adaptations to degradation of polymeric organic matter. *Environ. Microbiol.* 8, 2201–2213. doi: 10.1111/j.1462-2920.2006.01152.x

Benjamini, Y., Krieger, A. M., and Yekutieli, D. (2006). Adaptive linear step-up procedures that control the false discovery rate. *Biometrika* 93, 491–507. doi: 10.1093/biomet/93.3.491

Brussaard, C. P. D., Mari, X., Van Bleijswijk, J. D. L., and Veldhuis, M. J. W. (2005). A mesocosm study of *Phaeocystis globosa* (Prymnesiophyceae) population dynamics. II. significance for the microbial community. *Harmful Algae* 4 (5), 875–893. doi: 10.1016/j.hal.2004.12.012

Chan, K. M., Leung, K. M., Cheung, K. C., Wong, M. H., and Qiu, J. W. (2008). Seasonal changes in imposex and tissue burden of butyltin compounds in *Thais clavigera* populations along the coastal area of mirs bay. China. *Mar. pollut. Bull.* 57 (6–2), 645–651. doi: 10.1016/j.marpolbul.2008.02.040

Chen, J., Li, H., Zhang, Z., He, C., Shi, Q., Jiao, N., et al. (2020). DOC dynamics and bacterial community succession during long-term degradation of ulva prolifera and their implications for the legacy effect of green tides on refractory DOC pool in seawater. *Water Res.* 185, 116268. doi: 10.1016/j.watres.2020.116268

Cole, J. J. (1982). Interactions between bacteria and algae in aquatic cosystems. *Annu. Rev. Ecol. Syst.* 13, 291–314. doi: 10.1146/annurev.es.13.110182.001451

Comte, J., and Del Giorgio, P. A. (2010). Linking the patterns of change in composition and function in bacterioplankton successions along environmental gradients. *Ecology* 91, 1466–1476. doi: 10.1890/09-0848.1

Cottrell, M., and Kirchman, D. (2000). Natural assemblages of marine proteobacteria and members of the cytophaga–flavobacter cluster consuming low- and high-molecular weight dissolved organic matter. *Appl. Environ. Microbiol.* 66, 1692–1697. doi: 10.1128/AEM.66.4.1692-1697.2000

Csárdi, G., and Nepusz, T. (2006). The igraph software package for complex network research. *Inter. J. Complex Syst.* 1695. .Available at: http://igraph.sf.net.

Dang, H., Li, T., Chen, M., Huang, G., and Dang, H. Y. (2008). Cross-ocean distribution of rhodobacterales bacteria as primary surface colonizers in temperate coastal marine waters. *Appl. Environ. Microbiol.* 74, 52–60. doi: 10.1128/AEM.01400-07

Delmont, T. O., Hammar, K. M., Ducklow, H. W., Yager, P. L., and Post, A. F. (2014). *Phaeocystis antarctica* bloom strongly influence bacterial community structures in the amundsen Sea polynya. *Front. Microbiol.* 5. doi: 10.3389/fmicb.2014.00646

Edgar, R. C. (2013). UPARSE: highly accurate OTU sequences from microbial amplicon reads. *Nat. Methods* 10, 996–998. doi: 10.1038/nmeth.2604

Edwards, J., Johnson, C., Santos-Medellín, C., Lurie, E., Podishetty, N. K., Bhatnager, S., et al. (2015). Structure, variation, and assembly of the root- associated microbiomes of rice. *P. Natl. Acad. Sci. U.S.A.* 112 (8), E911–E920. doi: 10.1073/pnas.1414592112

Fang, J., Zhang, L., Li, J., Kato, C., Zhang, Y., Tamburini, C., et al. (2015). The POM-DOM piezophilic microorganisms continuum (PDPMC)-the role of piezophilic microorganisms in the global ocean carbon cycle. sci. *China Earth Sci.* 58, 106–115. doi: 10.1007/s11430-014-4985-2

Fuchsman, C. A., Kirkpatrick, J. B., Brazelton, W. J., Murray, J. W., and Staley, J. T. (2011). Metabolic strategies of free-living and aggregate-associated bacterial communities inferred from biologic and chemical profiles in the black Sea suboxic zone. *FEMS Microbiol. Ecol.* 78 (3), 586–603. doi: 10.1111/j.1574-6941.2011.01189.x

GB/T 12763.4-2007 (2007). *Specifications for oceanographia survey–part 4: Survey of chemical parameters in sea water* (Beijing: Standards press of china).

Higashi, A., Fujitani, Y., Nakayama, N., Tani, A., and Ueki, S. (2016). Selective growth promotion of bloom-forming raphidophyte *Heterosigma akashiwo* by a marine bacterial strain. *Harmful Algae* 60, 150–156. doi: 10.1016/j.hal.2016.11.009

Hothorn, T., Bretz, F., and Westfall, P. (2008). Simultaneous inference in general parametric models. *Biometrical J.* 50 (3), 346–363. doi: 10.1002/bimj.200810425

Huang, Y., Liu, Y., Geng, J., Lü, H., Zhao, H., Xiang, L., et al. (2022). Maize root-associated niches determine the response variation in bacterial community assembly and function to phthalate pollution. *J. Hazard. Mater.* 429, 128280. doi: 10.1016/j.jhazmat.2022.128280

Janse, I., Zwart, G., van der Maarel, M. J. E. C., and Gottschal, J. C. (2000). Composition of the bacterial community degrading *Phaeocystis mucopolysaccharides* in enrichment cultures. *Aquat. Microb. Ecol.* 22, 119–133. doi: 10.3354/ame022119

Kiørboe, T., and Jackson, G. A. (2001). Marine snow, organic solute plumes, and optimal chemosensory behavior of bacteria. *Limnol. Oceanogr.* 46 (6), 1309–1318. doi: 10.4319/lo.2001.46.6.1309

Lamy, D., Obernosterer, I., Laghdass, M., Artigas, L. F., Breton, E., Grattepanche, J. D., et al. (2009). Temporal changes of major bacterial groups and bacterial heterotrophic activity during a *Phaeocystis globosa* bloom in the eastern English channel. *Aquat. Microb. Ecol.* 58, 95–107. doi: 10.3354/ame01359

Li, J., Wei, B., Wang, J., Liu, Y., Dasgupta, S., Zhang, L., et al. (2015). Variation in abundance and community structure of particle-attached and free-living bacteria in the south China Sea. *Deep-Sea Res. Pt. II* 122, 64–73. doi: 10.1016/j.dsr2.2015.07.006

Li, N., Zhao, H., Jiang, G., Xu, Q., Tang, J., Li, X., et al. (2020). Phylogenetic responses of marine free-living bacterial community to *Phaeocystis globosa* bloom in beibu gulf, China. *Front. Microbiol.* 11. doi: 10.3389/fmicb.2020.01624

Liu, Y., Debeljak, P., Rembauville, M., Blain, S., and Obernosterer, I. (2019). Diatoms shape the biogeography of heterotrophic prokaryotes in early spring in the southern ocean. *Environ. Microbiol.* 21, 1452–1465. doi: 10.1111/1462-2920.14579

Ma, B., Wang, H., Dsouza, M., Lou, J., He, Y., Dai, Z., et al. (2016). Geographic patterns of co-occurrence network topological features for soil microbiota at continental scale in eastern China. *ISME J.* 10 (8), 1891–1901. doi: 10.1038/ismej.2015.261

Martinez-Garcia, M., Brazel, D. M., Swan, B. K., Arnosti, C., Chain, P. S., Reitenga, K. G., et al. (2012). Capturing single cell genomes of active polysaccharide degraders: an unexpected contribution of verrucomicrobia. *PloS One* 7, e35314. doi: 10.1371/journal.pone.0035314

Meyer, K. A., O'Neil, J. M., Hitchcock, G. L., and Heil, C. A. (2014). Microbial production along the West Florida shelf: responses of bacteria and viruses to the presence and phase of *Karenia brevis* blooms. *Harmful Algae* 38, 110–118. doi: 10.1016/j.hal.2014.04.015

Oksanen, J., Blanchet, F. G., Friendly, M., Kindt, R., Legendre, P., McGlinn, D., et al. (2019) *Vegan: community ecology package*. Available at: https://CRAN.R-project.org/package=vegan.

Orellana, L. H., Francis, T. B., Ferraro, M., Hehemann, J., Fuchs, B. M., and Amann, R. (2021). Verrucomicrobiota are specialist consumers of sulfated methyl pentoses during diatom blooms. *ISME J.* 16 (3), 630–641. doi: 10.1038/s41396-021-01105-7

Ortega-Retuerta, E., Joux, F., Jeffrey, W. H., and Ghiglione, J. F. (2013). Spatial variability of particle-attached and free-living bacterial diversity in surface waters from the Mackenzie river to the Beaufort Sea (Canadian Arctic). *Biogeosciences* 10, 2747–2759. doi: 10.5194/bg-10-2747-2013

Parada, A. E., Needham, D. M., and Fuhrman, J. A. (2015). Every base matters: assessing small subunit rRNA primers for marine microbiomes with mock communities, time series and global field samples. *Environ. Microbiol.* 18, 1403–1414. doi: 10.1111/1462-2920.13023

Parks, D. H., Tyson, G. W., Hugenholtz, P., and Beiko, R. G. (2014). STAMP: statistical analysis of taxonomic and functional profiles. *Bioinformatics* 30, 3123–3124. doi: 10.1093/bioinformatics/btu494

R Core Team (2018). *R: a language and environment for statistical computing* (Vienna, Austria: R foundation for statistical computing). Available at: https://www.R-project.org/.

Ren, L., Lu, Z., Xia, X., Peng, Y., Gong, S., Song, X., et al. (2022). Metagenomics reveals bacterioplankton community adaptation to long-term thermal pollution through the strategy of functional regulation in a subtropical bay. *Water Res.* 216 (5), 118298. doi: 10.1016/j.watres.2022.118298

Revelle, W. (2021). *Psych: procedures for personality and psychological research* (Evanston, Illinois, USA: Northwestern University). Available at: https://CRAN.R-project.org/package=psych.

Ruiz-Gonzalez, C., Proia, L., Ferrera, I., Gasol, J. M., and Sabater, S. (2013). Effects of large river dam regulation on bacterioplankton community structure. *FEMS Microbiol. Ecol.* 84, 316–331. doi: 10.1111/1574-6941.12063

Santolini, M., and Barabási, A. L. (2018). Predicting perturbation patterns from the topology of biological networks. *P. Natl. Acad. Sci. U.S.A.* 115 (27), E6375–E6383. doi: 10.1073/pnas.1720589115

Schloss, P. D., Westcott, S. L., Ryabin, T., Hall, J. R., Hartmann, M., Hollister, E. B., et al. (2009). Introducing mothur: open-source, platform-independent, community-supported software for describing and comparing microbial communities. *Appl. Environ. Microb.* 75 (23), 7537–7541. doi: 10.1128/AEM.01541-09

Sher, D., Thompson, J. W., Kashtan, N., Croal, L., and Chisholm, S. W. (2011). Response of *Prochlorococcus ecotypesto* co-culture with diverse marine bacteria. *ISME J.* 5, 1125–1132. doi: 10.1038/ismej.2011.1

Shi, R., Huang, H., Qi, Z., and Han, T. (2022). The extent and pattern of mariculture impacts on spatial and seasonal variations of sediment bacterial communities among three coastal waters. *Front. Mar. Sci.* 9. doi: 10.3389/fmars.2022.782456

Shi, R., Li, J., Qi, Z., Zhang, Z., Liu, H., and Huang, H. (2018). Abundance and community composition of bacterioplankton in the northern south China Sea during winter: geographic position and water layer influences. *Biologia* 73 (2), 197–206. doi: 10.2478/s11756-018-0023-8

Sichert, A., Corzett, C. H., Schechter, M. S., Unfried, F., Markert, S., Becher, D., et al. (2020). Verrucomicrobia use hundreds of enzymes to digest the algal polysaccharide fucoidan. *Nat. Microbiol.* 5, 1026–1039. doi: 10.1038/s41564-020-0720-2

Stelzer, R. S., Scott, J. T., Bartsch, L. A., and Parr, T. B. (2014). Particulate organic matter quality influences nitrate retention and denitrification in stream sediments: evidence from a carbon burial experiment. *Biogeochemistry* 119, 387–402. doi: 10.1007/s10533-014-9975-0

Sun, F., Wang, C., Wang, Y., Tu, K., Zheng, Z., and Lin, X. (2020). Diatom red tide significantly drive the changes of microbiome in mariculture ecosystem. *Aquaculture* 520, 734742. doi: 10.1016/j.aquaculture.2019.734742

Sun, F., Wang, Y., Wu, M., Sun, C., Jiang, Z., Cheng, H., et al. (2021). Bacterial community variations in the south China Sea driven by different chemical conditions. *Ecotoxicology* 30, 1808–1815. doi: 10.1007/s10646-021-02455-w

Sun, W., Xia, C., Xu, M., Guo, J., and Sun, G. (2017). Seasonality affects the diversity and composition of bacterioplankton communities in dongjiang river, a drinking water source of Hong Kong. *Front. Microbiol.* 8. doi: 10.3389/fmicb.2017.01644

Teeling, H., Fuchs, B. M., Bennke, C. M., Krüger, K., Chafee, M., Kappelmann, L., et al. (2016). Recurring patterns in bacterioplankton dynamics during coastal spring algae blooms. *eLife* 5, e11888. doi: 10.7554/eLife.11888

Wang, Q., Garrity, G. M., Tiedje, J. M., and Cole, J. R. (2007). Naive Bayesian classifier for rapid assignment of rRNA sequences into the new bacterial taxonomy. *Appl. Environ. Microbiol.* 73, 5261–5267. doi: 10.1128/AEM.00062-07

Wang, X., Huo, Y., Yang, F., and Wang, Y. (2021b). Induced allelopathic effects of *Thalassiosira weissflogii* on colony formation in *Phaeocystis globosa*. *Water* 13, 581. doi: 10.3390/w13050581www.mdpi

Wang, X., Song, H., Wang, Y., and Chen, N. (2021a). Research on the biology and ecology of the harmful algal bloom species *Phaeocystis globosa* in China: progresses in the last 20 years. *Harmful Algae* 107 (2), 102057. doi: 10.1016/j.hal.2021.102057

Wang, X., Tang, K. W., and Smith, W. O.Jr. (2010). Temperature effects on growth, colony development and carbon partitioning of three *Phaeocystis* species. *Aquat. Biol.* 9 (3), 239–249. doi: 10.3354/ab00256

Wang, X., Wang, Y., Ou, L., He, X., and Chen, D. (2015). Allocation costs associated with induced defense in *Phaeocystis globosa* (Prymnesiophyceae): the effects of nutrient availability. *Sci. Rep.* 5, 10850. doi: 10.1038/srep10850

Wolińska, A., Kuźniar, A., Zielenkiewicz, U., Izak, D., Szafranek-Nakonieczna, A., Banach, A., et al. (2017). Bacteroidetes as a sensitive biological indicator of agricultural soil usage revealed by a culture-independent approach. *Appl. Soil Ecol.* 119, 128–137. doi: 10.1016/j.apsoil.2017.06.009

Worden, A. Z., Follows, M. J., Giovannoni, S. J., Wilken, S., Zimmerman, A. E., and Keeling, P. J. (2015). Rethinking the marine carbon cycle: factoring in the multifarious lifestyles of microbes. *Science* 347, 1257594. doi: 10.1126/science.1257594

Xia, X., Leung, S. K., Cheung, S., Zhang, S., and Liu, H. (2020). Rare bacteria in seawater are dominant in the bacterial assemblage associated with the bloom-forming dinoflagellate *Noctiluca scintillans*. *Sci. Total Environ.* 711, 135107. doi: 10.1016/j.scitotenv.2019.135107

Yang, C., Li, Y., Zhou, Y., Zheng, W., Tian, Y., and Zheng, T. (2012). Bacterial community dynamics during a bloom caused by *Akashiwo sanguinea* in the xiamen sea area, China. *Harmful Algae* 20, 132–141. doi: 10.1016/j.hal.2012.09.002

frontiers | Frontiers in Marine Science

TYPE Original Research
PUBLISHED 14 April 2023
DOI 10.3389/fmars.2023.1133187

OPEN ACCESS

EDITED BY
Huang Honghui,
South China Sea Fisheries Research Institute (CAFS), China

REVIEWED BY
Shaowei Wang,
Nuclear and Radiation Safety Center, China
Baojun Tang,
East China Sea Fisheries Research Institute (CAFS), China

*CORRESPONDENCE
Xiang Pu
puxiang@snerdi.com.cn

SPECIALTY SECTION
This article was submitted to Marine Pollution, a section of the journal Frontiers in Marine Science

RECEIVED 28 December 2022
ACCEPTED 28 March 2023
PUBLISHED 14 April 2023

CITATION
Fu X, Du F, Huang X, Pei J, Zhang Z, Xing X and Pu X (2023) Cooling water intake system safety analysis based on impingement probability. *Front. Mar. Sci.* 10:1133187. doi: 10.3389/fmars.2023.1133187

Cooling water intake system safety analysis based on impingement probability

Xiaocheng Fu, Fenglei Du, Xiaodong Huang, Juan Pei, Zhenglou Zhang, Xiaofeng Xing and Xiang Pu*

Shanghai Nuclear Engineering Research and Design Institute Co., Ltd., Shanghai, China

Invasion or aggregation of marine organisms in cooling water intake systems (CWIS) has gradually become an important problem affecting the safety of nuclear power plants with environmental and climate changes. In this study, a 3-dimensional numerical model (TELEMAC-3D) was used to determine the impingement probability in a typical nuclear power plant with a once-through cooling system, and the effect on CWIS safety. The factors controlling impingement probability were also analyzed. Results show that (1) impingement probability decreased rapidly with an increase in distance from the CWIS. In addition, the distance of the impingement effect of a nuclear power plant with six units was mainly within 1 km of the CWIS. (2) Impingement probability increased with water withdrawal, and as distance to the CWIS increased, the increase in probability increased. (3) Generally, an increase in tide strength led to a decrease impingement probability. (4) Near the CWIS, the impingement probabilities of areas upstream or downstream of the CWIS along the tidal flow direction were much higher than those not in those areas. (5) An increase in water depth significantly reduced impingement probability. When the water depth of the CWIS increased from 5 m to 15 m, impingement probability was reduced up to 30%. Based on the above findings, the following suggestions were made to minimize the impingement effects on CWIS safety: first, the CWIS of coastal nuclear power plants should be set in an area with low aquatic biomass, strong tides, deep water, and few surface species within the range of 1 km, and second, the amount of cooling water withdrawal or velocity should be reduced as much as possible.

KEYWORDS

cooling water intake system, impingement probability, impact factors, numerical modeling, TELEMAC, nuclear power plant

1 Introduction

Nuclear power provides about 10% of the world's electricity from about 440 power reactors (World Nuclear Association, 2023). As the world's second largest source of low-carbon power, nuclear power plays an important role in confronting climate change. At

nuclear power plant (NPPs), cooling water is withdrawn from rivers, lakes, estuaries, and oceans through a Cooling Water Intake System (CWIS), for the purpose of dissipating waste heat. Most power plants use either once-through cooling or a closed-cycle cooling system. A once-through cooling system, which typically withdraws water in the range of tens of millions to billions of gallons per day, could lead to (1) the drawing of fish and shellfish eggs and larvae into and through the condenser cooling systems, and (2) trapping of fish against the screens that prevent debris from being drawn into the cooling water intake. These processes are referred to, respectively, as "entrainment" and "impingement" (Barnthouse, 2013). Impingement and entrainment could lead to loss of fish (eggs, larvae, juvenile, and adult), planktonic organisms, or other aquatic organisms (Merriman and Thorpe, 1976; Helvey, 1985; Boreman and Goodyear, 1988; Karas, 1992; Greenwood, 2008; White et al., 2010), and they also may result in the blockage of CWIS (WANO, 2007), thus threatening the stable operation of NPP. The increasing amount of waste, marine biota, sediment, sea ice, etc. could all aggravate the condition of blockage (Chen, 2009; Arefiev et al., 2015; Yan and Lu, 2016). The safety of cooling water intake has gradually become an important factor affecting the safe operation of nuclear power plants.

In a 2006 study, the World Association of Nuclear Operators found 44 blockages at NPPs since 2004 (WANO, 2007). Aquatic life was the most common material causing blockages, including algae and aquatic grasses, mussels, jellyfish, crustaceans (shrimp and crabs), and fish. Those materials contributed to 37 of the 44 blockage events. The remaining events resulted from accumulations of frazil ice (ice crystals forming in a body of water), depositions of sand and silt, and ingress of crude oil. An Electric Power Research Institute survey found that problems with debris are common (EPRI, 2015). Nearly 50% of facilities have been de-rated because of problems with debris, and slightly more than 10% have been shut down because of debris. In China, according to incomplete statistics, since 2014, there have been many incidents of sea creatures gathering and affecting unit operations (National Nuclear Safety Administration, 2016). For example, in July 2014, accumulations of jellyfish caused a rotating filter blockage at an NPP in northern China. Unit 1 and unit 2 of the circulating pumps jumped and the power plant ultimately shut down. In addition, in August 2015, many *A. molpadioide* (100–200 mm) invaded an NPP in southeastern China, which caused the circulating pumps to stop working and the emergency shutdown of unit 3. Such incidents not only lead to huge economic losses at NPPs but also affect power plant safety and stable operation. As a result, regulator departments, NPP owners, and related design institutes are focusing attention on the problem.

Studies currently primarily focus on how water intake blockage events develop in NPPs, feedback following blockages, and suggestions to improve early warning systems and prevent intake water blockage events (Ruan, 2015; Li et al., 2017; Meng et al., 2018). However, outbreaks of marine organisms as mechanisms causing blockage events of NPPs have not been fully investigated (Fu et al., 2020; Wang et al., 2022).

Chae et al. (2008) reported a seawater intake blockage event in a nuclear power plant at Uljin and discussed the impacts of warm surface current of the eastern Korean waters and the environmental factors related to the ecobiology of the large quantity of salpa. Prakash et al. (2012) found that the Salem power plant was invaded by seaweed from the intertidal swamp 3 miles away by using hydrological and seaweed migration models. Chen (2018) speculated that the blockage of nuclear power plants may be caused by the effect of ocean currents caused by typhoons, the disturbance of the bottom habitat, and the growth of *A. molpadioidea*. Yoon et al. (2022) analyzed the mechanisms and cause of the mass appearance and intrusion of *S.fusiformis* by field surveys and collected observational data.

To optimize water intake design and reduce the effects of water intake blockage, it is essential to determine the probability of biological impingement and its controlling factors. An empirical model has been applied for evaluating entrainment of aquatic organisms in NPPs ever since the 1970s (Eraslan et al., 1975; Swartzman et al., 1977; Boreman et al., 1978). With the development of computational fluid dynamics, numerical models became a useful tool for predicting blockages of water intake structures of NPPs through calculating the probability of biological impingement (Zhang et al., 1992; Prakash et al., 2014). In this paper, a high-resolution, non-structured, three-dimensional numerical model, the TELEMAC-3D, was used to systematically and quantitatively study the factors influencing the probability of biological impingement, including distance to water intake structure, quantity of water intake, tide pattern, tidal current direction, and water depth.

2 Materials and methods

2.1 Numerical model

The TELEMAC-3D system developed by the National Hydraulic and Environmental Laboratory of the Research and Development Directorate of the French Electricity Board (EDF-DRD. Website: http://opentelemac/org/) was used to simulate the hydrodynamic pattern in this study.

The model is based on continuity, momentum, and tracer equations and a turbulence closure scheme and solves each physical quantity of a fluid.

2.1.1 Continuity equation

The continuity equation (mass conservation equation) in the σ coordinate system is as follows:

$$\frac{\partial \eta}{\partial t} + \frac{\partial Hu}{\partial x} + \frac{\partial Hv}{\partial y} + \frac{\partial \hat{w}}{\partial \sigma} = 0 \qquad \text{(Eq. 1)}$$

where η is the free surface height, H = h + η is the total depth, and h is the depth under a flat free surface. Variables u and v are velocity components along x and y axes, respectively, in the Cartesian coordinate system, and $\hat{w}$ is the vertical velocity in the

σ coordinate system:

$$\hat{w} = \frac{\partial \sigma}{\partial t} + u\frac{\partial \sigma}{\partial x} + v\frac{\partial \sigma}{\partial y} + w\frac{\partial \sigma}{\partial z} \quad \text{(Eq. 2)}$$

where w is the vertical velocity component in the Cartesian coordinate system.

To account for complex bathymetry of a research area, the σ coordinate system is used for the vertical discretization of hydrodynamic equations:

$$\sigma = \frac{h+z}{h+\eta} \ (-h < z < \eta) \quad \text{(Eq. 3)}$$

2.1.2 Momentum equation

After the σ coordinate transformation, the momentum equations along the x and y axes are as follows (Hervouet, 2007):

$$\begin{aligned}&\frac{\partial Hu}{\partial t} + \frac{\partial Hu^2}{\partial x} + \frac{\partial Huv}{\partial y} + \frac{\partial u\hat{w}}{\partial \sigma} + gH\frac{\partial \eta}{\partial x}\\ &= \frac{\partial}{\partial x}(2HN_h\frac{\partial u}{\partial x}) + \frac{\partial}{\partial y}[HN_h(\frac{\partial u}{\partial y} + \frac{\partial v}{\partial x})]\\ &+ \frac{\partial}{\partial \sigma}(\frac{N_z}{H}\frac{\partial u}{\partial \sigma}) + fvH - \frac{gH^2}{\rho_0}\frac{\partial}{\partial x}(\int_0^\sigma \rho d\sigma)\\ &+ \frac{gH}{\rho_0}\frac{\partial H}{\partial x}\int_0^\sigma \sigma\frac{\partial \rho}{\partial \sigma}d\sigma \end{aligned} \quad \text{(Eq. 4)}$$

$$\begin{aligned}&\frac{\partial Hv}{\partial t} + \frac{\partial Huv}{\partial x} + \frac{\partial Hv^2}{\partial y} + \frac{\partial v\hat{w}}{\partial \sigma} + gH\frac{\partial \eta}{\partial y}\\ &= \frac{\partial}{\partial x}HN_h(\frac{\partial u}{\partial y} + \frac{\partial v}{\partial x})] + \frac{\partial}{\partial y}[2HN_h\frac{\partial u}{\partial y}]\\ &+ \frac{\partial}{\partial \sigma}(\frac{N_z}{H}\frac{\partial v}{\partial \sigma}) - fuH - \frac{gH^2}{\rho_0}\frac{\partial}{\partial y}(\int_0^\sigma \rho d\sigma)\\ &+ \frac{gH}{\rho_0}\frac{\partial H}{\partial y}\int_0^\sigma \sigma\frac{\partial \rho}{\partial \sigma}d\sigma \end{aligned} \quad \text{(Eq. 5)}$$

where f is the Coriolis parameter and ρ is the density of fluid. The subscript $(_0)$ denotes a reference value. Variables N_h and N_z are the horizontal and vertical eddy viscosities, respectively.

2.1.3 Tracer equation

The dynamic equation for a tracer is as follows (Hervouet, 2007):

$$\begin{aligned}&\frac{\partial HT}{\partial t} + \frac{\partial HuT}{\partial x} + \frac{\partial HvT}{\partial y} + \frac{\partial \hat{w}T}{\partial \sigma}\\ &= \frac{\partial}{\partial x}(HK_h\frac{\partial T}{\partial x}) + \frac{\partial}{\partial y}(HK_h\frac{\partial T}{\partial y}) + \frac{\partial}{\partial \sigma}(\frac{K_z}{H}\frac{\partial T}{\partial \sigma}) \end{aligned} \quad \text{(Eq. 6)}$$

where T is the density of a tracer (kg/m^3) and K_h and K_z are the horizontal and vertical eddy diffusivities, respectively.

2.1.4 Turbulence closure scheme

The k-ϵ turbulence closure scheme is used in the TELEMAC-3D model:

$$\begin{aligned}&\frac{\partial k}{\partial t} + u\frac{\partial k}{\partial x} + v\frac{\partial k}{\partial y} + w\frac{\partial k}{\partial z}\\ &= \frac{\partial}{\partial x}(\frac{N_z}{\sigma_k}\frac{\partial k}{\partial x}) + \frac{\partial}{\partial y}(\frac{N_z}{\sigma_k}\frac{\partial k}{\partial y}) + \frac{\partial}{\partial z}(\frac{N_z}{\sigma_k}\frac{\partial k}{\partial z}) + P + B\\ &- \epsilon \end{aligned} \quad \text{(Eq. 7)}$$

$$\begin{aligned}&\frac{\partial \epsilon}{\partial t} + u\frac{\partial \epsilon}{\partial x} + v\frac{\partial \epsilon}{\partial y} + w\frac{\partial \epsilon}{\partial z}\\ &= \frac{\partial}{\partial x}(\frac{N_z}{\sigma_\epsilon}\frac{\partial \epsilon}{\partial x}) + \frac{\partial}{\partial y}(\frac{N_z}{\sigma_\epsilon}\frac{\partial \epsilon}{\partial y}) + \frac{\partial}{\partial z}(\frac{N_z}{\sigma_\epsilon}\frac{\partial \epsilon}{\partial z}) + C_{1\epsilon}\frac{\epsilon}{k}[P\\ &+ (1 - C_{3\epsilon})B] - C_{2\epsilon}\frac{\epsilon^2}{k} \end{aligned} \quad \text{(Eq. 8)}$$

where k is the turbulent kinetic energy (TKE):

$$k = \frac{1}{2}\overline{u_i' u_i'} \quad \text{(Eq. 8)}$$

where u_i' is the turbulent fluctuation of velocity.

The variable ϵ is the dissipation rate of TKE:

$$\epsilon = v\overline{\frac{\partial u_i'}{\partial x_j}\frac{\partial u_i'}{\partial x_j}} \quad \text{(Eq. 9)}$$

where v is the kinematic viscosity.

The variable P is the shear production of TKE:

$$P = N_z\hat{S}^2 \quad \text{(Eq. 10)}$$

where $\hat{S}^2 = (\frac{\partial u}{\partial z})^2$ is the squared shear.

The variable B is the buoyancy production of TKE:

$$B = K_z N^2 \quad \text{(Eq. 11)}$$

where $N^2 = -\frac{g}{\rho}\frac{\partial \rho}{\partial z}$ is the squared Brunt–Väisälä frequency.

2.1.5 Initial conditions

A flat free surface and a quiescent velocity field are initialized as follows:

$$\eta(x, y, \sigma, 0) = 0 \quad \text{(Eq. 12 − 1)}$$

$$u(x, y, \sigma, 0) = 0 \quad \text{(Eq. 12 − 2)}$$

$$v(x, y, \sigma, 0) = 0 \quad \text{(Eq. 12 − 3)}$$

$$\hat{w}(x, y, \sigma, 0) = 0 \quad \text{(Eq. 12 − 4)}$$

The temperature field is initialized as follows:

$$T(x, y, \sigma, 0) = 25 \quad \text{(Eq. 13 − 1)}$$

The salinity field is initialized as follows:

$$S(x, y, \sigma, 0) = 32 \quad \text{(Eq. 13 − 2)}$$

Turbulent kinetic energy and dissipation rate are initialized as follows:

$$k(x, y, \sigma, 0) = k_{min} \quad \text{(Eq. 14 − 1)}$$

$$\epsilon(x, y, \sigma, 0) = \epsilon_{min} \quad \text{(Eq. 14 – 2)}$$

where $k_{\min}$ and $\epsilon_{\min}$ are the default minimum values of k and ϵ, respectively.

2.1.6 Boundary condition

The flow velocity at the intake is calculated based on the flow rate as follows:

$$U_q = \frac{Q_q}{A_q} \quad \text{(Eq. 15)}$$

where U_q is the flow velocity at the intake ($m{\cdot}s^{-1}$), A_q is the cross-sectional area of the intake (m^2), and Q_q is the flow rate at the intake ($m^3{\cdot}s^{-1}$).

The sea boundary of the model is an open boundary. The eight major tidal constituents of M_2, S_2, N_2, K_2, K_1, O_1, P_1, and Q_1 are considered at the sea boundary. Harmonic constants of the eight constituents are used to calculate the tidal elevation at each tidal boundary node. The harmonic constants were collected from the global ocean model TPXO7.2. Calculation of tidal elevation at the open boundary was based on the following equation (Doodson, 1928):

$$\eta(t) = \sum_{i=1}^{8} f_i^{\}} A_i^{\}} \cos[\omega_i t + (V_i^{\}} + u_i^{\}}) - g_i^{\}}] \quad \text{(Eq. 16)}$$

where f' And u' are the constants for a tidal constituent, A' and g' are the amplitude (m) and phase lag (°), respectively, ω is the tidal frequency ($°s^{-1}$), and V' is the initial phase (°). The subscript i denotes the number of each tidal constituent.

2.2 Mesh generation

The coastal NPP was in northeastern China (Figure 1). The water intake is shown in Figure 2. Bathymetry of the domain from admiralty charts was superimposed with survey data.

The mathematical model used an unstructured triangular grid, with partial nesting at the intake and outfall, a minimum grid scale of approximately 10 m, a maximum grid scale of approximately 2,000 m, and a total number of grids of approximately 40,000. The computational grid of the area around the plant site is shown in Figure 1.

2.3 Validation

The hydrodynamic model was validated by observed data from three tidal stations (WTZ, TPJ, and MJZ; Figure 1) and four gauging stations (Figure 3) with tide height and velocity. Validation results are shown in Figures 4–6.

2.4 Simulated scenarios

2.4.1 Quantity of water intake

The water intake of the power plant was an open channel near the shore. The quantity of water intake has important effects on impingement. According to the power plant design, it had six units, with a total intake of 330 m^3/s cooling water. Every two units used water at 110 m^3/s. In this paper, the effects of water withdrawal at 110 m^3/s and 330 m^3/s were simulated.

2.4.2 Tide

Tide pattern is also a possible factor influencing impingement. Spring, moderate, and neap tides were analyzed, but results for spring and neap tides were used in this article. Bathymetry differences were also considered, and bathymetry was set at –5 m and –15 m in simulations. The general settings of simulated scenarios are listed in Table 1.

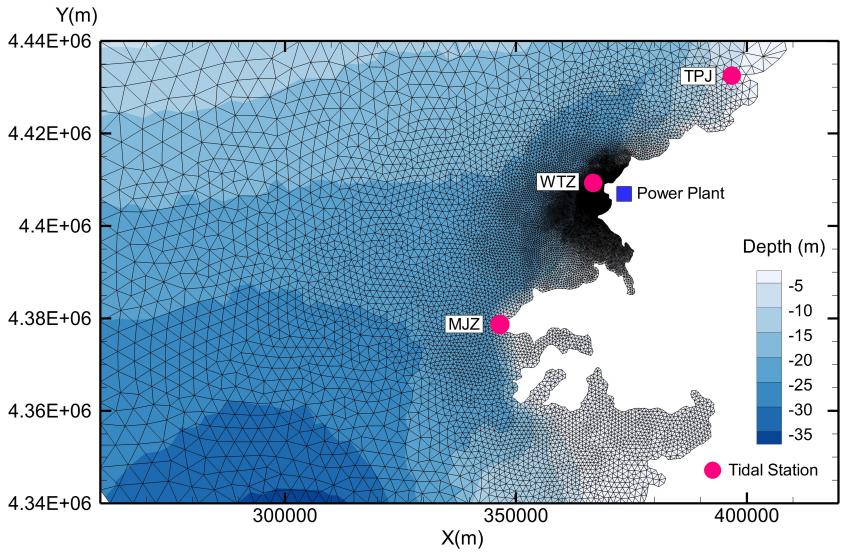

FIGURE 1
Bathymetry and mesh in the computational domain (red dots denote tidal stations).

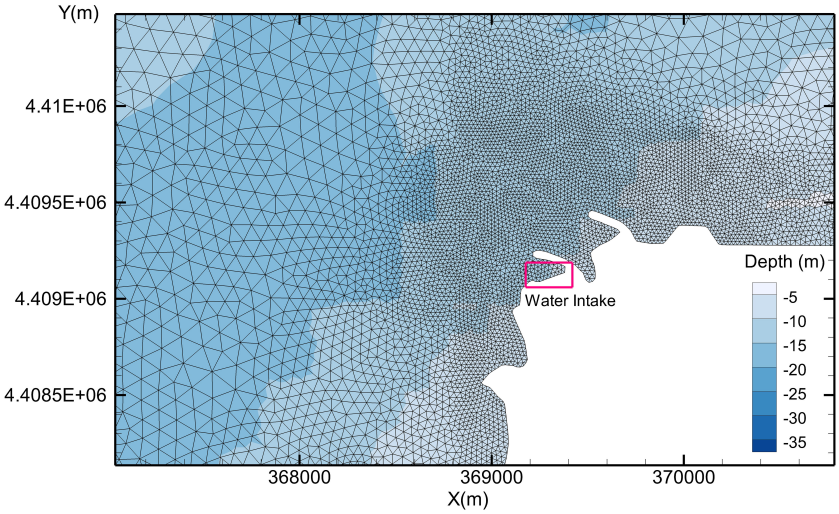

FIGURE 2
Bathymetry and mesh near the water intake.

2.5 Impingement probability calculation

The operation of water intake and discharge facilities can cause significant changes in the flow field of the surrounding sea area, and such changes vary with different locations. Therefore, the impingement probabilities of aquatic organisms at different locations are not the same. To determine the impingement probability at a given location, biological tracers were released into the volume of the water (W_0) at such a location with an initial density C_0, hence the initial number of biological tracers was C_0W_0. Over time the biological tracers will spread and reach the intake where its density at the intake, $C_i(t)$, will gradually decrease with time. Let Q_p be the withdrawal rate at the intake, then the cumulative number of the biological tracers withdrawn at the intake, $M(t)$, will be

$$M(t) = Q_p \int C_i(t)dt \qquad \text{(Eq. 17)}$$

Hence the impingement probability $I_p(t)$ could be calculated by Eq.18.

$$I_p(t) = \frac{M(t)}{C_0 W_0} \qquad \text{(Eq. 18)}$$

In this study, the above method used for calculating the impingement probability is termed as “mass transport model”. A similar method has been used in the literature (e.g. Edinger and Kolluru, 2000).

For the simulated scenarios, the intensity of impingement effect at different locations was estimated in two primary steps. Firstly, the impingement influenced area in the vicinity of the water intake was

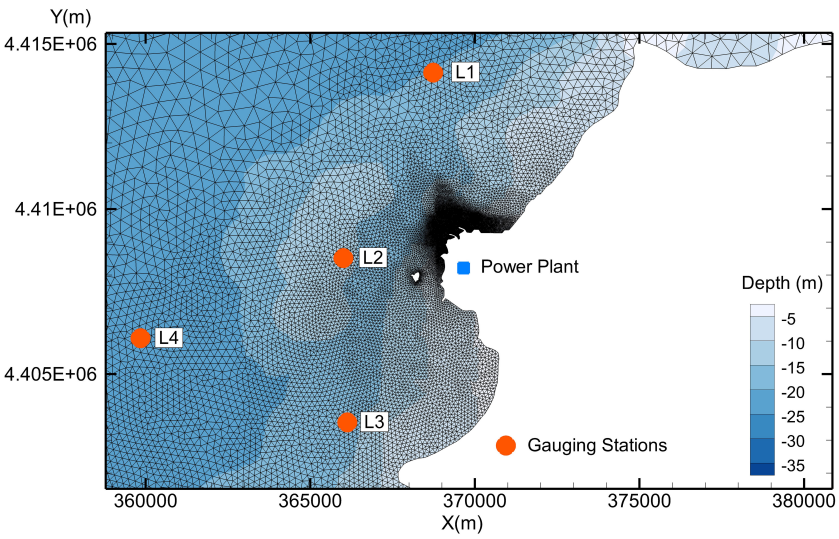

FIGURE 3
Gauging stations near the nuclear power plant.

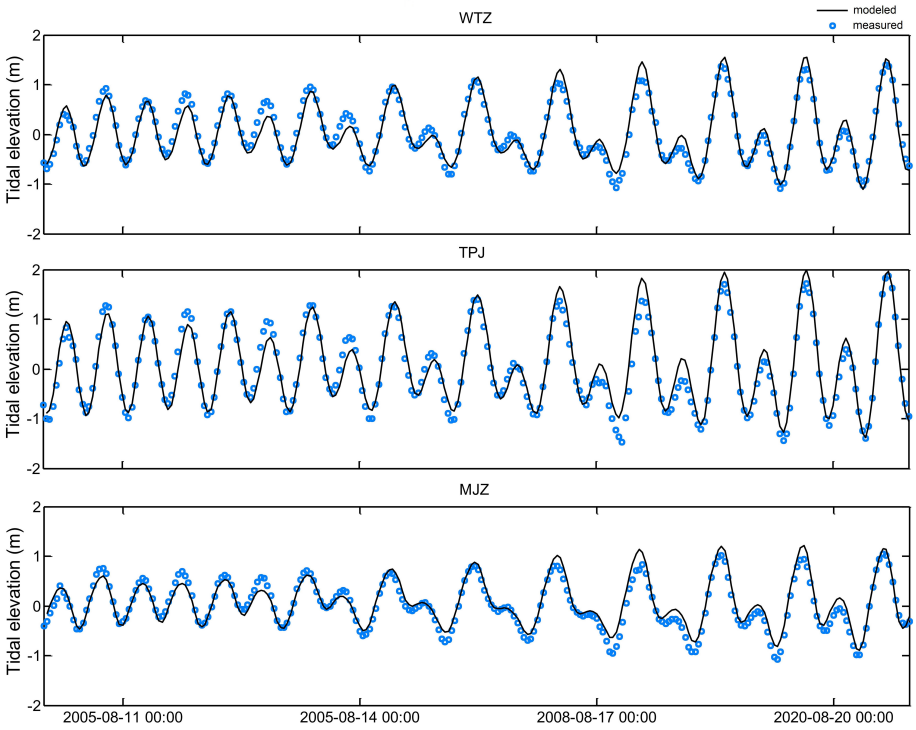

FIGURE 4
Comparison between modeled and measured tidal elevation at three tidal stations within the computational domain.

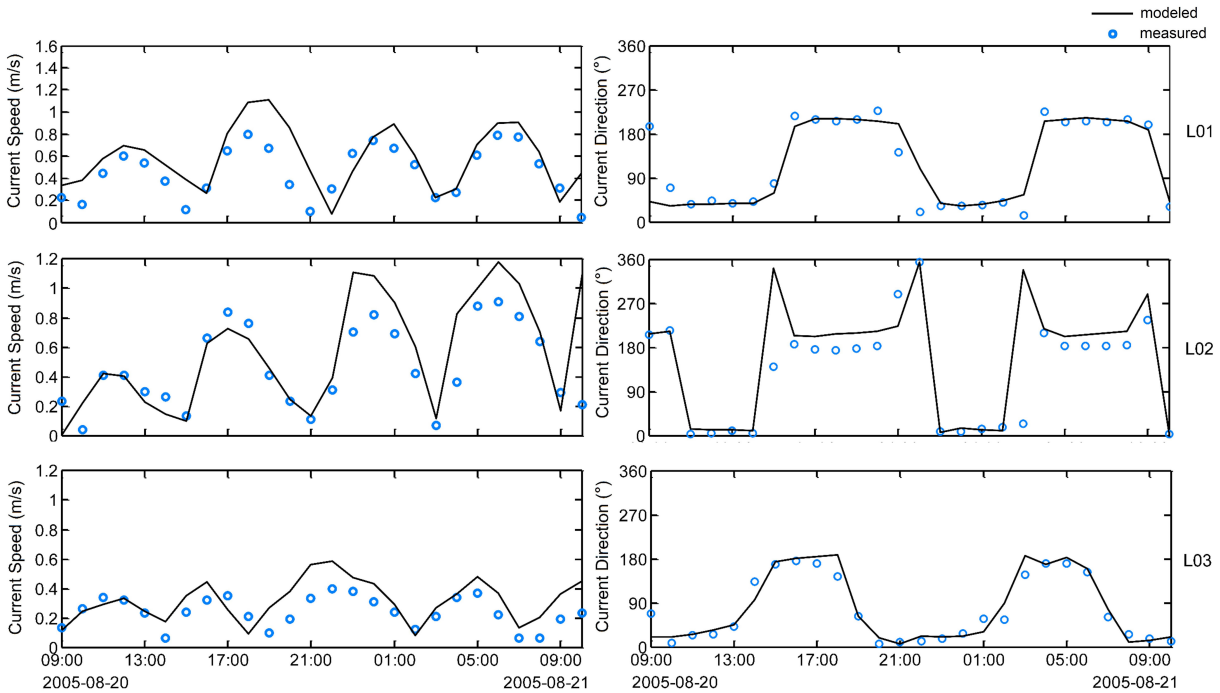

FIGURE 5
Comparisons between measured and simulated current speeds and directions on a spring tide at three gauging stations (L01, L02, and L03).

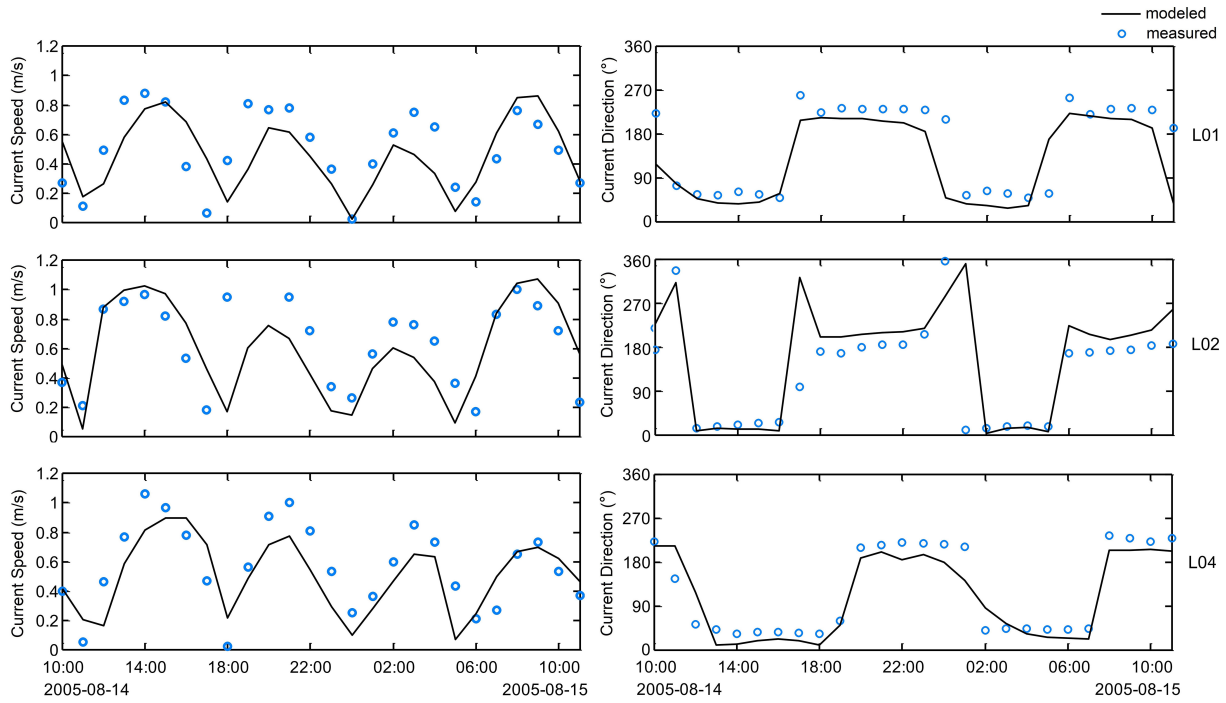

FIGURE 6
Comparisons between measured and simulated current speeds and directions on a neap tide at three gauging stations (L01, L02, and L04).

analyzed by using a numerical model without considering the tidal conditions. Secondly, the main influenced area was divided into several subregions, and the impingement probability in each subregion was calculated.

3 Results

3.1 Impingement influenced area

Nuclear power plants with a direct current circulation cooling scheme have large withdrawal and discharge volumes, which can significantly change the flow field in the nearby sea area. To quantitatively analyze the influences of withdrawal and discharge of a typical coastal plant site on the surrounding flow field, simulations were conducted of case 1 and case 2 without considering the tidal effect. This can be achieved by settling the amplitude of each tidal component to 0m at the tidal open boundary in numerical model. In case 1, when only the action of water intake was considered, the maximum flow velocity near the water intake reached 0.12 m/s, the flow velocity of the outermost area of the embankment on the north side of the intake (approximately 200 m from the intake) was approximately 0.05 m/s, and the flow velocity of the area approximately 400 m from the intake was approximately 0.01 m/s (Figure 7). Because the impingement mainly occurred by plankton with weak swimming ability and that drift with the waves, the area with flow velocity greater than 0.01 m/s was considered a conservative estimate of the possible influence range of the impingement.

In case 2, the maximum flow velocity near the water intake area reached 0.35 m/s, the flow velocity in the outermost area of the

TABLE 1 General settings of model scenarios.

Case no.	Installed capacity (MW)	Intake (m^3/s)	Tide	Bathymetry
1	2×1000	110	No	realistic
2	6×1000	330	No	realistic
3	2×1000	110	Neap tide	realistic
4	2×1000	110	Spring tide	realistic
5	6×1000	330	Neap tide	realistic
6	6×1000	330	Spring tide	realistic
7	2×1000	110	Neap tide	–5 m (uniform)
8	2×1000	110	Neap tide	–15 m (uniform)

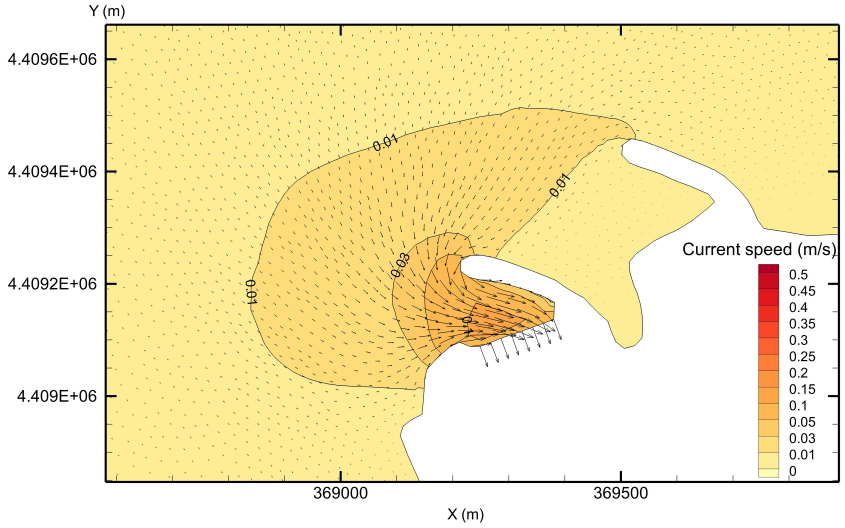

FIGURE 7
Flow field near the cooling water intake system in case 1 (no tide).

embankment on the north side of the intake (approximately 200 m from the intake) was approximately 0.15 m/s, and the flow velocity in the fan-shaped area approximately 400 m from the intake was approximately 0.05 m/s. Overall, in case 2, the water intake of 330 m^3/s influenced the flow field in the surrounding area to approximately 1,000 m (with the extent of 0.01 m/s as the limit; Figure 8).

According to the simulations, the possible area where the impingement effect takes place covered approximately 400 m in radius around the water intake when the water withdrawal of the power plant was 110 m^3/s. When water withdrawal of the power plant increased to 330 m^3/s, the impingement area enlarged to 1 km in radius from the water intake. The results are in general agreement with actual field measurements (Kang et al., 2018).

The distance influenced by impingement will differ at different sites with different water withdrawals, layout characteristics of water intake, and water depth around water intake. However, the results in this study are meaningful for further research. In this study, the focus area for simulation and analysis of impingement probability was set within 1 km from the water intake.

3.2 Distance from the water intake

Based on the determination of the influenced area, the area of the impingement probability analysis was set within an approximate range of 1 km from the water intake and expanded as appropriate.

To further quantify the probability of impingement at different locations near the water intake, the sea area near the water intake was divided into 11 subzones that were 500 m × 500 m (T1–T11; Figure 9). The initial density of biological tracers in 11 water bodies was separately set to 1 (normalized). The density of biological tracers in other areas was set to 0. When the model calculation began, density of biological tracers in a subzone gradually decreased due to water intake. After calculating for a certain time (e.g. several days), the total amount of tracers in the calculation domain remained almost unchanged, indicating that the tracers that remained were far from the water intake. At that time, the difference between the remained and initial number of tracers was the impinged part by water intake.

Probabilities of impingement in the subzones near the water intake in case 3 (neap tide, 2 units), case 4 (spring tide, 2 units), case 5 (neap tide, 6 units), and case 6 (spring tide, 6 units) are shown in Figures 10, 11. In case 3, the probability of impingement in the area within approximately 300 m from the water intake (subzone T8) reached 45.78%, and the probability in the adjacent subzones T10 (to the east) and T7 (to the south) also reached 32.97% and 35.84%, respectively. By contrast, the probability of impingement within 1 km from the intake was close to 1%. In case 5, the probability of impingement in the area within approximately 300 m from the water intake (subzone T8) reached 83.49%, and the probability in the adjacent subzones T10 and T7 also reached 72.34% and 60.23%, respectively. Within 1 km from the intake, the probability of impingement was close to 5%.

The results indicated that under the combined effect of water withdrawal and tide, the impingement effect of a typical coastal site mainly occurred within a 1-km area from the water intake, and as the distance to the water intake decreased, the probability of impingement increased.

3.3 Quantity of water intake

The difference in the probability of impingement at the same location under the same tidal pattern between different quantities of water intake can explain the effect of water withdrawal on the probability of impingement.

The probability of impingement for six units was significantly higher than that for two units (Figures 10, 11). In case 5, the probability of impingement was 83.49% in T8, 72.34% in T10, and 60.23% in T7. In case 3, the probability of impingement was 45.78% in T8, 32.97% in T10, and 35.84% in T7. The results indicated that

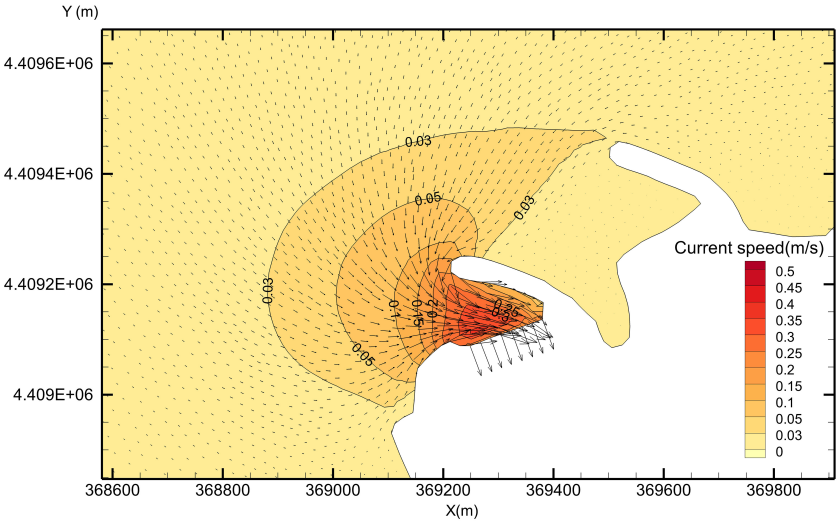

FIGURE 8
Flow field near the cooling water intake system in case 2 (no tide).

the increase in water intake significantly increased the probabilities of impingement. In case 3, the probability of impingement was 2.57% in subzone T5 (to the west) and 2.65% in subzone T9 (to the north). In case 5, the probability was 18.07% in T5 and 11.3% in T9. These indicated that increases in impingement probabilities due to increase in water withdraw were most significant in key impingement subzones, such as T8, T10, and T7.

3.4 Tide

For a coastal site, the tidal range is one of the most important factors affecting the flow velocity. Therefore, tide is also a possible factor in analyzing the probability of impingement.

In case 3, the probability of impingement was high in subzones of T8 (45.78%), T10 (32.97%), and T7 (35.84%). However, in case 4, the probabilities were 34.14% (T8), 27.76% (T10), and 24.28% (T7). The differences in probability were –11.64% (T8), –5.21% (T10), and –11.56% (T7) (Figure 10). In the other subzones in the range of 300 m to 800 m from the water intake, the differences in probability were 10.44% in T4, –0.33% in T5, –0.41% in T9, and –1.19% in T11. The results indicated that when the tide changed from neap tide to spring tide, the probabilities in some subzones increased, whereas in others, they did not.

In case 5, the probability of impingement was high in subzones T8 (83.49%), T10 (72.34%), and T7 (60.23%). However, in case 6, the probabilities were 70.29% (T8), 61.66% (T10), and 80.19% (T7). The differences in probability were –13.2% (T8), –10.68% (T10),

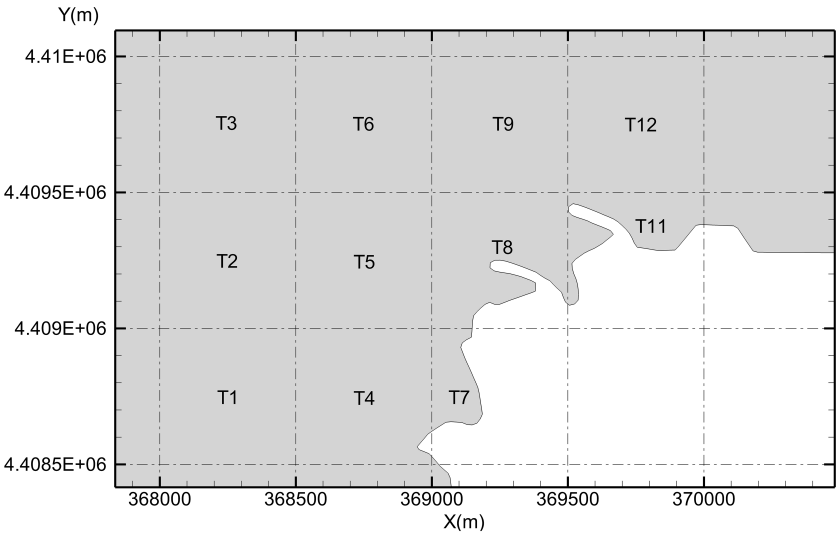

FIGURE 9
Computation subdomains for the probability of entrainment.

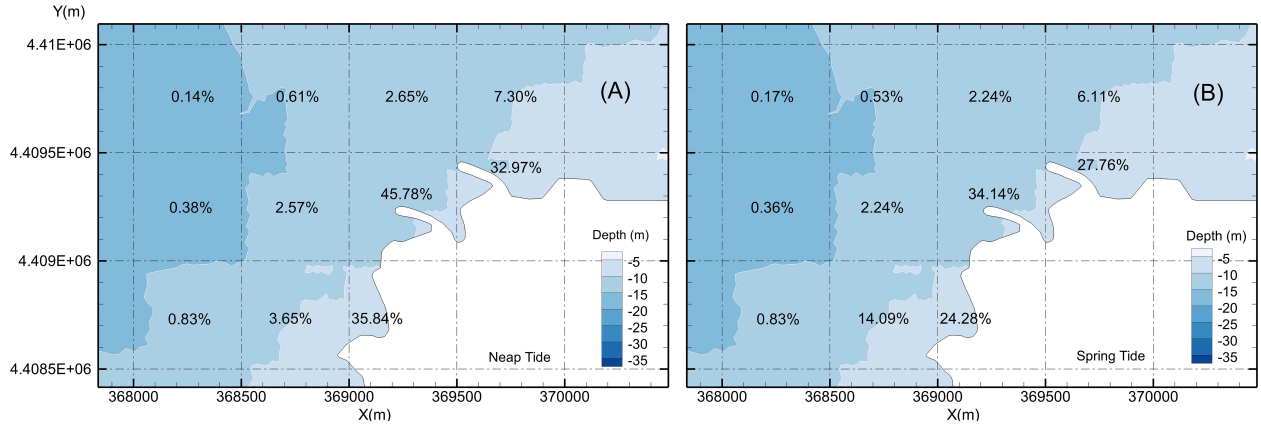

FIGURE 10
Probabilities of impingement near the cooling water intake system for the site with two units installed capacity. **(A)** Neap tide; **(B)** spring tide.

and 19.96% (T7) (Figure 11). In the other subzones in the range of 300 m to 800 m from the water intake, the differences in probability were 31.6% in T4, –6.99% in T5, –4.5% in T9, and –7.17% in T11. The results were almost the same as those in case 3 and case 4.

To conclude, an increase in tidal difference can lead to a decrease in the probability of impingement in the area near a water intake but to an increase in some other areas far from a water intake. Therefore, the effect of tide changes not only the total probability of impingement but also the spatial distribution of the probability.

3.5 Tidal flow direction

The probability of impingement in subzones T10 and T7 was significantly higher than that in subzones T9 and T5 (Figures 10, 11). The difference was mainly due to the local tidal field. The direction of the tide in the study area was generally parallel to the shoreline, with northeast the main direction of the rising tide and southwest the main direction of the falling tide. The tide constantly transported tracers in the northeast and southwest of the water intake to the water intake area, which led to higher probabilities of impingement in those subzones. This could also explain why the probability of impingement in subzone T7 (80.19%), an adjacent subzone nearby the water intake, was higher than that in subzone T8 (70.29%), a subzone where the water intake takes place.

Thus, areas up or down the main tidal current direction had a higher probability of impingement than areas not on the tidal current direction. To minimize the effect on probability of water intake blockage, the sites of NPPs need to pay special attention to the main tidal currents in local areas.

3.6 Water depth

Water depth conditions are often different at different sites, and therefore, the effect of water depth on the probability of impingement was analyzed. Two model cases (case 7 and case 8) were set with water depths of –5 m and –15 m.

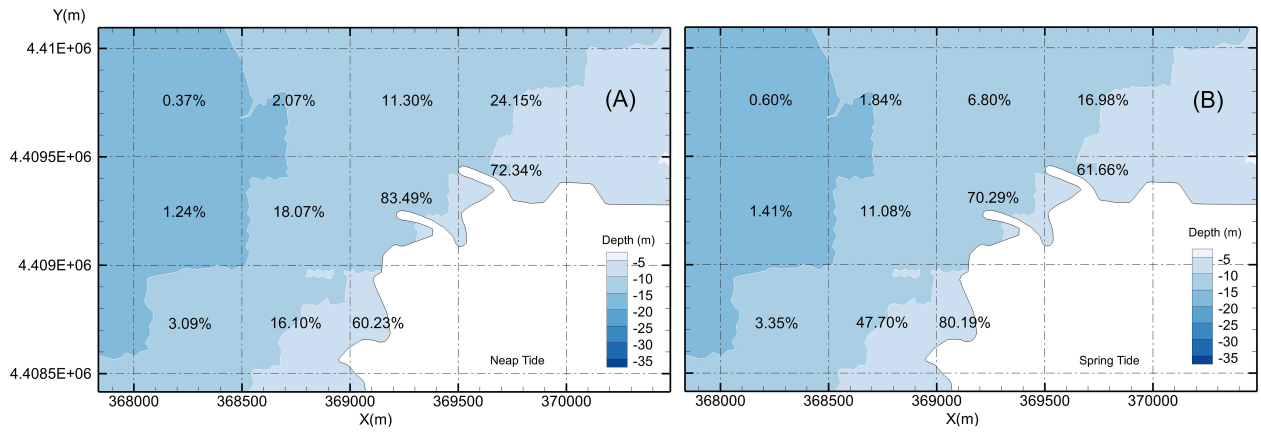

FIGURE 11
Probabilities of impingement near the cooling water intake system for the site with a capacity of six installed unit. **(A)** Neap tide; **(B)** spring tide.

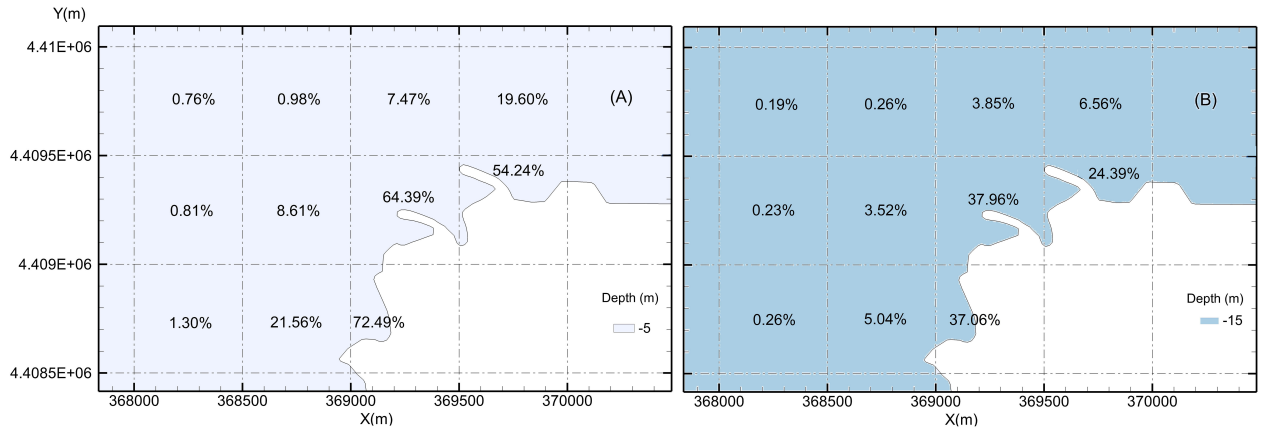

FIGURE 12
Probabilities of impingement near the cooling water intake system for the site with different water depths. **(A)** −5 m; **(B)** −15 m.

Probabilities of impingement in case 7 were significantly higher than those in case 8 (Figure 12). In case 7, the probability of impingement was 64.39% in T8, 54.24% in T10, and 72.49% in T7. In case 8, the probabilities of impingement were only 37.96% in T8, 24.39% in T10, and 37.06% in T7. The differences between the two cases were approximately 26.43% (T8), 29.85% (T10), and 35.43% (T7). In the other subzones, probabilities of impingement in case 7 were also higher than those in case 8, with differences of approximately 16.52% (T4), 5.09% (T5), 3.62% (T9), and 13.04% (T11).

The results indicated that water depth was an important factor affecting the probability of impingement. With an increase in depth, the probability of impingement decreased. Thus, when selecting an NPP site, a site with deep water would be best.

4 Discussion

4.1 Influenced area by water intake

It is essential to determine the influenced area by water intake in studying CWIS safety in NPPs. When the area is clear, targeted safety monitoring can be conducted, and the control areas can be divided to reduce the workload. Determining the area is also important in monitoring marine biota and cleaning blockages when under severe weather. However, at present, the influenced area by water intake has not been clearly defined. In a conservative approach, relatively large ranges for monitoring are selected, with a maximum radius up to 66 km (Shi et al., 2020). According to the characteristics of the monitoring object and technology, 10 km has been used as the monitoring range (Song et al., 2021). On the basis of emergency response time, 5 km has been defined as the control range. In this study, the actual effect of the flow field is proposed to set the range. Sea organisms entering that range are influenced by the flow field and have a certain probability of entering the water intake. This conclusion is generally consistent with actual field measurements (Kang et al., 2018). Such a range also does not conflict with the scope of security control proposed by other studies, because for monitoring and early warning, it is indeed necessary to expand the monitoring range to prepare for a response in advance. In addition, the area for safe water withdrawal proposed in this study can also be affected by coastal currents, and thus, for some coastal NPPs, the influenced area may expand in some directions.

4.2 Method to calculate impingement probability

This study was based on the method to calculate impingement probability. Two methods are commonly used in simulating the distribution of material. One method is the particle tracking method (Chu et al., 2010; Moon et al., 2010), and the other is the mass transport method (Zhang et al., 1992). In this study, the mass transport method was used to calculate impingement probability. The method is suitable for simulating marine organisms that are passively transported, such as jellyfish. Zhang et al. (1992) also used this method to analyze the effect of impingement from the Dayawan Nuclear Power Station on nearby water ranges. For marine organisms with strong movement ability (such as fish), the results will be affected to some extent. Currently, there is no reliable method to simulate the movement of marine organisms (Wu et al., 2015). Although jellyfish may also have certain migration abilities, those organisms generally follow the flow (Wu et al., 2016). On a large scale, based on the mass transport method, the overall estimates of impingement probability remain credible.

4.3 Subregion division

Dividing the influenced area by water intake into subregions is an important step in calculating probabilities of impingement. In this study, rectangular subregions were selected, and then impingement probabilities were calculated in those sub-regions. Such subdivision was relatively easy and facilitated subsequent calculations, however, it was also somewhat unreasonable because

the probability of impingement was significantly related to the distance from the CWIS. In NPP site surveys and selections, most use subregional division of a population according to distance from the site, with circular subdivisions (International Atomic Energy Agency, 2015). In fact, subregion shape and size both have important effects on impingement probability, and thus, it would be valuable to examine those factors in follow-up studies.

5 Conclusion

In this paper, based on a 3D hydrodynamic numerical model, the probability of impingement under different conditions in a typical coastal plant site was calculated. Water withdrawal volume, tide, tidal flow direction, and water depth were analyzed as important factors affecting the probability of impingement.

Considering water intake only and two units with volume of 110 m^3/s, the influenced flow field was approximately 400 m around the water intake (with 0.01 m/s as the limit). For six units with volumes of 330 m^3/s, the flow field influenced was approximately 1,000 m around the water intake (with 0.01 m/s as the limit). Thus, an increase in water withdrawal significantly increased the probability of impingement in the area near the water intake. Considering both water intake and tide effect, the impingement mainly occurred in the 1,000 m around the water intake, and as the distance to the water intake decreased, the probability of impingement increased. With an increase in tidal difference, the probability of impingement in the area around the water intake decreased, whereas that in peripheral areas increased. Therefore, the effect of tidal difference on impingement was mainly expressed in changes in the spatial distribution of the probability of impingement, and a decrease in total probability of impingement in the total sea area was limited. For the main tidal flow direction, the probability of impingement was higher than that in other directions. In addition, the probability of impingement decreased when the site had increased water depth. The results of this study can be used in plant site selection and water intake design.

Data availability statement

The original contributions presented in the study are included in the article/Supplementary Materials, further inquiries can be directed to the corresponding author.

Author contributions

All authors listed have made a substantial, direct, and intellectual contribution to the work and approved it for publication.

Funding

The research was supported by the projects “Technology development of keeping cold water intake system safety and security of nuclear power plants” (21FW018), “Research on a new sea organism control technology” (20YW118) and “Development of numerical simulation technology for the transport and diffusion of radioactive wastewater from nuclear accidents at the Global coastal sea scale” (21YW057).

Acknowledgments

We thank the topic organizers for their hard work and kind introductions.

Conflict of interest

All authors were employed by Shanghai Nuclear Engineering Research and Design Institute Co., Ltd.

Publisher’s note

Supplementary material

The Supplementary Material for this article can be found online at: https://www.frontiersin.org/articles/10.3389/fmars.2023.1133187/full#supplementary-material

References

Arefiev, N., Mikhalev, M., Zotov, D., Zotov, K., Vatin, N., Nikonova, O., et al. (2015). Physical modeling of suspended sediment deposition in marine intakes of nuclear power plants. *Proc. Eng.* 117, 32–38. doi: 10.1016/j.proeng.2015.08.120

Barnthouse, L. W. (2013). Impacts of entrainment and impingement on fish populations: A review of the scientific evidence. *Environ. Sci. policy.* 31, 149–156. doi: 10.1016/j.envsci.2013.03.001

Boreman, J., and Goodyear, C. P. (1988). Estimates of entrainment mortality for striped bass and other fish species inhabiting the Hudson river estuary. *Am. Fisheries Soc. Monograph* 4, 152–160.

Boreman, J., Goodyear, C. P., and Christensen, S. W. (1978). *An empirical transport model for evaluating entrainment of aquatic organisms by power plants (Vol. 78)* (Department of the Interior, Fish and Wildlife Service, Office of Biological Services, Power Plant Project).

Chae, J., Choi, H. W., Lee, W. J., Kim, D., and Lee, J. H. (2008). Distribution of a pelagic tunicate, salpa fusiformis in warm surface current of the eastern Korean waters and its impingement on cooling water intakes of uljin nuclear power plant. *J. Environ. Biol.* 29, 585–590.

Chen, F. (2009). The principle of choosing tunnel gate location for nuclear power plants in the coastal sites in China. *Nucl. Saf.* 2, 25–29. doi: 10.3969/j.issn.1672-5360.2009.02.005

Chen, H. (2018). Research on the causes, prevention and control measures of bioblogging on nuclear power cold source by acaudina molpadioidea. master thesis (Shanghai: Shanghai Ocean University).

Chu, Q. Q., Li, L., and Li, P. L. (2010). *The particle tracking numerical experiment of flow field in the jiaozhou bay* Vol. 40 (Periodical of Ocean University of China), 29–34. doi: 10.16441/j.cnki.hdxb.2010.11.004

Doodson, A. T. (1928). The analysis of tidal observations. *Philos. Trans. R. Soc. London.* 227, 223–279. doi: 10.1098/rsta.1928.0006

Edinger, J. E., and Kolluru, V. S. (2000). Power plant intake entrainment analysis. *J. Energy Eng.* 126, 1–14. doi: 10.1061/(ASCE)0733-9402(2000)126:1(1)

EPRI (2015). *Best management practices manual for preventing cooling water intake blockages. report no. 3002006735214* (Palo Alto, CA: EPRI).

Eraslan, A. H., Van Winkle, W., Sharp, R. D., Christensen, S. W., Goodyear, C. P., Rush, R. M., et al. (1975). Computer simulation model for the striped bass young-of-the-year population in the Hudson River. *[Effects of entrainment and impingement at power plants on population dynamics].* (United States). doi: 10.2172/7232009

Fu, X. C., Du, F. L., Pu, X., Wang, X., and Han, F. Z. (2020). Analysis on critical factors of marine organism impacts on water intake safety at nuclear power plants. *J. Nucl. Eng. Radiat. Sci.* 6, 1–6. doi: 10.1115/1.4048112

Greenwood, M. F. D. (2008). Fish mortality by impingement on the cooling-water intake screens of england's largest direct-cooled power plant. *Mar. pollut. Bull.* 6, 723–739. doi: 10.1016/j.marpolbul.2007.12.008

Helvey, M. (1985). Behavioral factors influencing fish entrapment at offshore cooling-water intake structures in southern California. *Mar. fisheries review.* 47 (1), 18–26.

Hervouet, J. M. (2007). *Hydrodynamics of free surface flows: Modelling with the finite element method* (West Sussex: John Wiley & Sons), 341.

International Atomic Energy Agency (2015). *Site survey and site selection for nuclear installations. IAEA safety standards series no. SSG-35* (Vienna: IAEA).

Kang, J. F., Fan, D. D., Zhou, C. L., and Lv, Y. X. (2018). The characteristic analysis of ocean current for the safety of cold resource of nuclear power station. *Mar. Environ. Sci.* 37, 70–77. doi: 10.13634/j.cnki.mes.2018.01.012

Karas, P. (1992). Zooplankton entrainment at Swedish nuclear power plants. *Mar. pollut. Bull.* 24 (1), 27–32. doi: 10.1016/0025-326X(92)90313-U

Li, J., Liu, X., Zhang, J., and Meng, Y. (2017). Research on sea creature detection technology for improving the safety of cold sources in nuclear power plants. *Chin. J. Electric Saf. Technol.* 19, 32–37. doi: 10.3969/j.issn.1008-6226.2017.10.011

Meng, Y., Liu, L., Guo, X., Liu, N., and Liu, Y. (2018). An early-warning and decision-support system of marine organisms in a water cooling system in a nuclear power plant. *J. Dalian Ocean Univ.* 33, 108–112. doi: 10.16535/j.cnki.dlhyxb.2018.01.017

Merriman, D., and Thorpe, L. M. (1976). *The Connecticut river ecological study: impact of a nuclear power plant* (American Fisheries Society Monograph).

Moon, J. H., Pang, I. C., Yang, J. Y., and Yoon, W. D. (2010). Behavior of the giant jellyfish *Nemopilema nomurai* in the East China Sea and East/Japan Sea during the summer of 2005: a numerical model approach using a particle-tracking experiment. *J. Mar. Syst.* 80, 101–114. doi: 10.1016/j.jmarsys.2009.10.015

National Nuclear Safety Administration (2016). *Bulletin on the recent incidents of marine organisms or foreign debris affecting the safety of water withdrawals of nuclear power plants. report no. 000014672/2016-00407* (Beijing, China: National Nuclear Safety Administration).

Prakash, S., Kolluru, V. S., and Tutton, P. (2012) "Semi-Lagrangian approach to studying grassing issue on a nuclear power plant cooling water intake," in *Proceedings of 10th International Conference on Hydroscience and Engineering.* 1–26(Orlando, Florida, USA), ICHE 2012.

Prakash, S., Kolluru, V., and Young, C. (2014). Evaluation of the zone of influence and entrainment impacts for an intake using a 3-dimensional hydrodynamic and transport model. *J. Mar. Sci. Eng.* 2, 306–325. doi: 10.3390/jmse2020306

Ruan, G. (2015). Reason analysis and corresponding strategy for cooling water intake blockage at nuclear power plants. *Nucl. Power Eng.* 36, 151–154. doi: 10.13832/j.jnpe.2015.S1.0151

Shi, W. Q., Yuan, S., Song, L. N., Zhuang, Y. J., Xu, N., Liu, X. Q., et al. (2020). A preliminary study on numerical simulation warning of the risk of ice blocking in water intake of the hongyanhe nuclear power plant. *Mar. Sci. Bull.* 39, 439–446. doi: 10.11840/j.issn.1001-6392.2020.04.006

Song, L. N., Wang, Z. Z., Zhao, B. Q., Yang, Y. J., Wang, P., and Yuan, S. (2021). Design of the radar monitoring system of sea ice for the safety of nuclear power cold source. *Chin. J. Mar. Environ. Sci.* 40, 619–624. doi: 10.12111/j.mes.20200008

Swartzman, G., Deriso, R., and Cowan, C. (1977) Comparison of simulation models used in assessing the effects of power-plant-induced mortality on fish populations. in *Proceedings of the Conference on Assessing the Effects of Power-Plant-Induced Mortality on Fish Populations. Pergamon*. p.333–p.361.

Wang, Y., Chen, X., Lin, Y., Zhang, S., Chang, L., Tang, X., et al. (2022). Potential risk from and prevention of phytoplankton outbreaks in blocking the cooling water system in a nuclear power plant on the southeast China coast. *Front. Mar. Sci.* 9. doi: 10.3389/fmars.2022.1034876

WANO (2007). *Intake cooling water blockage: Significant operating experience report (SOER). report no. 2007–2* (London: WANO).

White, J. M., Nickols, K. J., Clarke, L., and Largier, J. L. (2010). Larval entrainment in cooling water intakes: spatially explicit models reveal effects on benthic meta-populations and shortcomings of traditional assessments. *Can. J. fisheries Aquat. Sci.* 67 (12), 2014–2031. doi: 10.1139/F10-108

World Nuclear Association (2023) *Nuclear power in the world today [EB/OL].* Available at: https://world-nuclear.org/information-library/current-and-future-generation/nuclear-power-in-the-world-today.aspx.

Wu, L. J., Gao, S., and Bai, T. (2016). Review on the migration mechanisms of large jellyfish and techniques of the monitoring, forecasting, and warning of jellyfish disaster. *Acta Ecologica Sin.* 36, 3103–3107. doi: 10.5846/stxb201409251898

Wu, L. J., Gao, S., Liu, G. Y., and Bai, T. (2015). Study on the ensemble forecast of large jellyfish drift in the coastal waters of qingdao. *Mar. Forecasts* 32, 62–71. doi: 10.11737/j.issn.1003-0239.2015.02.010

Yan, G. C., and Lu, W. T. (2016). Prevention and management of invasions blockage in water intake of power plant. *Ind. Technol.* 14, 119–119. doi: CNKI:SUN:CXYY.0.2016-14-091

Yoon, W., Choi, B. J., Yoo, H., Kim, B., Bok, Y., and Chae, J. (2022). Unusual mass appearance of *Salpa fusiformis* (Thaliacea: Salpida) in early spring at a nuclear power plant at mid-western boundary of the East Sea. *Ocean Sci. J.* 57, 269–278. doi: 10.1007/s12601-022-00065-z

Zhang, C. L., Huang, Z. Z., Kong, L. F., and Peng, J. W. (1992). The numerical simulation on low-level radioactive waste water, low-temperature cooling water drained effect of impingement from the dayawan nuclear power station. *Chin. J. Comput. Phys.* 9, 587–591.

Frontiers in Marine Science

Explores ocean-based solutions for emerging global challenges

The third most-cited marine and freshwater biology journal, advancing our understanding of marine systems and addressing global challenges including overfishing, pollution, and climate change.

Discover the latest Research Topics

See more →

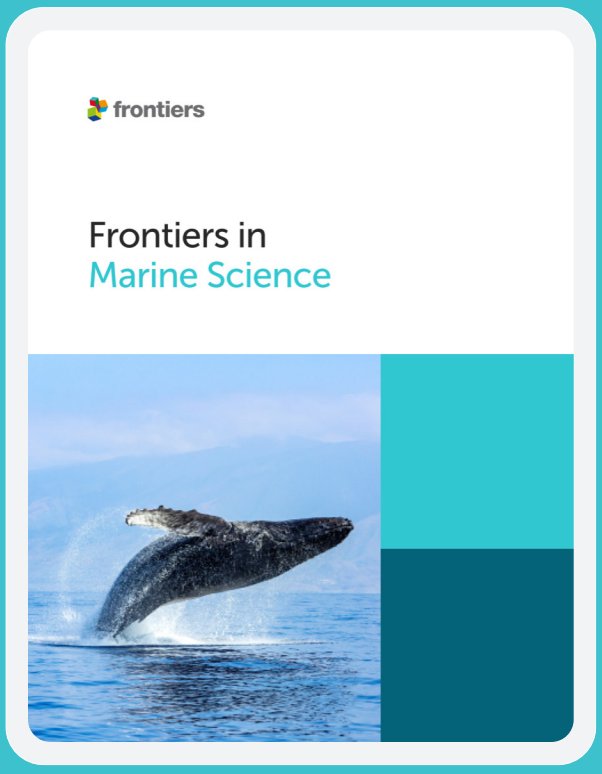

Frontiers

Avenue du Tribunal-Fédéral 34
1005 Lausanne, Switzerland
frontiersin.org

Contact us

+41 (0)21 510 17 00
frontiersin.org/about/contact